

University of Warwick institutional repository: <http://go.warwick.ac.uk/wrap>

A Thesis Submitted for the Degree of PhD at the University of Warwick

<http://go.warwick.ac.uk/wrap/69959>

This thesis is made available online and is protected by original copyright.

Please scroll down to view the document itself.

Please refer to the repository record for this item for information to help you to cite it. Our policy information is available from the repository home page.



Processing and Characterisation of Cementitious Materials Reinforced with Fibres

By

Abdalla Khalifa

A thesis submitted in partial fulfilment of the requirements for the degree of

Doctor of Philosophy

School of Engineering

THE UNIVERSITY OF
WARWICK

February 2015

I dedicate this thesis to the memory of my beloved grandfather, Omar Khalifa

Contents

Table of contents.....	ii
List of Figures.....	vii
List of Tables.....	xv
List of Abbreviations.....	xvii
Acknowledgements.....	xx
Declaration.....	xxi
Abstract.....	xxii
Terminology.....	xxiv
1 Introduction.....	1
1.1 General.....	1
1.2 Aims and Objectives.....	3
1.3 Structure of Thesis.....	5
2 Literature Review.....	7
2.1 Introduction.....	7
2.2 Key Difference Between FRC and FRP Composites.....	7
2.3 Clasification of FRC Composites.....	9
2.4 Fibres Reinforced Cementitious Materials.....	11
2.4.1 Glass Fibres (GF).....	13
2.4.2 Polyvinyl Alcohol Fibres (PVA).....	14
2.4.3 Polypropylene Fibres (PP).....	15
2.4.4 Carbon Fibres (CF).....	16
2.4.5 Mechanical Properties of Carbon Fibre Reinforced Concrete (CFRC).....	18
2.5 Textile Reinforced Concrete (TRC).....	21
2.6 Manufacturing Process.....	23
2.6.1 Hatschek.....	24
2.6.2 Hand Lay-up.....	24
2.6.3 Spray-up.....	25
2.6.4 Premixing.....	25
2.6.5 Pultrusion.....	25
2.6.6 Extrusion.....	26

2.6.7	Compression Moulding.....	26
2.6.8	Effect of Manufacturing Processes on The Mechanical Properties	26
2.7	Dispersion of Short Fibres.....	27
2.8	Additives.....	28
2.8.1	Silica Fume (SF).....	29
2.8.2	Pulverised Fuel Ash (PFA).....	31
2.8.3	Ground Granulated Blast Furnace Slag (GGBS).....	32
2.9	Mechanical Behaviour of FRC.....	33
2.9.1	Composite Rule of Mitures.....	33
2.10	Stress-Strain Curve in FRC Composite.....	34
2.11	Models of FRC Composites.....	39
2.12	Which Models to Use.....	40
2.13	ACK Model.....	43
2.14	Fibre Volume Fraction (V_f).....	47
2.15	The Critical Length (l_c).....	49
2.16	Interfacial Bond Strength (τ).....	52
2.17	The Fibre Efficiency Factors (η): Fibre Length and Orientation	59
2.18	Fracture Mechanics.....	65
2.18.1	Fracture Principles: LEFM and NLFM.....	66
2.19	Summary to Literature Review.....	67
3	Materials and Experimental Procedures.....	71
3.1	Introduction.....	71
3.2	Materials.....	71
3.2.1	Cement (C).....	72
3.2.2	Supplementary Cementing Materials (Additives).....	72
3.2.3	Aggregates.....	74
3.2.4	Reinforcement Fibres.....	75
3.2.5	Superplasticisers (SP).....	82
3.2.6	Water (W).....	83
3.3	Particle Size Distribution (PSD) Analysis.....	84
3.3.1	Sieve Analysis.....	84
3.3.2	Laser Diffraction Analyser.....	87
3.4	Scanning Electron Microscopy (SEM).....	89

3.5	Helium Pycnometry.....	90
3.5.1	Sample Preparation and Analysis.....	91
3.5.2	Porosity Measurement.....	92
3.6	Workability.....	93
3.6.1	Slump Test.....	94
3.7	Single Fibre Tensile Test.....	97
3.8	Mechanical Testing.....	99
3.8.1	Analysis of Four-Point Flexural Test Result.....	100
4	Manufacturing Process.....	104
4.1	Introduction.....	104
4.2	Dispersing Methods of Recycled Milled Carbon Fibres.....	105
4.3	Mixing of Materials Process.....	106
4.4	Hand Lay-up.....	106
4.4.1	Moulds for Hand Lay-up.....	107
4.4.2	Processing Green Forms by Hand Lay-up.....	107
4.5	Compression Moulding.....	110
4.5.1	Single Sample Trapezoidal Mould.....	110
4.5.2	Final Design of Single Sample Trapezoidal Mould.....	111
4.5.3	Six Sample Trapezoidal Mould.....	112
4.5.4	Single Rectangle Slab Mould.....	114
4.5.5	Processing Green Forms by Compression Moulding.....	116
4.6	Curing Process.....	120
5	Mix Design Optimisation.....	122
5.1	Introduction.....	122
5.2	Optimisation Step 1: The Influence of Curing Regime.....	124
5.3	Optimisation Step 2: The Influence of Loading Rate.....	125
5.4	Optimisation Step 3: The Influence of Additives (SF, PFA, and GGBS).....	127
5.5	Optimisation Step 4: The Influence of Aggregate Type and Composition.....	132
5.6	Optimisation Step 5: Influence of Fine Aggregate Content.....	135
5.7	Optimisation Step 6: Influence of Water/Binder (w/b) Ratio.....	137
5.7.1	Short Fibres.....	137
5.7.2	Continuous Fibres.....	140
5.8	Optimisation Step 7-Influence of Pressing on w/b.....	142

5.9	Summary.....	143
6	Test Results of Cementitious Materials Reinforced With Short Fibres.....	146
6.1	Introduction.....	146
6.2	Specimens Labelling Code.....	146
6.3	Test Results and Discussion.....	147
6.3.1	Control Materials ($V_f = 0\%$).....	150
6.3.2	Critical Length (l_c) and Combined Efficiency Factor (η)	156
6.3.3	Fibre Volume Fraction, V_f	162
6.3.4	Materials Reinforced With Milled Carbon Fibres (CF1).....	170
6.3.5	Materials Reinforced With Short Carbon Fibres of Types CF2 and CF3	177
6.3.6	Materials Reinforced With Polypropylene Fibre (PP).....	184
6.3.7	Materials Reinforced With Polyvinyl Alcohol Fibre (PVA).....	188
6.3.8	Summary of Mechanical Test Results with Short Fibres.....	192
6.4	Porosity Measurement.....	197
6.5	Statistical Analysis.....	200
6.6	Findings from Mechanical Testing of Materials with Short Fibres.....	202
7	Test Results of Cementitious Materials Reinforced With Continuous Fibres	204
7.1	Introduction.....	204
7.2	Specimens Labelling Code.....	204
7.3	Test Results and Discussion.....	205
7.3.1	Curing Regimes.....	208
7.3.2	Combined Efficiency Factor (η).....	209
7.3.3	Fibre Volume Fraction (V_f).....	210
7.3.4	Control Materials ($V_f = 0\%$).....	215
7.3.5	Materials Reinforced With Unidirectional Fabrics CF4, CF5 and CF6	218
7.3.6	Materials Reinforced With Biaxial Fabrics CF7, CF8 and GF.....	226
7.3.7	Materials Reinforced With Multi-axial Fabric CF9	236
7.4	Summary of Mechanical Test Results With Continuous Fibres.....	240
7.4.1	Mechanical Properties.....	240
7.4.2	Effect of Manufacturing Process on Mechanical Properties	243

7.4.3	Effect of Fabric Type.....	246
7.5	Improving Effectiveness of Unidirectional Reinforcement CF4 and CF5.....	247
7.6	Influence of Hybrid Fibre on Mechanical Properties.....	260
7.7	Porosity Measurement.....	266
7.8	Statistical Analysis	269
7.9	Findings From Mechanical Testing of Materials With Continuous Fibres.....	270
8	Conclusions and Further works.....	273
8.1	Conclusions.....	273
8.2	Further Works.....	278
9	Bibliography.....	280
	Appendices.....	313
	Appendix A.....	314
	Appendix B.....	320
	Appendix C.....	346
	Appendix D.....	353
	Appendix E.....	356

List of Figures

<i>Figure 2.1: Stress-strain curve for: a) FRP and b) FRC composites (Namaan, 2008)....</i>	<i>9</i>
<i>Figure 2.2: Classification of FRC composites based on their tensile stress-strain curve: (a) conventional strain-softening or FRC, (b) strain-hardening FRC or HPFRC (Naaman, 2008).....</i>	<i>10</i>
<i>Figure 2.3: Idealised tensile stress-strain curves for FRC (Purnell, 2010).....</i>	<i>35</i>
<i>Figure 2.4: Schematic description of the idealised stress-strain curves for FRC materials based on the ACK model (Purnell, 2010).....</i>	<i>44</i>
<i>Figure 2.5: Multiple cracking according to the ACK model: (a) crack spacing and bridging fibres; and (b) strain distribution in FR.....</i>	<i>46</i>
<i>Figure 2.6: Stress profile along a short fibre as a function of fibre length, when; a) $l < l_c$, b) $l = l_c$ and c) $l > l_c$.....</i>	<i>51</i>
<i>Figure 2.7: Forces on a fibre being pulled from a block of matrix.....</i>	<i>51</i>
<i>Figure 2.8: Principle of combined fibre pull-out and fibre fracture in a bundle FRC material (Wiberg, 2003).....</i>	<i>55</i>
<i>Figure 2.9: Fibre orientation, (a) in 2D and (b) in 3D (Lofgren, 2005).....</i>	<i>60</i>
<i>Figure 2.10: Typical estimated efficiency factors; length and orientation (η_l and η_θ), for a simple continuous fibre with different ply orientation (Harris, 1999).....</i>	<i>61</i>
<i>Figure 2.11: Combined Efficiency factor (η) for different fibre layouts (Purnell, 2010).....</i>	<i>63</i>
<i>Figure 2.12: Fracture process zone (FPZ) in FRC (Wecharatana and Shah 1983; Purnell 1998).....</i>	<i>66</i>
<i>Figure 3.1: Five types of short fibres: a) recycled milled carbon fibre (CF1); b) recycled chopped carbon fibre (CF2); c) chopped carbon fibre (CF3); d) chopped polypropylene fibre (PP); e) chopped polyvinyl alcohol fibre (PVA).....</i>	<i>77</i>
<i>Figure 3.2: Layer orientations for the fabrics: a) unidirectional fabric, b) biaxial fabric and c) multi-axial fabric.....</i>	<i>78</i>
<i>Figure 3.3: Seven types of continuous fibres: a) CF4, b) CF5, c) CF6, d) CF7, e) CF8, f) CF9 and g) GF.....</i>	<i>79</i>
<i>Figure 3.4: Toray's tensile strength and modulus grades of carbon fibres (Kamiura, 2010).....</i>	<i>81</i>
<i>Figure 3.5: PSD analysis of aggregates using sieve analysis.....</i>	<i>86</i>

<i>Figure 3.6: Particle size distribution analysis for types of binders and additives using laser diffraction technique</i>	88
<i>Figure 3.7: Schematic diagram illustrating the cones used during the slump test a) in-house ceramic cone and b) British Standard cone</i>	95
<i>Figure 3.8: Relationship between slump and water/binder (w/b) ratio</i>	96
<i>Figure 3.9: Relationship between slump and V_f of CF1 in presence of 3% of SP_B</i>	97
<i>Figure 3.10: The schematic diagram illustrating the testing arrangements and position of the extensometer during the mechanical testing for the trapezoidal cross section specimen</i>	100
<i>Figure 3.11: Cross-section of the trapezoidal specimen</i>	102
<i>Figure 4.1: Recycled milled carbon fibre. a) before grinding, b) after grinding</i>	105
<i>Figure 4.2: Steps in fabrication of FRC green forms by hand lay-up process, (a) laying a thin layer of mortar (b) laying a sheet of fabric (c) rolling to get better bind (d) covering with polythene sheet (e) placing 20 kg dead load</i>	109
<i>Figure 4.3: A typical green specimen using the single trapezoid mould of Figure 4.9</i> ...	112
<i>Figure 4.4: Four parts for six trapezoidal mould for DASSET machine</i>	113
<i>Figure 4.5: Mild steel components for the rectangular slab mould</i>	115
<i>Figure 4.6: Steps in the fabrication of the FRC green forms by the compression moulding process: (a) laying a filter paper into the base of the mould; (b) laying a thin layer of mortar; (c) laying a sheet of fabric; (d) covering with an upper layer of filter paper when the required slab thickness has been reached; (e) placing the mould in the centre of the Denison 7231 compression machine; (f) demoulding the FRC specimen after pressing.</i>	119
<i>Figure 4.7: Flexural strength of CF1 specimens exposed to different pressing regimes in compression moulding process</i>	120
<i>Figure 5.1: Mean flexural strength vs. different curing regimes</i>	125
<i>Figure 5.2: Mean flexural strength vs. SF content for evaluation optimum SF content.</i>	128
<i>Figure 5.3: Mean flexural strength vs. PFA content for evaluation optimum PFA content</i>	130
<i>Figure 5.4: Mean flexural strength vs. GGBS content for evaluation optimum GGBS content</i>	131
<i>Figure 5.5: Mean flexural strength vs. mix design 1C:1A and 1C:2A with different aggregate compositions at 7 days</i>	134

<i>Figure 5.6: Mean flexural strength vs. mix design 1C:1A and 1C:2A with different aggregate compositions at 28 days</i>	135
<i>Figure 5.7: Mean flexural strength vs. mix design. Aggregate (A=100%S) = 0.5, 1, 2, and 4</i>	136
<i>Figure 5.8: Manufacture specimen: (a) with a bad surface finish; (b) with good surface finish and without cracks</i>	139
<i>Figure 5.9: Flexural strength vs. w/b ratio for short fibres reinforced material</i>	140
<i>Figure 5.10: Mean flexural strength vs. w/b ratio for continuous fibres reinforced material</i>	142
<i>Figure 5.11: Water/binder ratio before and after pressing for six batches</i>	143
<i>Figure 6.1: Lower and upper bound stress-strain curves for control specimens produced with compression moulding</i>	154
<i>Figure 6.2: Lower and upper bound stress-strain curves for control specimens produced with hand lay-up</i>	154
<i>Figure 6.3: Fracture of control specimen after four-point bending test</i>	155
<i>Figure 6.4: Relationship between mean flexural strength and fibre volume fraction for the CF1 cementitious material</i>	165
<i>Figure 6.5: Cross-section of a material reinforced with CF1 fibre at $V_f = 2\%$ showing poor dispersion and clumping on the fibres into balls</i>	165
<i>Figure 6.6: Matrix reinforced with CF2 fibres with a V_f: a) 7%, b) 9%</i>	166
<i>Figure 6.7: Relationship between mean flexural strength and fibre volume fraction for the CF2 cementitious material</i>	167
<i>Figure 6.8: Comparison of the lower and upper bound stress-strain curves for CF1 cementitious specimens ($V_f = 2\%$) produced with compression moulding with lower bound curve from the control specimens</i>	173
<i>Figure 6.9: Comparison of the lower and upper bound of stress-strain curves for CF1 cementitious specimens ($V_f = 2\%$) produced with hand lay-up with lower bound curve from the control specimens</i>	173
<i>Figure 6.10: SEM photo for CF1 material made by compression moulding, (a) fibres stick together to form balls, (b) poor dispersion, (c) filaments are not coated with cementitious materials, (d) area of pure mortar with too few fibres</i>	175
<i>Figure 6.11: Brittle fracture of CF1 cementitious specimen after four-point bending test</i>	176

<i>Figure 6.12: Comparison of the lower and upper bound of stress-strain curves for CF2 cementitious specimens ($V_f = 2\%$) produced by compression moulding with lower bound curve from the control specimens.....</i>	<i>179</i>
<i>Figure 6.13: Comparison of the lower and upper bounds of stress-strain curves for CF2 cementitious specimens ($V_f = 2\%$) produced by hand lay-up with lower bound from the control specimens.....</i>	<i>179</i>
<i>Figure 6.14: Comparison of the lower and upper bound of stress-strain curves for CF3 specimens ($V_f = 2\%$) produced by compression moulding with lower bound of control specimen.....</i>	<i>180</i>
<i>Figure 6.15: Comparison of the lower and upper bounds of stress-strain curves for CF3 specimens ($V_f = 2\%$) produced by hand lay-up with lower boundary from the control specimens.....</i>	<i>180</i>
<i>Figure 6.16: CF2 and CF3 materials were made by hand lay-up; a) CF2 dispersed well throughout the matrix; b) CF3 covered with cementitious materials.....</i>	<i>183</i>
<i>Figure 6.17: CF2 filaments are coated with cementitious materials.....</i>	<i>184</i>
<i>Figure 6.18: Comparison of the lower and upper bound of stress-strain curves for PP specimens ($V_f = 2\%$) produced by hand lay-up with lower bound curve from the control specimens.....</i>	<i>186</i>
<i>Figure 6.19: Comparison of the lower and upper bound of stress-strain curves for PP specimens ($V_f = 2\%$) produced by compression moulding with lower bound curve from the control specimens.....</i>	<i>186</i>
<i>Figure 6.20: PP material was made by compression moulding and is clean, smooth and not coated with cementitious materials.....</i>	<i>188</i>
<i>Figure 6.21: Comparison of the lower and upper bounds of stress-strain curves for PVA specimens ($V_f = 2\%$) produced by hand lay-up with lower bound from the control specimens.....</i>	<i>190</i>
<i>Figure 6.22: Comparison of the lower and upper bounds of stress-strain curves for PVA specimens ($V_f = 2\%$) produced by compression moulding with lower bound from the control specimens.....</i>	<i>190</i>
<i>Figure 6.23: PVA material was made by compression moulding: a) PVA has rough surface and; b) PVA coated with cementitious materials.....</i>	<i>192</i>
<i>Figure 6.24: Mean LOP stress from flexural testing for control and short fibres materials.....</i>	<i>193</i>

<i>Figure 6.25: Mean peak stress from flexural testing for control and short fibres materials</i>	194
<i>Figure 6.26: Mean strain at peak stress for control and short fibres materials</i>	195
<i>Figure 6.27: Mean toughness at peak stress for control and short fibres materials</i>	195
<i>Figure 6.28: Excess water attained by using compression moulding process for control and short fibres materials</i>	197
<i>Figure 6.29: Percentage of porosity for control and five short fibre materials at $V_f = 2\%$ made by hand lay-up and compression moulding</i>	199
<i>Figure 6.30: The mean peak strength versus mean porosity for five FRC materials with CF1, CF2, CF3, PP and PVA fibres made by hand lay-up and compression moulding.</i>	199
<i>Figure 6.31: The mean peak strength versus mean water loss for five FRC materials with CF1, CF2, CF3, PP and PVA fibres made by compression moulding</i>	200
<i>Figure 7.1: Mean peak flexural Strength with two curing regimes; cured in hot water at 50°C and Relative Humidity condition of 100% for CF5 materials in sheet form that were produced by hand lay-up and compression moulding processes</i>	209
<i>Figure 7.2: Relationship between mean flexural strength and fibre volume fraction for the CF4 cementitious material that produced by hand lay-up and compression moulding processes</i>	212
<i>Figure 7.3: CF4 specimen having V_f equal to 13% has poor surface finish and delamination cracks throughout its thickness</i>	213
<i>Figure 7.4: Lower and upper bound stress-strain curves for control specimens produced with compression moulding</i>	217
<i>Figure 7.5: Lower and upper bound stress-strain curves for control specimens produced with hand lay-up</i>	217
<i>Figure 7.6: Comparison of the lower and upper bound stress-strain curves for CF4 cementitious specimens ($V_f = 5\%$) produced with compression moulding with lower bound curve from the control specimens</i>	220
<i>Figure 7.7: Comparison of the lower and upper bound stress-strain curves for CF4 cementitious specimens ($V_f = 5\%$) produced with hand lay-up with lower bound curve from the control specimens</i>	220
<i>Figure 7.8: Comparison of the lower and upper bound stress-strain curves for CF5 cementitious specimens ($V_f = 5\%$) produced with compression moulding with lower bound curve from the control specimens</i>	221

<i>Figure 7.9: Comparison of the lower and upper bound stress-strain curves for CF5 cementitious specimens ($V_f = 5\%$) produced with hand lay-up with lower bound curve from the control specimens.....</i>	<i>221</i>
<i>Figure 7.10: Comparison of the lower and upper bound stress-strain curves for CF6 cementitious specimens ($V_f = 5\%$) produced with compression moulding with lower bound curve from the control specimens.....</i>	<i>222</i>
<i>Figure 7.11: Comparison of the lower and upper bound stress-strain curves for CF6 cementitious specimens ($V_f = 5\%$) produced with hand lay-up with lower bound curve from the control specimens.....</i>	<i>222</i>
<i>Figure 7.12: Fracture of CF4 specimen after four-point bending test.....</i>	<i>224</i>
<i>Figure 7.13: Cementitious material penetrate CF4 fabric between the openings of the bundles by compressive pressure in compression moulding process.....</i>	<i>225</i>
<i>Figure 7.14: SEM image showing poor matrix penetration in CF5 (sheets form).....</i>	<i>225</i>
<i>Figure 7.15: SEM image showing voiding and poor matrix penetration in CF6 fabric..</i>	<i>226</i>
<i>Figure 7.16: Comparison of the lower and upper bound stress-strain curves for CF7 cementitious specimens ($V_f = 5\%$) produced with compression moulding with lower bound curve from the control specimens.....</i>	<i>230</i>
<i>Figure 7.17: Comparison of the lower and upper bound stress-strain curves for CF7 cementitious specimens ($V_f = 5\%$) produced with hand lay-up with lower bound curve from the control specimens.....</i>	<i>230</i>
<i>Figure 7.18: Comparison of the lower and upper bound stress-strain curves for CF8 cementitious specimens ($V_f = 5\%$) produced with compression moulding with lower bound curve from the control specimens.....</i>	<i>231</i>
<i>Figure 7.19: Comparison of the lower and upper bound stress-strain curves for CF8 cementitious specimens ($V_f = 5\%$) produced with hand lay-up with lower bound curve from the control specimens.....</i>	<i>231</i>
<i>Figures 7.20: Comparison of the lower and upper bound stress-strain curves for GF cementitious specimens ($V_f = 5\%$) produced with compression moulding with lower bound curve from the control specimens.....</i>	<i>232</i>
<i>Figures 7.21: Comparison of the lower and upper bound stress-strain curves for GF cementitious specimens ($V_f = 5\%$) produced with hand lay-up with lower bound curve from the control specimens.....</i>	<i>232</i>

<i>Figures 7.22: SEM Photo for CF7 material was made by compression moulding; (a) good penetration of the matrix into the fibre tow, (b) opening spaces between the two filaments neighbours are filled with cementitious materials, (c) evidence of fracture fibre failures</i>	233
<i>Figures 7.23: SEM Photo for CF8 material was made by compression moulding; (a) interface between fibres and matrix is intimate, (b) poor penetration of the matrix into the fibre tow, (c) evidence of voiding and few filaments are covered with binder materials.</i>	234
<i>Figure 7.24: Cementitious material cannot penetrate the GF filaments due to sizing</i>	235
<i>Figure 7.25: Comparison of the lower and upper bound stress-strain curves for CF9 cementitious specimens ($V_f = 5\%$) produced with compression moulding with lower bound curve from the control specimens</i>	239
<i>Figure 7.26: Comparison of the lower and upper bound stress-strain curves for CF9 cementitious specimens ($V_f = 5\%$) produced with hand lay-up with lower bound curve from the control specimens</i>	239
<i>Figure 7.27: CF9 material was made by compression moulding; (a) spaces in all direction between the carbon tows. (b) cement matrix is seen to penetrate between the individual CF9 fibres</i>	240
<i>Figure 7.28: Mean peak flexural strengths for control and continuous fibres materials</i>	241
<i>Figure 7.29: Mean strain at peak stress for control and continuous fibres materials</i>	242
<i>Figure 7.30: Mean toughness at peak stress for control and continuous fibres material</i>	243
<i>Figure 7.31: Excess water attained by using compression moulding process for control and seven continuous fibres materials</i>	245
<i>Figure 7.32: CF4 cut into strips to increase the penetration of the cement in between the tows and to improve the bond and enhance the mechanical performance</i>	249
<i>Figure 7.33: Photo shows CF4 (a) before and (b) after surface treatment</i>	249
<i>Figure 7.34: Stress-strain curves for CF4 cementitious specimens ($V_f = 5\%$) in strip form produced with compression moulding</i>	252
<i>Figure 7.35: Stress-strain curves for CF4 cementitious specimens ($V_f = 5\%$) in strip form produced with hand lay-up</i>	252
<i>Figure 7.36: Stress-strain curves for CF5 cementitious specimens ($V_f = 5\%$) in strip form produced with compression moulding</i>	253

<i>Figure 7.37: Stress-strain curves for CF5 cementitious specimens ($V_f = 5\%$) in strip form produced with hand lay-up.....</i>	<i>253</i>
<i>Figure 7.38: Stress-strain curves for Ethanol treated CF4 cementitious specimens ($V_f = 5\%$) produced with compression moulding.....</i>	<i>254</i>
<i>Figure 7.39: Stress-strain curves for Ethanol treated CF4 cementitious specimens ($V_f = 5\%$) produced with hand lay-up.....</i>	<i>254</i>
<i>Figure 7.40: Stress-strain curves for Ethanol treated CF5 cementitious specimens ($V_f = 5\%$) produced with compression moulding.....</i>	<i>255</i>
<i>Figure 7.41: Stress-strain curves for Ethanol treated CF5 cementitious specimens ($V_f = 5\%$) produced with hand lay-up.....</i>	<i>255</i>
<i>Figure 7.42: Photo shows surface treated CF4 fabric; (a) the matrix exists between fibres (b) and CF4 filament fully coated.....</i>	<i>256</i>
<i>Figure 7.43: Mean peak flexural strengths for CF4 and CF5 in three forms (sheets, strips, and treated) and control materials.....</i>	<i>258</i>
<i>Figure 7.44: Mean strain at peak stress for CF4 and CF5 in three forms (sheets, strips, and treated) and control materials.....</i>	<i>258</i>
<i>Figure 7.45: Mean toughness at peak stress for CF4 and CF5 in three forms (sheets, strips, and treated) and control materials.....</i>	<i>259</i>
<i>Figure 7.46: Stress-strain curves for hybrid (1%CF3+1%PVA+3%CF8) specimens ($V_f=5\%$) produced with compression moulding.....</i>	<i>262</i>
<i>Figure 7.47: Stress-strain curves for hybrid (1%CF3+1%PVA+3%CF8) specimens ($V_f = 5\%$) produced with hand lay-up.....</i>	<i>262</i>
<i>Figure 7.48: Mean peak flexural strength for materials reinforced with; CF3, PVA, CF8, hybrid (1%CF3+1%PVA+3%CF8) fibres and control materials.....</i>	<i>264</i>
<i>Figure 7.49: Mean strain at peak stress for materials reinforced with; CF3, PVA, CF8, hybrid (1%CF3+1%PVA+3%CF8) fibres and control materials.....</i>	<i>265</i>
<i>Figure 7.50: Mean toughness at peak stress for materials reinforced with; CF3, PVA, CF8, hybrid (1%CF3+1%PVA+3%CF8) fibres and control materials.....</i>	<i>265</i>
<i>Figure 7.51: Percentage of porosity for control and continuous materials made by hand lay-up and compression moulding.....</i>	<i>268</i>
<i>Figure 7.52: The mean peak strength versus mean porosity for seven FRC materials with CF4, CF5, CF6, CF7, CF8, CF9 and GF fabrics made by compression moulding.....</i>	<i>268</i>

List of Tables

<i>Table 2.1: Mechanical properties of the most commercial types of fibre (Bentur and Mindess, 2007)</i>	12
<i>Table 2.2: Typical mechanical Properties of PAN and pitch-based carbon fibres (Bentur and Mindess, 2007)</i>	17
<i>Table 2.3: Summary of interfacial bond strength (τ) for CF, GF, PP and PVA fibres</i>	56
<i>Table 2.4: Orientation efficiency coefficient (η_0) for short fibres (Brandt, 2009)</i>	62
<i>Table 2.5: Examples for how to calculate the effective fibre volume fraction (V_f')</i>	64
<i>Table 3.1: Physical properties for additives SF, PFA, and GGBS</i>	73
<i>Table 3.2: Manufacturer's data for short fibres</i>	76
<i>Table 3.3: Manufacturer's data for continuous fibres</i>	80
<i>Table 3.4: Grading limits for fine aggregate (from BS 882-1992)</i>	85
<i>Table 3.5 Sieve analysis result of GA, CL and S as BS 882-1992</i>	87
<i>Table 3.6: Range of particle size of C, SF, PFA, and GGBS by Laser Diffraction analyser</i>	89
<i>Table 3.7: Measured and manufacturer's data of single fibre tensile strength for seven continuous fibres (CF4, CF5, CF6, CF7, CF8, CF9 and GF)</i>	99
<i>Table 5.1: The mean flexural strengths and loading rate for the six groups</i>	126
<i>Table 5.2: Optimum percentage of additives; SF, PFA and GGBS by weight of cement obtained by a number of independent researchers</i>	132
<i>Table 5.3: Different aggregate type and composition scenarios for the two mix design of 1C:1A:0.4w/b and 1C:2A:0.4w/b</i>	133
<i>Table 5.4: Different water/binder ratio scenarios from pressing process for short fibres reinforced material</i>	140
<i>Table 5.5: Different water/binder ratio scenarios from pressing process for continuous fibres reinforced material</i>	141
<i>Table 5.6: Material proportions and moulds used for the hand lay-up process</i>	144
<i>Table 5.7: Material proportions and moulds used for compression moulding process</i> ...	145
<i>Table 6.1: Results from four-point bending test, water reduction, coefficient of variation, and standard deviation of six control specimens manufactured via compression moulding</i>	152

<i>Table 6.2: Results from four-point bending test, coefficient of variation, and standard deviation of six control specimens manufactured via hand lay-up.....</i>	<i>152</i>
<i>Table 6.3: Values of aspect ratio, critical length (l) and $2l_c$ for short fibres, CF1, CF2, CF3, PP and PVA.....</i>	<i>159</i>
<i>Table 6.4: Values of combined efficiency factor (fibre length and orientation) for short fibres, CF1, CF2, CF3, PP and PVA.....</i>	<i>160</i>
<i>Table 6.5: Values of η' for short fibres, CF1, CF2, CF3, PP and PVA.....</i>	<i>162</i>
<i>Table 6.6: Values of V_{fcrit} for, CF1, CF2, CF3, PP and PVA fibres.....</i>	<i>169</i>
<i>Table 6.7: Values of V_f' for, CF1, CF2, CF3, PP and PVA fibres.....</i>	<i>170</i>
<i>Table 6.8: Values of P-value for, CF1, CF2, CF3, PVA, PP fibres and control specimen.....</i>	<i>202</i>
<i>Table 7.1: Values of combined efficiency factor (fibre length and orientation) for seven fabrics, CF4, CF5, CF6, CF7, CF8, CF9 and GF.....</i>	<i>210</i>
<i>Table 7.2: Values of V_{fcrit} for CF4, CF5, CF6, CF7, CF8, CF9 and GF fabrics.....</i>	<i>214</i>
<i>Table 7.3: Values of V_f' for CF4, CF5, CF6, CF7, CF8, CF9 and GF fabrics.....</i>	<i>215</i>
<i>Table 7.4: Values of P-value for, CF4, CF5, CF6, CF7, CF8, CF9 and GF fabrics and control specimens.....</i>	<i>270</i>

List of Abbreviations

- A – Aggregates
ACK – Aveston, Cooper and Kelly
ANOVA – Analysis of variance
BS – British Standard
C – Cement
CF – Carbon Fibre
CF1 – Recycled Milled Carbon Fibre
CF2 – Recycled Chopped Carbon Fibre
CF3 – Chopped Carbon Fibre
CF4 – Unidirectional Carbon Fabric at 200 g/m²
CF5 – Unidirectional Carbon Fabric at 300 g/m²
CF6 – Unidirectional Carbon Fabric at 450 g/m²
CF7 – Biaxial Hybrid Fabric with 40% of Carbon Fibres and 60% of Glass Fibre
CF8 – Biaxial Carbon Fabric
CF9 – Multiaxial Carbon Fabric
CFRC – Carbon Fibre Reinforced Concrete
CL – Crushed Limestone
CM – Compression Moulding
C-S-H – Calcium Silicate Hydrate
CS – Control Materials without Short Fibre
CS1 – Control Materials without Continuous Fibre
E – Modulus of elasticity
E_c – Modulus of elasticity for the composite
EN – European Standard
FRC – Fibre Reinforced Cementitious Materials
FRP – Fibre Reinforced Polymer
G – Gram
GA – Crushed Granite
GF – Biaxial E-glass Fabric

GGBS – Ground Granulated Blast Furnace Slag
GHG – Greenhouse Gas
HEC – Hydroxyl Ethyl Cellulose
HP – Helium Pycnometry
HU – Hand Lay-up
HNO₃ – Nitric acid
K – Number of filaments in a bundle
l – Fibre Length
l_c – Critical Fibre Length
l/d – Aspect Ratio
LVDT – Extensometer
OPC – Ordinary Portland Cement
PAN – Polyacrylonitrile-Based Carbon Fibres
PFA – Pulverised Fuel Ash
PP – Chopped Polypropylene Fibre
PSD – Particle Size Distribution
PVA – Chopped Polyvinyl Alcohol fibre
RH – Relative Humidity
S – Sand
SD – Standard Deviation
SEM – Scanning Electron Microscopy
SF – Silica Fume
SP – Superplasticiser
SP_A – Superplasticiser type Tegla Extra
SP_B – Superplasticiser type Glenium 51
SP_C – Superplasticiser type Glenium 271
SP_D – Superplasticiser type Glenium ACE 333
TRC – Textile Reinforced Concrete
V_f – Fibre Volume Fraction
V_{fcrit} – Critical Fibre Volume Fraction
W – Water
w/b – The ratio of mixing water to the binder in a mix.
w/c – The ratio of mixing water to the cement in a mix

η – Fibre Efficiency Factor

τ – Interfacial Bond Strength

Acknowledgements

First of all, I would like to thank Allah, the almighty, for giving me the strength to carry on this project and for blessing me with many great people who have been my greatest support in both my personal and professional life.

I would like to thank my supervisors, Professor Toby Mottram and Professor Phil Purnell for their continual guidance, encouragement and valuable advice over the entire course of my PhD.

I wish to express my gratitude to the Ministry of High Education in Libya for their financial support for this study. Thanks are also extended to all staff members of the School of Engineering and the Civil Engineering Group, in particular, the technical staff of the Engineering Workshop for their help with manufacturing all my tools throughout this project. Special gratitude is expressed to Mr Colin Banks, Mr Ryan Griffith, and Mr Martin Davis for their advice and their supports in the laboratory, Dr. Mark Pharaoh, Dr. Ian Brzeski and Mr Neil Reynolds at Warwick manufacturing group, for their help and providing me the access to their thermoset Compression moulding machine. Thanks also to Mr Steve Yourk, for his assistance in the Scanning Electron Microscopy (SEM) and Mr Dave Hammond, for helping me with helium Picnometry.

I would also like to thank Formax UK Ltd, for supplying the biaxial and multiaxial carbon fabric, PG Lawton (Industrial Services) Ltd., for supplying the filter sheets, Hanson Heidelberg Cement Group, for supplying the GGBS, SGL Carbon Fibres Ltd., for supplying the short carbon fibre, Fothergill Engineered Fabrics Ltd., for supplying the E-glass fabric, and BASF UK Ltd. and Christeyns Oscrete for supplying the superplasticisers.

Last but not least, deep gratitude is expressed to a remarkable wife for her unlimited patience and encouragement. I am deeply indebted to her continuous support and extraordinary efforts to take the full responsibility of all shopping and home duties including supporting our three kids, Hani, Mohammed and Sohail. I would also like to thank my son Hani for his help. My sincere gratitude also goes to my great parents, brothers in particular, Ashraf for his support and sisters who always wished me every success.

This thesis is dedicated to the memory of my grandfather, Omer Khalifa, and to my Parents, wife and sons; Hani, Mohammed and Sohail.

Declaration

I hereby declare that the work presented in this thesis is my own work and effort and that where other sources of information have been used, they have been appropriately acknowledged. The research reported here has not been submitted, either wholly or in part, in this or any other academic institution for admission to higher degree. This copy has been supplied on the understanding that it is copyright material and that no quotation from the thesis may be published without proper acknowledge.

Abdalla Khalifa

Abstract

Presented in this thesis are the test results of combined processing and mechanical property characterisation studies using a developed cementitious mix reinforced by various fibre types and forms (with short and continuous lengths). The research is aimed to identify new Fibre Reinforced Cementitious (FRC) composites that have post-cracking ductility, much higher flexural strength and higher toughness than the control (matrix) material without reinforcement, and higher than traditional FRC composites. Laboratory work uses two methods to process the green forms, one by novel compression moulding and the other by hand lay-up that were both adapted from the fibre reinforced polymer industry. Results show a reduction in the hand lay-up water/binder ratio of 24 to 41% can be achieved by applying compression moulding with a pressure of 9MPa.

One key processing challenge with short recycled milled carbon fibres is to make the mix uniform, even when the volume fraction is low at 2%. Microstructural investigations confirm that the carbon fibres, having mean length of 0.085 mm, always gave a very poor dispersion, and this is due to static electricity causing the fibres to form into balls (5 to 30 mm diameter). Overall, the study with short fibre reinforcements found that, by adding 2% by volume of the polyvinyl alcohol (PVA) fibres, the stress-strain curve exhibits strain-hardening behaviour accompanied by multiple cracking. Furthermore, the flexural properties show the material to possess ductility, toughness and mean strength that, at 13 MPa, is two times higher than the control material. It is observed that the hydrophilic nature of PVA and the fibres surface roughness play a significant role in an increased bonding strength with this short fibre.

When introducing continuous fibre reinforcement in the form of fabrics it is shown that the volume fraction of fibres should be no more than 5%. Unsuccessful green form specimens

were a consequence of having a higher volume fraction by introducing more fabric layers. Test results show that materials reinforced with carbon fabrics give an FRC material with much improved mechanical properties, in terms of post-cracking strength, strain at peak stress and toughness (energy absorption) at peak stress. Higher overall bond strength might be attributed to an apparent increase in interfacial contact area between fibres and cement matrix and improved mechanical anchoring from the fabric's construction. Microstructural investigations confirm that good matrix penetrability between the filaments of the tow or bundle is essential in order to maximise the reinforcing efficiency of the fabric.

Investigated are two novel methods for modifying the continuous unidirectional carbon fibre reinforcements to improve the overall bond strength, by enhancing matrix penetration through and across the reinforcement plane. In one method the fabric is cut into strips to leave spaces (holes) between parallel reinforcement units for the matrix material to bridge across, while in the second method the fabric receives a surface treatment by immersion in Ethanol alcohol. Test results show that, with compression moulding and the strip form of reinforcement at 5% volume fraction the FRC composite has a flexural strength of 75 MPa. This flexural strength is ten times higher than the measured strength of the control material.

The experimental research reported in this thesis shows that to achieve 'unusual' composite action and a relative high stress at loss of proportionality requires a continuous fibre reinforcement that can be treated or non-treated. Given the considerable increase in mechanical properties achieved using such fibre reinforcement at 5% the most promising FRC materials require to be further evaluated to find suitable candidates for load bearing products.

Terminology

Technical terms used the thesis are introduced here:

Additives: Materials in the binder such as Pulverised Fuel Ash (PFA), Silica Fume (SF), or Ground Granulated Blast Furnace Slag (GGBS).

ANOVA: Refers to analysis of variance and is a statistical method used in order to analysis the differences between data sets and determines whether any of those data sets are significantly different from each other.

Aspect ratio: The ratio of length-to-diameter of the fibre.

Binder: It is an ingredient used to bind together two or more other materials in the cement mixture. Its two principal mechanical properties are for adhesion and for cohesion. In this thesis binders are from a combination of cement (C), silica fume (SF), pulverized fly ash (PFA), and ground granulated blast furnace slag (GGBS).

Bundle (also Tow): General term for a collection of essentially parallel filaments of continuous fibres.

Control Specimen: Specimen of cement matrix without fibre loading used to characterize baseline mechanical properties.

Calcium Silicate Hydrate (C-S-H): It is the gel “glue” that provides strength and holds the hardened cement paste together.

Filament: Single long fibre used to produce a tow or yarn for different types of reinforcement fabric.

Green Form: Refers to cementitious material that has set but not yet hardened, and is able to carry its own self-weight without fracturing.

Hydrophilic: Material having an affinity for water; readily absorbing or dissolving in water.

Hydrophobic: Material that repels water, tending not to combine with, or incapable of dissolving in water.

Loss of proportionality (LOP) or ‘Bend over point’ (BOP): On the stress-strain curve it is point for the end of the pre-cracking region and the onset of multiple cracking. It is often characterised by the first stress drop in stress along the stress-strain curve. Up to LOP the both matrix and the fibres are in their linear, elastic range. After LOP the stress-strain curve becomes non-linear (Purnell, 2010). In a number of publications, LOP is referred to as the ‘first crack stress’.

Roving: A number of tows collected into a parallel bundle with little or no twist of reinforcing fibres.

Sizing (Surface treatment): A chemical solution used to coat fibre filaments, facilitating operations such as weaving or braiding. Sizing protects the filament from water absorption and abrasion (to minimize fibre wear) and also can be used to bind together and stiffen warp yarns during weaving. Sizing is usually removed and replaced with a finish before polymer matrix application.

Strain at failure: It is the strain measured at the peak stress.

Toughness (absorption energy): It is the amount of energy per unit that a material can absorb before rupturing. In this thesis toughness is taken to be the area under the stress-strain curve up to the peak stress having units J/m^3 .

T700: It is a carbon fibre product from Japanese producer Toray’s with a high tensile strength reported to be about 5000 MPa.

T300: It is a carbon fibre product from Japanese producer Toray’s with a tensile strength reported to be about 3500 MPa.

Tow: A term used for an untwisted bundle of continuous fibre filaments.

Warp: Fibre bundles in a woven fabric that run parallel (at a 0° angle) to the length of the loom and lengthwise along the longer dimension of the finished fabric.

Weft: The fibre bundles in a woven fabric that run transverse (at a 90° angle) to the warp yarns; also known as fill.

Yarn: It is used mostly for glass fibre, usually meaning a twisted bundle of filaments.

Chapter 1

1. Introduction

1.1 General

Plain (un-reinforced) cementitious materials, such as concrete and mortar, exhibit several desirable characteristics including stiffness, compressive strength, low permeability, low cost, ease of manufacture and are readily available. They are, however, brittle in nature and exhibit undesirable mechanical properties such as low tensile and flexural strengths. This material weakness can be partially overcome by reinforcing with various types of fibres to produce a Fibre Reinforced Cementitious or Fibre Reinforced Cement (FRC) material. Throughout this thesis the abbreviation FRC will be used. Historically, the concept of reinforcing brittle materials with fibres is very old. As early as 2500 B.C. natural fibres were used to strengthen brittle matrices. Straw and horsehair were mixed with clay to form bricks and floors (Brandt, 2008). Though modest improvements in strength can be obtained, the primary purpose of fibre inclusion to cementitious materials is to increase toughness and ductility.

There are various types of fibrous materials for reinforcing cementitious based materials with the most commonly found to include fibre of glass, steel, nylon, polypropylene and carbon. Forms of reinforcement can be either: (i) as discrete short fibres, usually less than 50 mm long, which are processed by manufacturing processes such as spraying and mixing; or (ii) as continuous fibres (usual a fabric) in the form of continuous fibres, that are combined with the matrix by manufacturing processes, such as filament winding or by the hand lay-up (Bentur and Mindess, 2007). Advances in the manufacture of fibres have also been made. This has allowed previously ‘exotic’ fibres,

such as carbon and aramids, are beginning to drift downwards in price sufficiently for researchers to consider using them for FRCs (Purnell, 2010).

The presence of short fibres in the cement matrix can enhance mechanical properties such as tensile and flexural strength, and toughness. This is because fibre characteristics such as high tensile strength, length and aspect ratio enable fibres to bridge cracks. As an example the increase in tensile stress on the lower surface of a sagging beam member leads to hairline vertical cracks developing when the tensile strength of the matrix is reached. When these cracks open-up and propagate, and when the fibres crossing them have adequate bond strength with the matrix, the fibres will not be pulled-out and they will provide a crack-bridging force. This force will retard the crack's progression and supply a resistance to further matrix crack growth. Fabrics of continuous fibres provide additional benefits, such as improved fibre anchorage and further overall bond strength development. The penetration of the cement paste between the openings (holes) in a fabric's construction is a controlling factor towards the improved structural performance of the FRC material. As Mobasher *et al.* (2004) observed the degree of 'wet-out' will depend on the size of the fabric openings and the viscosity of the cement matrix

The performance of FRCs change depending on many variables. Key variables are fibre material properties (e.g., fibre strength, stiffness, and Poisson's ratio), fibre volume content, fibre geometry (smooth, end hooked, crimped, twisted), fibre length, fibre orientation and distribution, matrix properties (e.g., matrix strength, stiffness, Poisson's ratio), interface properties (adhesion, frictional, and mechanical bond) and manufacturing process method (Kim *et al.*, 2008). The critical fibre length (l_c) is an important physical property when the length of short fibre reinforcement is close to l_c . It is necessary for the fibre length to be sufficient ($> l_c$) to ensure fibres can rupture in tension before the bond

(i.e. the shear strength) with the matrix fails (Li and Obla, 1994). The effectiveness of short fibres depends on the degree of fibre dispersion that, ideally, should be a uniform distribution (Chung, 2005). The processing techniques must be compatible with the particular combination of reinforcement form and the matrix material. This depends not only upon the fibre type, but also on the geometry of the reinforcement (Bentur and Mindess, 2007).

FRCs have attracted a great deal of attention due to improvements achieved in their strength and toughness for civil engineering applications, with a wide variety of uses. An FRC material is preferred where thin sections (i.e. of thickness insufficient to provide cover for rebars) are required, such as roofing and cladding products. It is also often preferable where localised deformations are considerable and/or unpredictable, such as tunnel linings, industrial floors, marine structures and blast-resistant structures. Furthermore it is increasingly employed as a substitute for traditional asbestos cement sheet following the widely publicised revelations concerning the health hazards associated with asbestos fibres.

1.2 Aims and Objectives

One main aim of the PhD work is to develop a cementitious mix, and associated processing procedures, that will provide a homogeneous material reinforced with short fibres, devoid of cracks and voiding, and which has mechanical properties suitable for applications in building components (see Chapters 5 and 6). A second main aim of the research will be to use the ‘optimum’ concrete mix design to produce FRCs having layers of continuous fibre fabrics with dramatically improved mechanical properties compared to the control material (i.e. matrix without fibres) (see Chapters 5 and 7).

In this research short fibres (from different sources), having a volume fraction of 2%, are to be dispersed uniformly into a cementitious mix. Their presence is required to improve the mechanical properties in all directions. It is necessary to have a concrete mix that aid fibre dispersion. Previous work introduced in Chapter 2 shows that additives, such as silica fume can be used to improve dispersion. Chapter 3 considers the enhancement to the matrix's properties by partial substitution to cement with binder constituents of pozzolans (e.g. silica fume (SF), pulverised fuel ash (PFA), and ground granulated blast furnace slag (GGBS)).

The objectives of the FRC research are:

- To study variations in composition and processing of FRCs by measuring specific mechanical properties (for flexural strength and toughness) using a four-point bending test method.
- To develop and evaluate mixing and/or processing methods that will allow fibre volume fraction to exceed 2% and that will establish a limit on fibre loading.
- To compare the test results for the same FRCs processed by the two methods of compression moulding and hand lay-up.
- To maximise the flexural strength and toughness of FRCs either reinforced with short or continuous fibres (by way of fabric layers).
- To apply Scanning Electron Microscopy (SEM) to study the micro structure of FRCs and link the observations to the mechanical properties determined from the series of four-point bending testing.

1.3 Structure of the Thesis

This thesis is organised into eight chapters with Chapter 2 and 8 summarised as follows:

Chapter 2 provides a review of existing literature on processing and characterisation of FRC materials. It covers background and theoretical mechanics, key difference between FRC and FRP composites, manufacturing processes, fibre dispersion, pozzolans, textile reinforced concrete, the ACK model, fibre volume fraction, the critical fibre length, interfacial bond strength, fibre efficiency factors and fracture mechanics. It closes with a summary that gives the findings from the review in context with the new contribution presented and discussed in Chapters 3 to 7.

Chapter 3 describes the materials, the experimental programme, the testing procedures, and items of experimental equipment employed in the work.

Chapter 4 discusses the processing methods of compression moulding and hand lay-up that are used to produce green forms of FRCs having appropriate ‘green’ material strength (i.e. sufficient to enable the rectangular specimens to be handled as soon as practical after casting without fracturing).

Chapter 5 discusses the results of experimental work carried out to optimise the cement based mix design and its curing regime. This chapter gives an account of the development programme undertaken to establish suitable mix designs using different combinations of binder (cement, SF, PFA, and GGBS) and several types of aggregates (sand (S), crushed limestone (CL), and granite aggregate (GA)). Once the most promising combination of materials in the mix was identified, detailed examination was carried out to determine the

influence of aggregate type/combination, superplasticisers and curing regimes on the properties of the required cementitious matrix for fibre reinforcement.

Chapter 6 is for the presentation and findings of mechanical properties of FRCs having one of five different types of short fibres.

Chapter 7 reports the findings from the measurement of mechanical properties of FRCs using seven different types of continuous fibres in fabric form.

Chapter 8 presents the conclusions by summarising the research achievements from the findings of the test results presented in Chapters 5 to 7, along with suggestions for further work that will continue to characterise the most promising FRCs for possible applications in building products.

Chapter 2

2. Literature Review

2.1 Introduction

This chapter reviews previous work regarding the use of short and continuous fibres in cementitious materials to form an FRC with enhanced mechanical properties. It will focus on FRCs with the four fibre types of carbon, glass, polypropylene and polyvinyl alcohol having different fibre volume fractions. In the context of mechanical properties the review will consider: the theoretical mechanics of FRC; the nature of the fibre dispersion (how the fibres are oriented and their distribution in the matrix); the use of waste materials (pozzolanic) in the cementitious mix design and the manufacturing process. The discussion in this chapter, while taking into account existing literature and previous findings regarding aspects of FRCs, also justifies the need for the research reported in this thesis.

2.2 Key Difference Between FRC and FRP Composites

Compared to other fibre reinforced composite materials (e.g. fibre reinforced polymers (FRPs)), FRC composites are different. Unlike FRP, the modulus of elasticity of fibres (E_f) in FRCs does not play as important role in establishing E_c because the modulus of elasticity is dependent mainly on cement matrix modulus of elasticity (E_m). Li (2002) says this is feature because of the brittle nature of the cement and the lower fibre volume fraction ($V_f < 10\%$) in FRC compared to $\approx 50\% - 60\%$ in FRPs; in addition to the fibres often being short and randomly oriented.

As shown in Figure 2.1(b) the main common characteristic of FRCs is that the ultimate tensile strain of the matrix is very much lower than that of the fibre ($\epsilon_{mu} < \epsilon_{fu}$). The

opposite is true for FRPs. Under tension action the cement matrix cracks before the full potential of the fibres is achieved (i.e. before fibres reach their tensile strength). For this reason, the fibres in FRCs are present to enhance toughness and control cracking, implying that their contribution becomes effective, mainly, after the matrix has cracked and the fibres create beneficial bridges across the cracks. As shown in Figure 2.1(a) for the FRP the ultimate strain of the polymer matrix (e.g. epoxy) is considerably higher than that of the fibres, this is for $\varepsilon_{mu} \gg \varepsilon_{fu}$. Hence, failure in FRPs is caused either by fibre failure or complete fibre debonding while the matrix is or is not in a plastic behaviour state (Namaan, 2008).

Furthermore, in FRCs, the cement matrix has low tensile strength (σ_{mu}), is highly porous and the bond between fibre and cement is relatively weak (often ≈ 0.5 to 2 MPa). This is attributed to FRCs having fibres (with the exception of steel and natural fibres) introduced as bundles rather than as individual filaments. As discussed in details in Section 2.16 fibres have a considerable freedom of movement relative to others. It is difficult for the cement paste to penetrate into these bundles or completely surround the filaments (but may increasingly do so with time as the hydration process continues). How the bond strength in an FRC changes with time is discussed in more details by Purnell (2007; 2010) and Purnell *et al.* (1999; 2000).

Fibres are introduced into FRCs to increase toughness and/or energy absorption capability. In addition, the lower price of cement matrix compared to epoxy is of course an advantage. To do an economical evaluation is outside the scope of this thesis.

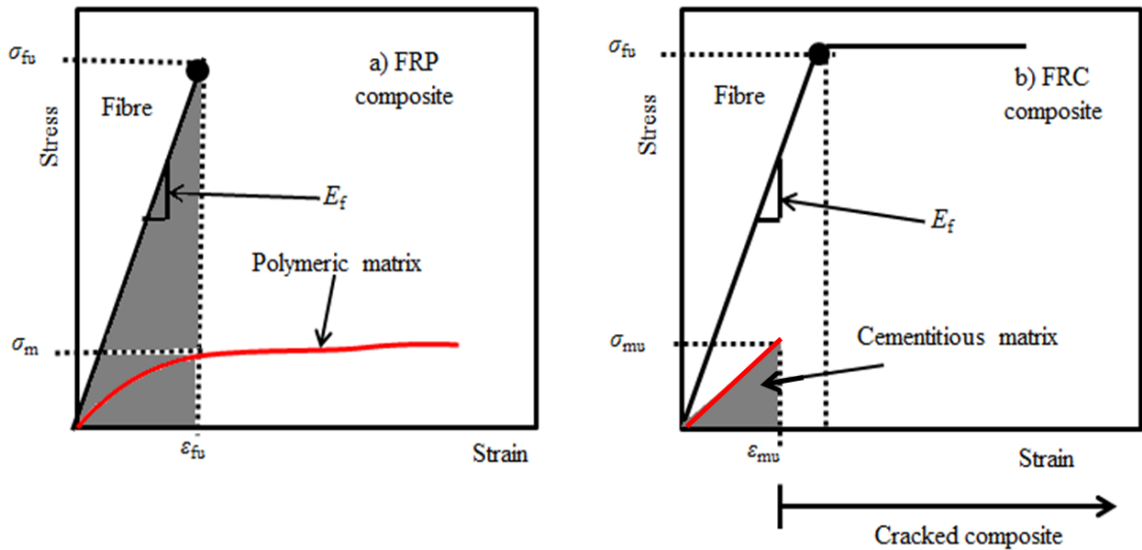


Figure 2.1: Stress-strain curve for: a) FRP and b) FRC composites (Namaan, 2008).

2.3 Classification of FRC Composites

FRCs can be classified according to the shape of tensile stress-strain curve into two categories: conventional FRC or simply FRC, and High Performance FRC, hereafter denoted HPFRC. It can be seen from the stress-strain curves in Figures 2.2(a) and 2.2(b) the FRC exhibits strain-softening behaviour after the linear elastic region I. If localisation (failure) occurs immediately following first cracking it results in no strain-hardening or multiple cracking (FRCs do not have the zone II shown in Figure 2.2(b)). In the case of a HPFRC, the stress-strain in Figure 2.2(b) exhibits strain-hardening behaviour after the initiation of matrix cracking, accompanied by multiple cracking as shown by the presence of a zone II. It can be seen in Figure 2.2(b) that the maximum tensile strain and load carrying capacity of HPFRCs are higher than for FRCs, and that the amount of stored energy (toughness) represented by the area under the curve in is going to be much higher (c.f. with Figure 2.2(a)). After localisation, the descending branch for strain-softening FRC (III) follows a path similar to that when the material is strain-hardening. The post-cracking

stress is labelled σ_{cu} in Figure 2.2, and for strain-hardening $\sigma_{cu} \geq \sigma_{c,A}$, while for strain-softening $\sigma_{cu} < \sigma_{c,A}$.

Strain-hardening in an FRC has been introduced by reinforcing the matrix with continuous (long) fibres. This is attributed to the two reasons of their ‘infinite’ length and for having fibres aligned with the loading direction (i.e. the fibre is fully effective as it is in a unidirectional fabric (0°)), as discussed in Section 2.17. Strain-hardening may be achieved in FRCs containing randomly distributed fibres if: V_f is higher than the critical fibre volume fraction (V_{fcrit}), as discussed in Section 2.14; fibre mean length (l) exceeds the critical fibre length by five times ($l > 5l_c$ (long fibres)), as discussed in Section 2.15; fibres have uniform dispersion throughout the matrix; the interfacial bond strength is sufficient during loading to transfer forces between matrix and fibres, as required to carry additional load during strain-hardening (see Section 2.16).

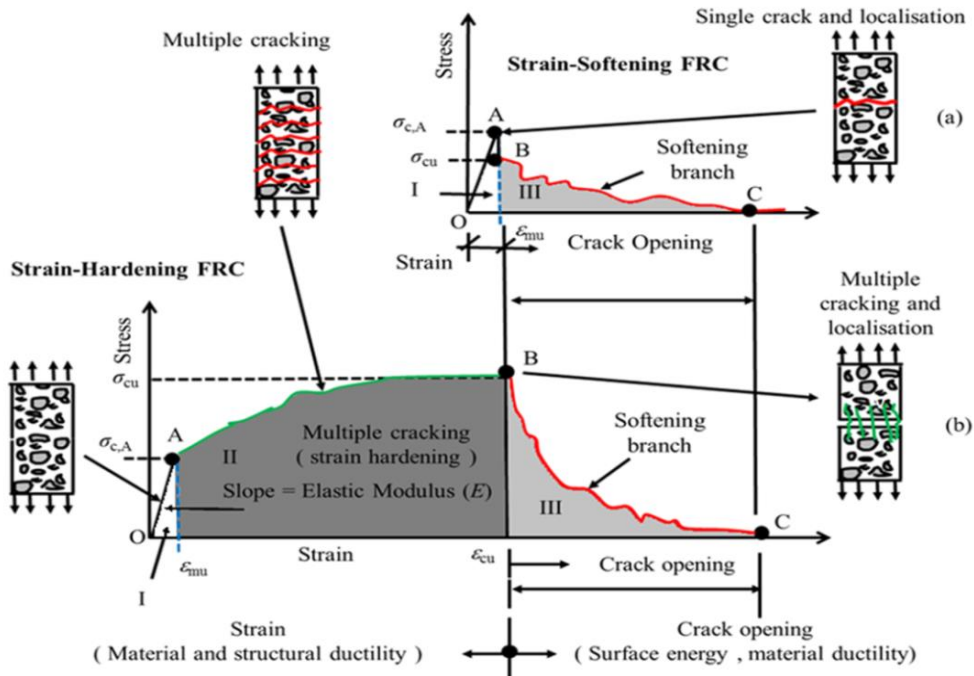


Figure 2.2: Classification of FRC composites based on their tensile stress-strain curve: (a) conventional strain-softening or FRC, (b) strain-hardening FRC or HPFRC (Naaman, 2008).

Classes of FRCs for strain-softening and hardening are fully discussed by Tjiptobroto and Hansen (1991), Shah *et al.* (1999), Stang and Li (2004), Naaman and Reinhardt (2006) and Naaman (2008). This recognised classification is used in this study to analysis the test results presented in Chapters 6 and 7 for FRCs with short and continuous fibres, respectively.

2.4 Fibres in Cementitious Materials

A wide range of fibres possessing different mechanical, physical and chemical properties have been used to reinforce cementitious matrices. As introduced in Section 2.2, the main advantage of introducing fibres into the brittle matrix is usually realised only after the cement paste starts to crack. Fibre bridging then acts to prevent a sudden loss in the load carrying capacity of the cracked material by providing a load transfer mechanism across the crack, resulting in a pseudo-ductile response (Suwannakarn, 2009). Thus fibres are found not only to suppress the formation of ‘brittle’ cracks, but also prevent further propagation and growth of these cracks.

Commercial fibres have different mechanical properties, cost and effectiveness. They also vary largely in their geometry. The steel and glass fibres used in the early work on FRC in the 1950s and 1960s had smooth surfaces and were straight. Over the years more complicated geometries have been employed, mostly to give mechanical interlock to enhance the mechanical bonding with matrix. Thus, modern steel fibres possess different profiled shapes, with hooked or deformed ends. Other fibres for FRCs and HPFRCs can be fibrillated films or bundled filaments, or woven fabrics or mats. As a result of these differences, there are applications where the reinforcement functions better than conventional reinforcing rebars. As an example, there are thin sheet cement products (for

flat and corrugated sheet roofing elements) with relatively high V_f of $> 5\%$. Conventional steel reinforcement cannot be used for obvious practical reasons. In applications with an FRC the fibres can increase both the tensile strength and the toughness. FRC materials are therefore widely found in industry applications (Purnell, 2010) such as: cladding in exterior building facade panels, bridge works, precast panels, shotcrete (tunnel linings), sewer pipes, drainage channels and agricultural purposes.

As discussed in Section 2.7 the uniformity of distribution of the fibres throughout the volume is very sensitive to the mixing and consolidation process, and in practice a uniform volume fraction is rarely achieved (Bentur and Mindess, 2007). The author's work will support the practical challenges faced for successful manufacture. In Section 2.4 the four types of fibre (carbon (CF), polyvinyl alcohol (PVA), polypropylene (PP) and glass fibre (GF)) are introduced for their effectiveness in previous research work in the public domain. To give a level of comparison typical mechanical properties for these and several other commercial fibres are summarised in Table 2.1.

Table 2.1: Mechanical properties of the most commercial types of fibre (Bentur and Mindess, 2007).

Fibre Type	Tensile Strength (MPa)	Young's Modulus (GPa)	Fibre Diameter (μm)	Alkali Stability (relative)
Asbestos	600-3600	69-150	0.02-30	Excellent
Carbon	600-4900	28-520	7-18	Excellent
Aramid	590-4800	62-130	11-12	Good
Polypropylene	200-700	0.5-9.8	10-150	Excellent
Polyamide	700-1000	3.9-6.0	10-50	Excellent
Polyester	800-1300	up to 15	10-50	Excellent
Rayon	450-1100	up to 11	10-50	Fair
Polyvinyl alcohol	850-1500	29-40	14-600	Good
Polyacrylonitrile	850-1000	17-18	19	Good
Carbon steel	3000	200	50-85	Excellent
Stainless steel	3000	200	50-85	Excellent
AR-glass	1700	72	12-20	Good
E-glass	1900	72	12-20	Poor

2.4.1 Glass Fibres (GF)

Glass fibre (GF) is used in FRCs and HPFRCs because it is readily available and inexpensive, and is supplied in various useful forms. The primary concern with the standard 'E' glass type, which is commonly the reinforcement in civil engineering FRPs, is that the fibres are not stable in most cement matrices. This is because they degrade in the highly alkaline environment (Purnell, 2010). The alkaline nature of concrete causes a damaging chemical reaction between cement and GF. This leads to a rapid deterioration process that involves strength and weight losses and reduction in the filament diameter (Purnell 1998; Bentur and Mindess 2007).

Robert and Benmokrane (2013) explain that GFs are damaged by the combination of the following two processes: (1) chemical attack by the alkaline cementitious environment, and (2) concentration and growth of cement hydration products between individual filaments. Fibre embrittlement is due to the nucleation of calcium hydroxide on the fibre surface. Hydroxylation can cause fibre surface pitting and roughness, which act as flaws, and in the long-term cause a severe reduction in strength, especially in the presence of moisture. In addition, calcium, sodium, and potassium hydroxides in the concrete pore solution are aggressive to GFs (Benmokrane *et al.*, 2002). Robert and Benmokrane (2010) investigated the short- and long-term durability of E-glass fibre in cementitious materials after 60, 120, 180, and 240 days of immersion in water at different temperatures. They found no significant loss before 240 days in tensile strength and elastic modulus. Their test results showed a slight decrease of 6-11% from the short-term tensile strength. This decrease is similar, and confirmed by the tensile strength measured by Robert *et al.* (2009). To prevent any durability issues a special glass fibre having alkali resistant (AR) (SiO_2 - Al_2O_3 - ZrO_2 -alkali oxide) was developed in 1967 by scientists of the United Kingdom

Building Research Establishment (BRE). GF is normally supplied as continuous rovings on a roll having up to 64 strands; each with 200 filaments having an average of diameter 14 μm . GF can be supplied continuous and in short lengths of 3 to 40 mm (Purnell, 1998).

Several researchers, including Marikunte *et al.* (1997), Purnell *et al.* (2000), Rols *et al.* (2000), Li *et al.* (2002), Kruger *et al.* (2003) and Cuypers *et al.* (2006) agree that either using a low alkalinity cement or densifying the interface between fibres and matrix with polymers, prevents the $\text{Ca}(\text{OH})_2$ diffusion into the GF. This can be used either with E-glass or AR-glass fibres to modify the matrix in order to improve the long-term resistance. Another technique to limit the alkali-silica reaction is to reduce the amount of portlandite (calcium hydroxide ($\text{Ca}(\text{OH})_2$)) in the matrix by employing the pozzolanic effect. As discussed in Section 2.8 the cement replacement materials of PFA, SF or GGBS can be added in order to replace part of the cement. The long-term performance of Glass fibre Reinforced Cementitious (GRC) materials is still the major criterion by which quality is assessed. As discussed by Bentur and Mindess (2007) considerable effort is continuously made to find out how to improve service life. The most common manufacturing process is spraying (with V_f at 5%) to produce thin sheet products (Purnell, 2010). Introduced in Section 2.6 are other manufacturing processes, such as filament winding (e.g. for pipes), hand lay-up, extrusion, pultrusion and pre-mixing.

2.4.2 Polyvinyl Alcohol Fibres (PVA)

Polyvinyl alcohol fibre (PVA) is organic and was first produced 50 years ago in Japan. It has been used in FRCs since the 1980s due to suitable characteristics as reinforcement (Nuruddin *et al.*, 2014). The surface chemistry of PVA fibres is hydrophilic so that the bonding strength (τ) is relative strong (Shen *et al.* 2008), ranging between 3 to 5 MPa and can be compared with other hydrophobic polymeric fibres having τ at 0.5 MPa

for polyethylene fibre (PE) and 0.1- 0.3 MPa for polypropylene (PP) fibre (Redon *et al.*, 2001). Li *et al.* (1990) confirmed these findings by an independent research study. They found that the bond strength is 0.16 and 1.02 MPa for hydrophobic nylon and Polyethylene fibres, respectively. Whereas, they found a much higher bond strength of 4.5 MPa for hydrophilic aramid fibre. These two studies give results to confirm that fibres with hydrophilic surface characteristics have bonding several times, to an order of magnitude, higher than hydrophobic fibres (Kanda and Li, 1998). The hydrophilic nature of PVA fibre provides a great challenge since good bond means the fibre is more likely to fail in rupture than by pull-out (Wang and Li, 2006). Due to their good mechanical properties and physical characteristics PVA fibres have been used to produce FRC sheet products as a replacement for asbestos (Bentur and Mindess 2007; Suwannakarn 2009). The fibres have to be surface treated to enhance their compatibility with the cement matrix and to enable their efficient dispersion (Bentur and Mindess, 2007). A study by Zheng and Feldman (1995) found that PVA fibres act very effectively to prevent micro-cracking.

PVA fibres offer more advantages as they offer: good alkali resistance (Ogawa and Hoshiro, 2011); good chemical compatibility; good affinity with water; faster drainage rate and no health risk. A PVA FRC can be produced by a number processing methods, including pre-mixing and shotcreting. Shao and Shah (1997) found that thin sheets, pipes and other shapes were being produced by an extrusion process.

2.4.3 Polypropylene Fibres (PP)

Polypropylene fibre (PP) was first used to reinforce cementitious materials in the 1960s. This fibre type can be introduced as discrete short fibres of length 6 to 60 mm, or as continuous rovings. PP fibre is hydrophobic which does not absorb the water and is non-corrosive. Moreover, it possess excellent resistance against chemicals (alkalis and

chloride), and PP is stable in the highly alkaline environment (Bentur and Mindess 2007; Ezeokonkwo and Nwoji 2011). Another advantage of PP as a reinforcement is that it does not intervene in the hydration of cement and thereby does not affect the constituents in the mix (Ezeokonkwo and Nwoji, 2011).

It has been proven by Hannant (1978), Currie and Gardiner (1989), Bentur and Mindess (2007), Felekoglu *et al.* (2009) and Sadrmomtazi and Fasihi (2010) that the interfacial bond strength (τ) between PP fibre and cement matrix is extremely poor. This is because of the fibres' low wettability. This weakness is most severe when mono-filaments are used. They have smooth surface texture and no surface treatment to improve the interfacial bond. For this reason, the flexural strength and toughness improvement with PP FRCs are claimed to be limited (Singh *et al.* 2004; Bentur and Mindess 2007; Felekoglu *et al.* 2009). Due to this known disadvantage most of the PP fibres used for FRCs will undergo various proprietary surface treatments to improve wettability, etc. (Currie and Gardiner 1989; Buendia *et al.* 2013). PP FRC can be produced by a number of different manufacturing processes, including Hatschek, extrusion, spraying and conventional mixing (casting).

2.4.4 Carbon Fibre (CF)

Carbon Fibre (CF) can be produced from different organic materials, such as polyacrylonitrile (or PAN), petroleum and coal tar pitch (pitch). PAN based carbon fibres are sometimes classified into two types; type I is for high modulus, having $E_f \approx 390$ GPa, and type II is for high tensile strength, having $\sigma_f \approx 2700$ MPa (Bentur and Mindess, 2007). There is no hard relationship between strength and stiffness. Pitch-based fibres ($E_f \approx 30$ GPa and $\sigma_f \approx 600$ MPa) are used because they are cheaper than PAN-based carbon fibres (Purnell, 2010). Despite their considerably lower mechanical properties it is observed that

pitch fibres still have superior properties over other synthetic fibres, such as polypropylene. Because of their overall property portfolio PAN fibres have been shown by Bentur and Mindess (2007) to be the most suitable to reinforce a cementitious matrix. Table 2.2 lists typical mechanical properties of PAN and pitch-based CFs.

CF can be supplied in untwisted bundles of fibres called tows and they are commercially available in three basic lengths, namely, continuous (> 50 mm), short (4-50 mm) and milled (7-3000 μm). Continuous fibres are far more effective than short fibres because of the good fibre bond; this fact will be developed further in Section 2.5. The bond between CFs and cement matrix is particularly important (see Section 2.16), because their relatively high cost requires the maximum utilisation of their potential advantages. A weakness is that their hydrophobic nature and low affinity to cement paste makes the transfer of force between fibres and matrix rather unreliable and discontinuous (Brandt, 2009). Fu *et al.* (1996) and Xu and Chung (1999) state that the surface treatment of CF by chemical treatments, such as silane, ozone and nitric acid treatments is an effective approach to adequately increase bond strength.

Table 2.2: Typical mechanical properties of PAN and pitch-based carbon fibres (Bentur and Mindess, 2007).

Type of carbon fibre	Diameter (μm)	Density (kg/m^3)	Modulus of elasticity (GPa)	Tensile strength (MPa)	Elongation at fibre rupture (%)
PAN type I	7.0 - 9.7	1950	390	2200	0.5
PAN type II	7.6 - 8.6	1750	250	2700	1.0
Pitch	18	1600	30 - 32	600 - 750	2.0 - 2.4

The primary advantage of CFs is that they are far more stable than GF in the presence of the highly alkaline matrix (Nakagawa *et al.* 1993; Johnson 2001). As the reinforcement in both FRCs and HPFRCs they improve tensile strength, flexural strength,

toughness, drying shrinkage and dimensional stability. Their main drawback has to be their relatively high cost; low cost is necessary for applications of FRCs in the construction industry. The principal factor in the price of CFs is the cost of the raw materials, followed by the cost of heat-treatment, which is higher the greater the treatment temperature. Although the literature reports promising results for CF FRC, they are currently limited by high production costs. If the manufacture of CF evolves to reduce their cost, their beneficial properties would make them the fibre type of choice (Nakagawa *et al.*, 1993). CF FRCs are being used successfully in curtain walls and roofing panels for exterior and interior of buildings, for cladding panels and for the repair and protective coating of structural elements exposed to aggressive environments. This gives an indication of the durability and dimensional stability of these cementitious composites (Bentur and Mindess, 2007). A CF FRC can be produced using manufacturing processes such as hand lay-up, filament winding, spraying and conventional mixing (casting) (Nishioka *et al.*, 1986).

Due to the superior properties of CF listed above, the effect of a number of parameters are investigated by the author, and are introduced in Chapters 3 and 5 with the test results presented in Chapters 5 to 7. The aim of the research has been to improve the mechanical (flexural strength and toughness) and microstructure properties of FRCs for building product applications.

2.4.5 Mechanical Properties of Carbon Fibre Reinforced Concrete (CFRC)

Much research with CFRCs has been conducted in Japan, and from the study by Ohama (1989) it is observed that the material reinforced with short CF at V_f of 2% doubles the flexural strength from that of the unreinforced matrix. Work by Park *et al.* (1991) found that the flexural and tensile strengths increased almost linearly as V_f is increased. They

concluded that for V_f of 5 % these two strengths are three to four times greater than for the matrix. The modulus of elasticity obtained from the stress-strain curves are found to decrease gradually as V_f increases. This is the result of higher porosity, caused by the presence of the CF. When V_f exceeded 5% Park *et al.* found that the workability of the mixes became so poor that the fibres formed into balls. Chen and Chung (1993) concluded that with short pitch-based carbon fibres at a V_f of 0.2%, together with SF at 15% by weight of cement, the flexural strength increases by 85% and the toughness by 205%.

A study by Park and Lee (1993) investigated the effect of different types of CF on mechanical properties. They concluded that a PAN fibre is more effective in increasing strength (tensile, compressive, and flexural) than a pitch-based fibre. This is due to the fact that, the fibre tensile strength of PAN fibre is four times greater than that of pitch-based fibre as given in Table 2.2. Flexural strength is determined to increase as V_f increased up to 3%. It then decreased at the higher fibre loading of 5%. More recently, Garces *et al.* (2005) studied mechanical properties to conclude that for a CF content at 0.5% of cement weight and substitution of 20% of the same weight by SF, the flexural strength increases by 14%. For reinforcement levels higher than 0.5%, the flexural strength gain is either small or negative, probably because of an increase in porosity leads to a reduction in FRC strength. There is also a significant reduction in porosity from 20-22% to 15-16% for all mixes when SF is a cement substitute. As discussed further in Section 2.16 this is attributed to the small SF particles (0.01-0.5 μm) filling-in the interstices between fibres and cement particles producing better packing and fibre-matrix contacts, thereby improving adhesion and reducing matrix porosity.

Using a direct pull-out test procedure Katz *et al.* (1995) measured the interfacial bond strengths of two CFs, having different diameters of 10 μm and 46 μm , with matrices

having different water/binder (w/b) ratios and SF contents. The results showed that for the 10 μm CF the bond strength is basically of a friction nature, and ranges from 0.5 MPa, for the matrix with high w/b of 0.52 and no SF, to 1.3 MPa, for the low w/b ratio of 0.35 and SF at 10% of cement weight. For the 46 μm CF matrices containing SF at 10% gave much better bond strengths of 2.44 and 3.02 MPa for the 0.50 and 0.35 w/b ratios, respectively. Due to the high bond many fibres were observed to fracture and not pull-out of the SF-cement matrices. These results indicate that the densification of the matrix surrounding the fibres, either by reducing the w/b ratio or by using SF has a positive effect on developing bond strength, as discussed in more details in Sub-sections 2.8.1 and 2.16. The influence of adding SF appears to be more effective when used with a relatively low w/b ratio, of 0.35.

As discussed in Section 2.16 the surface treatment of CF is very important to improve the bond (Fu *et al.*, 1996). It has been shown by Fu and Chung (1998) that the bond can be improved through different treatments, such as thermal, adding admixtures, and using chemical solutions. Admixtures can either be particles, such as SF or they can be liquids, such as methylcellulose aqueous solution and water reducing agents. A study by Zheng and Chung (1989) investigated cementitious materials reinforced with 0.3% V_f of a CF that had the surface treated by concentrated aqueous Nitric acid (HNO_3) solution and chlorosulfonic acid. Results showed that the treated surface fibre gave double flexural and tensile strengths. Xu and Chung (1999) reported that the combination of silane treated CFs and SF in the mix design increases the tensile strength by 56%. They also found that the void content is increased, whether or not the fibres have been surface treated. Banfill *et al.* (2006) concluded that the addition of CFs results in a less dense FRC with enhanced ductility, improved impact resistance and increased toughness. In addition, the reinforcing

effect of CFs often produces superior flexural strength and marked improvements in post-cracking behaviour.

2.5 Textile Reinforced Concrete (TRC)

The term Textile Reinforced Concrete (TRC) is often used for a composite of a cement matrix with continuous fibre (fabrics) as reinforcement. TRC is the most efficient ways to obtain strain-hardening behaviour that has been shown to be beneficial in Section 2.3. In addition, TRC materials with high V_f up to 10% can be achieved (see Section 2.14) using special manufacturing processes such as, Hatschek, sprayed, hand lay-up and pultrusion, as discussed in Section 2.6.

A reinforcement fabric is a manufactured assembly of continuous (long) fibres of carbon, aramid or glass, or a combination of these, to produce a thin flat sheet of one or more layers of fibres. These layers are held together either by mechanical interlocking of the fibres themselves or with a secondary material to bind them into the fabric product. Fabrics have fibre assemblies with sufficient integrity to allow handling without the pattern being disrupted. Mechanical properties are more effective in an FRC than when fibres are short, discontinuous and randomly distributed. This is due to their length giving higher bond strength and because they can be oriented parallel to the applied load, as discussed further in Section 2.17.

Fabric reinforcements can be stitched, woven or non-woven. Alongside several other factors, such as yarn density, the fineness and the number of filaments in the bundle means there are many different constructions (Peled and Bentur, 2000). Specific fabric characteristics can influence the stability and the mechanical properties of the whole fabric, ultimately affecting the penetration of the particulate cement matrix (Peled *et al.*, 2008). Fabric types are not only categorised by the orientation of the fibres, but also by the

various construction methods used to hold the fibres together. Gurit (2011) categorise the three fibre orientation as:

1. Unidirectional (0° or warp), in which a majority of fibres are aligned in one direction, for the principal loading direction. A relatively small amount of CF or other fibre can be in the perpendicular direction (90° or weft) with the purpose of holding the 0° fibres in position (see Section 3.2.4).
2. Biaxial ($0^\circ/90^\circ$ for warp/weft) are stitch-bonded, non-crimp, reinforcements comprised of unidirectional warp (0°) and weft (90°) plies, usually with the same V_f in the two orthogonal directions.
3. Multi-axial fabrics can, for example, consist of four unidirectional layers with the same V_f in the directions of 0° , 90° , -45° and $+45^\circ$. A polyester stitching thread is usually used in the through-thickness direction to bind the layers together.

Peled and Bentur (2000), Peled and Shah (2003), Peled *et al.* (2004) and Mobasher *et al.* (2006(a)) stated that fabrics could significantly improve the mechanical behaviour of an FRC in terms of flexural strength, toughness and bond strength. Cuypers and Wastiels (2006) found that a relatively high V_f of $> 5\%$ can be obtained when fabrics are used. The manufacturing process for the FRC must ensure good penetration of the cement particles between the spaces within both the fabric and the bundle filaments. Good penetration is essential in order to maximise the reinforcing efficiency by improving bond. If the geometry of the fabric is open to allow for matrix bridging across a layer thickness, this mechanical connection will enable transfer of force between the matrix and the reinforcement, significantly reducing the dependence of composite action on the interfacial bond. Another advantage of this mechanical interlocking is an enhancement in debonding (or pull-out) strength, which normally serves to limit the load transfer mechanism

(Mobasher *et al.*, 2006(b)). Therefore, matrix penetration between the filaments depends heavily on the nature of the fabric junctions, the structure of the fabric, the number of filaments in the bundle, and the FRC production process (Peled, 2009).

In order to achieve the highest degree of composite action it is known that fabric surface treatment is necessary, as it helps develop the matrix to penetrate between fibre gaps. This is particularly important when using multi-filament reinforcements as only the fibre close to a bundle's perimeter can be in direct contact with the matrix, as explained in Section 2.16. FRCs having fabric reinforcement are known to provide benefits, such as excellent anchorage and bond development, and improve the mechanical behaviour (Peled *et al.*, 2006). An earlier study by Mobasher *et al.* (1997) showed that cements containing 5% by volume of unidirectional E-glass fabrics achieved tensile strength of 50 MPa, compared to an average tensile strength of about 14 MPa with short glass fibre materials (produced by the hand lay-up method).

In 1998 a research group called Textile Reinforced Concrete (TRC) (at the collaborative research centre (SFB 532)), was established at RWTH Aachen University, Germany. Also, in 2002 the Technical Committee for Textile Reinforced Concrete (TC TRC) was established by RILEM in France. From these two groups there is a considerable volume of literature on TRCs from extensive and recent research programmes. In particular, there have been theoretical investigations carried out to understand important mechanical properties such as flexural strength, toughness and bond strength.

2.6 Manufacturing Process

The chosen manufacturing process can significantly affect the properties of an FRC or a HPFRC, even when the same matrix and fibre reinforcement are used. Peled *et al.*

(2008) reported that there must be an effective development of the interfacial bond during the manufacturing process. Various methods have been successfully employed to produce an FRC. Any method must allow for the incorporation and uniform dispersion of a sufficient volume of short fibres, say $V_f > 2\%$, to achieve an adequate reinforcing effect (Bentur and Mindess, 2007). The processing technology of composite reinforced with continuous fibres is expensive and may only be used for special products. Composite with short fibres are easy than continuous fibre to work with, and the cost of processing their FRCs is therefore relatively lower (Shao and Qiu, 2002).

In this section there is a brief description of the seven manufacturing process of Hatschek, hand lay-up, spray-up, premixing, pultrusion, extrusion and compression moulding. In the description the author highlights work relevant to how FRCs are processed for the characterisation work presented in Chapters 5 to 7.

2.6.1 Hatschek

This process was developed for paper making and the sheets produced can be reinforced with asbestos fibres up to 35% by volume. Due to the hazardous nature of asbestos, the existence of FRCs spurred interest in using other fibres with the Hatschek process. Polyethylene fibres and cellulose fibres (i.e. processed natural fibres derived from woody materials), both in pulp form, are the most widely investigated. In principle, any fibre that can be dispersed within a cementitious slurry to produce a dense fibre mat can be used (Bentur and Mindess 2007; Purnell 2010).

2.6.2 Hand Lay-up

Hand lay-up or hand laminating technique is one of the oldest, simplest and most commonly used methods for manufacturing FRP materials. This method allows more

control of fibre placing than the spray method of Sub-section 2.6.3, and can potentially produce a relatively high $V_f > 10\%$. Disadvantages of hand lay-up are that the method is labour intensive and has a comparatively low output (Purnell, 2010). The steps to make an FRC are very similar to those using hand lay-up for a FRP (see reference Purnell (2010) for more details).

2.6.3 Spray-up

Spraying is one of the main production processes for glass FRC materials having V_f up to 6%. This method can be used to combine short fibres with textile reinforcement and allows the production of two and three-dimensional forms (Pachow, 2003).

2.6.4 Premixing

Premixing is used to produce GFRC materials with a V_f up to 6%. In this method fibres are pre-chopped to a maximum length of 35 mm and are added at a lower rate at the end of the mixing process to avoid damage. The premix process typically yields an FRC with a three-dimensional random orientation of short fibres. With this process it is found that a uniform fibre dispersion is difficult to achieve, and usually a high w/c ratio is required; it is higher than spray-up method ($0.4 > 0.3$).

2.6.5 Pultrusion

In the Pultrusion process, fabrics are passed through a bath of slurry and then pulled through shaped rollers (replacing the die for FRP production) to consolidate the matrix and fibres into a FRC sheet with a V_f up to 10%. This automated method offers better control of orientation and mechanical properties. By using this process, sheets with various widths, lengths and thicknesses can be produced (Bentur and Mindess 2007; Purnell 2010).

2.6.6 Extrusion

Extrusion is a plastic-forming technique which can be employed to produce high performance FRCs with V_f up to 8% (Kuder and Shah, 2010). When this process is applied to a very low w/c ratio (≈ 0.2 to 0.3) is utilised, which contributes to a high strength matrix (Shen *et al.*, 2008). The advantage of extrusion is that the FRC is formed under high shear and compressive forces. This results in material with improved tensile and bending strength (Aldea *et al.*, 1998), from a dense matrix and strong bond. The method also gives control for good fibre alignment (Peled *et al.*, 1999).

2.6.7 Compression Moulding

Compression moulding is a widely used method for the manufacturer of a range of FRP components. Using this moulding method to produce a FRC is fairly novel; the only previous research is the preliminary study by Farahi (2009). Farahi used this process to produce a few specimens to show that the process is unsuccessful for the reasons explained in details in Sub-section 2.6.8.

2.6.8 Effect of Manufacturing Processes on the Mechanical Properties

Much research has studied the effect of manufacturing processes on the mechanical properties of FRC. Hannant and Hughes (1986) used the hand lay-up process to conclude that the flexural strength is in the range of 20 to 40 MPa with fibres in the form of several layers of polypropylene mats.

A study by Farahi (2009) used compression moulding and hand lay-up to process two FRCs with AR glass fabric at $V_f \approx 3\%$ and unidirectional carbon fabric with $V_f \approx 8\%$. Farahi found that by using the hand lay-up process a mean flexural strength of 17 MPa with glass fibres was achieved and 61 MPa with unidirectional carbon fibre mat. Farahi

reported that compression moulding of FRCs was unsuccessful because specimens reinforced with fabric were severely delaminated and longitudinal cracks developed in the direction of the fibres. In the case of short fibres, the process only permits the addition of fibres up to V_f of 3%. Further addition was found to make green processing difficult and FRC specimens exhibited weak 'green strength'. Farahi found to delaminate a few hours after demoulding.

2.7 Dispersion of Short Fibres

Mechanical properties of FRCs are very sensitive to the uniformity of volume distribution or dispersion of the fibres, which includes both how the short lengths are oriented and located within the matrix. Good dispersion reduces the fibre free area in the matrix and improves their composite efficiency. Bentur and Mindess (2007) have noted that uniform dispersion, particularly at $V_f > 1\%$ is difficult to achieve. When V_f exceeds about 1 to 2% (depending on the fibre type) there is tendency for the fibres to form 'tight' balls (static electricity attraction) that cannot easily be broken down. As a consequence the mixture has poor fibre distribution and tends to become unworkable (see Section 2.14) and difficult to compact in a mould (Purnell 2007; Wang *et al.* 2014). Bentur (1989), Mobasher *et al.* (1990), Banthia *et al.* (1998), Toutanji *et al.* (1993) and Nilufer *et al.* (2004) all confirmed that the effectiveness of short fibres depends on the degree of dispersion, since this affects both the fresh and hardened state properties of the FRC. Poor dispersion can negatively impact the flow characteristics of the fresh state, and can severely limit the otherwise beneficial effects of fibres (Nilufer *et al.*, 2004).

The degree of dispersion can be improved by the use of additives such as SF. This is due to the fine particles (see Sections 2.8.1 and 3.2.2) whose presence helps the fibres break loose from one another as mixing occurs (Chung 1992; Chen *et al.* 1997). The

advantages of having a uniform distribution are reduced shrinkage cracks and the improved post-crack strength as cracks always have fibre bridging (Sivakumar and Santhanam, 2007). Previous studies have therefore focused on how to improve fibre dispersion. Akkaya *et al.* (2000) observed that when fibres clump together and the volume of 'fibre-free' matrix increases and the initiation of a matrix crack requires less strain energy. Once the crack forms it can advance easily through any 'fibre-free' matrix regions. Chung (1992) stated that the degree of fibre dispersion can be improved by treating the fibre surface with ozone treatment. It is reported by Banthia *et al.* (1998) that fibre distribution is affected by the fibre length and diameter (see Section 2.15). The ease of dispersion increases with decreasing fibre length (Ohama *et al.*, 1985). Another fibre dispersion study by Chuang *et al.* (2008) investigated the dispersion of short CFs of 5 mm length and 7 μm diameter after the mix involved a new dispersant of Hydroxyl Ethyl Cellulose (HEC). Using an ultrasonic method of detection they found that the CFs were not well dispersed when HEC was not used. Because they observed a uniform distribution for the mix with HEC they concluded this additive helped with the desired fibre dispersion.

2.8 Additives

A pozzolan is broadly defined as a siliceous material, which when added reacts with the lime (or portlandite) to produce an additional amount of Calcium Silicate Hydrate (C-S-H) by hydration, the main cementing component. Thus the pozzolanic material reduces the amount of calcium hydroxide ($\text{Ca}(\text{OH})_2$) and increases the amount of C-S-H. In addition, a pozzolanic reduces the alkalinity of the pore solution (and thereby fibre corrosion) and greatly reduces or even eliminates CH from the matrix) (Purnell, 1998). Very fine pozzolan particles sized between 0.1 and 10 μm , such as SF, can fill the holes between cement grains and fibres.

The use of Pozzolans, as partial replacement to Ordinary Portland Cement (OPC) offers many advantages and results in cost savings, particularly when these materials are diverted away from waste sites (Uzal *et al.*, 2010). Their introduction is beneficial by: reducing the amount of cement; improving concrete properties; reducing the energy needed for processing natural materials; conserving natural resources. Another advantage is that there is a reduction in cement production which reduces CO₂ emissions and energy consumption (Suneel, 2004). Lothenbach *et al.* (2011) and Carrasco *et al.* (2014) have shown that Pozzolans can improve long-term strength and durability and reduce the porosity. The adverse effects of replacing cement are the increase in setting times and the decrease in workability due to an increase in the surface area of particles (Sahmaran *et al.*, 2006).

Several researchers (Bagel 1998; Khan *et al.* 2000; Pandey and Sharma 2000) reported that the combination of two or more kinds of pozzolanic materials emerges as a superior choice when improving concrete and mortar properties. A study by Toutanji *et al.* (2004) agreed with these studies and confirmed that a combination of SF, GGBS and PFA can produce cementitious materials with higher strength and effective resistance to freeze-thaw. Middendorf *et al.* (2005) characterised the effect of adding an additive to show that the matrix becomes denser. Recently, Zhou *et al.* (2012) stated that by partially replacing cement with PFA or GGBS the mix's setting times is delayed. The effect of the three common additives of SF, GGBS and PFA on mechanical properties of cementitious materials is described in the following three sub-sections.

2.8.1 Silica Fume (SF)

SF, known also as micro silica, is a waste product from the silicon industry and contains 95-99% active silica by weight. Since the 1970s the application and interest in SF

has increased. SF particles are extremely small; more than 95% can have a diameter less than 1 μm . They have a very high water demand, which necessitates the addition of a mix of high range water reducers or superplasticisers (Vitro, 2008). This is in part due to the adverse effect SF has on workability (Purnell, 1998). SF particles are usually grey in colour, darker or lighter grey depends on their carbon and iron content. The specific surface area of SF ranges from 13,000 to 30,000 m^2/kg with a bulk density range from 130 to 430 kg/m^3 (Siddique, 2011). The high specific surface increases the rate of the pozzolanic reaction and also that of hydration generally, probably due to the small SF particles acting as nucleation sites (El-Hadj and Duval, 2009). It has been stated by Larbi *et al.* (1990) and Duchesne and Berube (1994) that adding SF reduces the alkalinity in the cement pore solution. SF is generally added as a partial replacement for cement at lower weight fractions than GGBS and PFA, at about 5-25% according to Sengupta and Bhanja (2003). Yogendran *et al.* (1987), Toutanji *et al.* (1993), Mobasher and Li (1996), Fu and Chung (1998), Chung (2000), Shannag (2000), Chung (2002), Shihada and Arafa (2010), Ismeik (2010) and Zulkarnain and Ramli (2011) all confirm that the typically replacement level is 15%.

As shown in this review there is a considerable volume research papers on the use of SF. Larson *et al.* (1991) reported that SF fills the voids between the particles of cement hence, improving packing between fibre and cement particles to develop the fibre-matrix bond. Bentur and Diamond (1985), Zhu and Bartos (1993) and Bartos and Zhu (1996) experimented with adding SF directly to the fibre bundles by immersion in a SF slurries, prior to manufacturing the FRC. The rationale behind this procedure is that the SF will penetrate into the inter-filament spaces. Previous studies by Yogendran *et al.* (1987), Toutanji *et al.* (1998), Urban (2003), Chung (2005) and Yazdanbakhsh *et al.* (2009)

concluded that SF is effective in improving the dispersion of short fibres, this is has been introduced in Section 2.7. Chung (2000) reported that the dispersion of CFs of 15 μm diameter and 5 mm length at 0.2% V_f is enhanced by having SF at 15% by weight of cement. Badanoiu and Holmgren (2003) studied the bond for continuous CFs where the tows have 12k (12000) filaments at 7 μm diameter. Results from their study showed a 20% improvement in the bond properties when the matrices contained SF at 10%. Nili and Afroughsabet (2010) found that the addition of SF led to an increase in flexural strength of up to 38% (tested at 28 days). This work also agreed with previous studies that the presence of SF improves the uniformity of fibre dispersion. It is for this reason that the author involves SF in the series of FRC experiments to be reported and discussed in Chapters 5 to 7.

2.8.2 Pulverised Fuel Ash (PFA)

Pulverised fuel ash (also known as fly ash) is a by-product from the burning of pulverised coal in power stations. The major constituents of PFA are silica, alumina, and oxides of iron and calcium. The physical and chemical properties of PFA can vary considerably from one power plant to other due to the differences in the sources of coal. Generally, PFA is made up of glassy, spherical particles which range in size from 2 to 160 μm . PFA has been used in concrete production for over 50 years, and is used to replace up to more than 50% of cement by weight (Carette and Malhotra 1983; Rashad 2014).

The use of PFA in cementitious materials offers many advantages and results in saving costs, particularly when these materials are diverted away from waste sites. PFA is also used to reduce hydration heat and thermal cracking at early ages, to improve the mechanical and durability properties especially at later ages (Siddique and Khan, 2011) and to decrease the shrinkage of the hardened concrete (Atis, 2003). Yuan *et al.* (1982)

showed that the water demand increased when the PFA content is more than 20%. Carette and Malhotra (1987) concluded that by adding 20% there is increase in concrete strength. Yuan *et al.* (1982) confirmed that a mix having 20% PFA exhibited less shrinkage on curing than either the control matrix or a matrix containing PFA at 30 to 50%. Saraswathy *et al.* (2003) confirmed that a critical level of 20-30% replacement activated the PFA addition, to improve both the corrosion-resistance and strength. A study by Snelson and Kinuthia (2010) disagrees with the studies by Yuan *et al.* (1982), Carette and Malhotra (1987) and Saraswathy *et al.* (2003). They all concluded that the strength decreases as cement is replaced with PFA. The author involves PFA in the series of experiments reported in Chapters 5 to 7.

2.8.3 Ground Granulated Blast Furnace Slag (GGBS)

GGBS is produced as a by-product during the manufacture of iron. This cement replacement is rapidly cooled to form granules, and then ground (crushed) to a fine white powder. This cement material has many similar characteristics to OPC. GGBS contains around 30 to 40% active silica by weight. GGBS is angular in shape with a surface texture much smoother than OPC. The size of GGBS particles varies from 5 to 70 μm , whereas the surface area is between 450 and 685 m^2/kg . Replacement levels for GGBS vary from 30% to up to 85% by weight of the cement (Elahi 2009; Siddique and Khan 2011).

It has been demonstrated that GGBS improves the general performance of cementitious materials by decreasing chloride diffusion and chloride ion permeability (Luo *et al.* 2003; Yun and Kyum 2005), reducing creep and drying shrinkage, increasing sulphate resistance, enhancing the ultimate compressive strength (Barnett *et al.*, 2006), reducing the heat of hydration and bleeding and reducing the alkalinity of cement pore solution (Duchesne and Berube 1994; Pavia and Condren 2008). Zhou *et al.* (2012)

concluded that a matrix with 30% GGBS by weight of cement exhibited higher splitting tensile strength than plain concrete.

2.9 Mechanical Behaviour of FRC

The brittle matrix in FRCs is typically porous and has a relative high compressive strength, but much lower tensile strength. This behaviour is different from FRPs, as discussed in Section 2.2, and must be understood and taken into account in application development. The difficulty of increasing tensile strength is mainly due to the low tensile strain capacity of the matrix (ϵ_m). It is also due to the fact that the fibre addition may lead to the FRC having increased porosity. The mechanical properties of FRC such as strength can be predicted by theoretical models based on constituent properties as presented in the next sub-section.

2.9.1 Composite Rule of Mixtures

The simplest model to predict strength (σ_c) and modulus of elasticity (E_c) of an FRC composite is the Rule of Mixtures, in which it is assumed that a uniform strain exists throughout, and failure occurs when either of the constituents (fibre and matrix) reaches their (material) failure strain. The two stages of pre- and post-cracking can be considered.

E_c in pre-cracking stage can be predicted as:

$$E_c = E_m V_m + E_f V_f \quad (2.1)$$

$$V_m + V_f = 1 \quad (2.2)$$

then

$$E_c = E_m(1 - V_f) + E_f V_f \quad (2.3)$$

where E is modulus of elasticity and V is volume fraction, the subscripts c, m and f denoting composite, matrix and fibre properties, respectively. A similar expression to Equation (2.3) can be used to predict σ_c by substituting the stress terms for the modulus terms, as:

$$\sigma_c = \sigma_m(1 - V_f) + \sigma_f V_f \quad (2.4)$$

Equations (2.3) and (2.4) are only acceptable for continuous uniaxially aligned and continuous fibres. For randomly distributed discontinuous fibres the formulae can be modified by introducing efficiency factors (≤ 1.0); η_l for fibre length and η_θ for fibre orientation (see also Section 2.17, where values are presented and discussed):

$$E_c = E_m(1 - V_f) + \eta_l \eta_\theta E_f V_f \quad (2.5)$$

$$\sigma_c = \sigma_m(1 - V_f) + \eta_l \eta_\theta \sigma_f V_f \quad (2.6)$$

Equations (2.5) and (2.6) are valid in the pre-cracking stage (i.e. before matrix cracking) where the composite has elastic behaviour. For the post-cracking stage, Equations (2.5) and (2.6) can be modified, by neglecting the contribution from the matrix to predict E_c and σ_c from:

$$E_c = \eta_l \eta_\theta E_f V_f \quad (2.7)$$

$$\sigma_c = \eta_l \eta_\theta \sigma_f V_f \quad (2.8)$$

2.10 Stress-Strain Curve

The reinforcing mechanisms in FRCs are quite different from those of FRPs as detailed in Section 2.2. In FRC, the fibre reinforcement becomes effective, mainly after the

matrix has cracked and the fibres bridge across the cracks. There can be four zones in the stress-strain relationship and the curve in Figure 2.3(a) shows them to be: an elastic or pre-cracking stage (zone I), a multiple cracking stage (zone II), a post-cracking stage (zone III) and a failure zone (IV). They are now introduced.

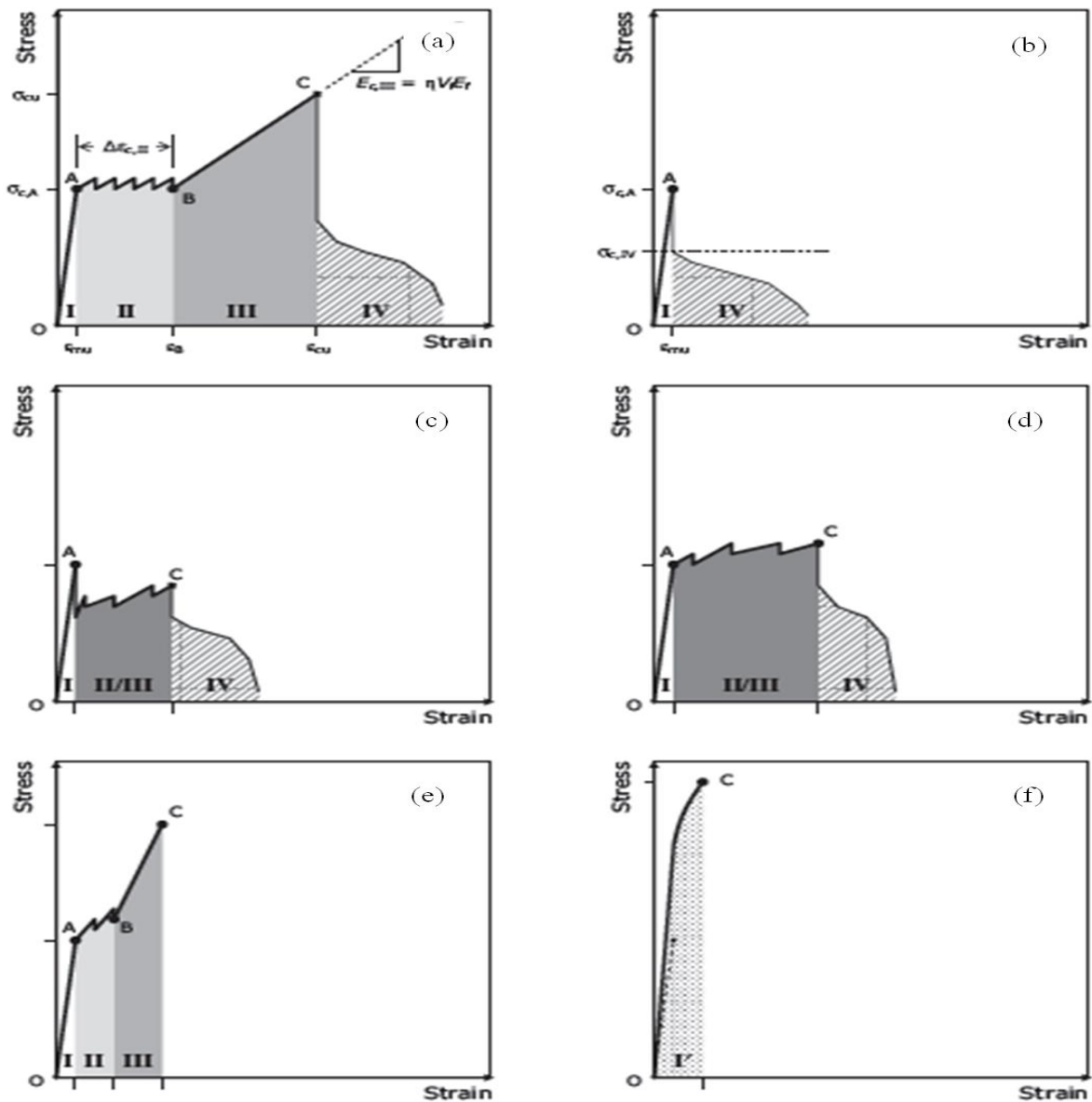


Figure 2.3: Idealised tensile stress-strain curves for FRC (Purnell, 2010).

Zone I: Elastic stage is from O up to point A for the first crack, as shown in Figures 2.3(a) to (f). This is often termed the pre-cracking response. In zone I the stress carried by the

composite immediately before the matrix cracks at $\sigma_{c,A}$ is shared by the matrix and fibres. The material exhibits linear behaviour up to $\sigma_{c,A}$ and E_c is given by the constant slope of line OA. The simplest model to predict E_c and σ_c is by the ‘Rule of Mixtures’ formulae (see Section 2.9.1).

At point A in Figure 2.3 the matrix will crack (this point is also referred to as a ‘Loss of Proportionality’, given abbreviation LOP). After this point new matrix cracks initiate, and the shape of the curves deviates from the linear response as the loss of continuity reduces the FRC’s stiffness. If the composite itself fractures immediately after matrix cracking, this can be because of inadequate V_f (see Section 2.14) at the critical section or, an insufficient fibre length, as discussed in Section 2.15. If the critical fibre volume fraction ($V_{f,crit}$) (see Section 2.14) is exceeded the tensile force can transfer across a crack (Mobasher and Shah, 1989).

Zone II: The Multiple cracking stage is labelled II in Figures 2.3(a) and 2.3(e). During this stage there is a fairly constant stress with increasing strain, in excess of the ultimate strain of the matrix (ϵ_{mu}). After the first crack has formed, if the load on the FRC is increased, the fibre-matrix bond stress transfers force into the matrix. Further, increases in stress will cause further matrix cracking until the matrix has a network of closely-spaced cracks.

Zone III: The Post-cracking stage is labelled III in Figures 2.3(a) and 2.3(e). Generally speaking, this is the stage where the development of new cracks stops and a localised critical crack starts opening-up, while other cracks formed during III commence unloading. In zone III, assuming that V_f is sufficiently above $V_{f,crit}$, the fibres enable the FRC to reach a peak (failure) stress at point C. Once full multiple cracking has occurred, only the fibres

further contribute to the stiffness in this post-cracking zone. The Rule of Mixtures can be used to predict E_c and σ_c by Equations (2.20) and (2.21), respectively in Section 2.17.

Zone IV: During the Failure stage the fibres begin to rupture or be pulled-out of the cracked matrix. In Figure 2.3(a) this region is labelled IV. Normally, the failure stage of the FRC occurs immediately after the peak stress has been reached. The shape of the stress-strain curve in this region, and the degree to which the stress continually decreases is an important indicator to the ability of the FRC to absorb, post-peak, energy.

Purnell (2010) provides an assessment of the six schematic, idealised stress-strain curves defined by Figures 2.3(a) to 2.3(f) that cover the response of most FRC (and HPFRC) materials. For a majority of FRCs E_c is not significantly different from E_m , thus we have that $\sigma_{c,A} \approx \sigma_{mu} = \varepsilon_{mu} E_m$. Immediately after the matrix cracks (when $\varepsilon_{fu} \gg \varepsilon_{mu}$) the matrix stress $\sigma_{m,A} = 0$. This condition should be valid for all FRCs, as introduced in Section 2.2. σ_{mu} is peak stress of the matrix.

Many FRCs retain some residual strength and toughness after the peak stress has been reached at point C; this is for zone IV. When V_f is $\geq V_{fcrit}$ the failure stress (σ_{cu}) will be significantly higher than $\sigma_{c,A}$. The FRC will now have a stress-strain curve similar to that shown in Figure 2.3(a). If $V_f \leq V_{fcrit}$ multiple cracking and post-cracking zones (II and III) will be small, or even absent from the stress-strain curve. This is a common when reinforcement is a relatively weak fibre or when there are workability problems (e.g., with steel fibres). In this case, the typical stress-strain curve is given in Figure 2.3(b) and toughness given by the area under the curve for zone IV.

Figures 2.3(c) and 2.3(d) show a stress-strain curves of FRCs where $V_f \leq V_{fcrit}$ (with fibres of steel, natural and many polymers). If $V_f < V_{fcrit}$ then the behaviour in Figure 2.3(c)

will be observed. The characteristic shape illustrated in Figure 2.3(d) is found when $V_f > V_{\text{crit}}$ and $l \leq l_c$ (i.e. bond is weak or fibres are short length) (see Sections 2.15 and 2.16). For these conditions many of the fibres are not fully effectively. The full stress capacity will be mobilised at peak stress (σ_{cu}) and the fibres will begin to pull-out of the matrix; although ultimate strength may be lower, the toughness will increase. In both Figures 2.3(c) and 2.3(d), the four zones (I, II, III and IV) exist; with II/III and IV overlapping in most FRCs. In FRCs with continuous fibres (i.e. bond is relatively very strong or fibre length is ‘infinite’), or short fibres with $l \gg l_c$ (i.e. $l \geq 5l_c$) (see Sections 2.15 and 2.16) zone IV can be very small or non-existent. This is because there is significant stress transfer between fibres and matrix on failure. The resulting stress-strain curve is similar to that illustrated in Figure 2.3(e).

The stress-strain behaviour shown in Figure 2.3(f) has rarely encountered in the past for FRCs. It requires $E_c > E_m$ (i.e. $E_c = \eta V_f E_f$) and $V_f \gg V_{\text{crit}}$ (i.e. $V_f > 10\%$) and can be achieved by applying recent developments with continuous carbon FRCs using manufacturing processes such as, the hand lay-up or Hatschek process (see Section 2.6). This response for the stress-strain relationship is unusual for FRC materials and happened when the $\sigma_{c,A} > \sigma_{\text{mu}}$ and/or $\varepsilon_{c,A} > \varepsilon_{\text{mu}}$. An effectively monotonic curve up to peak stress is observed, rather than the usual two or three-stage curve of the classic primary FRC (ACK model by Aveston *et al.* (1971)), as discussed in Section 2.13. The influence of relative high stiffness of carbon fibres on the response of the FRC makes it difficult to observe the first-crack stress (LOP) from the shape of the stress-strain curve. The transition between Region I and Regions II and III is ill-defined, and the crack width/spacing so small, that it cannot be detected without additional crack monitoring. We see that the strength and failure strain of the matrix has somehow been increased by the fibre reinforcement. This

behaviour is not the same as the suppression of initial matrix cracking (i.e. an increase in σ_m of the type proposed by Romauldi and Batson (1963)), suggesting that most of the pre-peak response is for Region I behaviour. The matrix is cracking, but there is no sudden drop in E_c because the carbon fibres have a high modulus of elasticity and V_f is sufficiently high (Purnell, 2010). There can be a sudden reduction in E_c when the fibres are of glass.

Generally, as discussed above the ideal tensile stress-strain behaviour for an FRC can be achieved if all the following requirements are satisfied: $V_f > V_{fcrit}$; $l \gg l_c$ and control the fibre orientation (i.e. the fibres aligned to the loading direction); made by appropriate manufacturing process. To achieve the ideal having strain-hardening behaviour with multiple cracking, the author in Chapters 5 to 7 investigate different types of fibres with different sources and forms (short and continuous) and different manufacturing processes.

2.11 Models of FRC Composites

For convenience in this thesis ‘FRC’ can be read to mean both standard ‘FRCs’ and ‘HPFRCs’. Modelling of crack formation and propagation is a major important topic over the last 50 years and its progress has been considered by, for example, Bazant (2002). It is complex in FRCs, as heterogeneities play an important role in crack initiation and progression (Bascoul, 1996). Most models for crack formation and propagation depend on fracture mechanics principles, either via Linear Elastic Fracture Mechanics (LEFM) or Non-Linear Fracture Mechanics (NLFM), as discussed in Section 2.18.1. The models for FRCs are classified into three main groups, as: empirical; analytical and numerical. They have been adopted based on different simplifying assumptions, with different degrees of reliability and complexity to describe and understand the fracture mechanics of FRCs.

Among existing nonlinear fracture models in the literature we find the: Smearred Crack Model (SCM) by Rashid (1968); ACK model by Aveston *et al.* (1971), the Cohesive Crack Model (CCM) or Fictitious Crack Model (FCM) proposed by Hillerborg *et al.* (1976) and developed for FRC materials by Hillerborg (1980); Crack Band Model proposed by Bazant (1976) and developed further by Bazant and Oh (1983); Two Parameter Fracture Model (TPFM) by Jenq and Shah (1985); discrete models, such as the well-known Lattice Model (LM) from Schlangen and Van-Mier (1992), the Variable Engagement Model (VEM) introduced by Voo and Foster (2003) and developed by Htut and Foster (2010), and the Double-K Fracture Model (DKFM) by Xu and Reinhardt (1999) and developed by Kumar *et al.* (2013).

2.12 Which Model to Use?

Many of the models are generally limited in their use, and are based on certain limiting assumptions; one observation is that more in-depth analyses are still needed to better understand the complex failure of FRCs. Complexity, as discussed in Section 2.2, is due to the cementitious material being heterogeneous, and exhibiting a highly nonlinear mechanical behaviour. To the best of this author's knowledge no one model has so far been able to handle the general cracking problem, and to fully capture all facets of the mechanical response. Any researcher who wants to simulate the fracture behaviour of FRCs has to decide which model to use. Design engineers require a simple and reliable model, which explains the fracture processes, with sufficient accuracy when measured against what is observed in practice. It is essential to choose the best model to describe the fracture behaviour and crack propagation.

As the aim of this PhD work is not to study the fracture process it has been decided by the author to look in detail only at the ACK model. The review will consider its

advantages and limitations. Readers wanting more information concerning details on the many models introduced in Section 2.11 and elsewhere can consult the following publications: Knott (1973); Mindess (1983); Gopalaratnam and Shah (1987); Broek (1989); Karihaloo (1995); Shah *et al.* (1995); Carpinteri and Massabo (1997); Van-Mier (1997); Oliver *et al.* (2002); Oliver and Huespe (2004); Purnell (2010); Sanchez *et al.* (2012) and Kumar *et al.* (2013). Three books, with an up-to-date description of different techniques and models, aimed at understanding crack propagation in cementitious materials have recently been published by Hofstetter and Meschke (2011), Kumar and Barai (2012) and Van-Mier (2013).

Although it is over 40 years since Aveston *et al.* (1971) proposed the ACK model we find that many researchers use it to model crack propagation in FRC materials, e.g., see Curtin (1999), Kulkarni (1998), Purnell (1998), Purnell *et al.* (1999), Purnell *et al.* (2000), Purnell *et al.* (2001), Da Silva *et al.* (2004), Cuypers and Wastiels (2006), Hegger *et al.* (2006), Mobasher *et al.* (2006(a)), Purnell (2007, 2010), Blom and Wastiels (2013) and Larrinaga *et al.* (2014). Purnell (1998) states that the ‘simple’ ACK model is valid for analysing glass FRCs. Konrad (2008) reported that the ACK model is one of the most frequently used analytical models to describe the stress-strain relationship of a FRC under tensile load.

According to several researchers the ACK model has some limitations. Mumanya (2007) reported that a major limitation is that the matrix and fibre reinforcement are characterised by linear elastic behaviour to failure. This condition is not always obeyed with FRCs. In addition, the ACK model is based on the assumption that the matrix has a single valued cracking stress over the multiple cracking region (zone II), which does not account for a strain-hardening zone III. Bentur and Mindess (2007) state that a drawback

with the model is that the force in the fibre must be totally transferred to the matrix. Moreover, crack localisation is not considered, nor is the contribution of broken fibres taken account for. The ACK model does not differentiate between the first cracking point and the end of multiple cracking with respect to energy changes, which are all combined into the model at the first cracking point. Mobasher (2011) stated that ACK does not address the tension stiffening effect, which is defined as the ability of the uncracked segments in between two parallel cracks that transmit the tensile force. A majority of tension stiffening models in the literature either don't take into account the gradual transition of bond-slip mechanism or simplify this mechanism by assuming a linear interfacial model.

These drawbacks are not so important to the author's study and can be ignored. The most important features of the ACK model are:

- 1- It is the simplest and most practical model, and is much more user-friendly for FRCs.
- 2- It is easily visualised and uses readily quantifiable parameters (e.g. matrix strength, crack spacing) to model the stress-strain behaviour of FRC and predict frictional bond values (Purnell *et al.*, 2000). The input parameters in the ACK model are derived from the Rule of Mixtures.
- 3- In general, the fracture mechanics of FRCs concerning the post-cracking region is complicate and the ACK model can adequately explained this process (Purnell, 1998). By paying particular attention to explaining and predicting the multiple cracking region, as mentioned in Sections 2.10 and 2.13, it copes with the strain-hardening behaviour.
- 4- It gives a satisfactory prediction of the real behaviour of many FRCs, such as TRCs (Hegger *et al.*, 2006). In spite of the useful predictive capabilities the ACK model still

has limitations in analysing FRCs with randomly distributed discontinuous fibres. This weakness is not so well documented for the original ACK model, but considered later in its derivatives by Aveston and Kelly (1973), Aveston *et al.* (1974), Budiansky *et al.* (1986), Naaman *et al.* (1991), Tjiptobroto and Hansen (1993) and Kullaa (1994; 1998). This can be achieved by introducing efficiency factors η_0 and η_1 , as will be discussed in details in Section 2.17.

The author decided to select the ACK model, as the most suitable model, to represent the results in Chapter 6 for short fibres and Chapter 7 for continuous fibres. Its theoretical background is described in the following section.

2.13 ACK Model

An attempt to model the behaviour of fibres in the post-cracking zone was undertaken in 1971 by Aveston, Cooper and Kelly that lead to the well-known ACK model. They described the behaviour of a brittle matrix composite with continuous aligned fibres as a function of V_f using the Rule of Mixtures. The basic assumption applied is that stress transfer between fibre and matrix is caused by purely frictional stress, with no adhesive or ‘elastic’ bonding (Purnell 1998; Cuyper and Wastiels 2006). Generally, the stress-strain response of an FRC (in flexural or tension) can be classified by the three stages that constitute the basis of the ACK model. Figure 2.4 shows the idealised tensile stress-strain curve, taken from Purnell (2010), with the three zones of linear elastic (zone I), multiple cracking (zone II) and post-cracking (zone III) that were detailed in Section 2.10.

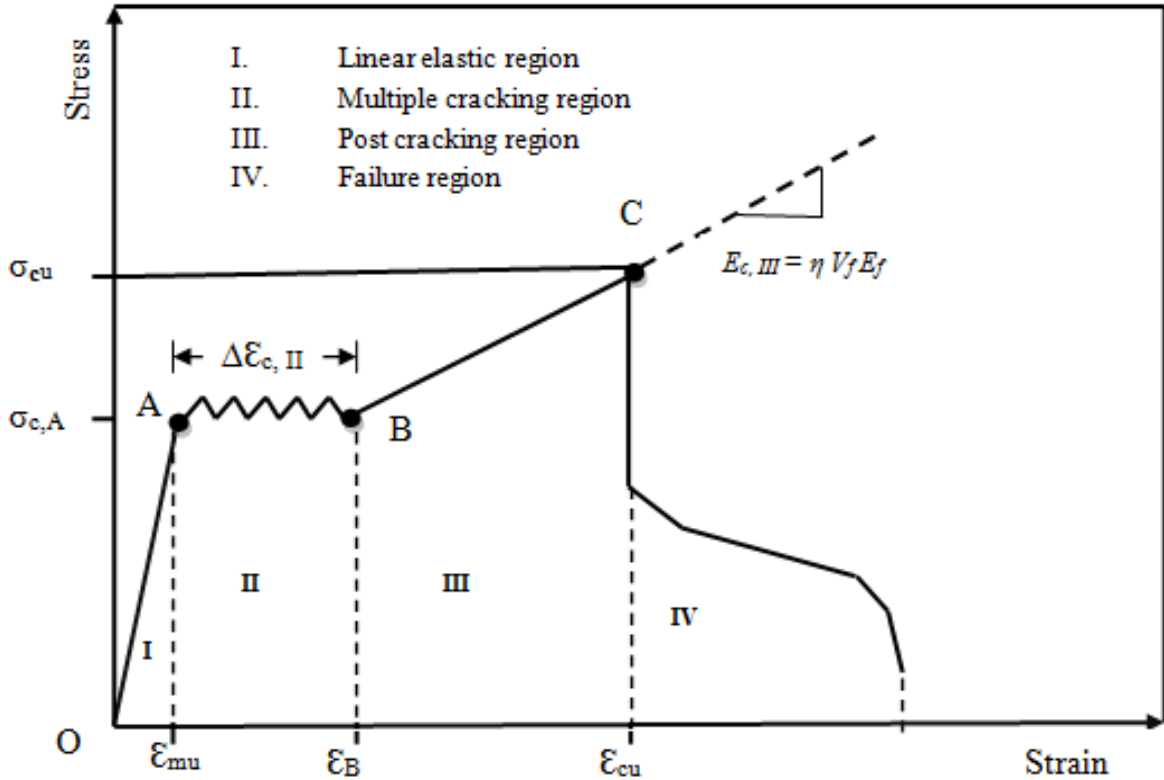


Figure 2.4: Schematic description of the idealised stress-strain curves for FRC materials based on the ACK model (Purnell, 2010).

Multiple cracking is one of the basic features for an FRC to possess a strain-hardening behaviour and toughness. Aveston *et al.* (1971) gave a big attention to describe the stress-strain behaviour in the multiple cracking zone II. The control of crack spacing and width during this stage of deformation has considerable influence on the serviceability of the composite (Bentur and Mindess, 2007). According to the ACK model, increasing the stress above σ_{mu} will lead to the multiple cracking zone, if $V_f > V_{crit}$. This will result in the matrix being broken into a series of blocks by parallel cracks with a crack spacing between x and $2x$ (i.e. x is the distance over which the load is transferred (half the block length) and $2x$ is the maximum block length). The average crack spacing is $1.364x$ (Purnell, 2010). The stress in the matrix must be zero at the crack faces and at each end of the block (as illustrated in Figure 2.5(a)), and this stress is assumed to vary linearly with distance away from the crack from zero to the maximum possible value, which can be the matrix strength

(σ_m) (Hibbertand and Hannant 1982; Purnell 2010; Blom *et al.* 2012). The length x can be derived from the balancing of the forces along the crack:

$$N P_f x \tau = V_m \sigma_{mu} \quad (2.9)$$

where σ_{mu} is the failure stress of the matrix, V_m is the volume fraction of the matrix, τ is the frictional shear stress at the interface, P_f is the perimeter of the fibre cross-section and N is the number of fibres per unit plan area (note that $N = V_f/A_f$ with A_f is fibre cross-sectional area).

Equation (2.9) can then be rewritten to calculate the length x :

$$x = \left(\frac{V_m}{V_f}\right) \cdot \left(\frac{\sigma_{mu}}{\tau}\right) \cdot \left(\frac{A_f}{P_f}\right) \quad (2.10)$$

For a given τ , multiple cracking will continue at a roughly constant stress ($\approx E_c \varepsilon_{mu}$) until the FRC completely separate into segments with lengths between x and $2x$ (i.e. the block length (i.e. crack spacing) becomes such that insufficient load can be transferred from the fibres to the matrix to produce further cracking). The strain distributions in the fibre reinforcement and matrix are presented in Figure 2.5(b). Thus, the upper and lower limits for the strain at the end of the multiple cracking zone II, ε_{mc} , are given by (Aveston *et al.*, 1971):

$$\varepsilon_{mu} \left(1 + \frac{1}{2} a\right) < \varepsilon_{mc} < \varepsilon_{mu} \left(1 + \frac{3}{4} a\right) \quad (2.11)$$

where
$$a = \left(\frac{E_m V_m}{E_f V_f}\right) \quad (2.12)$$

Beyond the multiple cracking region, no more cracking can take place, and additional tension will result in stretching and slipping of fibre in the matrix blocks. E_c will become

equal to $E_f V_f$ until failure, when σ_c is $\sigma_{fu} V_f$ (i.e. there is no contribution from the cracked matrix).

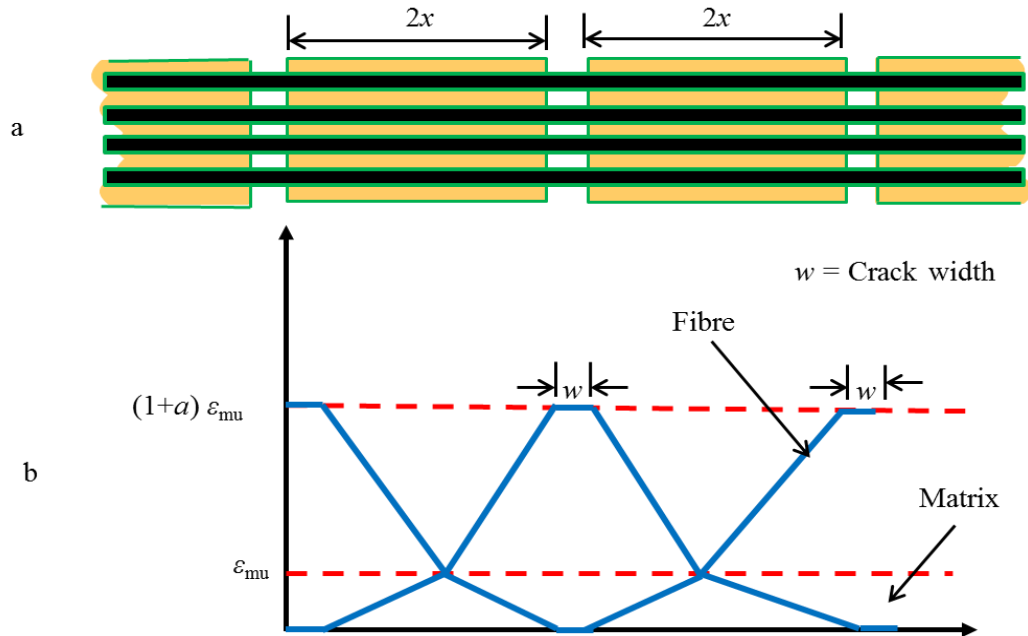


Figure 2.5: Multiple cracking according to the ACK model: (a) crack spacing and bridging fibres; and (b) strain distribution in FRC.

Aveston and Kelly (1973) showed that their ACK model is not sensitive to the assumed nature of the bond provided that the elastic bond strength does not exceed σ_{mu} , which is highly unlikely. Naaman *et al.* (1991) analysed the relative significance of frictional slip over elastic ‘adhesion’ bond for FRCs. By comparing their respective contributions to the energy absorbed during pull-out tests both analytically and experimentally they conclude that frictional stress transfer (i.e. bond) is the dominant component (Purnell, 1998). These findings validate the use of the ‘simple’ 1971 ACK model for modelling FRC.

2.14 Fibre Volume Fraction (V_f)

Fibre content is often measured as a fraction of the total volume in the composite material. Generally, V_f in FRCs is low at ≈ 1 to 2% for short fibres using normal mixing processing, and is due to the nature of the heterogeneous cement matrix. However, in recent years, $V_f \leq 10\%$ for materials reinforced with continuous fibres (see Section 2.5) have been successfully introduced using special manufacturing processes such as, Hatschek, hand lay-up, extrusion and pultrusion, as discussed in Section 2.6. To achieve multiple cracking and strain-hardening behaviour requires the higher V_f , as discussed in Section 2.3. This is due to the increasing effective bonding area and the increasing large number of fibres that can bridge the matrix cracks. In an FRC with low to medium V_f , 1 to 3%, the reinforcement does not enhance the tensile/flexural strength and so the benefits of having the fibres are limited to enhancement in energy absorption and/or toughness during the post-cracking zone. On the other hand, for a FRC with $V_f \geq 5\%$ the benefits are observed by increased tensile strength and toughness, and a strain-hardening behaviour as discussed in Section 2.3.

FRC models can be classified into three categories with regards to V_f , namely, low ($<1\%$), moderate (1 to 3%), and high ($> 5\%$); typical reinforcement level is 2% (Li, 2003). The workability of fresh mix decreases (Yusof *et al.*, 2011) when $V_f > 2\%$ and the other disadvantage is that porosity increases. As has been introduced in Section 2.7 short fibres have a tendency to form balls with increasing V_f and it becomes very difficult to distribute them uniformly. The optimal efficiency with short fibres is for a V_f between 1 and 2% (Hanjari, 2006).

The key parameter determining which type of post-cracking behaviour occurs is the critical fibre volume fraction, $V_{f,crit}$ (Purnell, 2010). $V_{f,crit}$ is the minimum fibre volume

fraction necessary to ensure the FRC strength (σ_{cu}), is at least equal to that of the matrix ($\sigma_{cu} \geq \sigma_{mu}$), and to avoid catastrophic failure. If V_f is too low ($< V_{fcrit}$) then when the matrix cracks, the fibres will be unable to carry any additional load. On the other hand, when $V_f > V_{fcrit}$ the fibres will be able to carry additional load imposed on them after the matrix cracks. Thus, we find that initiation of matrix cracking is not catastrophic, and the FRC will sustain more load and deformation; the material will be imbued with some post-cracking capability. V_{fcrit} can be calculated using the ACK model (Section 2.13) and is expressed by;

$$V_{fcrit} = \frac{\sigma_{mu}}{\eta\sigma_{fu}} \quad (2.13)$$

Where σ_{mu} and σ_{fu} are the tensile strength of the matrix and fibres, respectively and η is the combined efficiency factor accounting for orientation and length, i.e. $\eta = \eta_\theta \eta_l$. It is seen from Equation (2.13) that V_{fcrit} depends on matrix strength σ_{mu} . As the matrix becomes stronger, a greater proportion of fibres are required to take up load transferred into them as the matrix cracks. The common stress-strain curves with FRCs having different V_f is reviewed by Purnell (2010), and discussed in more detail in Section 2.10.

Balaguru and Shah (1992) stated that the growth of microcracks is hindered as V_f increases and as the fibres are more uniformly dispersed in the matrix. Also the localisation of deformation is delayed with a consequent substantial increase in the strength and strain capacities (Nicolaidis, 2004). Kullaa (1998) reported that V_f for cementitious materials with short fibres is typically $< 3\%$. This finding supports the outcome from a study by Larrinaga *et al.* (2014), who stated that the typical V_f is about 1 to 3%. If fibre content is higher, mixing and workability problems result. To overcome these weaknesses requires special mixing or placing techniques. Inagaki (1991) reviewed the introduction of CF in

FRCs by Japanese researchers. Inagaki concluded that the use of V_f from 2 to 4% made the strength two to three times higher than for the unreinforced matrix; there was also an increase in toughness. Purnell (2007) reported that, depending on the fibre type, as V_f exceeds about 1 to 2%, balling of fibre causes poor distribution and so the mix tends to become unworkable and difficult to compact. Farahi (2009) reported that there is a limitation and as more short fibres are added the mix becomes less workable, more difficult to pour it into a mould and to achieve the desired component shape with full compaction. Khorami (2011) concluded that V_f has to be limited to a maximum of 4%. He found that with higher V_f the fibres clump together and the mix was not homogeneous.

2.15 The Critical Fibre Length (l_c)

The fibre length (l) of the short fibres is important, especially when compared with the so-called critical fibre length (l_c). l_c is defined as the minimum fibre length required to achieve full strength capacity, σ_{fu} (i.e. fibres fracture rather than pull-out of the matrix). Figure 2.6 shows the stress transfer along a short fibre for the three lengths of: $l < l_c$ (Figure 2.6(a)); $l = l_c$ (Figure 2.6(b)); $l > l_c$ (Figure 2.6(c)). Fibre lengths $< l_c$, are insufficient in the FRC for the stress to reach σ_{fu} . In this case, failure is governed by fibre pull-out followed by matrix fracture; the strength is lower than the ultimate fibre strength, as shown in Figure 2.6(a). In order to achieve σ_{fu} for an effective reinforcement, l must be at least equal (Figure 2.6(b)) or exceeding l_c , as shown in Figures 2.6(c). In this case fibre strength can be attained and failure is governed by fibre fracture (Bentur and Mindess, 2007). The minimum fibre length to allow a fibre to be capable of transferring its maximum shear force at both ends is $\geq 2l_c$. For the FRC with $l \geq 2l_c$ the reinforcement will in theory behave structurally as though as the fibres are continuous (Purnell, 1998).

The fibre will tend to restrain the deformation of the matrix, and so a shear stress will be set-up in the matrix at its interface with the fibre. This shear stress is in equilibrium with a tensile stress in the fibre. This tensile stress is zero at the fibre ends and it reaches a maximum at a distance of $l_c/2$ from the end (see Figure 2.6(b)). The pull-out force required to extract an embedded length from a block of matrix should be greater than the breaking force (see Figure 2.7), at the fibre length l_c these two forces should be balanced. This equilibrium state can be written as:

$$\pi r^2 \sigma_f = 2 \pi r \frac{l_c}{2} \tau \quad (2.14)$$

where r is the fibre radius and τ is the frictional shear stress at the interface equal to the interfacial bond strength. The area of the fibre assumes a circular cross-section, and is A_1 in Figure 2.7. The surface area for the pull-out force is calculated for the cylindrical fibre, and is A_2 in Figure 2.7. Rearranging Equation (2.14) the expression for l_c is:

$$l_c = \frac{\sigma_f r}{\tau} \quad (2.15)$$

Equation (2.15) shows that l_c is linearly depends on the fibre strength and the inverse of the bond strength. Good τ and/or low σ_f , give low l_c , and *vice versa* (Purnell, 2010).

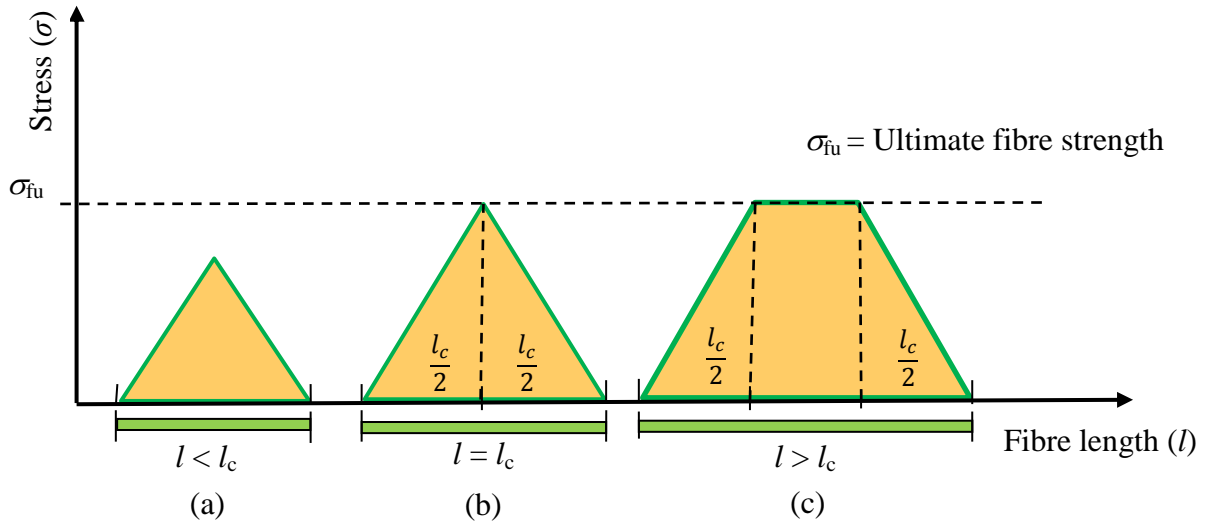


Figure 2.6: Stress profile along a short fibre as a function of fibre length, when; a) $l < l_c$, b) $l = l_c$ and c) $l > l_c$.

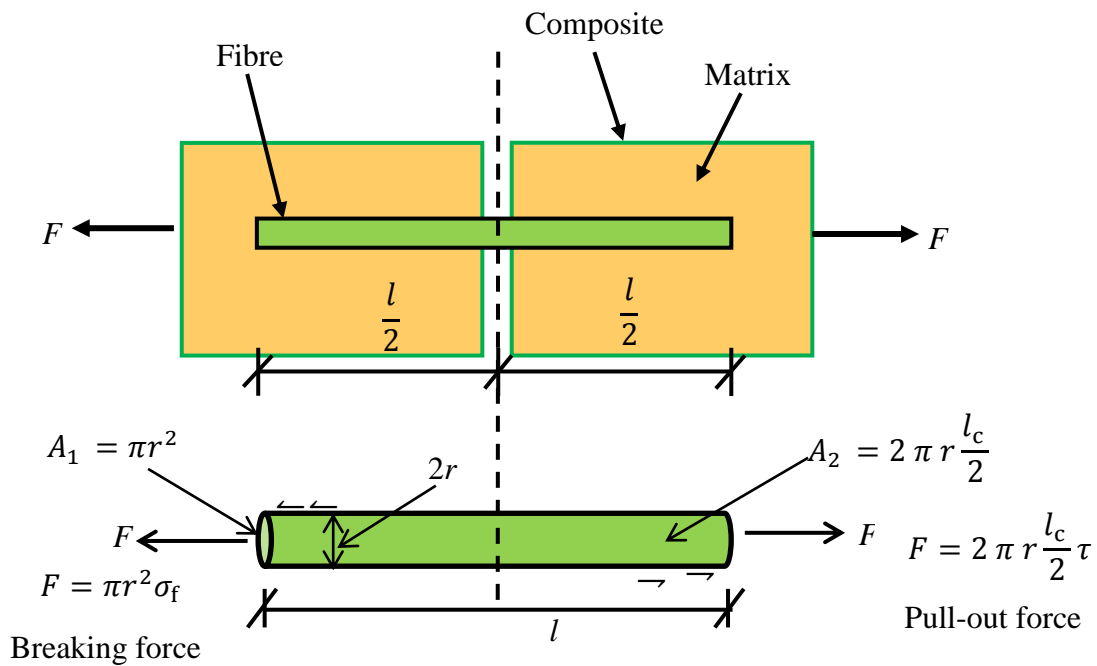


Figure 2.7: Forces on a fibre being pulled from a block of matrix.

As has been discussed in Section 2.7 other parameters, such as uniform dispersion of the fibre contribute to the mechanical performance. Betterman *et al.* (1995) reported that the distribution is influenced by the fibre length and fibre diameter. In the 1996 study by Banthia and Sheng a maximum flexural strength increase of about 360% was observed for

FRCs reinforced by CFs of lengths 6 and 10 mm and a V_f of 3%. Mobasher and Li (1996) studied the flexural and toughness properties with CFs at 1 mm length and a V_f of 8%. The results of the Mobasher and Li study showed that flexural strength increased on average by 90% when compared to the control material ($V_f = 0\%$). In addition, the failure mechanisms of fibre debonding and pull-out were observed, since the short length of 1 mm could not provide significant crack bridging. The lower efficiency found by Mobasher and Li can be attributed to the CF length being below the average aggregate size. Deng (2005) determined the energy absorption (toughness) of FRCs having CFs of 25 mm length. Deng concluded that there is a clear improvement in toughness when compared to the test results of Mobasher and Li (1996) who used a similar CF reinforcement of $1/25^{\text{th}}$ the length. Akkaya *et al.* (2000) studied the effect of PVA fibres at lengths of 2 and 6 mm on the toughness and tensile strength of FRCs. They concluded that mechanical behaviour was improved as l increased. Nishioka *et al.* (1986) suggested that l_c for CFs is in range from 0.8 to 1.4 mm. Larson *et al.* (1991) calculated l_c for another CF to show it fell in the range 0.6 to 0.8 mm.

From the discussion above, it can be concluded that an increase in l is advantageous for generating higher FRC tensile strength. When toughness is of consideration we find that an increase in l above l_c can be detrimental. In this study l_c is calculated by Equation (2.15) in Chapter 6 to investigate the effect of fibre length on flexural strength and toughness of FRCs having short fibres.

2.16 Interfacial Bond Strength (τ)

The performance of FRCs is often controlled by the strength and durability of the fibre-matrix interface. The effectiveness of the reinforcement depends on the quality of the bond, which is general much weaker compared to that for fibres in a polymer based matrix

(Lu *et al.*, 1998). The major parameters affecting the fibres interaction with its matrix are: condition of the matrix; matrix composition; fibre geometry and aspect ratio (l/d); type of fibre; fibre surface characteristics; fibre stiffness compared to matrix stiffness; fibre orientation (aligned or random distribution) and V_f (Balaguru and Shah, 1992).

Naaman and Najm (1991) state that there are four main factors to influence the bond, and they are:

- (i) physical and chemical adhesion;
- (ii) mechanical component of bond such as deformed, crimped and hooked end fibres;
- (iii) fibre-to-fibre interlock;
- (iv) friction (Silva *et al.*, 2011).

To enhance the mechanical bonding of steel fibres, as discussed in Section 2.4, they are purposely deformed to create mechanically interlocking with the matrix. Because τ is inversely proportional to l_c in Equation (2.15), a good bond requires a lower l_c , and *vice versa*.

Measuring the interfacial bond strength is not as simple as characterising the other mechanical properties because it is complicated for two reasons. First, the matrix in the interface region is quite loose and porous and this reduces the bond strength as discussed in Section 2.2. Bond strength can change significantly as the cement matrix ages and hydration continues, leading to contact between fibres and matrix becoming more intimate. The interface regions can become denser, and in a multifilament FRC the spaces within the fibre bundles may become partially filled with hydration products, particularly calcium hydroxide crystals. Over time this material change affects the bond strength positively

(Majumdar 1974; Purnell *et al.* 2000; Purnell 2010). Secondly, the unit reinforcing element in an FRC is usually a fibre bundle and not a single fibre (Peled *et al.* 2008; Peled 2009; Purnell 2010). It is very difficult to estimate the true contact perimeter of the bundle having a few hundred or thousands of filaments (i.e. for the P_f terms in Equation (2.16)). Purnell *et al.* (2000) developed a method to determine a bundle's perimeter using a digital image analysis with petrological thin sections. Their work showed that at early ages the matrix does not penetrate far into the bundle. This results in a reinforcing unit, in which the outer filaments are in direct contact with hydration products and can be said to be well bonded.

The inner filaments (in the core of the bundle) are relatively free of hydration products as shown in Figure 2.8(b). This leads to telescopic modes of failures, where the outer filaments fracture during tensile loading (see Figure 2.8(c)), whereas the inner filaments pulled-out under tension as seen in Figure 2.8(d) (Purnell 2010; Ombres 2012). It is to be understood that the contact perimeter is not the sum of the individual filament perimeters. Furthermore, the cross-sectional morphology of bundles is highly variable (Purnell *et al.*, 1999; 2000). This physical situation is different for an FRP as the polymer matrix completely penetrates between every filament (refer to Section 2.2).

τ can be determined either directly, for example, from pull-out tests on: single filaments; strands for GFs; tows for CFs; groups of strands or tows. The bond strength can also be obtained indirectly using the ACK model (see Section 2.13) from knowing the crack spacing (x) (Purnell *et al.*, 2001). The expression is:

$$\tau = 1.346 \left(\frac{V_m}{V_f} \right) \cdot \left(\frac{\sigma_{mu}}{x} \right) \cdot \left(\frac{A_f}{P_f} \right) \quad (2.16)$$

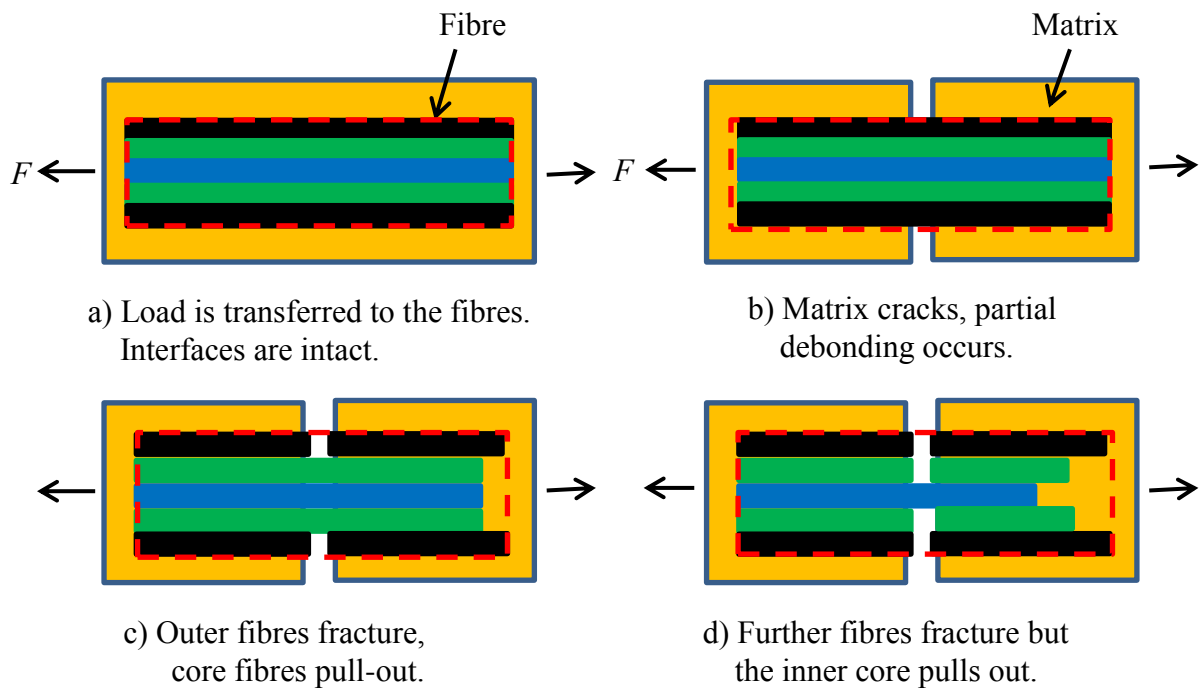


Figure 2.8: Principle of combined fibre pull-out and fibre fracture in a bundle FRC material (Wiberg, 2003).

Purnell *et al.* (2001) reports that there are a number of drawbacks when the ACK model is used to determine τ indirectly. In particular, the model relies on stress transfer between the fibres and matrix being purely frictional in nature. It has, however, been shown that there is elastic bond, and that the relationship between elastic and frictional bonds influence mechanical behaviour (Bartos, 1980; 1985). Although it would be of advantage to be able to measure bond strength directly, a practical (standard) test method is not available.

Surface treatments of fibres have been reported to be effective in improving the bond by enhancing the chemical affinity between fibres and matrix, and to add some roughening of the fibres' surface to generate mechanical anchoring (Bentur and Mindess, 2007). Bond enhancement can be obtained by either using fabric meshes or fibre grids or by providing mechanical anchoring to compensate for the poor interaction between hydrophobic fibres

(such as polypropylene) and the cement matrix (Peled *et al.* 1998; Ombres 2012). Badanoiu and Holmgren (2003) reported that if the matrix can penetrate into the interior of a tow of CFs, a higher number of filaments will be active leading to the increase in strength. Fu *et al.* (1996) concluded that surface treatment improved the bond strength. Table 2.3 is used to summarise results for the interfacial bond strength (τ) by a number of independent researchers.

Table 2.3: Summary of interfacial bond strength (τ) for CF, GF, PP and PVA fibres.

Fibre type	Interfacial bond strength (τ) (MPa)	Reference	Mean value of τ (MPa)
Carbon (CF)	0.52 to 3.02	Katz <i>et al.</i> (1995)	2
	3	Fu and Chung (1998)	
	2	Zhu <i>et al.</i> (1997)	
	0.8 to 2.5	Aveston <i>et al.</i> (1974)	
	0.5 to 1.5	Katz and Li (1996)	
	0.9 to 1.7	Li and Stang (1997)	
	2 to 4	Brandt (2009)	
Glass (GF)	2.3	Peled <i>et al.</i> (2006)	1.7
	0.6 to 1.6	Oakley and Proctor (1975)	
	1.4 to 2.2	Kakemi <i>et al.</i> (1996)	
Polypropylene (PP)	0.9 to 1.6	Li and Stang (1997)	1.9
	0.1- 0.3	Redon <i>et al.</i> (2001)	
	3.5	Peled and Bentur (2003)	
	2.7	Peled <i>et al.</i> (2006)	
Polyvinyl alcohol (PVA)	3 to 5 MPa	Li <i>et al.</i> (1990)	3
	2 to 3	Lin <i>et al.</i> (1999)	
	2.4	Peled <i>et al.</i> (2006)	

Next there is a brief introduction to the various studies. Stang (1996) and Peled and Bentur (2003) looked at the influence of varying E_f on the bond. They reported that increasing E_f enhances the strength. Brandt (2009) reported that an increasing bond improved flexural strength, but did not increase toughness, because the higher the bond strength the more brittle became the material behaviour. Oakley and Proctor (1975)

calculated the bond strength for FRCs with GFs. They found it generally ranges from 0.6 to 1.6 MPa. Kakemi *et al.* (1996) found the bond strength to be 1.4 to 2.2 MPa. The bond strength of CFs was investigated by Katz *et al.* (1995), and they found the mean ranged from 0.52 to 3.02 MPa. A study by Fu and Chung (1998) calculated the bond strength for CFs at 3 MPa, which is higher than 2 MPa reported earlier by Zhu *et al.* (1997). Aveston *et al.* (1974) concluded that the bond strength with CFs is from 0.8 to 2.5 MPa. Katz and Li (1996) reported typical bond strength for CF to be 0.5 to 1.5 MPa. Li and Stang (1997) studies with CF and PP fibres gave mean bond strengths from 0.9 to 1.7 MPa and from 0.9 to 1.6 MPa, respectively. Lin *et al.* (1999) studied PVA fibre to show that bond strength ranges from 2 to 3 MPa. Peled and Bentur (2003) concluded from their work that the mean value for PP fibre is 3.5 MPa. A study by Peled *et al.* (2006) determined the bond strength for GF, PVA and PP fibres by a pull-out test method, and they reported a mean of 2.3 MPa, 2.4 MPa and 2.7 MPa, respectively. Brandt (2009) used Equation (2.15) to calculate the bond strength with a CF. He showed it ranges approximately between 2 MPa and 4 MPa, and then confirmed the predictions by test results.

To achieve a strong interfacial bond with a cementitious matrix it is of great importance that the individual filaments are totally embedded in the matrix. This requirement is, as explained above, particularly difficult to meet when the matrix is in particle form and the particles have to be infiltrated between the fibres, there are at least two possible solutions. The first solution suggested by Larson *et al.* (1991), and much later by Stynoski *et al.* (2015) is to have smaller particles (less than 1 μm) in the mix (such as SF (Section 2.8.1)). SF particles will fill the interstices between fibres and cement particles producing better packing and fibre-matrix contact, thereby improving fibre-matrix adhesion. The second solution proposed is to manipulate the fibres either by forcing their

separation to allow cement particle penetration, or, to impregnate the fibre tow with a liquid matrix that avoids the difficulty of opening-up spaces between filaments. Briggs (1977) tested a special arrangement by creating voiding between filaments using compressed air in combination with filament winding processing. Wiberg (2003) found another way for fibre separate is to impregnate tows with a water soluble material. This addition is to be dissolved by water in the mortar at the time of application and thereby change places with cement particles.

In general, as mentioned above there is no easy method to measure interfacial bond stress. The results of pull-out tests generally exhibit a large scatter owing to unstable debonding effects (Purnell, 2001). Bartos and Zhu 1996, and Zhu and Bartos 1997 developed methods to measure the bond strength using high precision micro-indentation apparatus.

Aveston and Kelly (1973), Laws (1982) and Naaman *et al.* (1991) based their modelling on frictional load transfer, and showed that, in the post-cracking zone III, frictional bond controls behaviour. More recent models for FRCs invoke fracture mechanics to model debonding (and hence predict bond) as crack propagation along the fibre-matrix interface. They often require knowledge of parameters such as spacing factors and the shear modulus of the matrix (Shah, 1985) or the bond modulus and end slips of the fibres at the onset of full debonding. Such parameters are difficult for FRCs to measure or establish by analysis methods.

More details on the measurement of bond strength can be found in the work of Purnell *et al.* (1999; 2001). In this study the bond strength itself is not determined. The author decided to use the average bond strength for a fibre type using the values extracted

from the literature and collated in Table 2.3. Bond strength is only needed in this thesis to calculate the critical length l_c using Equation (2.15) in Section 2.15.

2.17 The Fibre Efficiency Factors for Fibre Length and Fibre Orientation

As will be discussed in Chapter 4 fibres distribution in an FRC is determined mainly by the manufacturing process. Choosing the right fibre, fibre length, layout or fibre architecture, is crucial in order that the fibres can be used most efficiently (Purnell, 2010). Fibre efficiency depends upon the three parameters of; fibre length (η_l), fibre orientation (η_θ) and the fibre-matrix shear bond strength (η_τ). Laws (1971) reports that these three factors are not independent, since the effects of both fibre length and orientation are highly sensitive to the bond (Bentur and Mindess, 2007).

The efficiency factors η_l and η_θ can be calculated either empirically, or analytical. As they are used in combination we can write η for the product $\eta_l \eta_\theta$, as introduced in Section 2.9.1, whereas the efficiency factor η_τ may be experimentally determined from a pull-out test. The reliable determination of η_τ is not straightforward because of the difficulties in measuring interfacial bond strength (Purnell, 1999). For this reason η_τ is out of scope in this study, and only the combined efficiency factor η , via η_l and η_θ , is discussed in the rest of the thesis.

In the case of short fibres η_θ is a function of l and l_c . These fibres are rarely oriented in the same direction as the tensile force that is necessary for them to provide maximum reinforcement efficiency. Short fibres should be distributed in a random two-dimensional (2D) or three-dimensional (3D) array as illustrate for a single fibre in Figure 2.9. Contribution of short discontinuous fibres to directional mechanical properties is clearly smaller than that of long continuous fibres; the latter can, for example, be oriented parallel

to the principal load direction. This leads to the concept of fibre efficiency (Purnell 2010, Bentur and Mindess 2007).

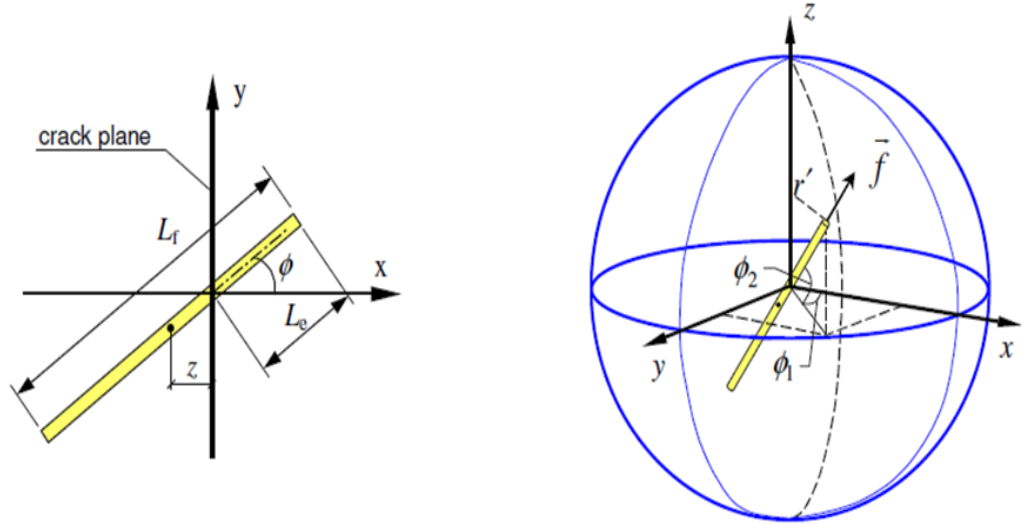


Figure 2.9: Fibre orientation, (a) in 2D and (b) in 3D (Lofgren, 2005).

Figure 2.10 shows estimates for η_1 and η_θ for continuous fibres with different ply orientations. It can be seen that $\eta_1 = 1.0$ in all four cases, because of the continuous length condition. η_θ is 1.0 for the unidirectional situation where filaments are aligned with the loading. For the other three situations in Figure 2.10 we have $\eta_\theta < 1.0$. A balanced biaxial fabric (equal 0° and 90°) has $\eta_\theta = 0.5$. When loading in the 0° direction it means 50% of the fibres are effectively. In case of a multi-axial fabric (equal 0° , 90° and $\pm 45^\circ$), η_θ is found to be 0.38. For more complex fabric layouts the Krenchel equation (1964) can be used for η_θ (see Laws 1971; Bentur and Mindess 2007). It is:

$$\eta_\theta = \sum a_\theta \cos^4 \theta \quad (2.17)$$

where a_θ is the fibre fraction oriented at an angle θ to the applied load.

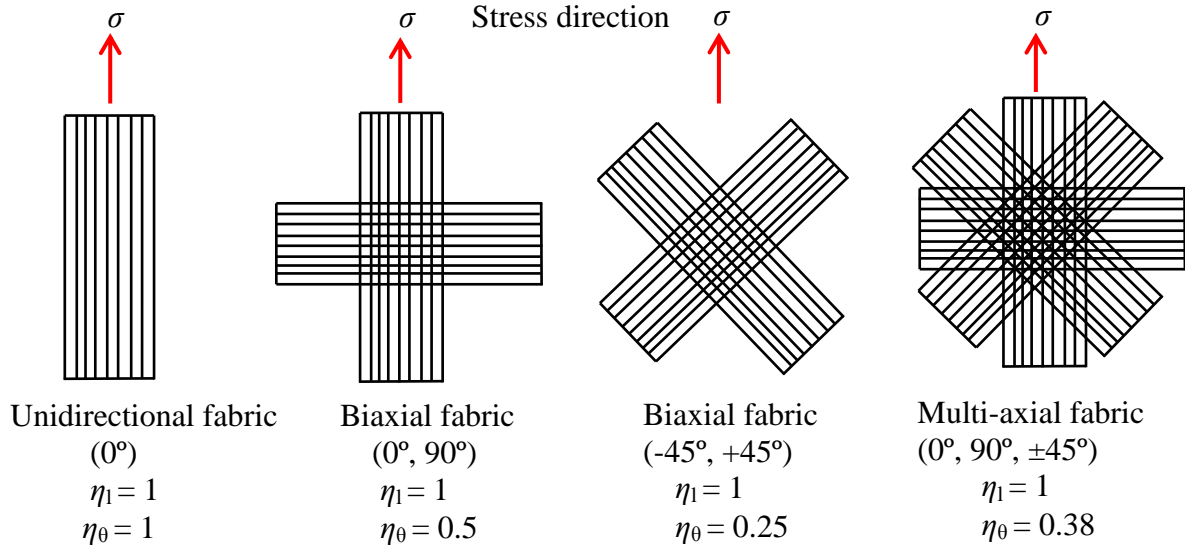


Figure 2.10: Typical estimated efficiency factors; length and orientation (η_l and η_θ), for a simple continuous fibre with different ply orientation (Harris, 1999).

For short fibres η_θ has been determined experimentally, and calculated, using various assumptions, by several researchers and their results do not give consistency as shown by the η_θ collated in Table 2.4. It is noted that all η_θ for 3D short fibres, except from Romualdi and Mandel (1964), Parimi and Rao (1971) and Aveston and Kelly (1973), are close, and in the range 0.17 to 0.33% for the percentage of the fibre properties that are theoretically effective. Romualdi and Mandel (1964), Parimi and Rao (1971) and Aveston and Kelly (1973) estimated higher η_θ in the range 0.41 to 0.64%. These values are seen to have increase by factor of 2. An explanation for this overestimation is based on how they introduce and define the η in their assumptions, which all these data and other information such as l and l_c are unknown and different from each other.

Table 2.4: Orientation efficiency coefficient (η_θ) for short fibres (Brandt, 2009).

Reference	η_θ for 2D	η_θ for 3D
Cox (1952)	0.33	0.17
Krenchel (1964)	0.38	0.2
Romualdi and Mandel (1964)	-	0.41
Laws (1971)	0.38	0.2
Parimi and Rao (1971)	-	0.5 - 0.64
Kar and Pal (1972)	0.44	0.33
Aveston and Kelly (1973)	0.64	0.5
Aveston <i>et al.</i> (1974)	0.5	0.21

Cox (1952) introduced η_l into the Rule-of-Mixtures to calculate E_c and σ_c in the pre-cracking zone I. Latter, Krenchel (1964) extended Cox's work by taking fibre orientation into account by adding η_θ into the Rule-of-Mixtures to give Equations (2.5) and (2.6) in Section 2.9.1. These equations are based on the model in which η_l and η_θ are combined into η , and so Equations (2.5) and (2.6) can be rewritten as:

$$E_c = E_m(1 - V_f) + \eta E_f V_f \quad (2.18)$$

$$\sigma_c = \sigma_m(1 - V_f) + \eta \sigma_f V_f \quad (2.19)$$

By introducing η , Equations (2.7) and (2.8) for the post-cracking zone II, can be written as:

$$E_c = \eta E_f V_f \quad (2.20)$$

$$\sigma_c = \eta \sigma_f V_f \quad (2.21)$$

η is maximum and 1.0 when all fibres are continuous and are all oriented parallel to the applied tensile stress. It is a minimum and zero when fibres are all oriented perpendicular to the deformation. This latter condition assumes that there is no improvement in matrix strength from having the fibres. Purnell (2007; 2010) summarised

the typical η for different fibre layouts and his results are reproduced in Figure 2.11. As an example the 3D short fibre layout having $\eta = 0.13$ requires seven times the V_f to achieve the same effective V_f (for same FRC stiffness and strength) as does the 1D long fibre layout with $\eta = 1.0$.

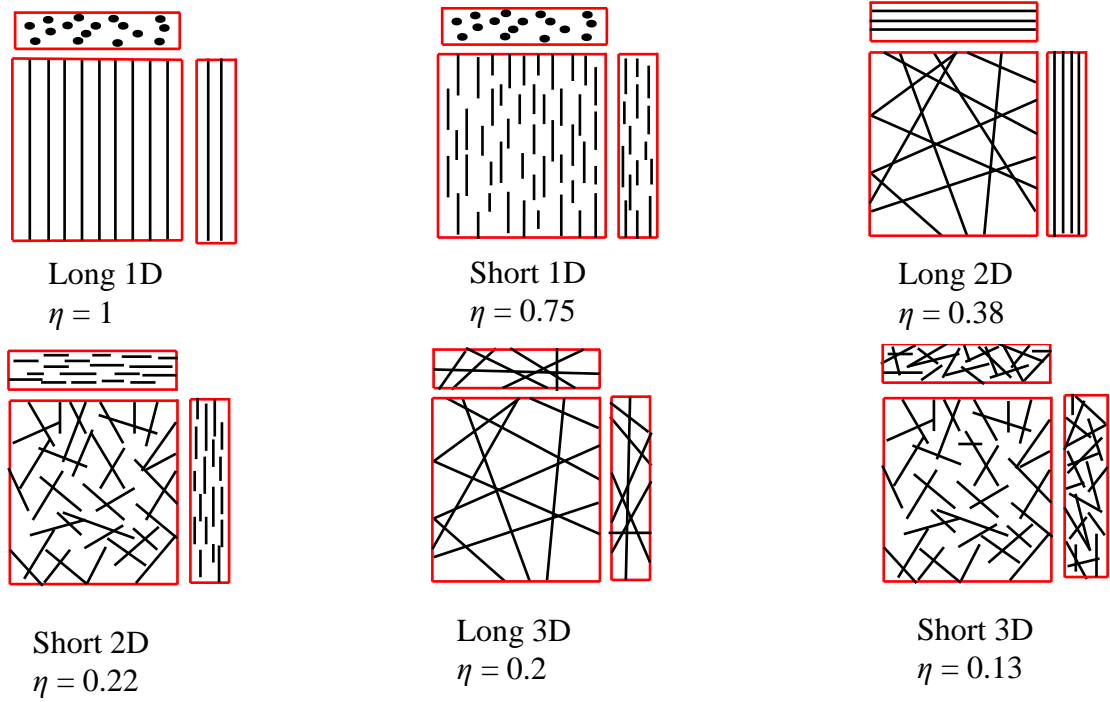


Figure 2.11: Combined Efficiency factor (η) for different fibre layouts (Purnell, 2010).

Discussion on what η should be may be considered an interesting refinement because it is difficult to verify quantitatively. η for short fibres in a 3D randomly distribution can be calculated from (Laws, 1971):

$$\text{If } l \geq \frac{10}{7}l_c \quad \eta = \frac{1}{5} \left(1 - \frac{5}{7} \cdot \frac{l_c}{l} \right) \quad (2.22)$$

$$\text{For } l \leq \frac{10}{7}l_c \quad \eta = \frac{7}{100} \left(\frac{l}{l_c} \right) \quad (2.23)$$

Equations (2.22) and (2.23) depend on l_c and l , and from work by Bentur and Mindess (2007) and Purnell (2010) they appear to have become accepted as giving reasonable results for η . The author decided to use them in Chapter 6 to predict η for short fibre FRCs produced for the PhD work.

η values taken from Figure 2.10 are used with the continuous fibre FRCs investigated by the author and reported in Chapter 7.

The combined efficiency factor (η) is used to obtain the effective fibre volume fraction V_f' from,

$$V_f' = \eta V_f \quad (2.24)$$

For example, for a continuous unidirectional reinforcement (0°) aligned to the load direction we have $\eta = 1$ and therefore $V_f' = V_f$ (i.e. the fibres are fully effectively). This is rarely the layout and so for the majority of FRCs $\eta < 1$. Table 2.5 gives some examples using Equation (2.24) for how to calculate V_f' for FRCs with continuous fibre reinforcement. It can be seen from Table 2.5 that V_f is taken to be 5% for the FRC with biaxial fabric ($+45^\circ, -45^\circ$). Using Equation (2.24) V_f' is determined to be 1.3%, and so we see that the reinforcement is 25% effective. This result is similar to the case of having short fibres in a 3D random distribution.

Table 2.5: Examples for how to calculate the effective fibre volume fraction (V_f').

Fibre type	V_f (%)	η_l	η_θ	$\eta = \eta_l \eta_\theta$	$V_f' = \eta V_f$ (%)
Unidirectional fabric (0°)	5	1	1	1	5
Biaxial fabric ($0^\circ, 90^\circ$)	5	1	0.5	0.5	2.5
Biaxial fabric ($+45^\circ, -45^\circ$)	5	1	0.25	0.25	1.3
Multiaxial fabric ($0^\circ, 90^\circ, \pm 45^\circ$)	5	1	0.38	0.38	1.9

2.18 Fracture Mechanics

We know that FRCs are heterogeneous materials with complex microstructures. They can be modelled at various scale levels, including at: nano; micro; meso; macro (Gdoutos, 2005). In their fracture analysis there is a micro-cracking zone adjacent to a crack front (known as the Fracture Process Zone (FPZ)) having non-linear material behaviour. A model for the physical situation is given in Figure 2.12 (Purnell, 1998). As discussed in Section 2.18.1 application of LEFM requires the FPZ to be relatively small. The stress distribution within the FPZ has to be considered explicitly in the analysis of crack propagation (Zhang and Li, 2004). The dimensions of the FPZ depend on the size of the structure and the length of the initial crack, as well as on the loading and FRC material properties too. In the zone's sphere of influence the interlocking crack surfaces contribute to a gradual decline in stress that prevents sudden failure (Esfahani, 2007).

Wecharatana and Shah (1983) first proposed the ideal crack model illustrated in Figure 2.12. It is divided into the following three distinct zones:

- a traction free zone where no fibres and/or aggregates interlock is available for bridging.
- a fibre bridging zone.
- an aggregate bridging zone, where both fibre and aggregate bridge the crack.

The latter two zones are for the FPZ.

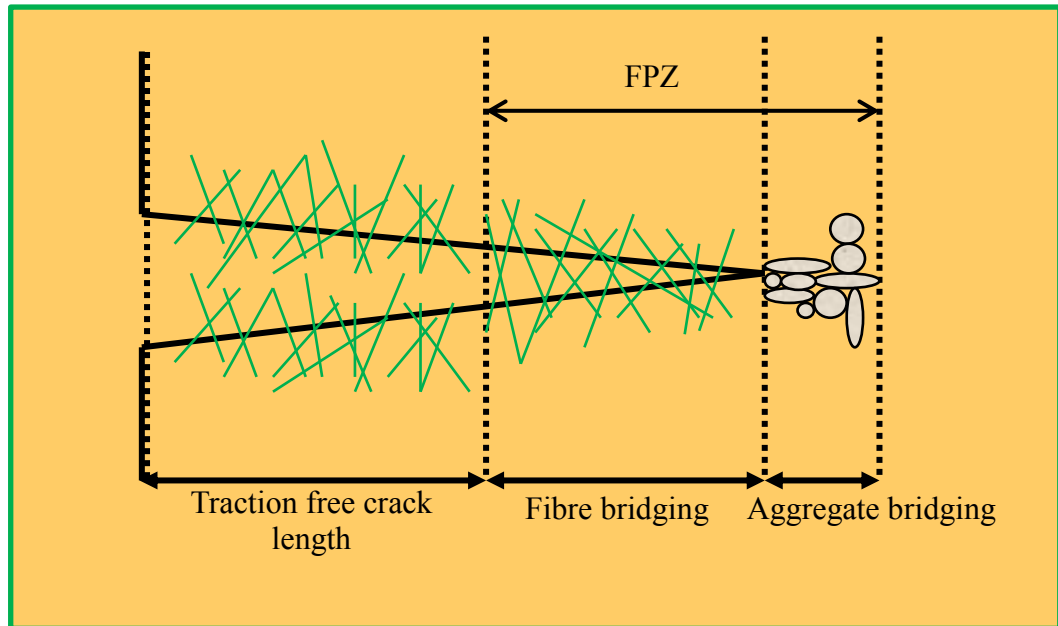


Figure 2.12: Fracture process zone (FPZ) in FRC (Wecharatana and Shah 1983; Purnell 1998).

2.18.1 Fracture Mechanics Principles: LEFM and NLFM

Griffith (1921) introduced Linear Elastic Fracture Mechanics (LEFM) with an energy balance approach for fracture of brittle materials, such as glasses. Griffith's work was significant, yet it did not cover materials that were not brittle on failure. Irwin (1957) began to see how the theory could be applied to ductile materials, such as metals. He determined that there was an energy contribution from plastic deformation that had to be added to the surface energy from Griffith, in order for the theory to work. Irwin created what we understand as the strain energy release rate.

Griffith theory forms the basis for LEFM (Denneman, 2011) and Romualdi and Batson (1963) were the first to use it with FRCs. They reported that there is a strain mismatch between the matrix and fibres caused by stress concentrations at the crack tip, as the cracks begin to form. The assumption in LEFM implies that the energy dissipation occurs only at the crack tip, while the rest of the body remains linear elastic. This limiting

assumption is only valid when the FPZ is small in size compared to the size of the specimen. In general the application of LEFM is very limited with heterogeneous materials such as FRCs. With metals the material in the non-linear zone undergoes either hardening or perfect plasticity and because the size of FPZ is negligible LEFM applies (Gdoutos 2005; Idiart 2009). In concretes the material undergoes softening damage (quasi-brittle) and the size of the FPZ is sufficiently large that its size must be taken into account. This is why NonLinear Fracture Mechanics (NLFM) is appropriate (Section 2.18) and was first proposed by Hillerborg *et al.* (1976) by the introduction of their celebrated Fictitious Crack Model (FCM). To explain why the fracture processes in FRC materials is complex we note that in addition to crack closing pressure from aggregate interlocking the presence of fibre bridging behind the tip of a propagating crack (where fibres undergo bond-slip processes) also provides additional closing pressures. Previous studies by Kaplan (1961), Hibbert and Hannant (1982), Wittmann and Hu (1991), Shah *et al.* (1995), Zhang and Li (2004), Mobasher (2011) and Shahbazpanahi *et al.* (2013) have applied LEFM to FRC materials. They found LEFM is not suitable because of heterogeneity in the microstructure, strain softening, a large FPZ, chaotic crack propagation and a difficulty in determining where the crack tip is because of fibre bridging. Their work can be used to make the conclusion that the fracture analysis of FRCs requires NLFM.

2.19 Summary to the Literature Review

The theoretical mechanics for the mechanical properties of an FRC have been reviewed based on the Rule of Mixtures approach (Section 2.13). According to the ACK model there are three distinct zones in the tensile stress-strain curves. They are zones for pre-cracking, multiple cracking and post-cracking. In general, it has been found from the literature that non-uniform dispersion and a non-uniform fibre orientation limits the stress

development in short-fibre FRCs. To improve bond between fibres and matrix many researchers have introduced pozzolanics, such as, SF, PFA, and GGBS into the mix as they reduce the amount of calcium hydroxide and increases the amount of calcium silicate hydrate (Section 2.8). For strain-hardening to occur the FRC must enable the multiple cracking zone to develop and grow without ultimate failure. This requires a relatively high fibre volume fraction and continuous fibres (Sections 2.13 and 2.14).

From the literature covered it can be seen that changes in the mechanical properties of FRCs are influenced by the: type of fibre; fibre volume fraction; geometry aspect ratio; distribution of fibres; orientations of fibres; manufacturing process and interfacial bonding strength. Most researchers agreed that the fibres having hydrophilic characteristics, such as polyvinyl alcohol (PVA), will develop the best bond (Section 2.4.2). On the other hand, it is feasible to use hydrophobic fibres, such as polypropylene (PP), which result in relatively weaker bonding. One important aspect coming out of the literature review is that the interfacial bond strength increases with time. Another major issue is that this shear strength is the difficulty to measure (Section 2.16).

By way of the literature review it is noted that previous work has studied FRCs with short fibre having V_f from 0.1 to 2 %, and continuous fibres having V_f from 3 to 10% (Section 2.14). There are several methods to produce an FRC, which have difference in fibre processing and manufacturing procedures. Conventional mixing (casting) is the manufacturing process for short fibre FRCs and other methods when reinforcement is continuous fibres include Hatschek, spray-up, hand lay-up, pultrusion, extrusion and compression moulding (Section 2.6). It is observed that the processing method of compression moulding is novel and has not previously been thoroughly investigated. Given that this method for processing FRCs should improve the quality of green form material,

(in terms of consolidation and lower water/binder ratio) there is justification for the research work reported in Chapters 4 to 7.

From the review it can be observed that the simple and conventional process of hand lay-up (Section 2.6.2) has a major advantage, in that a $V_f > 10\%$ can be achieved. The resulting FRC should be able to provide the desirable multiple cracking zone leading to improved toughness (energy absorption). Given this processing benefit the hand lay-up method is used by the author to produce FRCs with V_f up to 15%. Fully discussed in Chapters 6 and 7 is the influence of hand lay-up and compression moulding methods on the mechanical properties (flexural and toughness) of FRCs of both short and continuous fibre reinforcements.

The theoretical models found in the literature have been shown to give a good indication of the developing crack pattern. Moreover, they are seen to be useful for researchers to understand and explain the fracture behaviour observed in FRCs subjected to tensile loading. The review highlights that there are problems related to the application of these models because none is found to be consistent enough to describe all failure mechanisms. This weakness is attributed to the fact that the fibre-matrix interface is quite complex (as discussed in Section 2.11).

The next two chapters report on a development programme undertaken to establish a suitable mix design that can address the gaps in knowledge that have been uncovered from the literature review. Two manufacturing processes are investigated in Chapter 4 to produce 'green' forms, one by novel compression moulding and the other by hand lay-up. To make the matrix have sustainable credentials in FRC materials it is practical to consider pozzolans (e.g. silica fume (SF), pulverised fuel ash (PFA), and ground granulated blast furnace slag (GGBS)) as partial substitution to cement (see Chapter 5).

As much as the author can be aware of from the literature review, the use of the compression moulding process to make FRC materials has not previously been thoroughly investigated. Farahi (2009) did make a few specimens at the University of Warwick and found the process to be unsuccessful. There is justification for the new research work reported in Chapters 4 to 7 given that compression moulding has the potential to improve the quality of 'green' form material, by minimising porosity, increasing the degree of consolidation, reducing the water/binder ratio and improving the penetrability of the cement matrix into the fabric and the filaments of the tows or bundles,

The review of literature has further informed the author to conduct research work that considered the following challenges of:

- ensuring a uniform distribution of short fibres in a cementitious mix having the highest practical volume fraction.
- finding out what is the most suitable fibre type for reinforcement by short fibres.
- finding out what is the required volume fraction of fabric reinforcement for the highest properties determined using a four-point bending test method.
- determining what fabric type(s) give the highest mechanical properties.
- modifying reinforcement fabrics that have been produced to manufacture polymer composite materials so that they are more suitable for reinforcing a cementitious matrix, and, thereby, achieving a relatively high overall bond strength as established by higher mechanical properties determined using a four-point bending test method.

Chapter 3

3. Materials and Experimental Procedures

3.1 Introduction

This chapter describes the raw materials used in the PhD work, the processing methods employed to manufacture the test specimens (referred to as green forms), sample preparation and equipment. It also considers preliminary design and planning such as: the selection of coarse and fine aggregates, fibres and additives, and mix design and the number of mix batches and concrete specimens required to meet the scope of the research aims and objectives.

This chapter then discusses the mechanical and microstructural analysis employed to determine the influence of the mix design, curing process, etc; on the mechanical properties of specimens. The results of flexural strengths are presented in Chapter 6 for short fibres and Chapter 7 for continuous fibres.

3.2 Materials

A wide range of mixes from the cementitious matrix were examined in this study to determine the optimum mix design. Here the term “optimum mix design” refers to the range of mix combination that, as well as being capable of producing green forms with adequate green strength, gives a quality surface finish and exhibits significant enhancement in both mechanical and microstructural properties. In this study, the binders used were combinations of cement (C), silica fume (SF), pulverised fuel ash PFA, and ground granulated blast furnace slag (GGBS). Green forms were produced from various

combinations of binder and filler (aggregates) as well as a range of additives, fibres and fabrics, and manufactured from different novel processing techniques that are explained in Chapter 4.

3.2.1 Cement (C)

To prevent influences resulting from the use of different types of cement, only Rugby premium Portland-limestone cement was used. The cement, given label C is produced in Rugby by CEMEX UK and complies with BS EN 197-1:2000 – CEM II/A-L32, 5R. It contains 6-20% limestone, but no PFA added. This is also the most common type of cement used for making conventional concrete and is suitable for use in general concreting and cements related works. C has relatively small particles with sizes in the range of 5 μm to 125 μm . The C particles sizes were measured by two methods; laser diffraction analyser as discussed in Section 3.3.2 and by Scanning Electron Microscopy (SEM) as discussed in Section 3.4.

3.2.2 Supplementary Cementing Materials (Additives)

As introduced in Chapter 5 three additives, silica fume (SF), pulverised fuel ash (PFA), and ground granulated blast furnace slag (GGBS) were added into the mix as cement replacement materials. These three additives were used to:

- improve strength in the hardened state and durability by creating a denser cement matrix.
- reduce cost.
- improve dispersion of short fibres using SF.
- decrease the alkali-silica reactivity.

- reduce drying shrinkage.
- reduce creep rate.
- reduce permeability due to small particles.
- control the rate of hydration, confer environmental benefits.
- reduce cement contents and improved service life (see Section 2.8).

Table 3.1 presents the typical physical properties for the three additives of SF, PFA, and GGBS, as received from the suppliers. It can be seen from the data in Table 3.1 that the additives have spherical or microspheres particles with sizes in the range of 0.1 to 160 μm .

Table 3.1: Physical properties for additives SF, PFA, and GGBS.

Physical Property	SF	PFA	GGBS
Surface area (m^2/kg)	13000 – 30000	500	450 to 550
Bulk density (kg/m^3)	Standard 280 approx. Compacted 500 approx. Densified 640 approx.	1200 to 1700	1000 to 1100 (loose)
			1200 to 1300 (vibrated)
Specific gravity g/cm^3	2.2	1.8 to 2.4	2.9
Average particle size (μm)	0.1 - 0.2	2 - 160	5-70
Particle shape	Spherical Irregular angular	Spherical	Spherical Irregular angular
Colour	light and dark grey	grey	Off white

SF, also known as micro silica, is waste product of the silicon industry and contains 95-99% active silica by weight as discussed in Section 2.8.1. SF was supplied by Rockbond SCP Ltd. and consists mainly of spherical particles or microspheres. SF particles are extremely small; with more than 95% of the particles having a diameter $< 1 \mu\text{m}$. SF particles are usually grey in colour and darker or lighter according to their carbon and iron content. The specific surface area of SF ranges from 13,000 to 30,000 m^2/kg (Table 3.1). It also has a bulk density of 280 kg/m^3 (Siddique, 2011). Due to the small particles SF can fill the voids between the particles of cement hence improving packing between the fibre and

cement particles to develop the fibre-matrix bond (Larson *et al.*, 1991). The SF sourced conformed to European Standard BS EN 13263-1:2005+A1:2009.

PFA is a by-product produced from the burning of pulverized coal in power stations (see Section 2.8.2). It was supplied by Tarmac Ltd and consists mostly of silicon dioxide (SiO_2). Generally, PFA particles are spherical and they range in size from 2 to 160 μm . The advantage of PFA into cementitious materials is discussed in Section 2.8.2. The PFA sourced conformed to European Standard BS EN 450-1:2005+A1:2007.

GGBS is produced as a by-product during the manufacture of iron as discussed in Section 2.8.3. GGBS was supplied by the Hanson Heidelberg Cement Group, and has particles ranging in size from 5 to 70 μm (Table 3.1). The GGBS sourced conformed to either BS 6699:1992, or the European Standard BS EN 15167-1:2006, which has replaced the British Standard. These two standards contain similar requirements and, generally, GGBS that conforms to one standard will conform to the other.

3.2.3 Aggregates (A)

Aggregates (A) for the mix designs were combinations of foundry sand (S) for the fine aggregates, crushed limestone (CL), and crushed granite aggregate (GA) for the coarse aggregates. S, which is silica sand, has uniform physical characteristics and was supplied by Sibelco UK Ltd. It contains a high proportion of silica (normally more than 95% SiO_2). Physical and chemical characteristics of S depend upon the type of casting process. For most applications, silica sands have to conform to very closely defined specifications and consistency in quality is of critical importance. Particular uses often require different combinations of properties. The grain size distribution of S is uniform, with 85-95% of the material between 150 to 300 μm and only 5 to 12% smaller than 75 μm . S is generally sub-

angular to round in shape. In cementitious materials S provides excellent compaction, thereby helping to maximise bond strength and promote a good casting finish. It is used to improve both the flexural and tensile strengths of cementitious materials. For these reasons, S was selected in this study as a replacement for conventional fine aggregates.

GA and CL were both supplied by Tarmac Ltd. Given that the aggregates were stored outside, before adding into a mix they were dried in an oven with a temperature set at 105°C for 24 hours. The drying procedure removed the excess water locked within the particles. Given that the trapezoidal cross section of the flexural specimens is typically, 22/33 mm wide × 16 mm deep (as discussed in Chapter 4), it was decided that aggregate particles of a size > 2.36 mm should not be in the mix. Both the GA and CL materials were therefore passed through a 2.36 mm mesh sieve to collect and remove the larger particles. A sieve analysis was then performed on all aggregate types to investigate the range of Particle Size Distribution (PSD) within them. The technique and analysis procedure is fully discussed in Section 3.3.1. The influence of GA and CL on flexural strength of FRC is explained in Section 5.5.

3.2.4 Reinforcement Fibres

In this study, the influence of the manufacture processing (compression moulding and hand lay-up) on the engineering properties, flexural strength, toughness, and the microstructure of fibre reinforced specimens made from different types, forms, and resources of fibres was studied. The influence of twelve different types of fibres (short and fabric forms) was scoped. Five types were of short fibres, and the other seven types were of continuous fibres (fabrics), all types gave a different fibre volume fraction (V_f) (over 2%).

All of these reinforcements were chosen after a careful preliminary examination for the matrix penetration and flexural strength. A limit in choice was the fibre types available in the UK. Densities of the fibres were measured using Helium pycnometer (Section 3.5) and this data used in Chapters 6 and 7 to calculate V_f for each batch of FRC. The short fibres consisted of:

- a) recycled milled carbon fibre (CF1). b) recycled chopped carbon fibre (CF2).
- c) chopped carbon fibre (CF3). d) chopped polypropylene fibre (PP).
- e) chopped polyvinyl alcohol fibre (PVA).

The first three reinforcements were of carbon and the last two of polypropylene and polyvinyl alcohol. The manufacturer's data is given in Table 3.2 and Figure 3.1 shows how these short fibres look. The strengths of a single filament and the technical information such as the sizing were provided by the manufacturers. CF1 and CF2 fibres were made by recycling CF from waste carbon fibres products and supplied from the same manufacturer (see Table 3.2).

Table 3.2: Manufacturer's data for short fibres.

Fibre type	Tensile strength (MPa)	Modulus of elasticity (GPa)	Diameter (μm)	Length (mm)	Fibre density (g/cm^3)	Supplier name
CF1	3150	200	7	0.085	1.71	Recycled Carbon Fibre Ltd.
CF2	3150	200	7	3-25	1.77	Recycled Carbon Fibre Ltd.
CF3	3600	225	8	6	1.85	SGL Carbon Fibres Ltd.
PP	413	5	38	12	0.92	Propex Concrete Systems Ltd.
PVA	780	31	31	8	1.40	Morgan

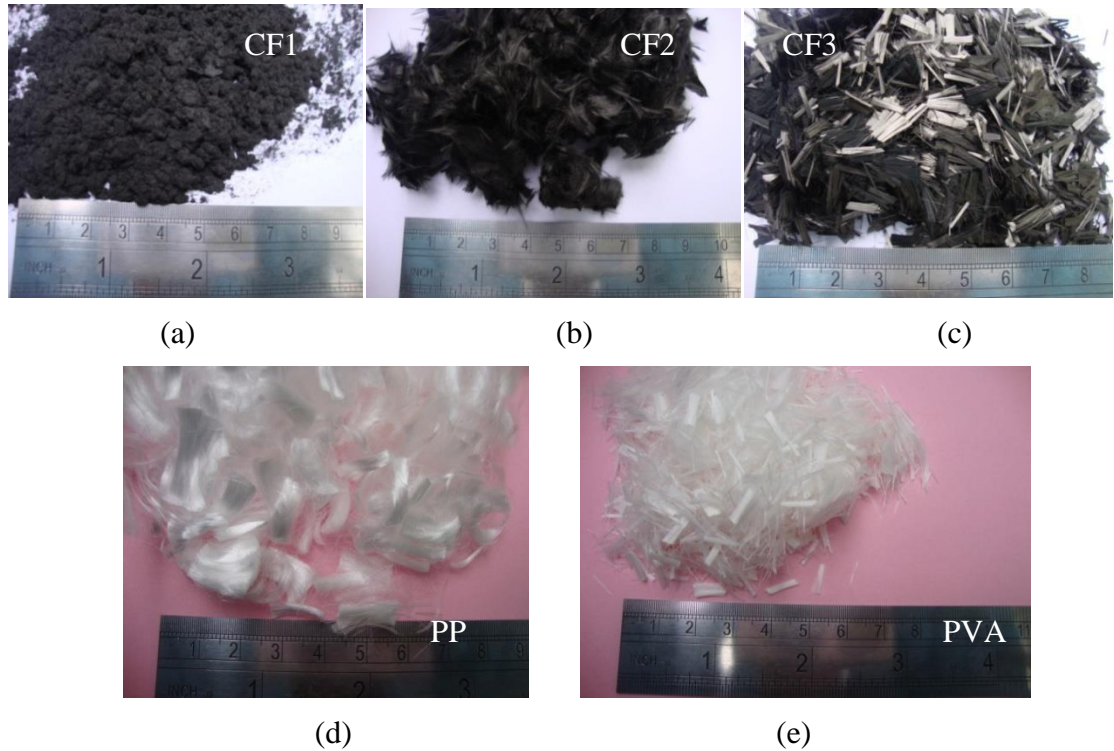


Figure 3.1: Five types of short fibres: a) recycled milled carbon fibre (CF1); b) recycled chopped carbon fibre (CF2); c) chopped carbon fibre (CF3); d) chopped polypropylene fibre (PP); e) chopped polyvinyl alcohol fibre (PVA).

In this study, six of the seven continuous fibre reinforcements are of carbon, and only one is of E-glass. All of the reinforcements are in a fabric form and were produced to be used with a polymer based matrix. None had been designed specially to be used with a cementitious matrix. There are three forms of carbon fabric. One of these forms is a unidirectional fabric (0°); three of these fabrics CF4 at 200 g/m^2 ; CF5 at 300 g/m^2 and CF6 at 450 g/m^2 . A second form is a biaxial fabric ($0^\circ, 90^\circ$). One type has a hybrid form (CF7) with 40% of carbon fibres in the 0° direction and 60% of glass fibres in 90° direction. The second type (CF8) had 100% of carbon fibres in both directions (0° and 90°). The third form was a multiaxial fabric (CF9). It comprised of four unidirectional fibre layers, one in each direction of $0^\circ, 90^\circ, -45^\circ$ and $+45^\circ$. The final fabric is the E-glass biaxial fabric (GF) ($0^\circ, 90^\circ$). Figure 3.2 provides various general sketches of the layer

orientations in the various fabrics and Figure 3.3 shows the seven types of continuous fabrics. The supplier's data for the fibres is given in Table 3.3.

The basic carbon fibre forms are bundles of continuous fibres called tows. A carbon fibre tow consists of thousands of continuous, untwisted filaments, with the filament count designated by a number followed by "K," indicating multiplication by 1,000 (e.g., 12K indicates a filament count of 12,000) (see Table 3.3). The surface of GF as informed by the supplier is treated with a proprietary mineral filled organic binder system. The suppliers told the author that the surfaces of carbon fibres are sized with silane materials.

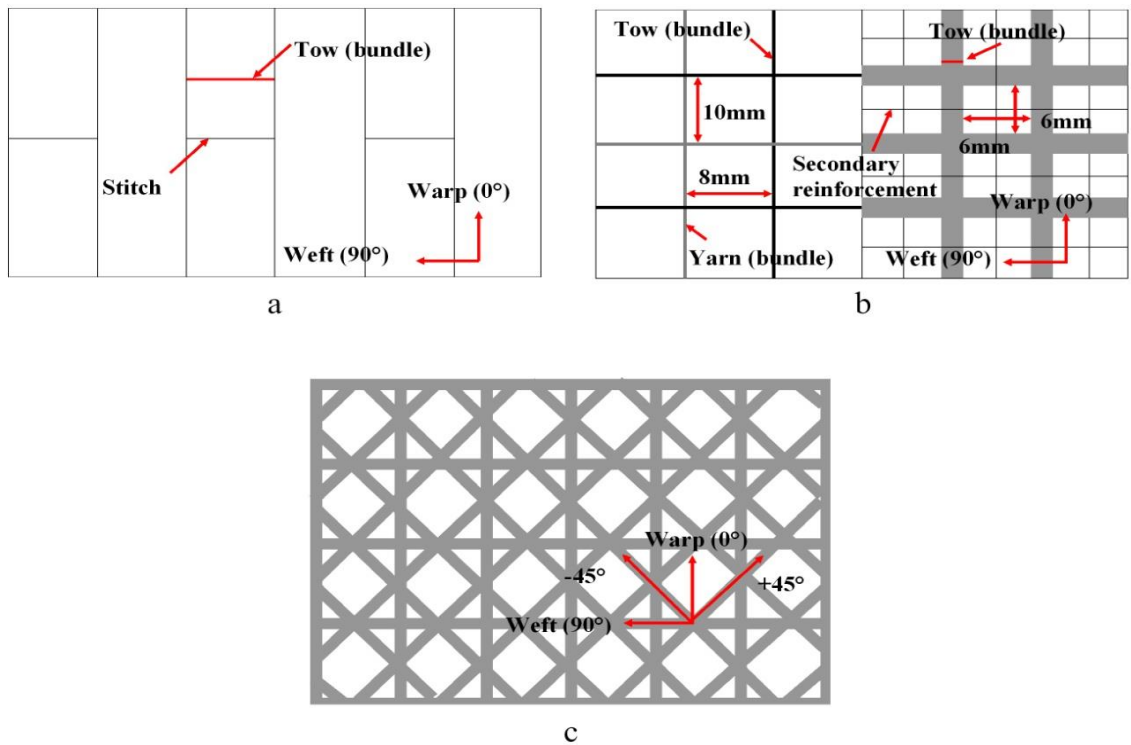


Figure 3.2: Layer orientations for the fabrics: a) unidirectional fabric, b) biaxial fabric and c) multiaxial fabric.

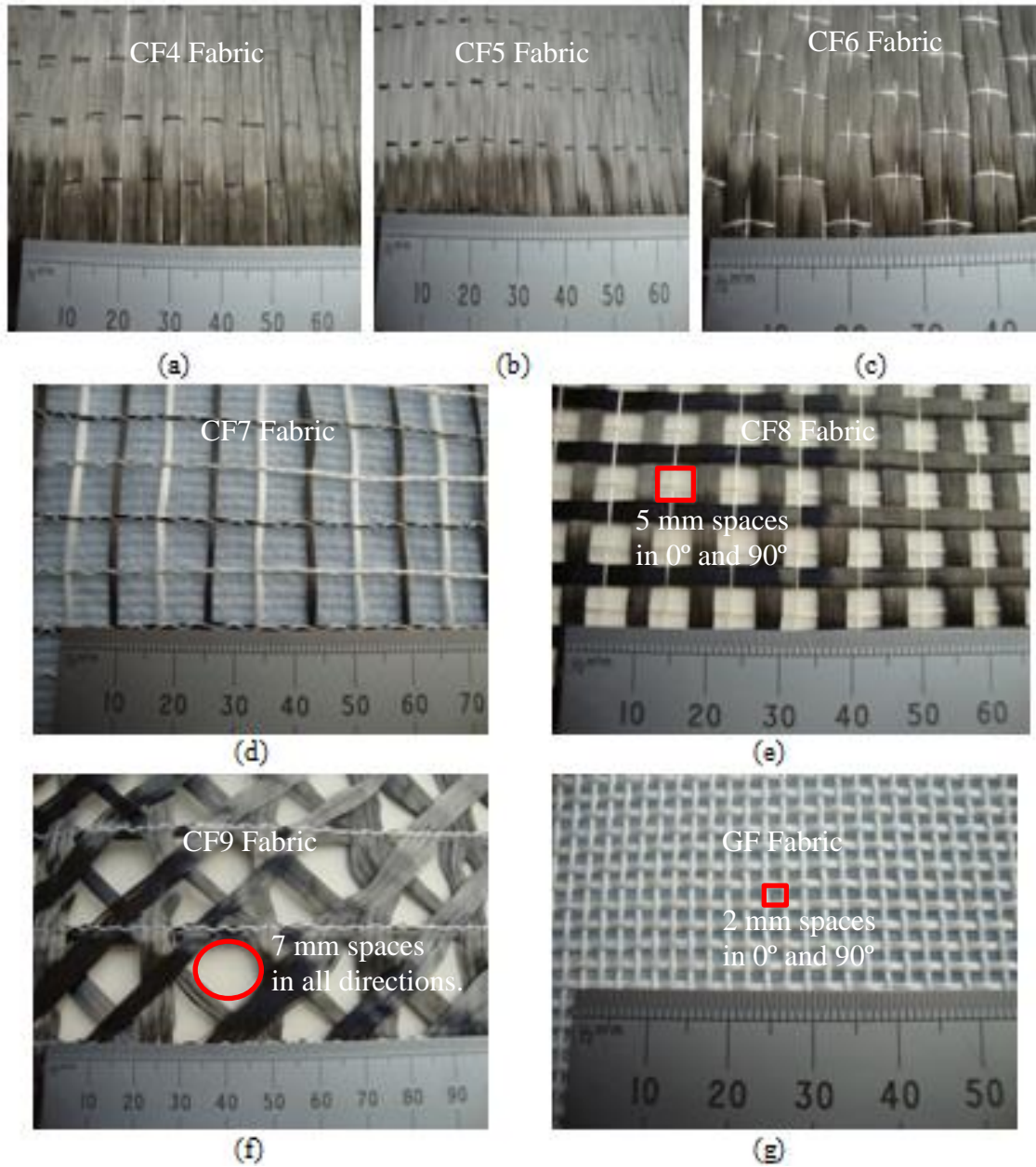


Figure 3.3: Seven types of continuous fibres: a) CF4, b) CF5, c) CF6, d) CF7, e) CF8, f) CF9 and g) GF.

Table 3.3: Manufacturer's data for seven continuous fibres.

Fibre type	Tensile strength (MPa)	Modulus of elasticity (GPa)	Filament diameter (μm)	Thickness (mm)	Fibre density (g/cm^3)	Weight (g/m^2)	No. of filaments in a bundle (K)	Supplier name
CF4	3800	236	7	0.25	1.78	200	12000	Marineware Ltd.
CF5	3800	236	7	0.50	1.79	300	12000	Marineware Ltd.
CF6	4900	230	7	0.55	1.84	450	12000	Carr Reinforcements Ltd.
CF7	1860	135	7	0.40	1.77	155	3000	Formax UK Ltd.
CF8	3500	200	7	0.50	1.99	67	12000	Cristex Ltd.
CF9	4900	240	7	0.65	1.78	170	12000	Formax UK Ltd.
GF	1900	70	9	0.70	2.54	357	204	Fothergill Eng. Fabrics Ltd.

All the carbon fabrics in this study were manufactured from single filaments produced by Toray in Japan. Toray fibres are classified into two main types, labelled T and M in Figure 3.4 which plots fibre tensile modulus against tensile strength. T denotes high tensile strength, while M indicates high tensile modulus. Originally the three or four digit numbers in Figure 3.4 for T type designated the approximate tensile strength. In the case of M type fibres; the two digit numbers in Figure 3.4 designates the approximate tensile modulus. According to Toray's classification the fabrics CF4, CF5, CF6, CF8, and CF9 are T700 (see terminology), while CF7 is T300 (see terminology). Both of these fibres have a standard tensile modulus of about 230 GPa. The difference is that T700 has a tensile strength close to 5000 MPa and this is about 3500 MPa higher than for the fibre T300.

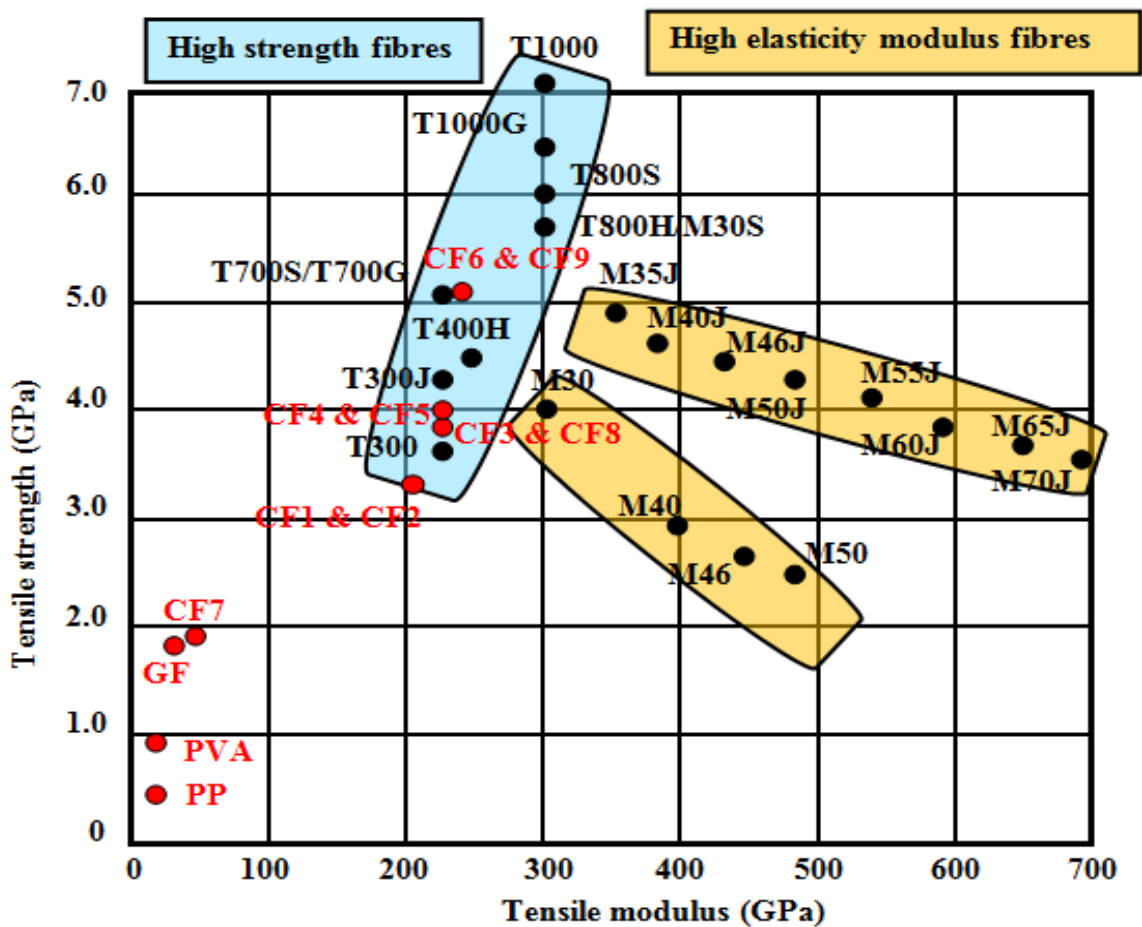


Figure 3.4: Toray's tensile strength and modulus grades of carbon fibres (Kamiura, 2010).

In general carbon fibres are considered to have very good durability in both alkaline and acid environments (Machida, 1993). E-glass fibres on the other hand, are known to be highly susceptible to attack in the strongly alkaline environment of the cementitious matrix (see Section 2.4.1). This alkaline environment damages GF fibres through loss in strength and through embrittlement. The author's research doesn't aim to study the long-term durability; specimens were only tested in four-point bending after 28 days (short-term). As previous work by Robert and Benmokrane (2010), shows there to be no loss in strength in the short-term durability of FRC with GF fibre. However, they concluded that the results showed a slight decrease 6 to 11% in the tensile strength after 240 days as discussed in details in Section 2.4.1. For this reason, it was decided to use the E-glass fabric preliminary fact finding in this study. The geometry of GF fabric provided a mesh having different distinctive openings between every two adjacent roving in 0° and 90° directions, as shown in Figure 3.2(g), to allow the matrix to bridge cross the reinforcement layers. As the spacing of 2 mm is between two bundles in both directions (0° and 90°) the openings have a plan area of 4 mm^2 .

3.2.5 Superplasticisers (SPs)

Superplasticiser (SP), also known as a high range water reducing admixture, is a high molecular weight and water soluble polymer, capable of achieving specific mix workability at a much lower w/c ratio. Thus addition of SP makes the cementitious mixture workable and suitable to cast, without any reduction in cement content and strength. A SP can reduce water content by about 15- 40%, or even higher. The reason for the higher workability is that the addition of a SP causes cement particles to disperse and repel each other (Neville, 2003).

To obtain the most effective SP in mix design required the type and the optimum dosage of SP must be determined early in the design stage by testing trial mix designs. The influence on the workability of various SP products was tested by measuring the slump and rheological properties. To obtain sufficient consistency in short fibre reinforced mixes, four SPs of the polycarboxylic type were studied. The influence of the following four types of SP on the slump and flexural strength of FRC specimens were investigated and CF1 fibre was used in all mixes:

1. Tegla SP Extra is an admixture based on the polycarboxylate technology.
2. Glenium 51 is an innovative admixture based on modified polycarboxylic ether.
3. Glenium 271 is a unique based on modified polycarboxylic ether.
4. Glenium ACE 333 is part of the innovative range of polycarboxylic ether.

Tegla SP Extra was supplied by Christeysn Oscrete Construction Products, with the other three supplied by BASF UK Ltd. These four types comply with BS EN934 Part 2 (2009). In the rest of the thesis they are given the labels SP_A, SP_B, SP_C, and SP_D, respectively.

3.2.6 Water (W)

Water quality has been a matter of concern in concrete construction for long time (Neville, 2001). Water is needed to chemically react with the cement (hydration) and to provide the workability with the concrete. Most specifications require the use of potable water because its chemical composition is known and well regulated. When water contains sufficient amounts of dissolved or solid impurities, it must not be used to prepare concretes. Because the quality of the mixing water can influence the setting time, the strength of fresh and hardened concrete and corrosion to the reinforcement. For these reasons, potable tap water was used in this study for mixing the FRC. Water for

production of concrete complies with European Standards BS EN 1008:2002 and AASHTO T 26-79 (2004).

3.3 Particle Size Distribution (PSD) Analysis

Particle Size Distribution (PSD) analysis was carried out for the range of aggregates (S, CL, and GA) and binders (C, SF, GGBS, and PFA), using two methods; sieve analysis for S, CL, and GA and laser diffraction analysis for C, SF, GGBS, and PFA.

3.3.1 Sieve Analysis

The sieve analysis, commonly known as the "gradation test", determines the gradation (the distribution of both fine and coarse aggregate particles, by size, within a given sample) in order to determine compliance with design, production control requirements, and verification specifications. The aggregate grading influences the water demand and the workability of the concrete and can affect the strength and other properties of the hardened concrete. It is possible to see whether the grading of the sample matches up to the specification, or whether it is too coarse, too fine or 'deficient in a particular size' (Neville, 1995). Sieve analysis was carried out on S, GA, and CL before their use in the experimental work. Suitable stacks of sieves were used for each analysis in accordance with BS 812: Part 105:1989 and BS 410-1:2000.

Before any sieve analysis was performed, all the aggregates must be air dried. Neville (1995) noted that the main reasons are to avoid lumps of fine particles being classified as large particles and to prevent the clogging of finer sieves. GA and CL were sieved to limit the maximum size of 2.36 mm, while S was sieved to confirm it meets the specification stated in BS 882: 1992. The grading limits for aggregates according to BS 882-1992 are given in Table 3.4. The sieve analysis technique works by dividing the

sample into fractions, each fraction containing particles between specific limits. For this work, seven sieve sizes ranging from < 5 mm to < 75 µm were mounted in the frame in order of size; the largest sieve size was at the top. The test begins by placing 1 kg of the material in the top sieve. The vibrator is turned and left for 30 minutes. After shaking, the retained materials on top of each sieve represent the fraction of aggregate coarser than the sieve in question, but finer than the sieve above.

Table 3.4: Grading limits for fine aggregate (from BS 882-1992).

Sieve size	Percentage by mass passing BS sieve			
	Overall limits	Additional limits for grading		
		Coarse	Medium	Fine
10 mm	100	100	100	100
5 mm	89-100	89-100	89-100	89-100
2.36 mm	60-100	60-100	65-100	80-100
1.18 mm	30-100	30-90	45-100	70-100
600 µm	15-100	15-54	25-80	55-100
300 µm	5-70	5-40	5-48	5-70
150 µm	0-15	0-15	0-15	0-15

The PSDs plotted in Figure 3.5 show that GA has similar distribution to that of CL and so it is known that when substituting GA with CL there is no effect on the material from a change in the PSD. The GA, CL, and S plots in Figure 3.5 show that these three materials are suitable for concrete mixes as their PSDs fit the limits set out in BS 882-1992. The results in Table 3.5 and Figure 3.5 show that 61% of GA and 70% of CL contained particles ranging in size from 150 to 600 µm, and an average of 26% for both GA and CL have particles ranging from 1.18 to 2.36 mm. The results of sieve analysis of the GA and CL samples show that the percent passing through the 2.36 mm sieve size is 99%. The value can be located within the standards limits by BS 882:1992 in the range of 30 to 100%. It can also be seen from the gradation table (see Table 3.5) and chart (Figure

3.5), that the GA aggregate in the 150 and 300 μm sieves, tend to contain a larger percentage of finer particles (11% and 31%) than CL ones (6% and 18%).

While S has 96% of particles ranging from 150 to 300 μm , only 4% have a size $\leq 75 \mu\text{m}$. This means that the S is almost constant sized and poorly graded. This can be seen in Figure 3.5, together with the fact that the percentages passing through sieves of 5 mm, 2.36 mm, 1.18 mm and 600 μm are very close to the lower limit specified by BS 882 1992. The counter the lower limit distribution the percentages passing through sieves of 150 μm and smaller tend to be closer to the upper limit.

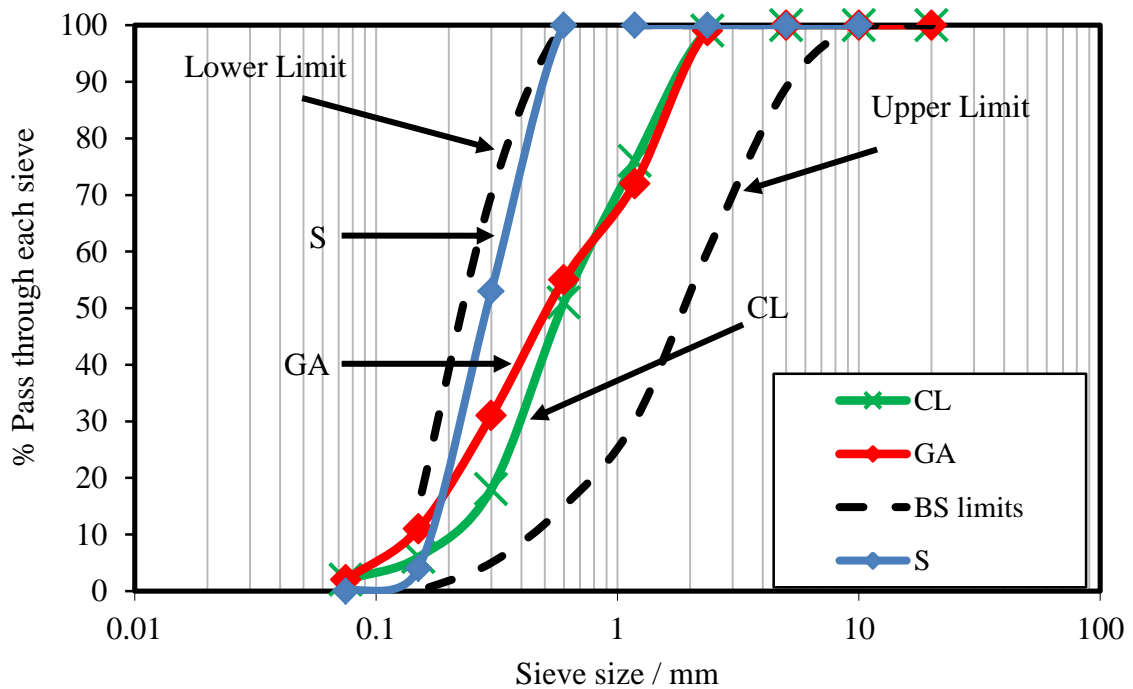


Figure 3.5: PSD analysis of aggregates using sieve analysis.

Table 3.5: Sieve analysis result of GA, CL and S as BS 882-1992.

Sieve size	CL		GA		S		% Passing (Overall limits from BS 882)
	Retained %	Cumulative passing (%)	Retained %	Cumulative passing (%)	Retained %	Cumulative passing (%)	
10 mm	0	100	0	100	0	100	100
5 mm	0	100	0	100	0	100	89-100
2.36 mm	1	99	1	99	0	100	60-100
1.18 mm	23	76	27	72	0	100	30-100
600 µm	25	51	17	55	0	100	15-100
300 µm	33	18	24	31	47	53	5-70
150 µm	12	6	20	11	49	4	0-15
75 µm	4	2	9	2	4	0	
Pan	2	0	2	0	0	0	

3.3.2 Laser Diffraction Analyser for PSD When particle size < 100 µm

Laser diffraction is now becoming more popular due to the increased amount of information generated by this analysis technique. It is quick and easy to use. For C and additives (SF, GGBS, and PFA), which all have very fine particles (< 100 µm), conventional sieve analysis was not possible. PSD analysis was therefore carried out using a Malvern laser diffraction particle size analyser in the Physics Department at the University of Warwick. This technique is widely used for sizing materials with particles ranging from 0.05 µm to 3500 µm in size. The instrument comprises a helium neon laser beam which has been spatially filtered and collimated to produce a clean parallel beam of light. This is then focused down by a Fourier or reversed Fourier lens to a point at the centre of a detector. This consists of a large number of photosensitive segments radiating outwards from the centre, increasing in size as they do so. The laser beam passes through a pinhole at the centre of the detector array and falls on to a detector tray, known as an obscuration detector. When a particle enters a beam, it scatters light at an angle inversely

proportional to its size. The Fourier lens focuses the scattered light onto a detector array, using inversion algorithm. The PSD is inferred from the collected diffracted light data (Cooper, 1998).

The results of PSD plotted in Figure 3.6 for C, SF, PFA, and GGBS samples show that the size of particles ranges from 0.5 to 164 μm . The maximum and minimum values are listed in Table 3.6. It can be seen from the gradation charts (see Figure 3.6) that the maximum size of C and PFA are 124 and 164 μm respectively. This means that the C and PFA particles have double the size particles of GGBS and SF (59 and 71 μm). Figure 3.6 showed that 75% of GGBS contained fine grains ranging in size from 2 to 30 μm , and 80% of SF has particles ranging in size from 4 to 50 μm .

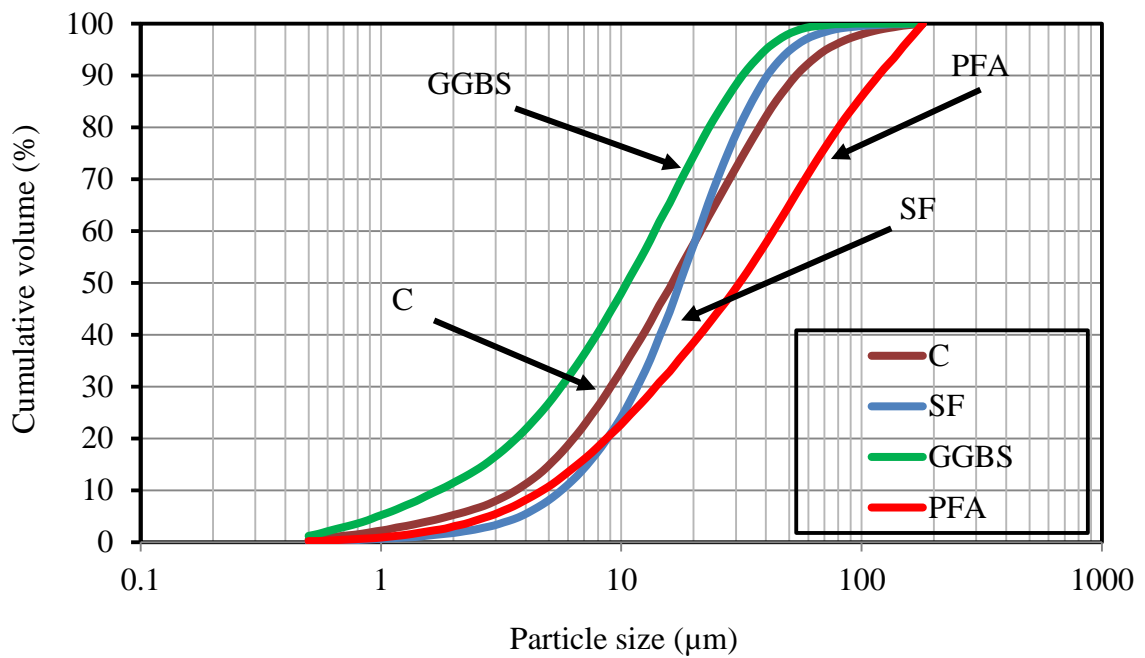


Figure 3.6: Particle size distribution analysis for types of binders and additives using laser diffraction technique.

Table 3.6: Range of particle size of C, SF, PFA, and GGBS by laser diffraction analyser.

	Minimum size (μm)	Maximum size (μm)
GGBS	0.5	59
SF	0.5	71
C	0.6	124
PFA	1.0	164

3.4 Scanning Electron Microscopy (SEM)

Scanning Electron Microscopy (SEM) is a technique used for the visual analysis of specimens and it has many advantages over traditional microscopes. The SEM analysis has a large depth of field, which allows the large amount of the six samples to be in focus at any one time. The SEM also produces images of high resolution, which means that closely spaced features can be examined at high magnification. The SEM uses a focused beam of high-energy electrons to generate a variety of signals at the surface of solid specimens. The signals that derive from electron sample interactions reveal information about the sample including external morphology (texture), chemical composition and crystalline structure and the orientation of materials making up the sample. The technique has the ability to create surface images with magnifications ranging from 10X to 100,000X (Stutzman, 2001). The ZEISS SUPRA 55VP SEM model used in this study is shown in Figure C1 in Appendix C.

Investigations on the microstructure of FRCs were carried out to characterise the fractured surfaces following the four-point bending strength tests. In each case, the specimens were cut into sections ≈ 5 mm height. They were mounted on an aluminium stub with the fracture surface facing upwards. They were then dried in sealed desiccators over a layer of dry silica gel and sputter coated with a thin layer of gold in the vacuum. This is because these specimens are electrically non-conducting materials and in order to prevent a

charge build-up on their surface, a uniform layer of conducting coating must be applied. The prepared specimens were then placed into the sample holder and left in the vacuum chamber with sufficient clearance to enable them to move freely. It is important when mounting samples into the vacuum chamber that their surface is placed normal to the electron beam so that the magnification will be the same in all areas of the viewing screen.

The constituent materials for FRC were examined by SEM to determine the shape, grain texture and size of the particles (for C, SF, PFA, GGBS and S), the diameter and cross-sectional shape and length for single short fibres. The results showed that the shape of C, GGBS, and SF particles were irregular, angular, and rough. The size of the particles was variable giving a range from 5 to 30 μm for C and 5 to 10 μm for GGBS. Noticeably SF particles were smaller than C and GGBS and were ranged from 30 nm to 0.1 μm . PFA particles were observed to be spherical, smooth and ranged in size from 2 to 7 μm . The S particles had sub-rounded shape which is, smooth and their size was from 250 to 435 μm .

Micrographs were then taken at various magnifications providing a view of the whole surface and a close-up of the interlocking area between fibres and matrix. Particular attention was paid to how the short fibre milled type was distributed and orientated (fibre dispersion). The results of this SEM study are reported in Chapter 6. One objective of this investigation was to study the microstructure of the bond, and the penetration of the cement matrix between the openings of the filament strands and between the openings of bundles of the fabric reinforcements. The results of this SEM study are given in Chapter 7.

3.5 Helium Pycnometry (HP)

Helium Pycnometry (HP) used as a technique to measure the density of the materials that used in this project such as, all short fibres, fabrics and binders (C, SF, GGBS and

PFA). Knowledge of densities of constituent materials and FRCs will enable the author to estimate the percentage porosity and to compare the porosity changes from the control in the FRCs materials. Helium was used in these experiments as it is believed to produce the most reliable density results (Aligizaki 2006; Krus *et al.* 1997). This is because:

- it behaves as an ideal gas and unlike many gases, it does not absorb on the surface of the materials.
- it does not interact or chemically react with most materials.
- helium is a monomolecular gas with the smallest atomic diameter of about 0.22 nm. This small size of helium atom permits it to penetrate pores as small as its size.

The instrument comprises of two cells, one that holds the sample and the other knowns the reference cell. For this study, tests were performed using the gas pycnometry kit, model AccuPyc 1330 made by Micromeritics. It provides a density resolution of about 0.0001 g/cm^3 , which makes it capable of providing a relatively accurate measurement of the true density.

3.5.1 Sample Preparation and Analysis

Since the sample holder used can only accommodate specimens of up to 35 mm high and 18 mm in diameter, the specimens cut to form $20 \times 10 \times 13$ mm cuboids. To minimise the damage to their pores structure, and to avoid the micro cracks associated with the cutting process, specimens were cut using a special fine blade saw, normally reserved for cutting ceramics. The copper bonded diamond saw was manufactured by Applied Diamond Ltd. A block of material was first glued onto a glass plate using melted wax. Cutting was then accompanied by an oil based lubricant to prevent any unnecessary chemical reaction with the samples. After cutting, the specimen was immersed in a white spirit solution for 24 hours in order to dissolve the wax. Then it was removed from the white spirit and gently

wiped with tissue to remove any wax remaining on the surface. The specimen was dried by the vacuum drying technique using the following processes (Aligizaki, 2006):

- i. To remove the water from the pores and to prevent any further hydration reaction, every specimen was fully immersed in acetone solution for 48 hours.
- ii. After removing from the acetone and they were exposed to a fan heater (blow drier) for hour. The heat dried the surface and any excess acetone was evaporated from it.
- iii. Finally, each specimen was placed in a sealed dessiccator under vacuum with a dry silica gel. Under the vacuum, pore water was turned into vapour and removed from the specimen.

The vacuum drying technique is a relatively slow process and with specimens was under vacuum for between 14 to 21 days, depending on their moisture content, until it reached a constant weight. To monitor the drying process, each specimen was weighed regularly until no evidence of continued weight loss could be recorded. After the drying process, the specimens were stored in the dessiccator to ensure that they remained dry before the density was measured.

3.5.2 Porosity Measurement

For each test, the weight of the specimen was recorded just before porosity measurement. It was then placed inside the sample holder (and the AccuPyc 1330) where helium gas under a known pressure (1.35 bar) enters the specimen holder and fills the pores. The change of helium volume in a chamber of constant volume allows the determination of the true volume of the specimens from pressure measurements via Mariottes's law (Aligizaki, 2006). The porosity measurement instrument then determines

the true density by dividing the sample mass by the true volume. To ensure accuracy, each test was repeated 10 times. At the end of each test, the true volume and density were calculated as an average of volume and density measured by each run. Measurements were performed in a temperature control laboratory at 22°C.

Percentage volume of porosity was then calculated by subtracting the bulk volume of the sample from the true volume determined by helium pycnometry. The bulk volume of the specimens was calculated by measuring the dimensions of the cuboids with a micrometer to ± 0.01 mm. To enhance the reliability, the author determined average porosity from five specimens using control (without fibres), short and continuous FRC materials. The results of porosity measurements are presented and discussed in Chapters 6 and 7 for short and continuous fibres, respectively.

3.6 Workability

Workability is defined as the property of freshly mixed concrete or mortar which determines the ease and homogeneity with which it can be mixed, placed, compacted and finished (Gambhir, 2006). The workability of fresh concrete is a complex system of two critical parameters, consistency and homogeneity. Consistency is the relative mobility or ability of a freshly mixed concrete to flow and is usually measured in terms a slump test method. Major factors affecting consistency are: water content; cement content and its characteristics; air content; temperature; mixing conditions; chemical admixtures and the mineral additives used. Addition of superplasticisers improves consistency by dispersing cement particles and reducing the viscosity of the cement paste. A slump test is used to measure the consistency of concrete, which has a close indication to workability. A low

slump has a stiff consistency. The following sub-section describes the fundamentals of the used with slump test of fresh properties of FRC specimens.

3.6.1 Slump Test

The slump test is the most well-known and widely used test method to characterise the workability of fresh concrete. The test method is widely standardised throughout the world, including in ASTM C143 and BS EN 12350-2:2009. The slump test is normally performed with a mould in the form of a cone frustum. The cone frustum is normally 300 mm high, with a diameter of 200 mm at the bottom narrowing to 100 mm at the top, which is open (Neville, 1995). However in this study, due to the relatively small size of the mixes produced the slump test was performed using a ceramic mould of similar geometric shape to the actual slump mould but, of smaller dimensions. The apparatus consisted of a ceramic mould as shown in Appendix C Figure C2, in the shape of a cone frustum with a base diameter of 80 mm, a top diameter of 45 mm and a height of 120 mm. Figure 3.7 gives the geometries of the two cones and shows that the angles are similar at 8.5° for the in-house ceramic cone and 9.4° for the British Standard one. However, the volume of the in-house ceramic mould (375000 mm^3) is fifteen times smaller than that of the British Standard cone (5500000 mm^3). The in-house method to measure slump can only provide an indication and not a standard measure of workability.

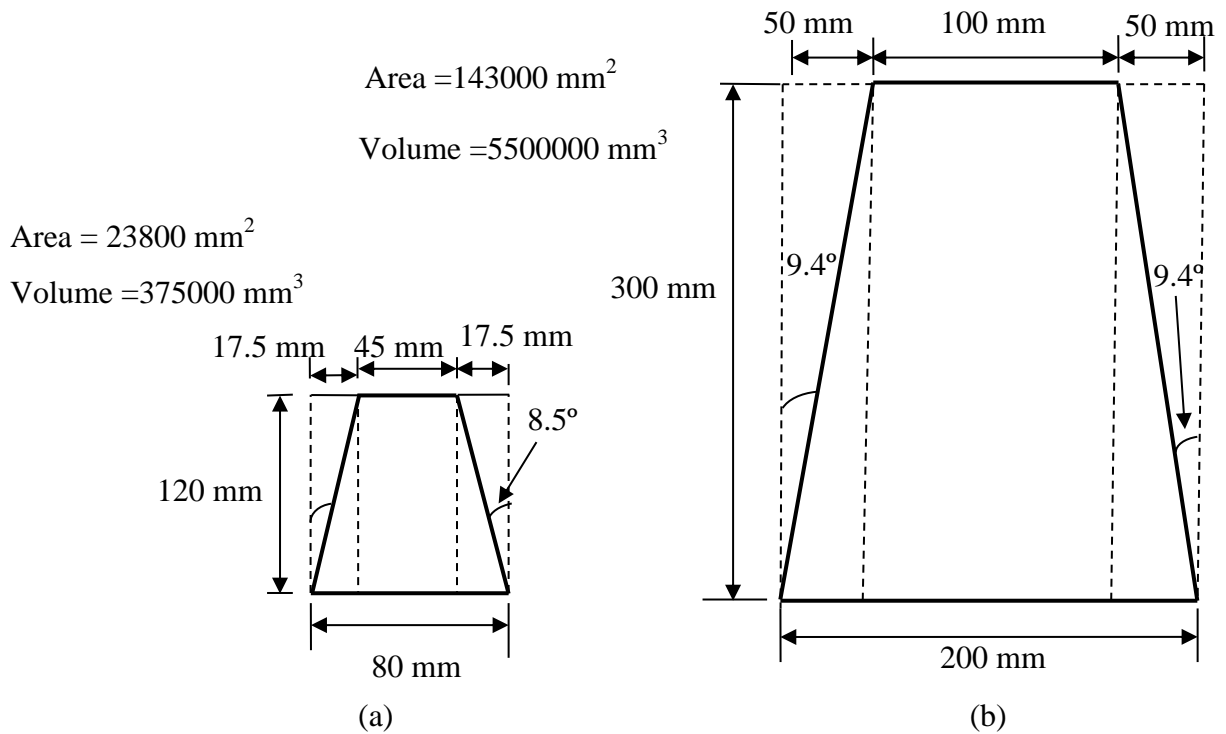


Figure 3.7: Schematic diagram illustrating the cones used during the slump test: a) in-house ceramic cone and b) British Standard cone.

Slump test were carried out using cementitious with CF1 fibres and four types of SPs (SP_A, SP_B, SP_C, and SP_D) to select the one that can increase the workability FRCs, for the reason given Sub-section 3.2.5. Results plotted in Figure 3.8 show that the mix containing SP_B achieved the highest slump at all four water/binder (w/b) ratios levels. The slump with SP_B and w/b ratios of 0.35 and 0.5 are 100% and 36% higher if superplasticiser is SP_D. Because SP_B was found to be most effective in increasing the workability it was selected as the superplasticiser in this thesis. The use of fibres is known to affect the workability. The influence of the addition of CF1 on the workability was investigated by repeating the slump test using SP_B (3% by mass of cement) and two mixes made from mix design; 1C:2A, one with CF1 at V_f of 9% and one without, at a w/b ratio of 0.35.

Figure 3.9 shows the relationship between slump and V_f of CF1 with two of water/binder (w/b) of 0.35 and 0.50. Four different V_f of 5%, 7%, 9%, and 12% were used in this section to represent the results to evaluate the low and high V_f on the slump of FRC and compared to control material ($V_f = 0\%$). The author has selected these values as it is more practical. Results in Figure 3.9 indicate that the specimens without CF1 achieved the highest slump at w/b ratio of 0.35 and 0.5. The slump with 0.35 w/b ratio of 100% matrix ($V_f = 0\%$) is found to be 10 times higher than for the FRC with CF1 at 12% V_f . This latter mix was unworkable because it was too dry; the FRC was difficult to place in a mould and fibre distribution was not uniform. The mixes without CF1 at both w/b ratios were more workable. They were both found to be too wet. The slump with SP_B and 9% CF1 at 0.50 w/b ratio had the same slump as the mix without CF1 at 0.35 w/b ratio (see Figure 3.9). It is concluded that there is an adverse relation because when the V_f increases the workability decreases.

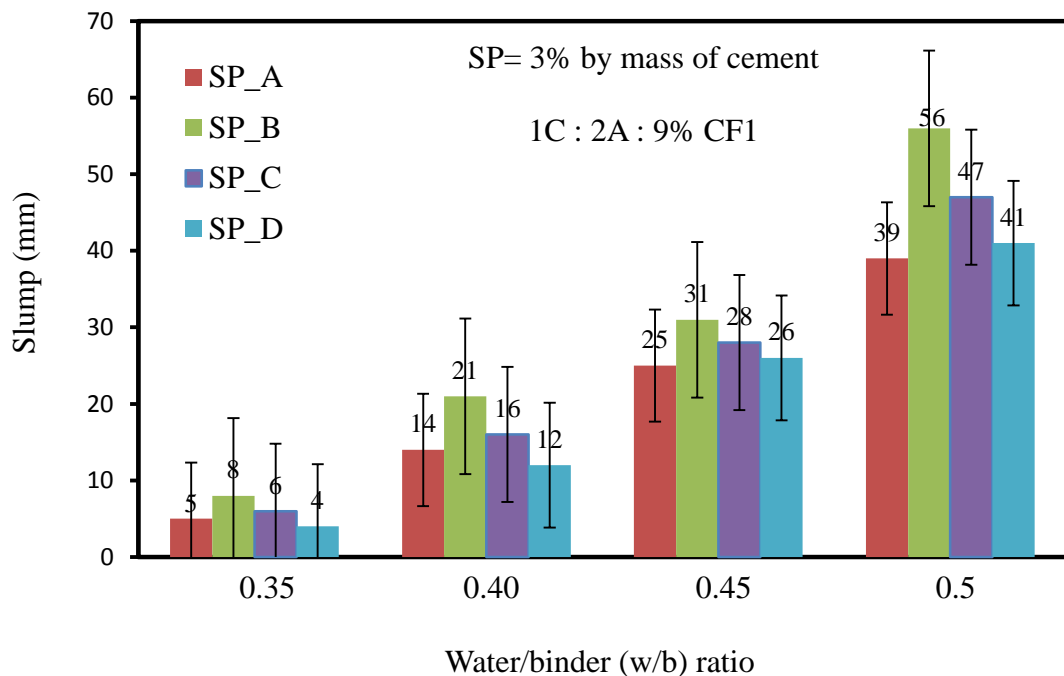


Figure 3.8: Relationship between slump and water/binder (w/b) ratio.

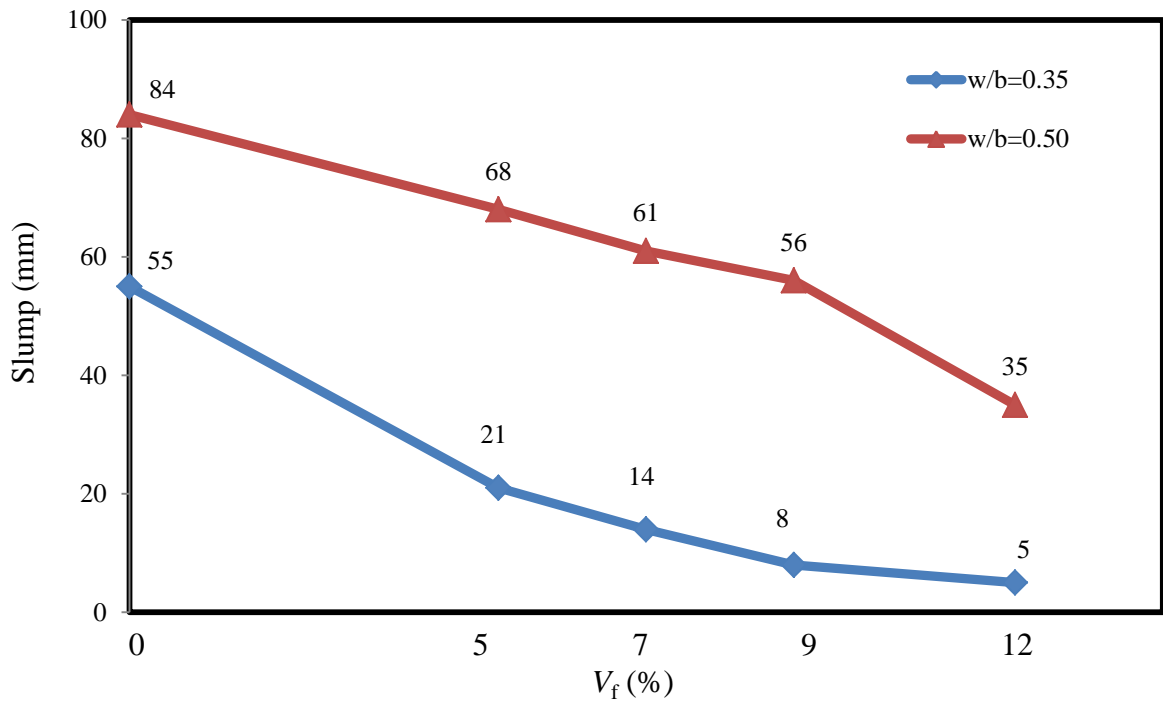


Figure 3.9: Relationship between slump and V_f of CF1 in presence of 3% of SP_B.

3.7 Single Fibre Tensile Test

Single fibre tensile strength was tested at Coventry University's Civil Engineering Department using a Lloyd's universal testing machine with a load cell of 10 N. The test set-up is shown in Appendix C Figure C3(a). The special clip-type grips from Lloyds shown in Figure C3(a). The grips are simple and lightweight and they are designed to hold single fibres with very small diameters (7 to 14 μm), during tension loading. Because each fibre has a diameter of 7- 14 μm it is not easy to handle when placing them into the grips. It was impossible to test the short fibres; CF1, CF2, CF3, PP, and PVA, due to their small length which ranged from 0.085 to 25 mm. For this reason, thirty five specimens were tested of seven fabric types of CF4, CF5, CF6, CF7, CF8, CF9 and GF. A single fibre specimen had a length of 100 mm and they were prepared following standard ASTM D-3822 (Standard Test Method for Tensile Properties of Single Textile Fibres).

Due to the small diameter of these single fibres specimens ranging from 7 to 14 μm , the author faced two difficulties when attempting to place specimen in the grips: (1) the single fibre specimens slipped and (2) because it was not easy to see the fibre and therefore it was difficult to ensure the ends were positioned correctly. Given that, the author created two methods to overcome the difficulty in locating a fibre in the grips. The first was to have two pieces of double-sided tape attached at the fibre ends to obtain a better grip. This is shown in Appendix C Figure C3(b). The second method was to have a lighting magnifying lens to magnify single fibre allowing the author to hold them. This aspect of the test procedure is shown in Appendix C Figure C3(c). The stroke rate was constant at 1 mm/min. Table 3.7 presents the mean of the five single fibre tensile test results for the seven fabric types and also presents the tensile strength provided by the manufacturers for comparison purposes.

The results in Table 3.7 showed that the measured fibre tensile strengths are lower than reported in the data sheets from the manufactures. The fibre manufacturers do not provide provenance to how a data sheet fibre strength was established in-house. Because the test method employed by the manufacture is unknown the condition of the fibre at the time of the tensile testing is unknown. Producing the fabric and the handling of this reinforcement until the FRC was made at Warwick University can create surface damage to the fibres for the lower fibre strength determined by the author's testing at Coventry University. Another factor that could lead to a lower measured strength is the effectiveness of the gripping of a single fibre since any stress concentration at the end of the gripping will lead to premature failure at a lower fibre strength. The results are listed in Table 3.7 can be used in Chapters 6 and 7.

Table 3.7: Measured and manufacturer's data of single fibre tensile strength for seven continuous fibres (CF4, CF5, CF6, CF7, CF8, CF9 and GF).

Fibre Type	Single fibre tensile strength (MPa)	
	Manufacturers data	Mean measured
CF4	3800	2460
CF5	3800	2495
CF6	4900	2350
CF7	1860	1445
CF8	3500	2240
CF9	4900	3290
GF	1900	1345

3.8 Mechanical Testing

To investigate the effectiveness of the mix design, processing method and curing regimes on the strength of FRC material all specimens were tested for flexural strength. Testing was conducted with a fully articulated four-point bending fixture in a 100 kN Testometric test machine (Machine type; Testometric Micro 100 kN PCX). Figure 3.10 shows a schematic diagram, illustrating the steel four-point bending test arrangement and the position of the extensometer (LVDT) during the mechanical testing for the trapezoidal cross section specimen. The rate of loading is quite important as it affects the amount of time taken to ultimate failure. All tests were performed with a 1 kN load cell. The effect of the loading rate on the flexural strength was investigated and the results are presented in Chapter 5.

The lower part of the bending has two support pins. These pins are separated by 135 mm for the trapezoidal cross section specimen and 200 mm for the rectangular cross section specimen. One end is fixed and at the other end the pin support is free to rock about one axis. The upper part of the flexural strength rig comprises of two loading pins for the trapezoidal specimen they are 45 mm apart and 66.7 mm for the rectangular cross section specimen. These provide fully articulated loading points of two equal line loads across the

full width of the specimen. The upper part is fixed onto the Testometric machine via a 1 kN load cell. To monitor deformation the central deflection was measured by attaching LVDT to the upper surface of the specimen.

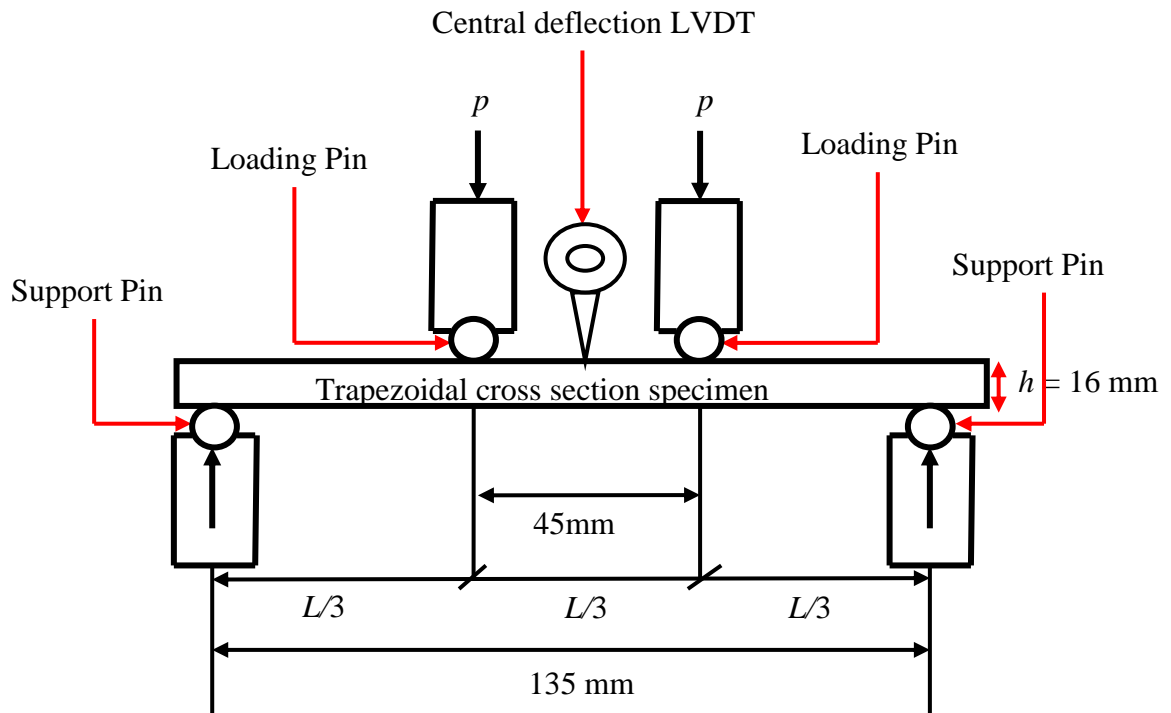


Figure 3.10: The schematic diagram illustrating the testing arrangements and position of the extensometer during the mechanical testing for the trapezoidal cross section specimen.

3.8.1 Analysis of Four-Point Flexural Test Results

The raw data consists of readings for load and central deflection, which after analysis can produce results for stress and strain. Stress-strain curves can subsequently be plotted. Due to the large volume of data involved the analysis is carried out using Microsoft Excel spreadsheets. The maximum applied load at the failure was taken from the software and the flexural strength at maximum stress at failure was calculated using:

Flexural strength $\sigma_{\max} = \frac{M y_{\text{tension}}}{I_{\text{xx}}} \quad (\text{MPa}) \quad (3.1)$

where: M is the maximum applied bending moment (N.mm), given by

$$M = p \frac{L}{3} \quad (3.2)$$

where L is the span of the beam between two supports. In this case $L= 135$ mm for the trapezoidal specimen cross-section and 200 mm for the rectangular specimen cross-section. p is the point load. y is the distance from the Neutral Axis to the outer surface with tensile (direct) stress. The value of y_{tension} is for the trapezoidal cross-section (see Figure 3.11) is

$$\frac{h(2a + b)}{3(a + b)} \quad (\text{mm}) \quad (3.3)$$

and for the rectangular cross-section is

$$\frac{h}{2} \quad (\text{mm}) \quad (3.4)$$

I_{xx} is the second moment of area of the cross-section;

where I_{xx} for trapezoidal cross-section is

$$\frac{h^3 (a^2 + b^2 + 4ab)}{36(a + b)} \quad (\text{mm}^4) \quad (3.5)$$

and

I_{xx} for rectangular cross-section is

$$I_{xx} = \frac{bh^3}{12} \quad (\text{mm}^4) \quad (3.6)$$

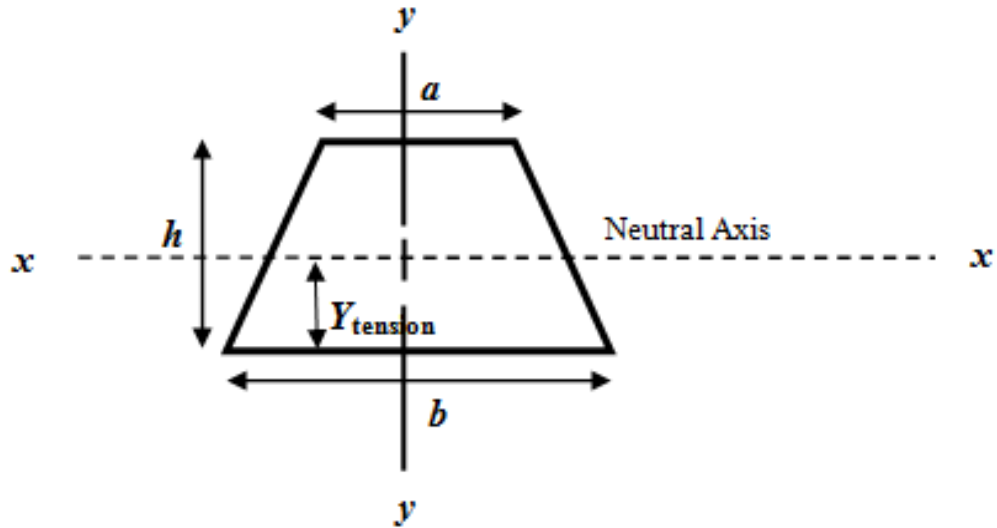


Figure 3.11: Cross-section of the trapezoidal specimen.

The maximum tensile strain at the section below a loading pin was calculated by the following equation:

$$\varepsilon = \frac{\sigma}{E} \quad (3.7)$$

E is the modulus of elasticity and is found from;

$$\delta = \frac{px}{24 EI} [3L^2 - 4x^2] \quad (3.8)$$

where δ is the central deflection (mm). x is $L/3$ the length from the support to the point load and is either 45 or 66.67 mm depending on the geometry of the test specimen.

On rearranging Equation (3.8) the modulus of elasticity is given by

$$E = \frac{px}{24 \delta I} [3L^2 - 4x^2] \quad (3.9)$$

The maximum tension strain (ϵ_{\max}) is determined from:

$$\epsilon_{\max} = \frac{216}{31} \times \frac{\delta_{\max} y}{L^2} \quad (3.10)$$

Chapters 6 and 7 discuss and evaluate the findings from the series of mechanical tests to characterise the properties of short and cementitious materials reinforced with different volume fraction and forms of carbon or glass fibres.

Chapter 4

4. Manufacturing Process

4.1 Introduction

A suitable manufacturing process is required to combine and consolidate the composite materials for a green state. When using short fibres (Section 3.2.4) the choice of the manufacturing process is governed by the need to achieve a uniform dispersion of the fibres in the cementitious matrix. One objective of this study was to investigate manufacturing processes not normally applied to cementitious composites. In particular an investigation has been made with regard to the production of FRC materials with enhanced flexural strength and toughness.

Following the review in Section 2.6 of manufacturing processes and an evaluation of the laboratory apparatus in the School of Engineering it was decided that the hand lay-up and compression moulding methods would be studied. Although the feasibility of using these two methods to produce green forms was studied comprehensively, most of the experimental works (see Chapter 3) to investigate the influence of mix designs (see Chapter 5), curing regimes, etc., on the flexural strengths and toughness (Chapters 6 and 7) of green specimens used, compression moulding. This was mainly due to the direct and regular access to a hydraulic press machine throughout this study. An introduction to the two processes (hand lay-up and compression moulding) and the necessary modifications made in order to make them successful are presented in the following Sections 4.4 and 4.5. The test results for cementitious materials reinforced with short and continuous fibres using these two manufacturing processes will be presented and discussed in detail in Chapters 6 and 7.

4.2 Dispersing Methods of Recycled Milled Carbon Fibre

Due to static electricity, the author found that recycled milled carbon fibres always clumped together. It was observed that fibre balling of 5 to 30 mm diameter or fibre clumping, as shown in Figure 4.1(a), usually occurs before the fibres are added into the mix and that they remain as clumps throughout the mixing process. In an attempt to breakdown these balls for uniform fibre dispersion the author used several methods from previous studies (discussed in Section 2.7) and found them all to be unsuccessful. The methods that failed are: fibre sieving; ultrasonic disturbance; various techniques of fibre mixing such as either mixing with water or just mixing dry fibres; silica fumes to be followed by other solid ingredients and, lastly, water. Given that previously tried methods were found to be unsuccessful, the author developed the novel method of grinding down the milled carbon fibre balls immediately before mixing; this dispersion method used a coffee grinder to breakdown the clumps. Following the grinding process balls were on average, 60% smaller in size and the difference can be seen when comparing the images in Figures 4.1(a) and (b). The method was then partially successful, at least superior to all those that were unsuccessful.

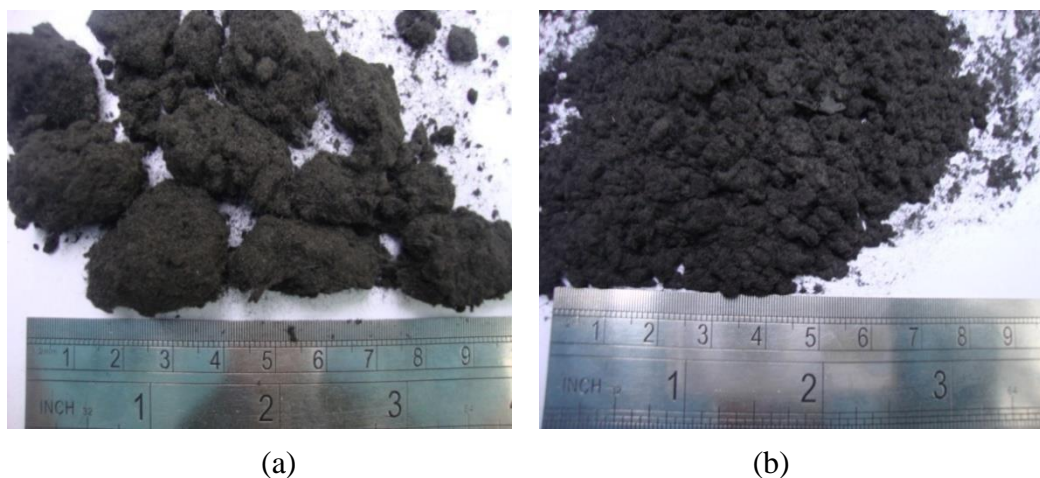


Figure 4.1: Recycled milled carbon fibre (CF1): a) before grinding, b) after grinding.

4.3 Mixing of Materials Process

The Hobart mixer with a five litre capacity stainless steel bowl shown in Figure C4 (Appendix C) was used. The Hobart has three Speed settings; Speed 1, low – 136 rpm, Speed 2, inter-mediate – 281 rpm and Speed three, high – 580 rpm. All the batches underwent the same mixing process. They were mixed for four minutes at Speed 2, after eight minutes at Speed 1. Mixing time at the lower speed was necessary to pre-mix the materials. Premixing the constituent materials at the lower speed avoided water and semi-dry material being thrown from the mixer.

The cement, short fibres and silica fume were first mixed in a dry condition in the Hobart mixer for two minutes. Fine aggregate and additives, GGBS and PFA, were then added and mixed for a further two minutes. 70% of the calculated amount of water was then added to the dry mix and mixed thoroughly for four minutes. The remaining 30% of the water was mixed with the superplasticiser type SP_B (see Sub-section 3.6.1), poured into the mixer and mixed for four minutes. The total mixing time was required for all mixes to disperse the short fibres and obtain a uniform mix was 12 minutes.

4.4 Hand Lay-up

Hand lay-up was used to produce the green forms that are reinforced with layers of fabric. The steps are very similar to fibre reinforced plastic (FRP) lay-up. Hand lay-up allows more control of the fibre placing than the spray methods and can potentially produce very high volume fractions, > 10%. However, labour intensive and results in a comparatively low output (Purnell, 2010). This process is not commonly used for cementitious matrix materials given that hand lay-up uses reinforcing fibres in textile form which is not compatible with the traditional concrete casting technology (RILEM, 2006).

4.4.1 Moulds for Hand Lay-up

Two moulds were manufactured for the hand lay-up process; one made from stainless steel, the other from softwood.

- 1- The stainless steel mould which accommodates five nominally identical rectangular specimens is shown in Appendix C Figure C5. Their dimensions are for a specimen of 225 mm long, 50 mm wide and 20 mm in depth. Figure C6 in Appendix C shows a typical specimen from the stainless steel mould.
- 2- The softwood mould made for a single specimen is shown in Figure C7 in Appendix C. Made of 15 mm thick softwood its rectangular designed frame is 15 mm depth by 50 mm wide by 170 mm long. The shape, width and thickness for the flexural specimen were chosen for easy use of the four-point bending test, which is introduced in Section 3.8.

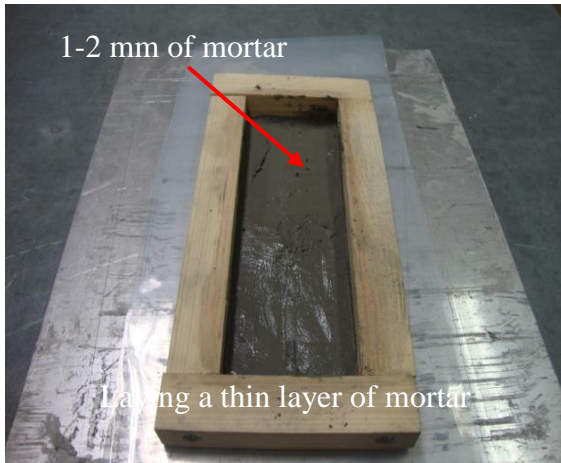
4.4.2 Processing Green Forms by Hand Lay-up

In what follows the author summarises the steps that were followed to manufacture a green form specimen by hand lay-up. To ensure a quality surface finish, and ease of demoulding green form specimens, the two moulds were connected to a polythene sheet with double sided tape and placed on a firm, smooth surfaced worktop before coating the inner moulded walls with a layer of releasing grease.

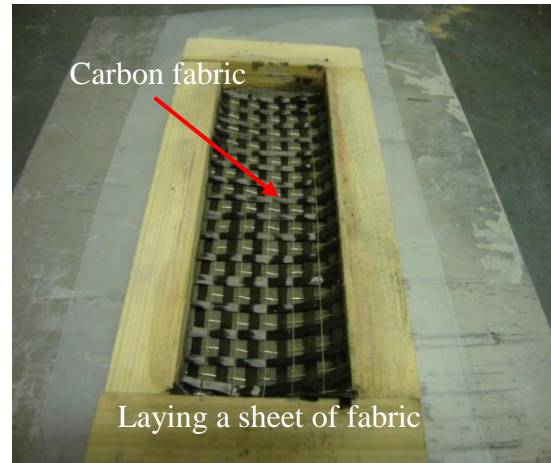
The green form was prepared by pouring a thin layer (\approx 1-2 mm) of the mortar into the mould, as can be seen in Figure 4.2(a). After pouring the mortar spread out evenly over the base before a layer of glass or carbon fibre mat is placed manually on top, and pressed gently into the mortar using the finger tips. This step in the processing is shown in Figure

4.2(b). A 20 mm diameter smooth steel roller, shown in Figure 4.2(c), is rolled over the reinforcement to encourage wet-out and composite consolidation, and to squeeze out excess water and entrapped air. The rolling action goes a stage further and helps the fibres to bind with the mortar. The specimen is then built-up by repeating these steps until the required thickness of either 15 mm or 20 mm is achieved. The final layer of reinforcement must be covered with a suitable mortar layer (1 to 2 mm) to enable the specimen to achieve its final thickness requirement. The specimen is next carefully covered with a polythene sheet as seen in Figure 4.2(d) and a dead weight of 20 kg mass is then placed on top of the mould, as shown in Figure 4.2(e). This compressive load compacts the specimen during the initial setting stage and will assist with further matrix/reinforcement consolidation. After 24 hours the dead load is removed and the green form specimen is demoulded.

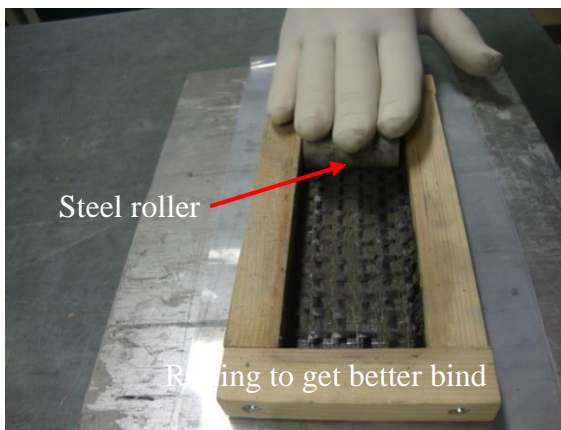
For each mix design (Chapter 5) a minimum of eight specimens from the softwood mould and ten from the stainless steel mould were produced. 50% were left in trays and cured in 100% Relative Humidity (RH) (Section 4.6), while the remaining 50% underwent a water bath process at 50°C (Section 4.6). All the hand lay-up specimens were cured for 26 days, after which they were kept at room temperature for 24 hours until their flexural properties were measured.



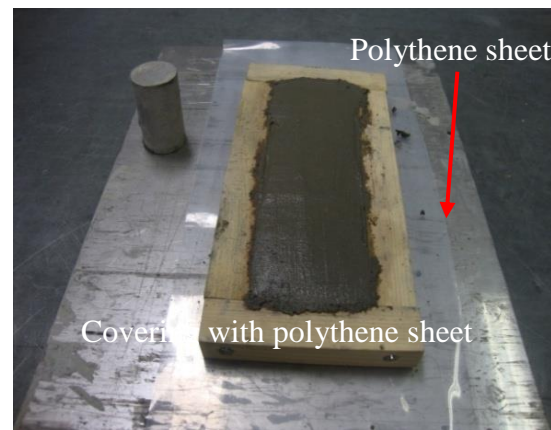
(a)



(b)



(c)



(d)



(e)

Figure 4.2: Steps in the fabrication of FRC green forms using the hand lay-up process: (a) laying a thin layer of mortar; (b) laying a sheet of fabric; (c) rolling to get a better bind; (d) covering with a polythene sheet; (e) placing a 20 kg dead load for consolidation.

4.5 Compression Moulding

A compression moulding process has been developed to minimise, if not eliminate, porosity by increasing the degree of consolidation. The concept behind the compression moulding is to reduce the water/cement (w/c) ratio after the concrete has been placed, thereby eliminating the problem of low workability (Haupt, 1997).

Three steel moulds were used, two of them from the PhD work of Farahi (2009). These two consisted of a trapezoid tool for a single specimen and a stainless trapezoid tool for six specimens. The third mould of mild steel was for a single rectangular specimen and was designed by an undergraduate student for his individual project (Wates, 2009). These moulds were manufactured in the Engineering Workshop in the School of Engineering at the University of Warwick.

The single sample, trapezoid tool was manufactured specifically for use with the Denison 7231 compression testing machine shown in Figure C8 in Appendix C. The six samples trapezoid tool was made to be used with the DASSET thermoplastic compression moulding machine shown in Figure C9 in Appendix C. The single rectangular slab plate mould can be used on either of the machines that apply a compression load. The trapezoidal cross-section was chosen for ease of demoulding. Green form specimens were manufactured using all three moulds depending on the availability of the Denison 7231 and DASSET machines.

4.5.1 Single Sample Trapezoidal Mould

This mould was comprised of two parts, one with a trapezium cross-section for the specimen. The mould shape was chosen given the expectation that pressing the mixes would be the best approach to achieve green forms when the mix design has the low

water/binder (w/b) ratio of 0.3. The tool was manufactured from mild steel, and as can be seen from Figure C10 it consists of six components connected together using cap head screws. Its design allows for easier demoulding and gives the specimens a good surface finish. As seen in Figure C10 in Appendix C, there are three rows of $\text{Ø}2$ mm holes at 10 mm spacing in the base of the mould to allow the draining of excess water. When the upper part mould parts meet and the tool is compressed, the protrusion of $150 \times 34 \times 2$ mm with the upper part locate into the bottom part (cavity) to enable the load transfer directly into the mix. The shape and size of the mould was chosen for both ease of specimen demoulding and testing for flexural strength by four-point bending, as discussed in Section 3.8.

4.5.2 Final Design of Single Sample Trapezoidal Mould

From an evaluation of the preliminary specimens using the mould shown in Figure C10 in Appendix C the study revealed some remarks during pressing. To improve the quality of manufacture the author decided that the mould design needed to be modified in the Engineering Workshop to improve consolidation and improve the uniform distribution of the 100 kN load over the top surface (34×150 mm) of the specimen. The height of the protrusion in the upper part was increased by another 1 mm to be 3 mm. Additionally, the 1 mm holes in the bottom part of the mould were increased to 3 mm diameter (see Figure C11 in Appendix C) to encourage removal of all excess water when the specimen was compressed. To aid sample removal the mould was lightly oiled before the mix was added. To collect the excess water the steel mould was horizontal placed onto a tray, centrally located on the lower platen of the Denison 7231. It is essential that the mould is positioned centrally in order to achieve a uniform downwards force. This is because the top platen of Denison 7231 has a joint that allows a degree of rotation from the horizontal plane.

To prevent blockage of the drawing holes, filter paper is placed in the base of the mould before adding the mortar. Filter paper consists of Polypropylene and Nylon and the composition of these filter papers help the filtration of the water, along with holes that are punched into the fabric. It was supplied by PG Lawton, Hebden Bridge. The applied compressive force of 100 kN over a contact area of 0.005 m² is equivalent to a uniform compression stress of 9 MPa (see Sub-section 4.5.4). Figure 4.3 shows that this mould produces a specimen of 150 mm in length with a trapezoidal cross-section of width from 22 to 34 mm linearly, varying over a thickness of 16 mm.

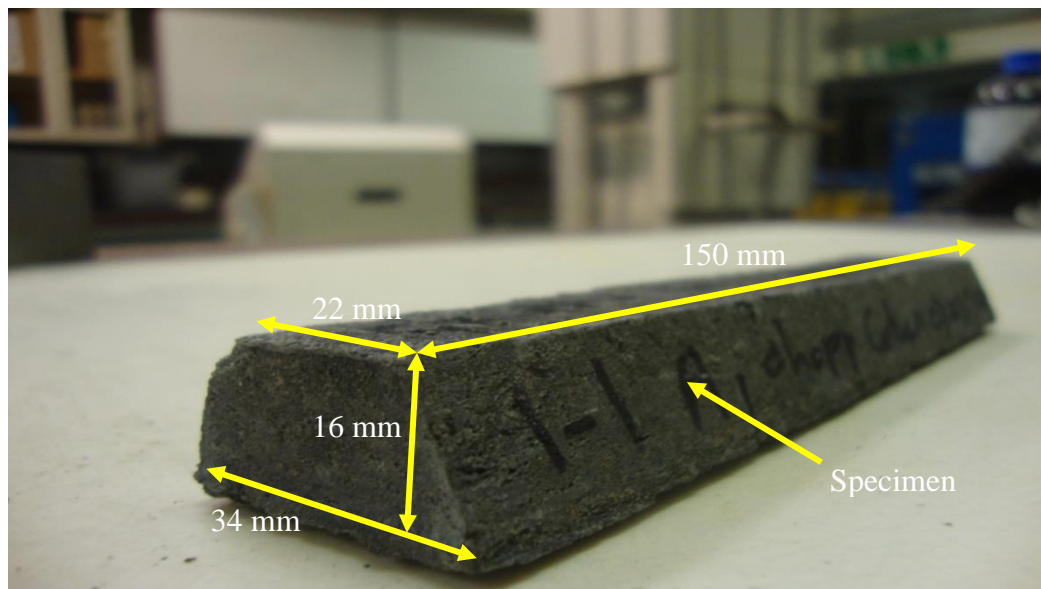


Figure 4.3: A typical green specimen using the single trapezoid mould.

4.5.3 Six Samples Trapezoidal Mould

This mould is shown in Figure 4.4 and comprises of two 300 mm wide by 170 mm long parts capable of producing six samples at a time. Each sample is 170 mm long and has a trapezoidal cross-section of 22 to 34 mm in 16 mm thickness. The mould is made of stainless steel tooling plate and was manufactured in the Engineering Workshop at the University of Warwick. For dewatering, during pressing, each cavity in the lower part has

three rows of $\text{Ø}2$ mm holes at a spacing of 10 mm. In the upper part two rows of $\text{Ø}2$ mm holes at 20 mm spacing were drilled. Six holes in the side of the upper part were connected to the vacuum pump via sets of manifolds and pipes. These were designed to create suction, uniformly distributed from the top for all six cavities while the mould is under pressure. The vacuum equipment extracts excess air and water from the top section of the mould. The vacuum manifold is used to connect the vacuum pump to the six trapezoidal and single rectangular plate tools. The manifold is attached to each side of the top section of the tool and a tight seal is provided through the use of rubber O-rings.

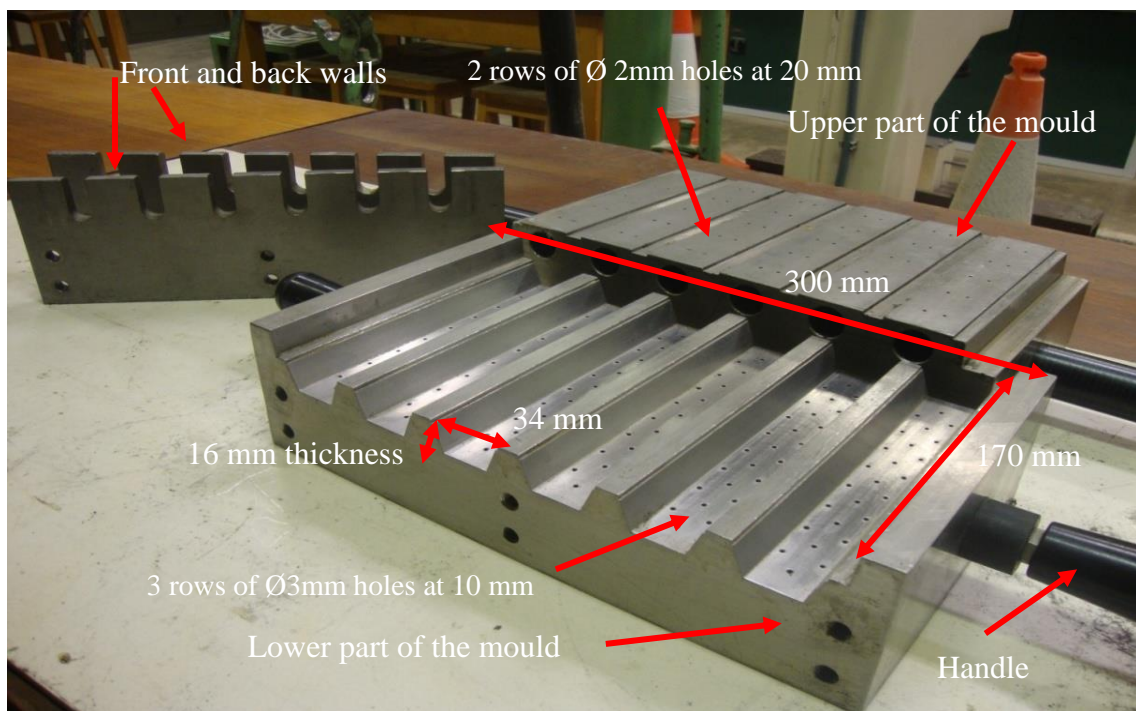


Figure 4.4: Four parts for six trapezoidal mould for DASSET machine.

To use the mould in the DASSETT compression moulding machine the upper part of the mould was screwed to the machine's lever arm at the point at which it moves up. This stage in the compression moulding process is shown in Figure C12 (Appendix C) and was needed to be able to apply mould pressure onto the mould while the pipes were connected to the vacuum machine that is located next to the compression moulding machine. The

lower part of the mould was placed onto an aluminium tray (see Figure C12 in Appendix C) and clamped to the base of the machine. The aluminium tray was covered with a polythene sheet shaped to collect the excess water drained from the moulds, while also preventing the machine from getting wet. The magnitude and duration of the applied compressive pressure was controlled by both computer software and the machine. The compressive force was set to 680 kN which, for a contact area of 0.035 m², is a mean compression stress of 9 MPa (see Sub-section 4.5.5) on the top surface of the specimen.

4.5.4 Single Rectangular Slab Mould

The main purpose of creating slab specimens was to establish whether they can, in green state, be removed undamaged from the mould. The mould comprises of an upper and lower part, each 240 mm width by 170 mm long. This mould can be used with both the DASSET and Denison 7231 compression machines and as seen in Figure 4.5, it has six components that connect together with cap head screws. The mould produces one single green specimen at a time of 240 mm long by 170 mm width by 15 to 45 mm depth.

As seen in Figure C13 in Appendix C the top and bottom contact faces of the mould are perforated. The compressive force is set to 800 kN over the contact area of 0.041 m², is equivalent to a pressure of 9 MPa to allow for the extraction of water and air (see Section 4.5.5). This pressure is transmitted to all other faces of the mould in contact with the sample, in a direction normal to these faces. The mould allows samples to be compressed by up to 30 mm for slabs of variable thicknesses from 15 to 45 mm. This will be particularly useful for the production of specimens containing fibre reinforcement at high volume fractions because they are likely to require a high vertical displacement of the upper part to consolidate the green form. The main disadvantage of this mould is that only

one sample can be produced at a time. To overcome this limitation each slab can be cut into a number of strips for flexural strength testing.

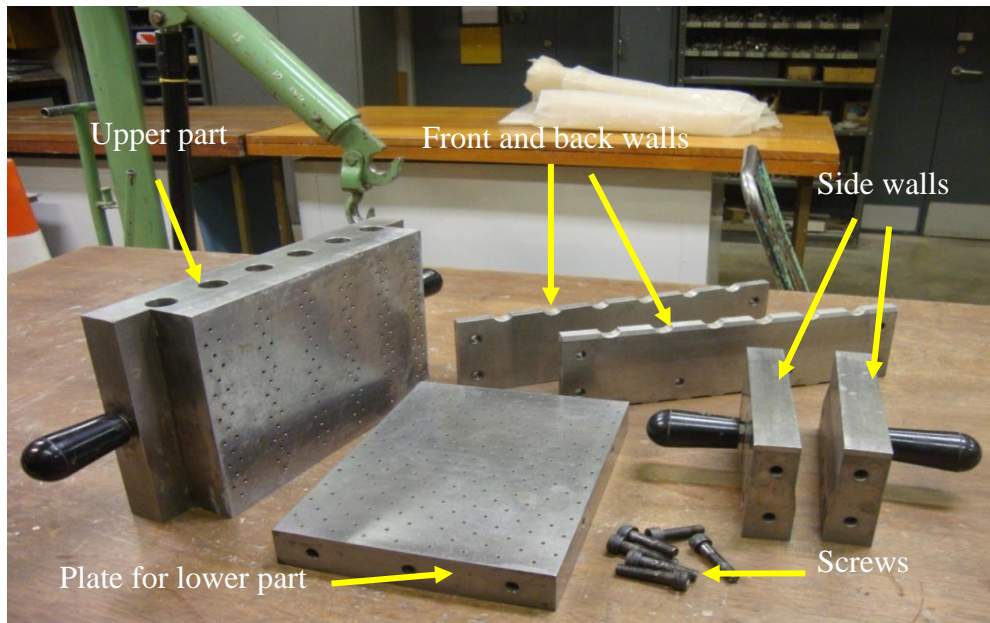


Figure 4.5: Mild steel components for the rectangular slab mould.

To ensure that the samples can be removed intact, the mould was designed with a significant draft angle of 10° along the lower section of the side walls (see Figure C14 in Appendix C). This not only achieves successful extraction but also slabs with a good surface finish. It was an expectation of the mould specimen design that sample extraction could be achieved by the removal of the front and back walls only. As a precaution, and because the specimen removal of samples is a key manufacturing issue, the mould was designed so that it can be disassembled completely. With all of the walls removed there will be little resistance to the extraction of samples. The components had to be kept clean and dry each part thoroughly after every use. It also requires that the tool is kept well-oiled and stored in a dry place between slab manufacturing.

4.5.5 Processing Green Forms by Compression Moulding

Green form specimens were produced using the moulds introduced in Sub-sections 4.5.2 to 4.5.4. The following steps were applied:

1. As shown in Figure 4.6(a) a sheet of filter paper was placed into the bottom of mould. Once the mixing process of Section 4.3 was finished, a 1 to 2 mm layer of the matrix was placed into the mould and evenly spread over the mould area using a spatula. Figure 4.6(b) shows the mould after one of these thin layers had been added. This layer was then tamped repeatedly by a 150 mm long and 20 mm diameter steel tamping rod before the next thin layer is added. When required, a sheet of glass or carbon fabric (Section 3.2.4) is placed on top of the mortar; it was then gently placed into the mortar by hand, as seen in Figure 4.6(c). The layered sample was built-up by repeating this procedure until the required thickness, higher 15 mm was achieved. The number of fabric layers differs dependent on the type of fabric and this feature of slab manufacturer is presented in Chapter 7.
2. Once the mould is full, a sheet of filter paper was placed on the top surface of the sample as seen in Figure 4.6(d).
3. It was especially important when using the six trapezoidal specimen mould to ensure that equal amounts of mix were placed into each cavity. Casting took place in the concrete laboratory of the Engineering Workshop and the loaded tool was transported to the WMG building on a trolley. The weight of material required to fill just one cavity before pressing was measured for each mix. This was achieved by fully filling a cavity, excavating it completely and measuring the weight of the removed cementitious materials. The remaining cavities were then filled with the same volume of mix.

4. The mould was then placed centrally on the lower platen of the either the Denison 7231 or the DASSET machine; in Figure 4.6(e) the Denison 7231 is shown. It is essential that the mould was positioned centrally in order to achieve a uniform downward pressure. The upper steel platen to the testing machine has a ball joint and is free to rotate when finding the state of static equilibrium.
5. The mould was then subjected to a compression force equivalent to a 9 MPa pressure, over the top surface area of the sample. The compressive stress was kept constant for one minute. During that time, the excess water was squeezed out of the samples and removed by vacuum through filter sheets and holes in the tool. Once the compression settings had been programmed into the machine, the vacuum pump turned on and the machine was instructed to compress the mix.
6. The applied pressure was then released.
7. To prevent a significant upward force that might damage the green form material when the upper platen of either the Denison 7231 or the DASSET was lifted the vacuum pump had to be turned off and the machine's ram lifted slowly.
8. The mould was then returned to the concrete lab and disassembled. A specimen was always carefully extracted by pushing it using a special tool designed for demoulding purposes. This step is shown in Figure 4.6(f). It is essential to be as gentle as possible when removing a sample as excessive deformation will induce deformation that could lead to undesirable micro-cracking (Miller, 1993). Although these micro-cracks may not be visible, Miller discovered that the in presence weakens the cured material significantly.

9. Finally, the tool was cleaned and dried thoroughly. Although laborious, due to the large number of drainage holes, this stage was absolutely essential if the mould was to be repeatedly used to produce green samples. Compressed air was used to clear the small holes and was found to minimise the time taken to complete this necessary stage. Once the steel had fully dry a light coating of the oil Aquaseal 777 was applied to prevent oxidation.
10. To ascertain the amount of water extracted during the pressing process, the weight of the specimens was recorded immediately after demoulding.
11. A specimen was then covered with a damp hessian sack and left overnight in the moist environment. Specimens were cured for 26 days using the procedures introduced in Section 4.6.

To determine the optimum pressing condition the author used material CF1 at 2% of V_f to investigate the influence of compression stress and the pressing time on flexural strength. All the specimens had the same mix design 1C:2A:0.58W. Following this, the specimens were cured for 28 days in hot water at 50 °C following the procedure given in Section 4.6. The aim was to identify when the flexural strength was a maximum. For this, the single trapezoid mould (Section 4.5.1) was used to produce batches of four specimens for the three compression forces of 50 kN (4.50 MPa), 100 kN (9 MPa), and 150 kN (13.5 MPa). The pressing times were of 1, 3, 6 and 9 minutes. To determine flexural strength, the test procedure outlined in Section 3.8 was used.

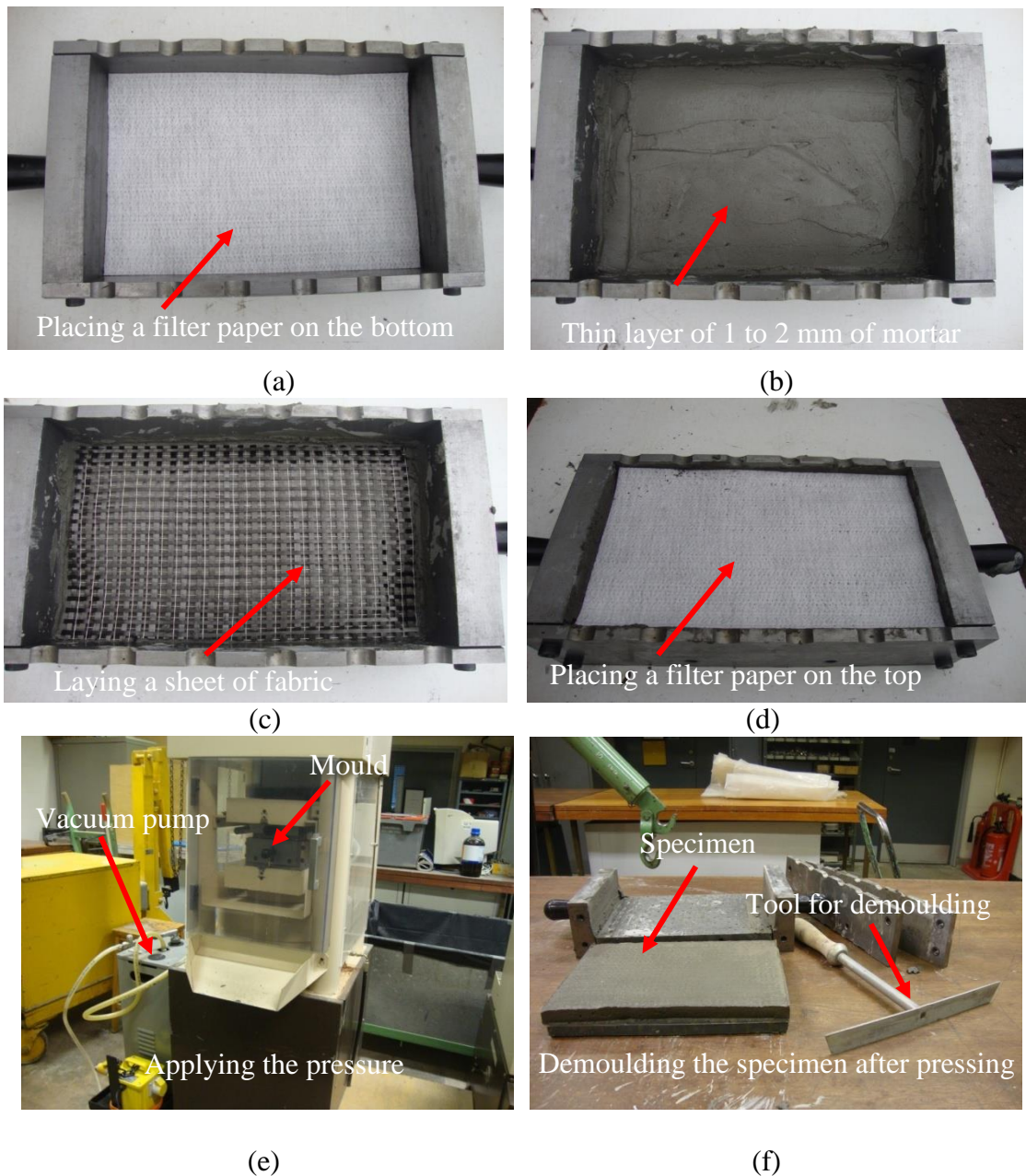


Figure 4.6: Steps in the fabrication of the FRC green forms by the compression moulding process: (a) laying a filter paper into the base of the mould; (b) laying a thin layer of mortar; (c) laying a sheet of fabric; (d) covering with an upper layer of filter paper when the required slab thickness has been reached; (e) placing the mould in the centre of the Denison 7231 compression machine; (f) demoulding the FRC specimen after pressing.

Plotted in Figure 4.7 are the mean flexural strengths from the twelve batches. It can be seen that as the pressing time increases, the strength decreases; this is contrary to the desired outcome of using compression moulding. The maximum mean flexural strength of

8.4 MPa was achieved when the applied compression stress was 9 MPa with a pressing time of 1 minute. This maximum mean can be compared with the hand lay-up flexural strength of 7.6 MPa from having a pressing of time of zero minute. The hand lay-up strength is lower and is found to be similar to the mean flexural strengths for pressing times of 3 to 9 minutes. Based on this experimental study it was decided that one minute was the optimum pressing condition for the programme of characterizing FRC materials reported in Chapter 5 to 7.

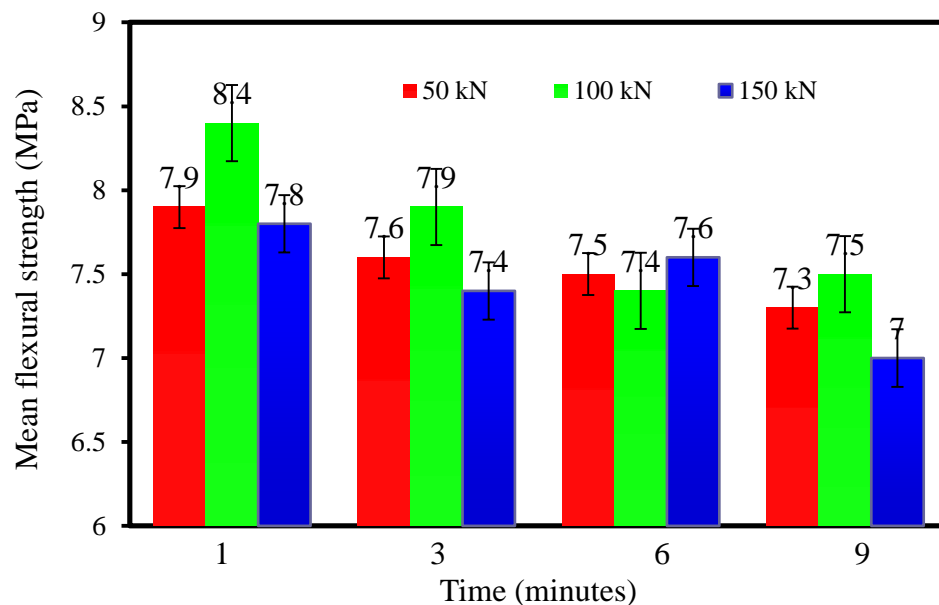


Figure 4.7: Flexural strength of CF1 specimens exposed to different pressing regimes in compression moulding process.

4.6 Curing Process

The influence of different curing regimes on the flexural properties of specimens was investigated. Twelve green specimens were produced for each mix design using the two methods process introduced in Sections 4.4 and 4.5. Since the green forms manufactured by the compression moulding method were immediately demoulded, they were found to be too fragile and weak for immersion under water. As a result, they were

covered with wet hessian for 24 hours before starting the curing process. Specimens from the hand lay-up method were demoulded after 24 hours (see Section 4.4) to provide samples with sufficient stiffness and strength to be immediately immersed in water.

Previous studies; Marikunte *et al.* (1997); Purnell (1998); Peled *et al.* (2005) and Purnell and Beddows (2005) studied the hot-water durability of glass fibre reinforced composites (GFRC). They cured GFRC by immersed the specimens in a hot water bath at different degrees; 20, 38, 50 and 65°C. Because high temperatures used in accelerated aging affect the nature of hydration products in the cement matrix. For this study 50° was chosen for curing. Hot water aging of the GFRC composite at 50° for 1 day is considered to be equivalent to about 100 days of aging when exposed to weathering in the UK (Purnell and Beddows, 2005).

Two curing processes were used. One batch of four samples was taken and cured in 100% Relative Humidity (RH). A second batch of four samples was cured by fully immersing them in hot water at 50° until the day before testing. When the single rectangular mould was used, it was necessary to cut the 240 by 170 by 15 mm slab into four flexural strength specimens of size 240 by 35 mm by 15 mm. Dependent on the strength of the material cutting was performed within four or five days of casting.

Chapter 5

5. Mix Design Optimisation

5.1 Introduction

Optimisation is the set of procedures used to make a system as effective as possible. FRC material is a system that has to meet varying and frequently, opposing criteria. These criteria include amongst others, strength, workability, and the availability of resources for the mix design. A choice in material proportioning is another criterion that can affect the mechanical properties of FRC materials. For example, those with higher cement content tend to increase shrinkage within the concrete, although this may also aid an increase in compressive, flexural, and tensile strengths. Cement is one of the most expensive components in concretes. The amount of the cement paste should be sufficient to cover all of the aggregates and fibres, binding them together to provide mobility to fresh concrete. It is however, also responsible for drying shrinkage and heat generation. Consequently, minimising the amount of cement paste in the mix design has to be one of the optimisation goals. One of the objectives of the study reported in this chapter is to evaluate the range of mix designs for FRC materials that could be capable of producing green forms of sufficient handling strength and structural integrity. Based on the goals of this research, fibres and materials such as those described in Chapter 3 were selected. The experimental work was divided into two main parts:

1. Short fibre reinforced cementitious materials with different types and sources of fibres, such as, recycled milled carbon (CF1), recycled chopped carbon (CF2), non-recycled chopped carbon (CF3), polyvinyl alcohol (PVA) and polypropylene (PP).

2. Continuous fibre reinforced cementitious materials using different fibres forms, such as unidirectional (0°) (CF4, CF5 and CF6), biaxial (0° , 90°) (CF7, CF8 and GF), and multiaxial (0° , 90° , $\pm 45^\circ$) (CF9) fabrics, and a hybrid, combining short and continuous reinforcements.

According to the previous research described in the literature review chapter, there are many parameters influencing the mechanical properties (flexural strength) of FRC materials. This chapter discusses the experimental procedures involved to establish the optimum cement based mix designs. The seven mix design, processing and testing parameters considered were; curing regimes, loading rate in flexural testing, additives content (SF, PFA and GGBS), aggregate type, aggregate composition, water/binder (w/b) ratio and pressing conditions on the mechanical properties of specimens manufactured by the compression moulding and hand lay-up processes. Processing of green specimens by these two methods has been fully discussed in Sections 4.4 and 4.5. Three moulds for the hand lay-up process; the single softwood, the five specimen stainless steel and the single rectangular slab plate moulds, were used as discussed in Sub-section 4.4.1. Three moulds for the compression moulding process; the single sample trapezoidal, the six samples trapezoidal, and the single rectangle slab plate moulds were used, as discussed in Sub-sections 4.5.1 to 4.5.3. As explained in Chapter 4 specimens were demoulded at two different stages, immediately after casting and pressing with compression moulding method and 24 hours after casting with the hand lay-up method. The necessary delay in removing material that is when using the hand lay-up method was due to the fact that the specimens were still fresh and did not have enough strength to remain intact throughout the demoulding process. Four-point bending test was carried out for all specimens to examine the materials in flexure. The test procedure is discussed in Section 3.8 and as will be seen, the mixes were modified to gain the highest flexural strength. Sub-sections 5.2 to 5.8 report

each of the seven stages. After preparing the moulds and the other equipment discussed in Chapter 4, many trial specimens were made to find the suitable proportion of ingredients to make the laboratory specimens.

5.2 Optimisation Step 1: The Influence of Curing Regime

In the concrete industry, it is common practise to place the manufactured product in a suitable moist environment during the early stages of cement hardening. This is essential given that any loss of water during its early age can adversely influence cement hydration, which can only take place with water filled capillaries. The consequence of this poor curing is a cement based material having a reduction in mechanical properties and long-term durability (Neville, 1995).

The optimisation step was based on evaluation using the optimum curing regime type i.e. cured in 100% RH and by fully immersing in hot water at 50°C. The curing period is 7 and 28 days. This series of experiments was carried out using mix design 1 C: 2 A: 0.4 W. In this experimental series only recycled milled carbon fibre (CF1) with 9% V_f was used and it was kept constant for comparison purposes. By visual inspection, it is found that the mix with 9% V_f is still workable due to the short length (0.085 mm) of CF1. Selecting the superplasticiser type to be SP_B (Glenium 51) with a loading at 3% by mass of cement was based on early results from the preliminary study outlined in Section 3.6.1. The green forms were processed by compression moulding using the six samples trapezoidal mould with the DASSET machine, as discussed in Sub-section 4.5.4. Before flexural testing, the two batches of twenty four specimens were prepared and cured in two different regimes following the procedure given in Section 4.6. Twelve specimens were cured in 100% RH, six for 7 days and the remaining six for 28 days. The other twelve specimens were cured by

fully immersing them in hot water at 50°C, six for 7 days and the remaining six for 28 days.

Figure 5.1 shows the mean flexural strength results for the specimens that were cured in 100% RH and by fully immersing in hot water at 50°C for 7 and 28 days. The results in Figure 5.1 clearly indicate that the specimens cured in hot water at 50° for both 7 and 28 days achieved the highest mean peak flexural strength of 10.8 and 14.4 MPa, being 24% (8.7 MPa) and 22% (11.8 MPa) respectively, higher than the specimens cured in 100% RH. Consequently, it can be seen that the curing regime by fully immersing in hot water at 50°C gives a higher material strength than the 100% RH condition. It was therefore decided to use this curing regime to cure all mixes during this study.

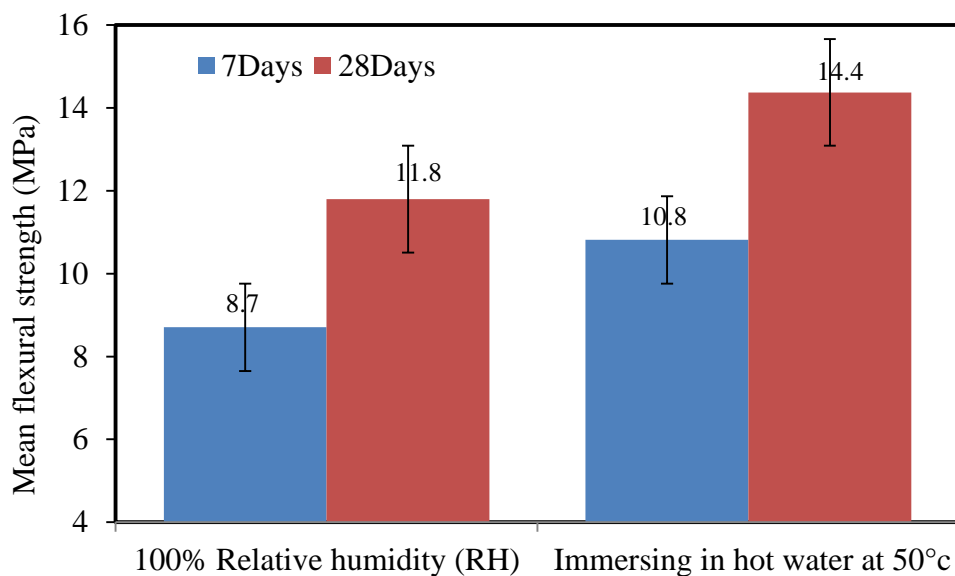


Figure 5.1: Mean flexural strength vs. different curing regimes.

5.3 Optimisation Step 2: The Influence of Loading Rate

The second optimisation step was based on evaluating the effect of loading rates during the four-point bending test on the flexural strength of FRC materials. The mix design, fibre type and content, constituent materials, and the mixing procedure were the

same as introduced in Section 5.2. The compression moulding method was used to process the green forms (see Sub-section 4.5.4) using the six samples trapezoidal mould (see Section 4.5.2) and the DASSET machine.

Based on the finding from the curing regime study in Section 5.2, the two batches of twenty four specimens were cured for 28 days in hot water at 50 °C (following the procedure given in Section 4.6). The specimens were then divided into six groups; each group had four specimens that were tested at loading rates of 0.5 (low), 1, 5, 10, 15, and 20 mm/min (fast). Four specimens were tested at each loading rate.

Table 5.1: The mean flexural strengths and loading rate for the six groups.

Loading rate (mm/min)	Mean flexural strength (MPa)
0.5	10.7
1	11.1
5	10.3
10	10.8
15	11.3
20	10.5

The results presented in Table 5.1 do not clearly indicate a change in flexural strength caused by the loading rate. For each batch the mean flexural strength remained around 11 MPa; such results indicate that an increase in the load rate would not be detrimental. Practically speaking, a four-point bending test for each specimen can be completed within \approx 25 to 30 minutes at 0.5 and 1.0 mm/min, \approx 5 minutes at 10 mm/min, and in less than 5 minutes for 15 and 20 mm/min. It was decided that a loading rate of 10 mm/min was the best compromise between time to failure and a possible strain rate effect changing the materials strength.

5.4 Optimisation Step 3: The Influence of Additives (SF, PFA and GGBS)

According to previous work developed in the literature review chapter, the use of additive materials (e.g. SF, PFA and GGBS), as partial replacement for cementitious materials offers many advantages. These advantages are discussed in Section 2.8. Optimisation Step 3 was based on evaluating the optimum additives (SF, PFA and GGBS) content. Again, the mix design, constituent materials, fibre type and content, curing regimes and the mixing procedure were the same as in Section 5.2. The adverse effects of the additives were an increase in the setting times of the mix and a decrease in workability due to an increase of particles in the surface area as discussed in Section 2.8. Compression moulding was used for the processing of all green forms, this time using the single sample trapezoidal mould with the Denison 7231 compression machine as discussed in Sub-section 4.5.4.

The first stage in this optimisation step was to evaluate the optimum silica fume (SF) content. Initial work was carried out using mix design 1 C:2 A with a w/b of 0.4 and with six different scenarios for SF content by increasing the additive in increments of 5%, from 0% to 25% by weight of cement. The maximum percentage of SF of 25% as replacement in cementitious materials used in the mixes in the present work agrees with the previous works in Sub-section 2.8.1 as SF was added in lower rate (5 to 25%) (Sengupta and Bhanja, 2003). Before flexural testing, the six batches of six specimens were cured in hot water at 50°C for 28 days.

The results of flexural testing for these mixes are shown in Figure 5.2. The material made with a SF content of 15% achieved the highest mean peak flexural strength of 13.6

MPa. Strengths for the mixes with SF content of 5% and 20% are similar at 10.7 and 10.1 MPa respectively, and so are the mean strengths for the materials having SF content of 10% and 25% at 11.5 and 11.2 MPa. Figure 5.2 shows that mean strengths increases continuously the SF content increased from 0 up to 15% and then the strength decreased with higher percentage of SF. The increase is known to be due to the decrease in voiding as result of the small ($\approx 1 \mu\text{m}$) SF particles filling the gaps between the cement grains and between the cement and fibres. Moreover, the trend is depicted by lower range of SF in Figure 5.2, seems to suggest that this tendency is linear. However, this trend is disrupted for values of SF content above 15%. In Figure 5.2, the cases with SF content $>15\%$ show a lower mean flexural strength, as compared to the peak reached by the 15% content. Nevertheless, given the range of percentage of SF studied in the present work, (0-25%). It is difficult to conclude if the later trend can achieve a higher flexural strength for mixes with percentage of SF $> 25\%$.

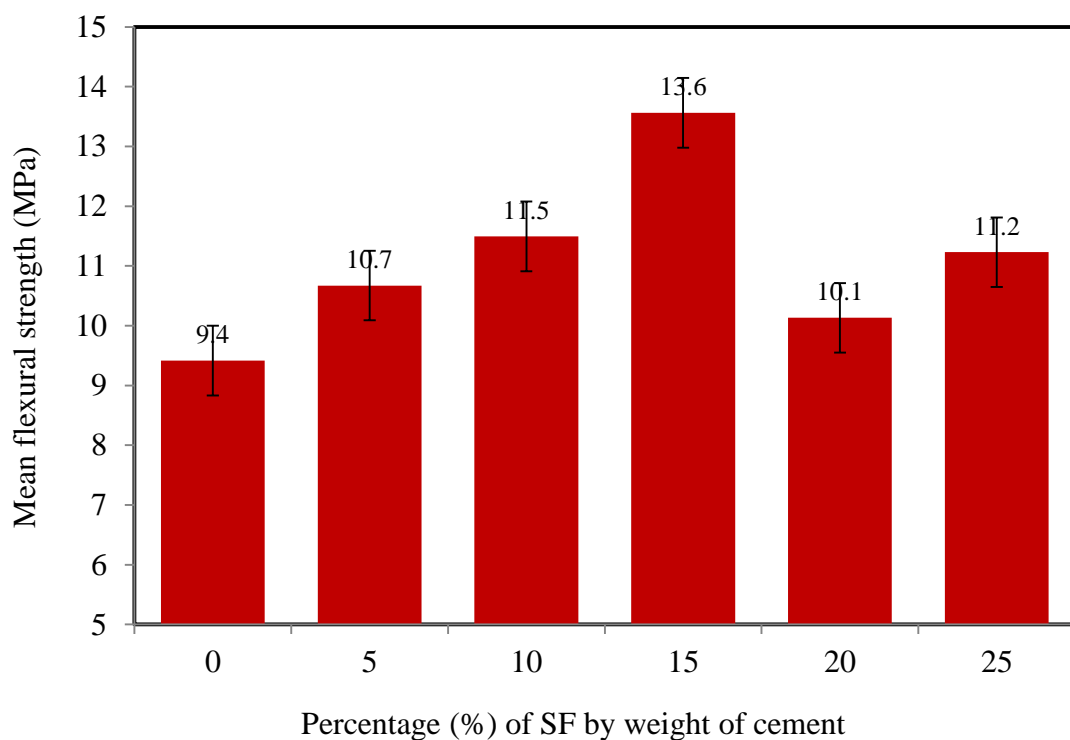


Figure 5.2: Mean flexural strength vs. SF content for evaluation optimum SF content.

It can be concluded, that the best SF content with regard to flexural strength is 15% by weight of cement. This important finding agreed with results from the previous studies by Yogendran *et al.* (1987); Toutanji *et al.* (1993); Mobasher and Li (1996); Fu and Chung (1998); Chung (2000); Shannag (2000); Chung (2002); Shihada and Arafa (2010); Ismeik (2010) and Zulkarnain and Ramli (2011) as discussed in detail in Sub-section 2.8.1.

The second stage of this optimisation step evaluated the optimum pulverised fly ash (PFA) content. Work was carried out using similar mix design as introduced in Section 5.2 with six different scenarios for a PFA content that was increased in increments of 10%, from 0% to 50%, by weight of cement. Before flexural testing the six batches of six specimens were cured in hot water at 50 °C for 28 days following the procedure out-lined in Section 4.6. As shown in Figure 5.3, for the range of mix designs studied, specimens of 1 C:2 A with a PFA of 20% achieved the highest mean peak flexural strength of 11.7 MPa. Results show that the strengths of materials with PFA at 10, 30 and 50% are similar at 9.9, 9.4, and 9.2 MPa so are the strengths of 11.7 and 10.9 MPa for the materials made with PFA at 20 and 40%. Test results give an increasing mean flexural strength for the PFA increasing from 0 up to 20%, strengths drop for further percentage increase. It can be concluded that the optimum PFA content with regard to flexural strength is 20%. This finding agrees with observations made by Yuan *et al.* (1982); Carette and Malhotra (1987); and Saraswathy *et al.* (2003) that were discussed in details in Sub-section 2.8.2.

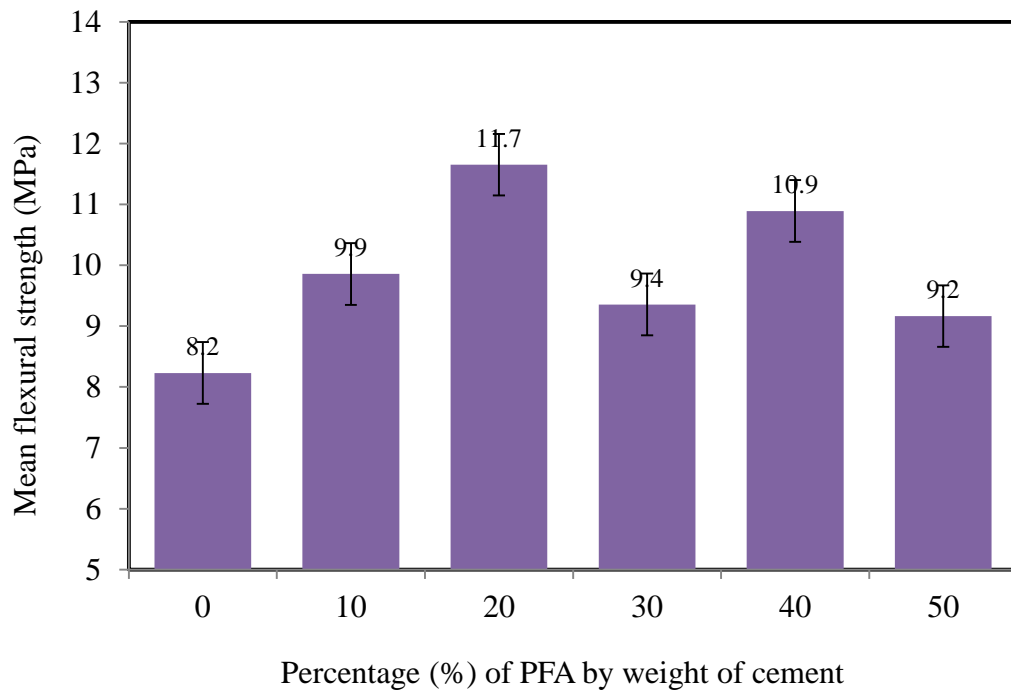


Figure 5.3: Mean flexural strength vs. PFA content for evaluation optimum PFA content.

The third stage of this optimisation step was to evaluate the optimum content for the additive of ground granulated blast furnace slag (GGBS). Work was carried out using a similar mix design as introduced in Section 5.2 with five different scenarios for GGBS content that was increased in increments of 15%, from 0% to 60%, by weight of cement. Five batches of six specimens were cured in hot water at 50°C for 28 days following the procedure given in Section 4.6. As presented in Figure 5.4, the six specimens containing GGBS at 30% achieved the highest mean peak flexural strength of 12.8 MPa. The bar chart show that this strength increased for GGBS increasing from 0% up to 30%. For higher percentages by weight the strength is found to be lowered. The optimum amount of GGBS is 30% and this conclusion is supported by a previous study by Zhou *et al.* (2012) that was introduced in Sub-section 2.8.3.

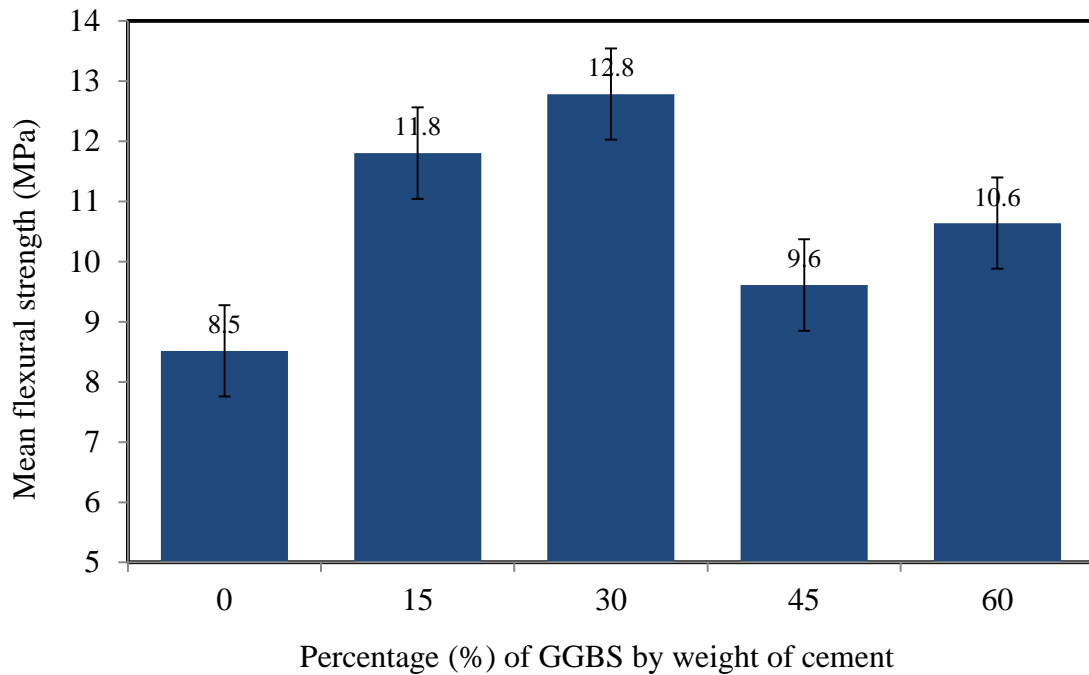


Figure 5.4: Mean flexural strength vs. GGBS content for evaluation optimum GGBS content.

The results obtained for this optimisation step with the three additive materials of SF, PFA and GGBS agreed with the previous studies by Bagel (1998); Khan *et al.* (2000); Pandey and Sharma (2000) and Toutanji *et al.* (2004), as discussed in Section 2.8. Moreover they confirm that a combination of SF, PFA and GGBS additives is likely to be a superior choice over any one of the additives. Regardless of the low strength in early age the additive materials were used: to reduce the amount of $\text{Ca}(\text{OH})_2$; increase the amount of calcium silicate hydrate (C-S-H) that holds the aggregates together; reduce the alkalinity of cement and to reduce the porosity. Based on the work in previous studies by Yogendran *et al.* (1987); Toutanji *et al.* (1998); Urban (2003); Chung (2005) and Yazdanbakhsh *et al.* (2009), all whom stated in their papers that the addition of SF can improve the uniformity of fibre dispersion in FRC materials. Knowing this fact and using the results of Section 5.4 it was decided to use in all mixes a combination of the additives SF, PFA, and GGBS as a replacement for cement. In terms of weight they were kept constant as 1 C: 0.15 SF:0.20

PFA :0.30 GGBS or in percentages the mix design had 60.6% C+9.1% SF+12.1% PFA+ 18.2% GGBS. These findings for binder proportions are confirmed by the results of the previous studies that are summarised in Table 5.2.

Table 5.2: Optimum percentage of additives; SF, PFA and GGBS by weight of cement obtained by a number of independent researchers.

Additive Type	Percentage of additive by weight of cement (%)	Reference
SF	15%	Yogendran <i>et al.</i> (1987)
		Toutanji <i>et al.</i> (1993)
		Mobasher and Li (1996)
		Fu and Chung (1998)
		Chung (2000)
		Shihada and Arafa (2010)
		Zulkarnain and Ramli (2011)
PFA	20%	Yuan <i>et al.</i> (1982)
		Carette and Malhotra (1987)
		Saraswathy <i>et al.</i> (2003)
GGBS	30%	Zhou <i>et al.</i> (2012)
		Gadpalliwar <i>et al.</i> (2014)
		Awasure and Nagendra (2014)

5.5 Optimisation Step 4: The Influence of Aggregate Type and Composition

Aggregates take up between 60 to 70% of the total conventional concrete materials volume. The aggregate mix design is an essential part of concrete mix design. It is therefore, most important that the correct aggregate type, proportion and particle size distribution are selected given that they have an effect on workability and mechanical properties strength of the FRC materials.

The fourth optimisation step considers aggregate type and aggregate combination (fine with coarse) by examining the effect of aggregates on the flexural strength of the FRC

materials. As discussed in Section 3.2.3 the cementitious material involved as the three types of aggregate; sand (S), crushed granite (GA) and crushed limestone (CL). The particle size distribution (PSD) analysis of S, CL and GA using sieve analysis is presented in Sub-section 3.3.1. For each aggregate combination study green forms were produced by compression moulding using the single sample trapezoidal mould and the Denison 7231 compression machine. The procedure followed to prepare the flexural specimens is given in Section 4.5.5.

One set of experimental work was carried out using a mix design with 9% V_f of CF1. The superplasticiser type SP_B (Glenium 51) was kept constant at 3% by mass of cement as introduced in Section 3.6.1. The best combination of binder materials for all mixes is 1 C:0.15 SF:0.20 PFA:0.30 GGBS as discussed in Section 5.2. By visual inspection, the water/binder (w/b) ratio was selected of 0.4. For the first stage of the investigation, characterisation work was carried out using the two different trials of aggregate proportions of 1 C:1 A and 1 C:2 A. Seven scenarios for aggregate composition that ranged different percentage compositions of GA, S, CL and S are listed in Table 5.3.

Table 5.3: Different aggregate type and composition scenarios for the two mix design of 1C:1A:0.4w/b and 1C:2A:0.4w/b.

	Aggregate combination (A)
Scenario 1	67% GA & 33% S
Scenario 2	67% CL & 33% S
Scenario 3	50% GA & 50% S
Scenario 4	50% CL & 50% S
Scenario 5	33% GA & 67% S
Scenario 6	33% CL & 67% S
Scenario 7	100% S

Notes: CL: Crushed limestone, GA: Crushed granite, S: sand

Compression moulding was used to process the green forms (see Section 4.5.5) using the six samples trapezoid mould (see Sub-section 4.5.3) with the DASSET machine. To

ensure that the CF1 fibres were distributed as uniformly as practical the mixture, as explained in Section 4.3, was agitated in a Hobart mixer for 12 minutes. Before flexural testing the fourteen batches of twelve specimens per batch were cured in hot water at 50 °C following the procedure given in Section 4.6. Six specimens from each batch were cured for 7 days and the remaining six of twelve for 28 days. Figures 5.5 and 5.6 show the mean flexural strength at 7 and 28 days for batches made with overall similar mix designs having different aggregate type and compositions. Results in these figures indicate that the flexural strength, at both 7 and 28 days, increases with increasing sand (S) content from 33% to 100% and decreasing coarse aggregate (GA and CL) contents from 67% to 0%.

For the range of mix designs studied the batch of 1 C:2 A with 100% S achieved the highest mean flexural strength of 17.3 MPa. It can be concluded that the optimum aggregate type and content with regard to strength is 1 C:2 A and only 100% sand with no coarse aggregate.

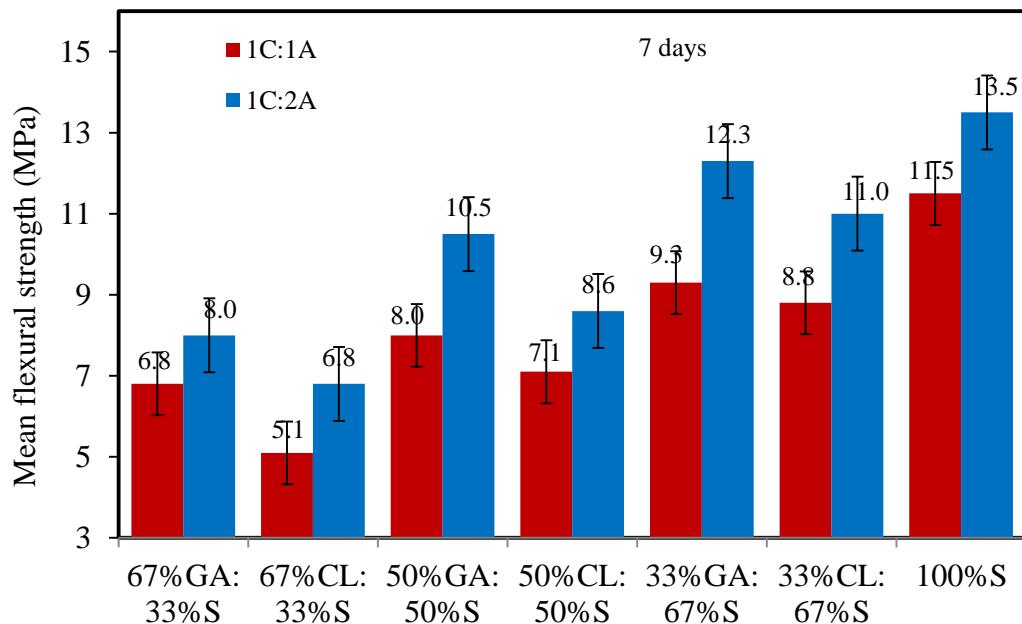


Figure 5.5: Mean flexural strength vs. mix design 1C:1A and 1C:2A with different aggregate compositions at 7 days.

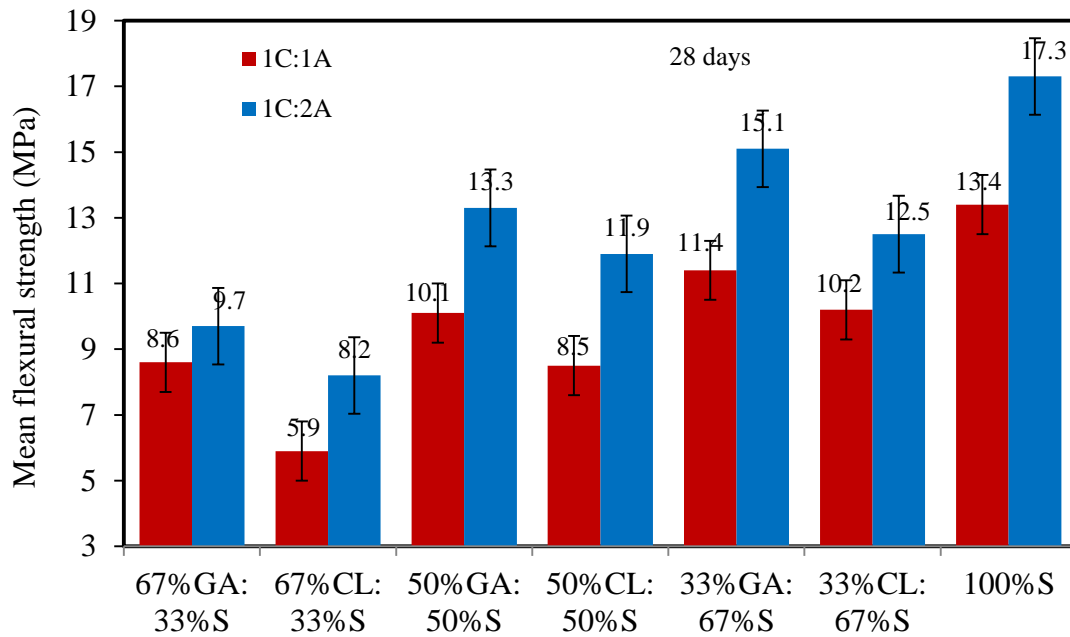


Figure 5.6: Mean flexural strength vs. mix design 1C:1A and 1C:2A with different aggregate compositions at 28 days.

Based on the test results presented in Figures 5.5 and 5.6 it can be seen that flexural strength at both 7 and 28 days increases when fine aggregate (S) content is increased from 33% to 100% and decreases with the coarse aggregate (GA and CL) contents reducing from 67% to 0%. It was therefore decided that no coarse aggregate (GA and CL) should be added to the cementitious formulations used in Chapters 6 and 7. The effect of fine aggregate content (S) on the flexural properties of FRC is investigated in next section.

5.6 Optimisation Step 5: The Influence of Fine Aggregate Content

This optimisation step is to determine the optimum fine aggregate (S) content. The mix design study of Section 5.5 indicates that a fine aggregate content of 100% S and no coarse aggregate is going to offer the highest flexural strength. For the mix design the constituent materials, fibre type and V_f , superplasticiser type and amount, binder type and amount and the mixing procedure were not change from that outlined in Section 5.2. The aggregate was 100% S with content per unit weight of 0.5, 1, 2, and 4. The four mix

designs are therefore Scenario 1 with 1 C:0.5 A, Scenario 2 with 1 C:1 A, Scenario 3 with 1 C:2 A and Scenario 4 with 1 C:4 A. Compression moulding was used to process the green forms (see Sub-section 4.5.5) using the six samples trapezoidal mould (see Sub-section 4.5.3) and the DASSET machine.

It was noted that when more aggregate was added to the mix, more water than for w/b ratio of 0.4 was required to maintain the same mix workability. To ensure similar workability, the water content in the mixes was adjusted during several trials, until they all reached the similar slump value of mm, i.e. a similar consistency. The workability of the mixes was measured by the modified slump test as discussed in Sub-section 3.6.1. Before flexural testing, the four batches of twelve specimens were cured in hot water at 50°C following the procedure given in Section 4.6. Six specimens from each of the four batches were cured for 7 days and the other six specimens from each batch were cured for 28 days. The mean flexural strength results given in Figure 5.7 show that there is a significant difference between batches cured for 7 and those cured for 28 days. The reason for a considerable decrease in flexural strength when the mix is 1 C:4 A is an increase in voids.

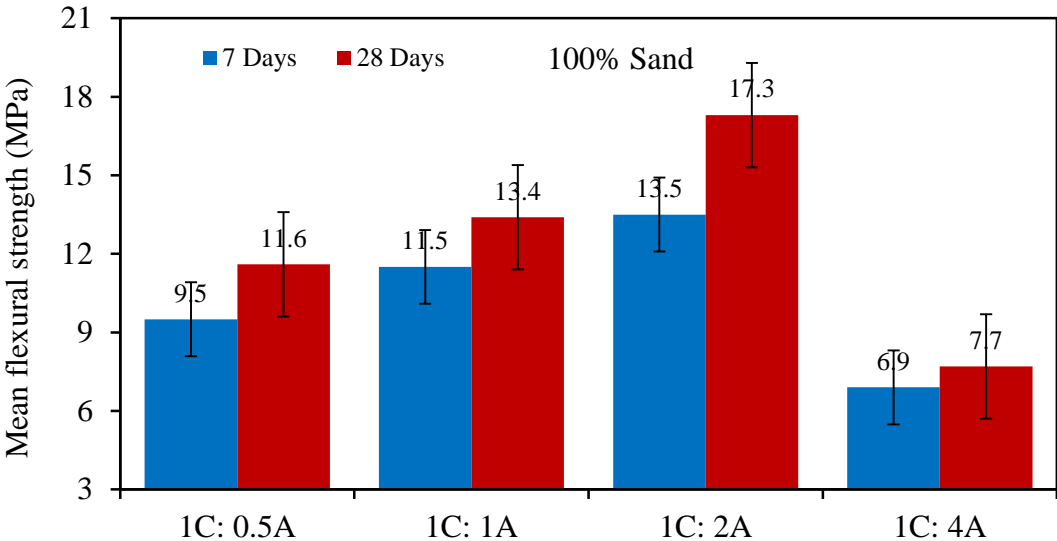


Figure 5.7: Mean flexural strength vs. mix design. Aggregate (A=100% S)= 0.5, 1, 2, and 4.

The results given in Figure 5.7 show that the specimens with a fine aggregate (S) ratio of 2 achieved a highest mean peak flexural strength for both 7 and 28 days of 13.5 and 17.3 MPa; 42% (9.5 MPa) and 49% (11.6 MPa), 17% (11.5 MPa) and 29% (13.4 MPa), and 96% (6.9 MPa) and 125% (7.7 MPa), respectively. This was higher than the specimens made from S of 0.5, 1, and 4. The results therefore indicate that the optimum fine aggregate ratio with regard to strength is 2.

5.7 Optimisation Step 6: The Influence of Water/Binder (w/b) Ratio

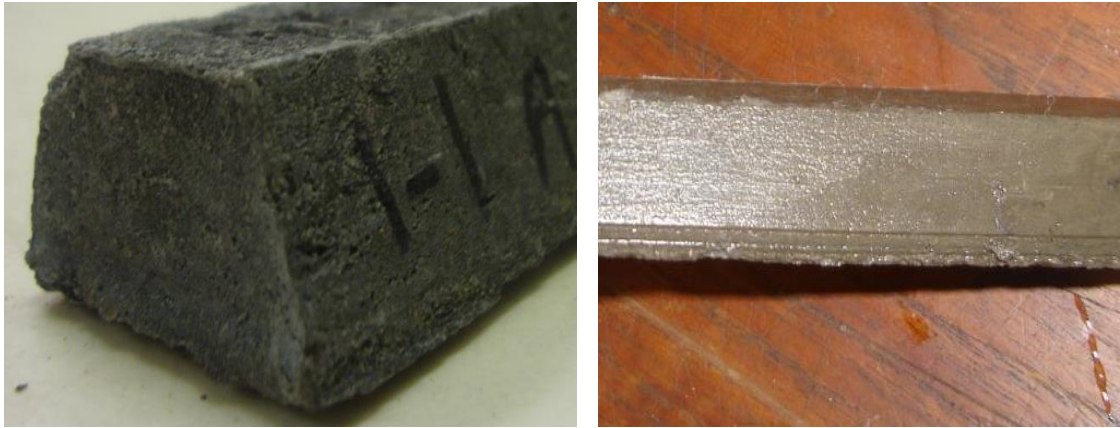
The ease of working with FRC materials depends on the water content. The use of less than the optimum amount of water may make setting difficult and reduce workability. On the other hand, greater shrinkage and a reduction in strength will occur when more water than the optimum amount is used. The best water-cement ratio therefore, depends on the particular mix design.

Optimisation step 6 is to establish the effect of changing the water content on the flexural strength. The experimental work was divided into the two main parts for cementitious materials reinforced with short fibres and for cementitious materials reinforced with continuous fibres as discussed in Sub-sections 5.7.1 and 5.7.2 below.

5.7.1 Short Fibres

This optimisation step is to determine the optimum w/b ratio for FRC materials reinforced with short fibres ($V_f = 9\%$) that will be studied in Chapter 6. The mix design, constituent materials and mixing procedure were as in Section 5.2. The combination of binder materials given the highest mean flexural strength is 60.6% C+9.1% SF+12.1% PFA +18.2% GGBS. This combination is now used in all mixes. These binder proportions were selected based on the processing investigations reported in Section 5.2. The aggregate

was 100 per cent S for the reason given in Section 5.5. According to previous research by Yusof *et al.* (2011) described in the literature review chapter in Section 2.14, there is an inverse relationship between the short fibre content (V_f) and workability; as the V_f increases the workability decreases. To characterise this change the w/b ratio was increased in increments of 0.05 from 0.40 to 0.60. These ratios were selected based on a preliminary study during which it was observed, by visual inspection, that a mix with short fibres and containing a w/b ratio of 0.35 or lower, was too dry, not workable, had lower strength and gave the poor surface finish seen in Figure 5.8(a). These differences in the cementitious material were due to a lack of water content to hydrate the cement given the presence of a 9% by volume of short fibre type CF1. The batches of specimen having w/b ratios from 0.40 to 0.60 were found to have workable mixes that also exhibited the best structural stability. That is after demoulding, they did not crack or rupture or become misshapen under their own weight. They also possessed good surface quality as seen in Figure 5.8(b). Compression moulding process was used for processing all the green forms using the single sample trapezoidal mould (see Section 4.5.3) and the Denison 7231 compression machine (see Section 4.5.5). Before flexural testing the five batches of twelve specimens were cured in hot water at 50 °C as investigated in Section 5.2. Then, following the procedure introduced in Section 4.6 six of the specimens were cured for 7 days and the remaining six cured for 28 days.



(a)

(b)

Figure 5.8: Manufacture specimen: (a) with a bad surface finish; (b) with good surface finish and without cracks.

The four-point bending test was carried out to determine flexural strength. The test procedure is discussed in Section 3.8 and the results of the flexural testing for these mixes are shown using the bar chart in Figure 5.9. The w/b ratios for each batch were calculated after demoulding to estimate the extraction water during the pressing process. It ranged from 33% to 42% as given in Table 5.4. As expected from previous study (Farahi, 2009), the results in Figure 5.9 show that when the water content increases the strength decreases. Specimens with the added w/b ratio of 0.40 that had been cured for 28 days achieved the highest mean peak flexural strength of 17.3 MPa. Assessment of this study indicates that the optimum w/b ratio with regards to strength and workability is going to be 0.4. In Chapter 6 all mixes with short fibres therefore used this w/b ratio.

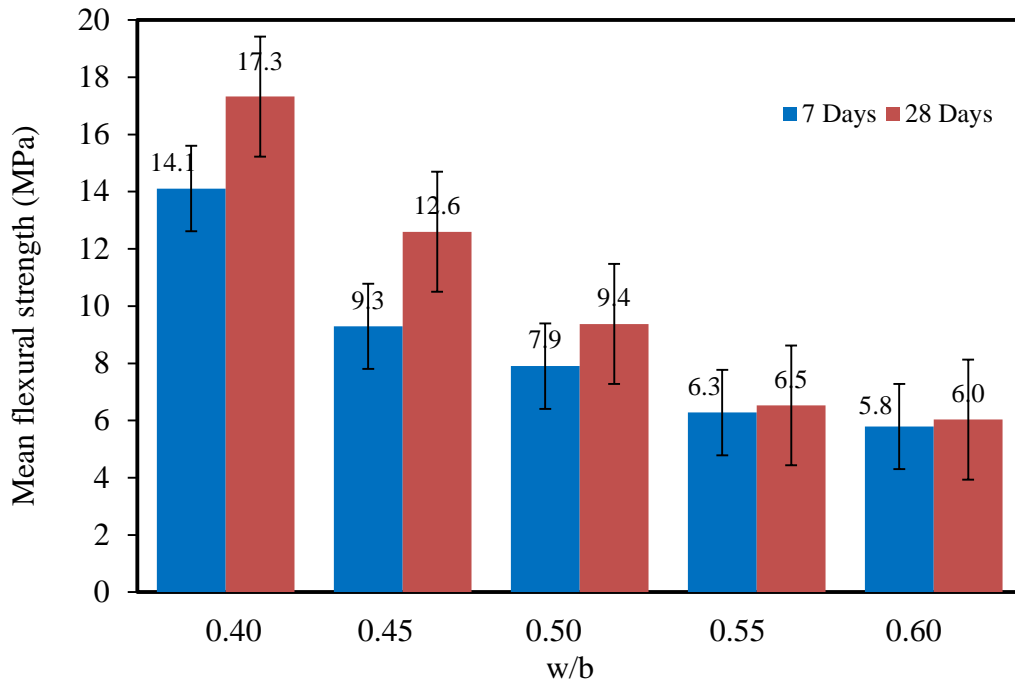


Figure 5.9: Flexural strength vs. w/b ratio for short fibres reinforced material.

Table 5.4: Different water/binder ratio scenarios from pressing process for short fibres reinforced material.

Mix No	w/b		
	Before pressing	After pressing	Difference (%)
Batch 1	0.40	0.27	33
Batch 2	0.45	0.27	40
Batch 3	0.50	0.33	34
Batch 4	0.55	0.34	38
Batch 5	0.60	0.35	42

5.7.2 Continuous Fibres

It is now important to establish the optimum w/b ratio for mix in Chapter 7 that will be reinforced with continuous fibre reinforced cementitious materials. The mix design, number of batches and curing regimes are the same as for the short fibres discussed in Section 5.7.1. For this study, the mix was reinforced with the continuous fibre type of CF9. Compression moulding was used for processing all green forms in accordance with the

method as discussed in Section 4.5 using a single rectangular slab plate mould and the DASSETT compression machine. To ensure a matrix of suitable workability the w/b ratio was increased in increments of 0.05 from 0.35 to 0.55.

Water extraction during the pressing process ranged from 28% to 38% as shown in Table 5.5. The results in Figure 5.10 show that when w/b ratio increases the strength decreases. The CF9 specimens had a V_f of 5%. With w/b equal to 0.35 and cured for 28 days the material achieved the highest mean peak flexural strength of 44.9 MPa, 15% (39 MPa), 42% (31.6 MPa), 64% (27.4 MPa) and 94% (23.2 MPa), respectively, and higher than the specimens made from w/b of 0.4, 0.45, 0.50 and 0.55. It can be concluded therefore, that the optimum w/b ratio with regard to strength is 0.35 and was used for all seven continuous fibres.

Table 5.5: Different water/binder ratio scenarios from pressing process for continuous fibres reinforced material.

Mix No	w/b		
	Before pressing	After pressing	Difference (%)
Batch 1	0.35	0.24	31
Batch 2	0.40	0.29	28
Batch 3	0.45	0.29	36
Batch 4	0.50	0.34	32
Batch 5	0.55	0.34	38

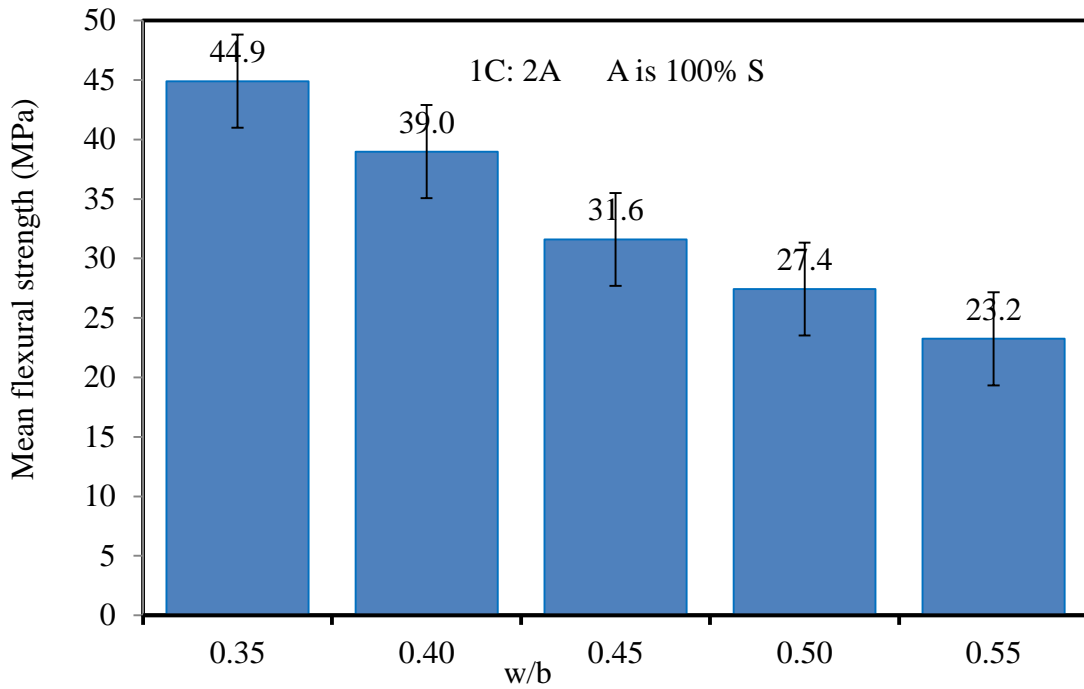


Figure 5.10: Mean flexural strength vs. w/b ratio for continuous fibres reinforced material.

5.8 Optimisation Step 7: The Influence of Pressing on w/b

As stated in Chapter 4 the compression moulding process was used to reduce the w/b ratio of the green form specimen. The change in w/b was investigated with the aim of estimating the water extraction during the pressing process. Again, the mix design, constituent materials and mixing procedure were the same as given in Section 5.2. Compression moulding using the single rectangular slab plate mould and the Denison 7231 compression machine was used for the processing of all green forms as discussed in Section 4.5.5. As explained in Section 4.5.5 an average compression stress of 9 MPa was applied with a pressing time of one minute.

This series of experiments was carried out using mix design 1 C:2 A (A is 100% S) with 9% V_f of the recycled milled carbon fibre type CF1. The mixes had superplasticiser type SP_B (Glenium 51) at 3% by weight of cement (see Section 3.6.1). The variable was

the w/b which was increased in increments of 0.05 from 0.35 to 0.6. Before flexural testing the six batches of six specimens were cured in hot water at 50°C for 28 days following the procedure given in Section 4.6. Plotted in Figure 5.11 is the mean w/b ratio from the six batches that had contained six specimens per batch. The pressing process achieved excess water extraction from the mould which ranged from 24% to 43%. This resulted in green forms with an average w/b of 0.20 to 0.40 as shown in Figure 5.11. Full consolidation and wet-out is essential in obtaining quality material.

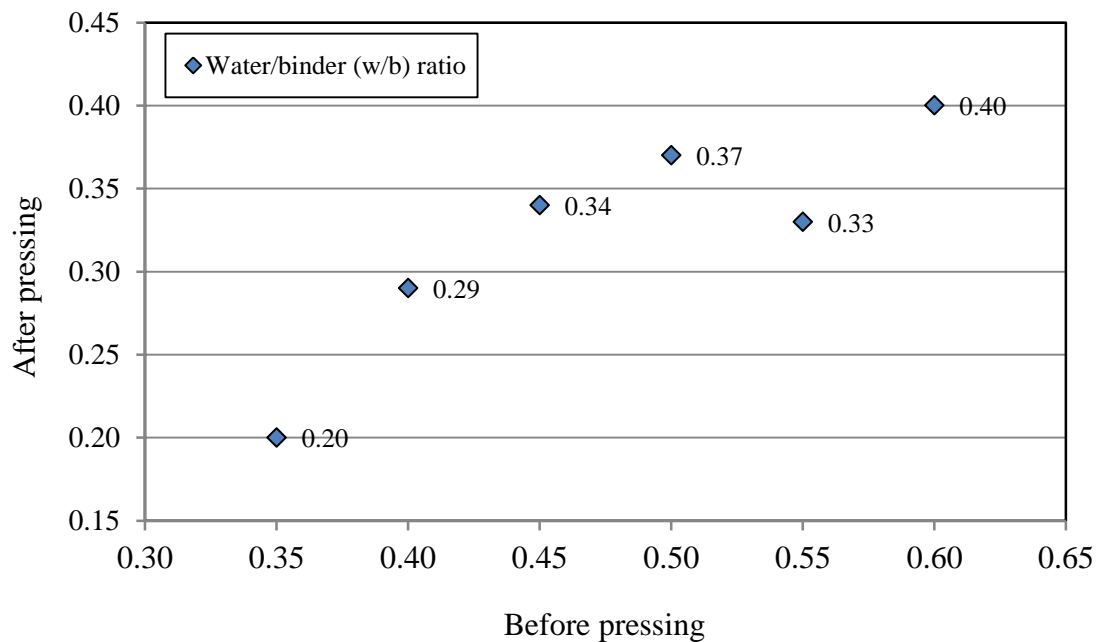


Figure 5.11: Water/binder (w/b) ratio before and after pressing for six batches.

5.9 Summary

Working with a wide range of mix designs the author set out to find the optimum mix design. Results confirmed that the aggregate type/combination given an increasing flexural with increasing sand (S) content and decreasing coarse aggregate contents. Specimens made from 1 C:2 A with an aggregate of 100% S achieved the highest mean flexural strength of 17.3 MPa. Results found that a w/b ratio 0.40 for short fibres and 0.35 for

continuous fibres gave the material with the best properties of strength and workability. The compression moulding process achieved an excess water extraction of 24% to 43%. Specimens cured in hot water at 50°C achieved a mean peak flexural strength of 22% higher than the specimens cured in 100% relative humidity (RH). The best combination of binder materials for all mixes was found to be 60.6% C+9.1% SF+12.1% PFA+ 18.2% GGBS.

Tables 5.6 and 5.7 present a summary of the materials proportions in grams for both hand lay-up and compression moulding processes for materials reinforced with short and continuous fibres using different moulds. Only the w/b ratio changes when the reinforcement is using a type of continuous fibre. Two mixes design were used in this study; 1 C:2 A:0.66 W for short fibres and 1 C:2 A:0.58 W for continuous fibres. These materials were used in the research developed work in Chapters 6 and 7.

Table 5.6: Material proportions and moulds used for the hand lay-up process.

Material by mass	Mould type		
	Single wood mould	5 Stainless steel mould	Rectangular mould
Cement (g)	48	450	300
Aggregate= 100% Sand (g)	96	900	600
Water* (g), for short fibres, w/b =0.4	31.68	297	198
SF= 15% by weight of cement (g)	7.2	67.5	45
PFA= 20% by weight of cement (g)	9.6	90	60
GGBS= 30% by weight of cement (g)	14.4	135	90
Superplasticiser = 3% by weight of cement (g)	1.4	13.5	9
Binder** (g) =	79.2	742.5	495
* Water/binder ratio (w/b) = 0.35 for continuous fibres, water = 27.72 g.			
** : Binder = 60.6% C + 9.1% SF + 12.1% PFA + 18.2% GGBS			

Table 5.7: Material proportions and moulds used for compression moulding process.

Material by mass	Mould type		
	Single mould	6 Stainless steel mould	Rectangular mould
Cement (g)	30	180	300
Aggregate= 100% Sand (g)	60	360	600
Water* (g), (w/b) = 0.4, for short fibres	19.8	118.8	198
SF= 15% by weight of cement (g)	4.5	27	45
PFA= 20% by weight of cement (g)	6	36	60
GGBS= 30% by weight of cement (g)	9	54	90
Superplasticiser = 3% by weight of cement (g)	1	5.4	9
Binder** (g)	49.5	297	495
*Water/binder ratio (w/b) = 0.35 for continuous fibres, water = 17.33 g.			
** : Binder = 60.6% C + 9.1% SF + 12.1% PFA + 18.2% GGBS			

Chapter 6

6. Test Results of Cementitious Materials Reinforced with Short Fibres

6.1 Introduction

In this chapter, the results of four-point bending tests, in accordance with Sub-section 3.8.1 are reported, analysed and discussed. Small batches of specimens are characterised for five short fibre types, as introduced in Section 3.2.4, to determine flexural strength, strain at peak stress and a measure of toughness (energy absorption) for FRCs, often with V_f of 2%. Based on the outcomes of Chapter 5, one mix design was chosen to manufacture all specimens made by compression moulding and hand lay-up processes. Its proportions of constituent parts are 1 C: 2 A: 0.66 W. A comparison is made between the reinforced materials (the FRCs) and the properties of the control where the cementitious matrix is without fibres.

6.2 Specimens Labelling Code

It is important to have a specimen labelling that clearly identifies the material. The parts of the system used are: fibre type; manufacturing method; curing regime; specimen number. The various entries to the four parts for a label are now explained. The fibre type is 'CF1', 'CF2', 'CF3', 'PP' and 'PVA'. 'CS' is for control material. The type of manufacturing process is 'HU' for hand lay-up, and 'CM' for compression moulding.

Curing regime codes are '50' for 50°C hot-water ageing. To help the reader know the system examples are now given:

- CF1-CM-50-01 is the material with recycled milled carbon fibre CF1, produced by compression moulding and cured in hot water at 50°C, and is specimen #1.
- PVA-HU-50-02 is the material with polyvinyl alcohol fibre (PVA), produced by hand lay-up and cured in hot water at 50°C, and is specimen #2.
- CS-CM-50-01 is for control specimen produced by compression moulding, and cured in hot water at 50°C, and is specimen #1.

6.3 Test Results and Discussion

Mix proportions are given by the weight of cement, as presented in Tables 5.6 and 5.7 (see Section 5.9). Preliminary experiment results show that no coarse aggregate is to be added to the matrix; only fine aggregate (100% sand) with SPD < 1.18 mm, as discussed in Section 5.5. It is worth reminding the reader that two key processing findings are; firstly, to have 3% by weight of cement of superplasticiser type SP_B (Glenium 51), selected based on study the effect of water/binder (w/b) ratio on the slump, as discussed in Section 3.6.1; and, secondly, that the required combination of the binder materials is: 60.6% C+ 9.1% SF+ 12.1% PFA+ 18.2% GGBS. In other words, the matrix contains these binder materials by weight of cement as: 15% of SF; 20% of PFA; 30% of GGBS. These proportions were selected based on the processing investigations presented in Section 5.4.

Preliminary experiments are reported in Section 5.7 and showed that (to maintain workability) the w/b ratio in the mixes with short fibres is to be kept constant at 0.40 (i.e. 0.66 W). It was kept constant for comparison purposes as it can be easy to compare with other specimens reinforced with other types of short fibres or without. The processing findings presented in Chapter 5 were adopted to produce the cementitious matrix for the work reported in this chapter.

In this chapter the influences of five types of short fibres on mechanical properties are investigated, using different values of V_f . Three of the fibres are of carbon (namely CF1, CF2 and CF3), of which two are from recycled sources (CF1 and CF2). Using type CF1 as reinforcement for cementitious materials is novel. Its average length is 0.085 mm. The length of CF2 fibre ranges from 3 to 25 mm, its average is 14 mm. CF3 is not from a recycled source and has an average length of 6 mm. The other two short fibres types are polypropylene (PP) having average fibre length of 12 mm and polyvinyl alcohol (PVA) with an average of 8 mm. These short fibres are briefly introduced in Section 3.2.4 and their properties on interest are presented in Table 3.2.

Tensile testing is in theory most appropriate for determining the stress-strain behaviour of FRCs, but is often very difficult to carry out in practice owing to issues with suitable test equipment. In this study, due to the shape and size of specimen (being relatively thick (16 mm) and trapezium in cross-section) tensile loading was deemed to be too difficult to execute. Hence, a flexural test was performed to determine mechanical performance. The author is aware of the limitations, and the fact that failure stress in flexure is slightly higher than would be the strength by testing tensile coupon. In accordance with Section 3.8.1 four-point bending tests were carried out. The results of the load against central deflection were recorded using software on a PC connected to the 100 kN Testometric machine. These data points were used to generate plots for the bending stress- bending strain curves. The procedure employed to convert load vs. deflection into stress vs. strain is presented in Section 3.8.1. Comparisons and analyses of the flexural behaviour are made using such plots, and in Sub-section 6.3.8 bar charts are used to summarise the main test results.

Test results and statistical analysis for batches of specimens reinforced with the five short fibres at $V_f = 2\%$ are presented in Tables A.6.1 to A.6.10 in Appendix A, and for the controls in Tables 6.1 and 6.2. In this series of tests, the number of nominally identical specimens per batch is normally six, with five in a few batches. The twelve tables have the following content. Column (1) gives the specimen label and the name of the property that has entries in the row of columns to the right of it. Column (2) is the w/b ratios for hand lay-up method or for the compression moulding before and after pressing. Columns (3) to (5) are for peak stress, peak strain at peak stress, and toughness, respectively. The third to eighth rows give information for the individual specimens. For each batch, the mean, standard deviation (SD) and characteristic values are given in rows nine to eleven, on the assumption that the strength population fits the Gaussian distribution. In row eleven the characteristic values for stress at first cracking (or ‘Loss of Proportionality’ with abbreviation LOP), and at peak load are determined using the guidance in Annex D7 (General principles for statistical evaluation) of Eurocode 0 (BS EN 1990:2002). Eurocode 0 and its commentary by Gulvanessian *et al.* (2002) give details of how characteristic properties are to be determined. The final two rows give maximum and minimum values for stress, strains, toughness and the water/binder (w/b) ratio; before and after pressing and the difference between them, for the compression moulding.

At each loading step flexural stress is calculated using Equation (3.1) and the mid-span deflection is calculated with Equation (3.8). The mean flexural strength for each batch is obtained by taking the mean of the maximum flexural stress for the specimens in a batch. In order to avoid confusion, due to the large number of specimens, the lower and upper bounds for the stress-strain curves have been chosen for figures as they can represent the flexural behaviour for each batch.

To allow for the pairs of curves in the twelve figures to be easily compared with each other, the plotting has the same ordinate and abscissa axis scales. By inspecting the curves the reader will be able to establish the relative differences in upper and lower test results from each batch of six (or five) specimens, and can from the area under a curve can evaluate the energy absorption capacities of various material characterised by the four-point bending testing. The microstructure of the five types of short fibres is investigated using Scanning Electron Microscopy (SEM) to examine how the fibres were dispersed in the matrix, and to observe the interaction between fibres and matrix. The preparation process and the SEM technique used are fully discussed in Section 3.4.

6.3.1 Control Materials

The mix design, constituent materials and mixing procedure were the same as previously mentioned in Section 6.3. In order to provide a basis for comparison and control, the flexural strength of mortar, without fibres, was investigated. Before flexural testing, the two batches of twelve control specimens were prepared; six were produced using compression moulding, and the other six by the hand lay-up processing method. Following this, the specimens were cured for 28 days in hot water at 50 °C following the procedure given in Section 4.6. The control specimens were produced with the same dimensions as the FRC specimens, as reported in Chapters 4 and 5. They were identified as series CS-CM-50-01 to CS-CM-50-06 for compression moulding process and CS-HU-50-01 to CS-HU-50-06 for hand lay-up². Tables 6.1 and 6.2 present the test results and statistical analysis. Inspecting column (3) in Tables 6.1 and 6.2 it is seen that LOP and the peak stresses are the same (i.e., $\sigma_{mu} = \sigma_{cu}$). This is because when the control material first cracks it results in ultimate failure.

A slight difference for the overall mechanical behaviour was observed between the control specimens produced with hand lay-up and compression moulding. The results in columns (4) and (5) of Tables 6.1 and 6.2 show that the mean strain at peak stress and toughness with hand lay-up is 36% and 25% higher than by compression moulding. All tests ended with tensile rupture for a mean failure strain of 0.026%. The strengths (i.e. peak stresses) reported in Tables 6.1 and 6.2 are for a range from 4.7 to 7.3 MPa, with an average of 6.4 MPa. The lower variability with the compression moulding is due to greater consistency in mixing, curing and testing. In this thesis, the author decided that a difference up to 15% between any two properties is not considered to be significant (see Section 6.5). The mean peak stress at 6.7 MPa with compression moulding is 10% higher than by hand lay-up at 6.1 MPa. Due to the applied compression pressure of 9 MPa (see Section 4.5.5) in casting there is reduced capillary porosity, and an improvement in the strength.

The strain and toughness of the control material is, as expected, very low, because the matrix exhibits no ductile behaviour owing to the inherent brittleness. As might be expected from the specimen consolidation by compression moulding the characteristic strength of 4.9 MPa from the hand lay-up control batch is slightly lower by 18%. The standard deviations (SD) are 0.5 and 0.8 in Tables 6.1 and 6.2, respectively, indicating that the data points tend to be close to the mean.

Table 6.1: Results from four-point bending test, water reduction and standard deviation of six control specimens manufactured via compression moulding.

(1)	(2)			(3)		(4)	(5)
Specimen code	Water binder ratio			Stress (MPa)		Strain at peak stress (%)	Toughness at peak stress (J/m ³)
	Before pressing	After pressing	Difference (%)	LOP	Peak		
CS-CM-50-01	0.4	0.22	45	6.8	6.8	0.021	0.0008
CS-CM-50-02	0.4	0.25	38	6.4	6.4	0.025	0.0008
CS-CM-50-03	0.4	0.24	40	5.8	5.8	0.014	0.0004
CS-CM-50-04	0.4	0.23	43	7.1	7.1	0.009	0.0003
CS-CM-50-05	0.4	0.25	38	6.9	6.9	0.022	0.0009
CS-CM-50-06	0.4	0.23	43	7.3	7.3	0.041	0.0019
Mean	0.4	0.24	41	6.7	6.7	0.022	0.0008
SD				0.5	0.5	0.011	0.001
Characteristic strength (MPa)				5.8	5.8		
Max		0.25	45	7.3	7.3	0.041	0.0019
Min		0.22	38	5.8	5.8	0.009	0.0003

Table 6.2: Results from four-point bending test and standard deviation of six control specimens manufactured via hand lay-up.

(1)	(2)	(3)		(4)	(5)
Specimen code	Water binder ratio	Stress (MPa)		Strain at peak stress (%)	Toughness at peak stress (J/m ³)
		LOP	Peak		
CS-HU-50-01	0.4	6.0	6.0	0.027	0.0008
CS-HU-50-02	0.4	6.6	6.6	0.084	0.0026
CS-HU-50-03	0.4	6.5	6.5	0.015	0.0009
CS-HU-50-04	0.4	6.4	6.4	0.021	0.0007
CS-HU-50-05	0.4	4.7	4.7	0.013	0.0005
CS-HU-50-06	0.4	6.7	6.7	0.011	0.0004
Mean		6.1	6.1	0.030	0.001
SD		0.8	0.8	0.028	0.001
Characteristic strength (MPa)		4.9	4.9		
Max		6.7	6.7	0.084	0.0026
Min		4.7	4.7	0.011	0.0004

Figures 6.1 and 6.2 show the lower and upper bound stress-strain curves for the two control materials. It can be observed from the figures that the stress-strain curves for compression moulding and hand lay-up show a similar relatively brittle behaviour, having linear elasticity up to the first crack. In this case, LOP is the peak stress occurring at approximately 5 and 7 MPa for lower and upper bounds, respectively. The peak stresses in both hand lay-up (4.7 and 6.7 MPa) and compression moulding (5.8 and 7.3 MPa) specimens varied similarly. Curve OA in Figure 6.1 represents the initial, linear, uncracked behaviour of the strongest control specimen. What is shown in this plot is for the pre-cracking Region I introduced in Section 2.13.

As shown in Figure 6.1(a) a control specimen failed almost immediately the maximum load is reached. This attributed to the following: heterogeneous and complex nature of cement matrix; strain limit of the cement matrix is low; macro-cracking rapidly traversed the whole depth of the specimen starting at the tension face. Brittleness is due to no stress transfer being possible, because of the relative non-efficiency of the cement mortar as a resistance mechanism and any bridging of macrocrack is very short. As Van-Mier (1997) noted the only crack bridging available, which is limited, is provided by aggregate locking action.

The first formal presentation of practical FRC stress-strain curves was published by Aveston and co-workers (1971, 1973 and 1974), leading to the ACK model. This model has been introduced in Section 2.13. There are four distinct regions in the stress-strain curve, with Regions II and III for flexural behaviour when there are multiple cracks and the specimen's stiffness is non-linear due to progressive damage growth. For the control specimens, these regions are totally absent as expected (see Figure 6.1) and as the photograph in Figure 6.3 shows a specimen fails with a single vertical (tension) crack

located directly below one of the two loading pins (where the maximum moment (and shear force coincide)).

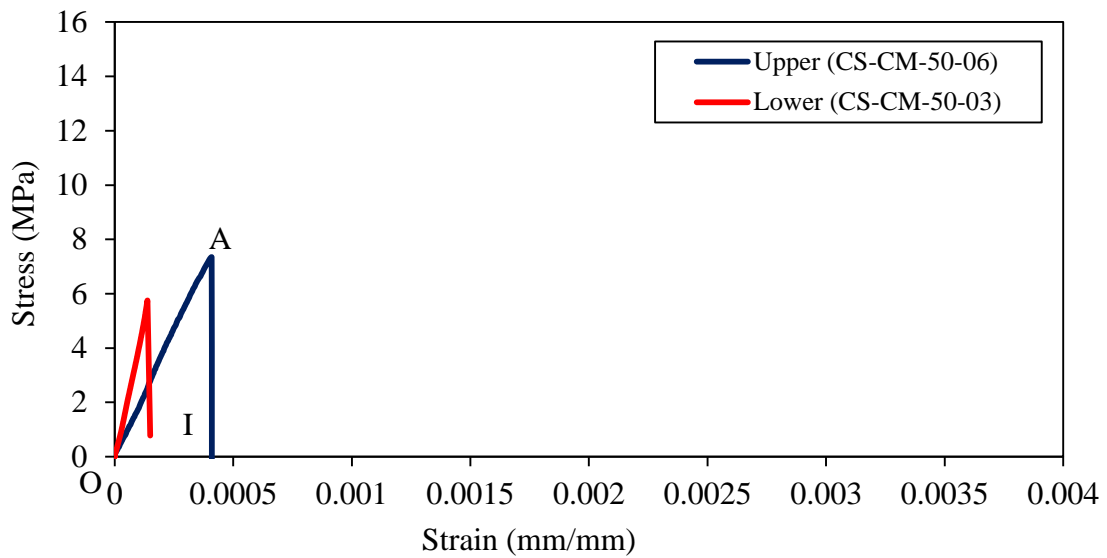


Figure 6.1: Lower and upper bound stress-strain curves for control specimens produced with compression moulding.

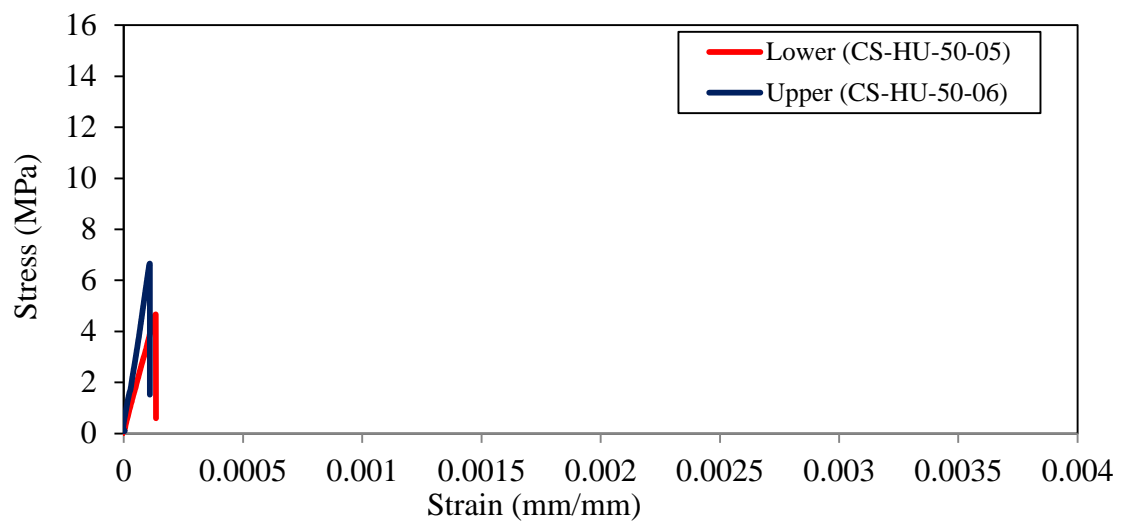


Figure 6.2: Lower and upper bound stress-strain curves for control specimens produced with hand lay-up.

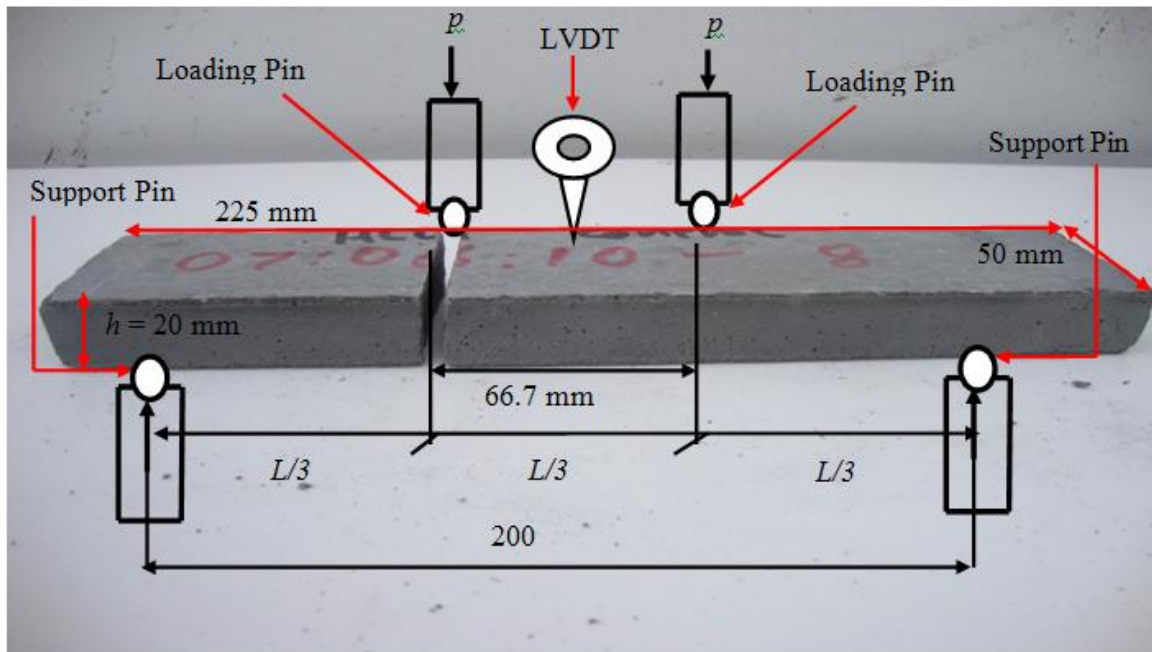


Figure 6.3: Fracture of control specimen after four-point bending test.

Generally, as expected the results and the findings from studying the control specimens support and confirm the outcomes of the previous studies by Kollé (2006); Farahi (2009); Suwannakarn (2009) and Khorami (2011). The overall performance of the control materials are similar to each other as they exhibit the strain-softening behaviour introduced in Section 2.3. There will always be localisation occurring immediately after first cracking. There will be no strain-hardening and multiple cracking (no regions II and III as shown in Figure 2.2(b)). The reported flexural strength of between 5 to 7 MPa is doubled that of 3.1 MPa determined by Khorami's (2011). This is attributed to this work having a mixture of the pozzolans, SF, PFA and GGBS, whose addition leads to lower porosity, lower permeability and lower bleeding. By adding pozzolanic materials there is a hydration reaction with lime giving additional Calcium Silicate Hydrate (C-S-H). Thus, a pozzolanic material reduces the amount of calcium hydroxide ($\text{Ca}(\text{OH})_2$) by increasing the amount of C-S-H. The main positive results of pozzolanic reactions are: lower heat liberation and strength development; lime-consuming activity; smaller pore size

distribution. To greatly improve packing the particles of SF can fill the voids between the cement particles as they are 100 times smaller (Section 2.8.1). Neville (1995) reported that because SF reduce the size and volume of voids near the surface of the aggregate, the so-called interface zone has improved properties, especially in terms of microcracking and permeability.

Following on from the discussion for the control materials the effect of adding different types of short fibres will be investigated in Sub-sections 6.3.2 to 6.3.6. In particular the study will look at how to achieve strain-hardening behaviour accompanied by multiple cracking, as this leads to a high failure strain capacity a less catastrophic/brittle mode of failure.

6.3.2 Critical Length (l_c) and Combined Efficiency Factor (η)

As discussed in Section 2.15, fibre length (l) is an important parameter that influences the fibre-matrix bond strength and strength and toughness. l is expressed in terms of critical length, l_c , which is the minimum length required for developing the full strength capacity of the fibre, and it is calculated for the five short fibres using Equation (2.15) in Section 2.15. Here σ_{mu} is the mean failure stress of the control materials and is given by the results in Tables 6.1 and 6.2. σ_{mu} is 6.1 MPa for hand lay-up and 6.7 MPa for compression moulding. Taking the mean of the two processing batches we can assume σ_{mu} is 6.4 MPa. σ_{fu} is the single fibre tensile strength, and as explained in Section 3.7 testing for this strength was carried out at Coventry University. A single fibre of types CF1, CF2, CF3, PP or PVA was not tested because the minimum practical length required to do the test is ≈ 60 mm, whereas their lengths ranged from 0.085 to 25 mm. For this reason it was decided to take the lowest value for σ_{fu} reported in Table 3.7 for a single continuous carbon fibre. It is therefore assumed that σ_{fu} is 2240 MPa the fibre types of CF1, CF2 and CF3. It

was observed that the tensile strength of single PP and PVA fibres provided by the suppliers, at 413 and 780 MPa, respectively (see Table 3.2), are close to strengths given in the literature. For example, Shi *et al.* (2013) reported the average tensile strength for PP as 437 MPa. Fidelis *et al.* (2013) stated that the tensile strength of PP fibres ranges from 400 to 550 MPa, with an average of 475 MPa. Bentur and Mindess (2007) reported that the tensile strength for PVA fibre as being from 850 to 1500 MPa (see Table 2.1 in Section 2.4). Asano and Kanakubo (2012) stated that the tensile strength for PVA fibre is 1690 MPa. Based on information known, it was decided by the author to take σ_{fu} as the fibre strengths in Table 3.2; namely 413 MPa for PP and 780 MPa for PVA. r is the fibre radius and was measured for the five short fibres using a SEM in accordance to the method in Section 3.4. These measurements are presented in Table 3.2.

Measurement of the interfacial bond strength (τ) is complicated for the reasons given in details in Section 2.16. As a consequence τ was not measured in this study and an estimate was made for τ for the five fibre types. The author decided to use the quoted mean of test results for carbon, glass, PP, and PVA fibres taken from the previous studies summarised in Table 2.3 of Section 2.16. For τ these means were used in Equation (2.15) to calculate l_c . From Table 2.3 the τ values for the CF, PP, and PVA fibres are 2.0, 1.9, and 3.0 MPa, respectively. These values could be on the low side, which means that the actual l_c can be lower than predicted. Measured fibre radii (r) are; 3.5, 3.5, 4, 19, and 15.5 μm for fibre types of CF1, CF2, CF3, PP, and PVA, respectively. An example on how to calculate l_c is given next. Substituting known and estimated parameters for CF1 into Equation (2.15) gives:

$$l_c = \frac{\sigma_{fu} r}{\tau} = \frac{2240 \times 0.0035}{2} = 3.92 \approx 4 \text{ mm}$$

Table 6.3 presents l_c for the five short fibres. The length of CF1 was measured to be 0.085 mm (l) and this is $\ll 4$ mm (l_c). It is found that it will be impractical for CF1 fibres to fracture, as all, will pull-out of the matrix before their tensile strength can be mobilised. A critical length of 4 mm is also estimated for CF2, PP and PVA fibres. Their mean lengths, as presented in Table 3.2, are 14 (3 to 25 mm), 12 and 8 mm, respectively and so they are $> l_c$. The length of CF3 is also greater than l_c (i.e. 6 mm $>$ 4.5 mm).

As discussed in Section 2.15 the minimum fibre length for effective reinforcement has to be $\geq 2l_c$ to make sure the fibre is capable of transferring shear stress at both ends. This minimum length is also needed to achieve strain-hardening behaviour (see Section 2.3) accompanied by multiple cracking and a higher failure strain capacity. For these two reasons, $2l_c$ is considered to be the minimum fibre length for reinforcement. For smaller lengths the stress in the FRC will be less than the maximum and the reinforcement is not utilised efficiently. From the literature Nishioka *et al.* (1986) quoted typical $2l_c$ for CFs of about 1.6 to 2.8 mm. Values for $2l_c$ are calculated for five fibres and results are presented in Table 6.3. They will be used in the analysis and discussion in Sub-sections 6.3.2 to 6.3.6.

It is clear from the information in Table 6.3 that there are three cases for l , when compared with $2l_c$, which are: 1) $l < 2l_c$ for CF1 (0.085 \ll 8 mm) and CF3 (6 $<$ 9 mm); 2) $l = 2l_c$ for PVA (8 = 8 mm); 3) $l > 2l_c$ for CF2 (14 $>$ 8 mm) and PP (12 $>$ 8 mm). The change in mechanical properties (i.e. for flexural strength, max strain and toughness) will be investigated in the following sections to Section 6.3. l_c in Table 6.3 will be used to calculate the combined efficiency factor (η) from Equations (2.22) and (2.23) in Section 2.17. This analysis will help to see how effective the fibre types are.

Table 6.3: Values of aspect ratio, critical length (l) and $2l_c$ for short fibres, CF1, CF2, CF3, PP and PVA.

Fibre Type	l (mm)	Aspect ratio (l/d)	l_c (mm)	$2l_c$ (mm)
Recycle milled carbon fibre (CF1)	0.085	12	4	8
Recycle chopped carbon fibre (CF2)	14*	2000	4	8
Chopped carbon fibre 6 mm (CF3)	6	750	4.5	9
Chopped polyvinyl alcohol (PVA)	8	258	4	8
Chopped polypropylene (PP)	12	315	4	8

Notice: *: 14 mm is the mean value as the length of CF2 ranged between 3-25 mm.

Contribution of discontinuous fibres to the mechanical properties of FRCs is likely to be smaller than for continuous fibres, which have length $\gg 2l_c$ and can be aligned parallel to the applied load. These two features result in higher bond strength (τ) and higher fibre efficiency. As discussed in Section 2.17 fibre efficiency depends upon the three efficiency factors for fibre length (η_l), fibre orientation (η_θ) and fibre-matrix shear bond strength (η_τ). The determination of η_τ is complicated, due to the difficult procedures for a satisfactory bond strength (pull-out) test. For this reason η_τ is not considered in this study, and only η_l and η_θ are, via $\eta = \eta_l \eta_\theta$. The value of η with unidirectional fibres (0°) is 1.0, i.e. the fibres are fully effectively. However, this is a very rare reinforcement arrangement and so for most commercial applications $\eta < 1.0$, and it must be calculated. When short fibres are 3D randomly distributed η is calculated using the Equations (2.22) and (2.23) in Section 2.17. The η is referred to as the theoretical fibre efficiency factor. An example on how to calculate the theoretical η for CF1, via Equation (2.23) is as follows:

For

$$l \leq \frac{10}{7} l_c = (0.085 \text{ mm} < 5.7 \text{ mm}),$$

$$\eta = \frac{7}{100} \left(\frac{l}{l_c} \right) = \frac{7}{100} \left(\frac{0.085}{4} \right) = 0.0015 \approx 0.002$$

Table 6.4 for the theoretical η is constructed using Equations (2.22) and (2.23) for the five fibre types. It is noted that η for CF2, CF3, PVA and PP fibres are similar and from 0.10 to 0.16. This implies that a maximum of 10 to 16% of the fibre properties can be mobilised. This finding for short fibres, except CF1 with a theoretical η that is relatively very small, supports the results in the previous studies by Farahi (2009) and Purnell (2007, 2010). Farahi (2009), used the equation by Laws (1971) to calculate η to be 0.11 for short glass fibres having $l = 12$ mm. Purnell (2007, 2010) summarises the typical efficiency values for different fibre layouts, as has been discussed in Section 2.17 and shown in Figure 2.11. Purnell (2007, 2010) estimated the value of the theoretical η for 3D short fibre materials to be 0.13.

Because η for CF1 is determined to be only 0.002 it is found that this fibre type cannot be a reinforcement in FRCs. This is because the mean fibre length (l) of 0.085 mm is well below the critical lengths l_c at 4 mm. It has been found that fibre types CF3, PP, PVA and CF2 offer an efficiency factors at least fifty times higher than 0.002. These fibres are more likely to bridge cracks as their l exceeds their l_c , as reported in Table 6.3.

Table 6.4: Values of combined efficiency factor (fibre length and orientation) for short fibres, CF1, CF2, CF3, PP and PVA.

	Fibre Type	Theoretical fibre efficiency factor (η)
1	Recycle milled carbon fibre (CF1)	0.002
2	Recycle chopped carbon fibre (CF2)	0.16
3	Chopped carbon fibre 6 mm (CF3)	0.10
4	Chopped polyvinyl alcohol (PVA)	0.13
5	Chopped polypropylene (PP)	0.15

Furthermore, the actual fibre efficiency factor, which is η' can be estimated from the experimental results by comparing theoretical and actual in cases where the FRC failure strength was above that of the matrix. The simplest model to predict the theoretical

strength (σ_t) is the Rule of Mixtures using Equation (2.4), by neglecting the contribution from the matrix it can be rewritten as:

$$\sigma_t = \sigma_f V_f \quad (6.1)$$

The actual strength of the composite, σ' , is the mean failure stress obtained from the four-point bending testing and their values are reported in Tables A.6.1 to A.6.10. η' can be calculated from:

$$\eta' = \frac{\sigma'}{\sigma_t} \quad (6.2)$$

An example on how to obtain η' for the CF2 fibre is given next. σ' for the CF2 materials having V_f at 2% is given by the results in Tables A.6.3 and A.6.4, and is 10.2 MPa for hand lay-up and 11.4 MPa for compression moulding. Taking the mean of the two processing batches we can take σ' to be 10.8 MPa. σ_f is the single fibre tensile strength, and for CF2 fibre is assumed to be 2240 MPa for the reasons introduced earlier in this section, and explained in Section 3.7. Substituting known and estimated parameters into Equations (6.1) and (6.2) we have:

$$\sigma_t = \sigma_f V_f = 2240 \times 0.02 = 44.8 \text{ MPa}$$

and

$$\eta' = \frac{\sigma'}{\sigma_t} = \frac{10.8}{44.8} = 0.24 .$$

Table 6.5 summarises the η' is calculated by this method for the five short fibre types. It is noted that the actual efficiencies for CF1, CF2, CF3 and PVA fibres ranged from 0.18

to 0.70. It actually means that 18 to 70% of the fibre properties are found to be mobilised. It is seen in all cases that $\eta' > \eta$. It has increased by a factor of 90 (from 0.18/0.002), 1.5 (from 0.24/0.16), 2 (from 0.20/0.10) and 5 (from 0.70/0.13) for CF1, CF2, CF3 and PVA fibres, respectively. It is also found that η' is > 1 for PP fibre. An explanation for this overestimation is that σ_f of 413 MPa of the PP fibre taken from the literature review is lower than for the fibres used to manufacture the short fibre FRC materials.

Table 6.5: Values of η' for short fibres, CF1, CF2, CF3, PP and PVA.

Fibre Type	σ_f (MPa)	V_f	σ_t $= \sigma_f V_f$ (MPa)	σ' (MPa)	η' $= \sigma / \sigma_t$	η by Laws (1971)	Difference $= \eta / \eta'$ (%)
CF1 fibre	2240	0.02	44.8	7.9	0.18	0.002	99
CF2 fibre	2240	0.02	44.8	10.8	0.24	0.16	33
CF3 fibre	2240	0.02	44.8	8.8	0.20	0.10	50
PVA fibre	780	0.02	15.6	10.85	0.70	0.13	81
PP fibre	413	0.02	8.26	9.5	1.1	0.15	86

It is not only l which is responsible for the fibre type achieving their ultimate strength and for the FRC to exhibit a strain-hardening behaviour. Another factor is V_f , which will be investigated in Sub-section 6.3.3. Values for η will be used to obtain the critical fibre volume fraction ($V_{f,crit}$) from Equation (2.13) and to determine the effective fibre volume fraction (V_f') using Equation (2.24).

6.3.3 Fibre Volume Fraction, V_f

The area below the stress-strain curve (for toughness) is expected to increase with an increase in V_f (see Section 2.2), as fibres act as ties between the two fracture interfaces of the cement matrix to prevent sudden failure. This behaviour should improve with the number of fibres, since when fibres break or pull-out there are adjacent fibres to bare load

by the crack-bridging mechanism. The crack development throughout the matrix is delayed until more flexural deformation has been applied.

Given that one objective of the research is to have the highest practical V_f , five different values of 2, 4, 7, 9 and 12% were used in the series of flexural tests. The author selected these particular percentages, as it is practical to compare new results at the low V_f of 2 and 4% and at the higher V_f of 7, 9, and 12 % with results from previous studies. The first attempt in producing relatively highly loaded FRCs was with fibres CF1 and CF2. These two types were selected because CF1 has the shortest length (average is 0.085 mm) and CF2 has the longest length, ranging from 3 to 25 mm. This means that choosing these two fibre types covered all five lengths in this investigation.

The mix design, constituent materials and mixing procedure were the same as previously mentioned in Section 6.3. Ten batches were prepared; five batches with CF1 and the other five with CF2; each batch had twelve nominally identical specimens. Twelve specimens reinforced with CF1 or CF2 were prepared; six made by hand lay-up, introduced in Sub-section 4.4.2, and another six by compression moulding processes, introduced in Sub-section 4.5.5. Before flexural testing, the ten batches of twelve specimens were cured in hot water at 50 °C for 28 days, as detailed in Section 4.6. To ensure that fibres CF1 and CF2 were distributed as uniformly as practical, the mixture was agitated in a Hobart mixer for 12 minutes, as explained in Section 4.3.

The influence of V_f at 2, 4, 7, 9, and 12% on mean flexural strength with CF1 is plotted in Figure 6.4. The mean for each batch is for the mean of the maximum flexural strengths from six tests. Along with reporting the mean there is an error-bar to show the spread within a batch. The test results for hand lay-up are given in blue with a circular symbol and for compression moulding they are in red with a square symbol. Straight lines

are used to join the individual mean results to give an indication of change in strength with V_f .

Comparing mean flexural strengths in Figure 6.4 it can be seen that they are similar for V_f of 2 and 4% for both processes. It can be observed that there is a tendency for a linear increase in mean strength as V_f increases towards its maximum of 12%. Nevertheless, given that V_f is 2-12%, it is difficult to conclude if a higher flexural strength can be achieved with $V_f > 12\%$. For compression moulding the 10% increase in CF1 loading leads to an 87% mean strength increase, from 8.2 to 15.4 MPa. The strength increase at 43% (from 7.6 to 10.9 MPa) is lower for hand lay-up. From this preliminary comparison there is evidence to suggest that there might be a V_f limit that needs to be exceeded for a significant increase in mean strength. Results in Figure 6.4 show that the mean flexural strength of the CF1 FRCs is fairly constant when V_f lies in the range of 2 to 9%.

It was observed during the mixing process that when V_f is 12% the mix was still workable. It is believed this advantage is because the fibres are < 0.1 mm long. It was, however, found to be difficult to disperse the fibres uniformly through a mix, even when V_f is 2%. This weakness is because static electricity causes the CF1 fibres to form into balls of diameters ranging from 5 to 30 mm (as shown in Figure 4.1(a)). To overcome the electrostatic flocculation the author applied the grinding method introduced in Section 4.2. The outcome of this processing was to generate balls of 1 to 2 mm diameter. These can be seen, as red circles, in Figure 6.5. This grinding allows for the penetration of the cement particles between the fibres to be limited and so only the outer fibres are in direct contact with the cement matrix. Inner fibres remain uncoated and have no bond with the matrix. This results in a poor bond strength as discussed in Section 2.16.

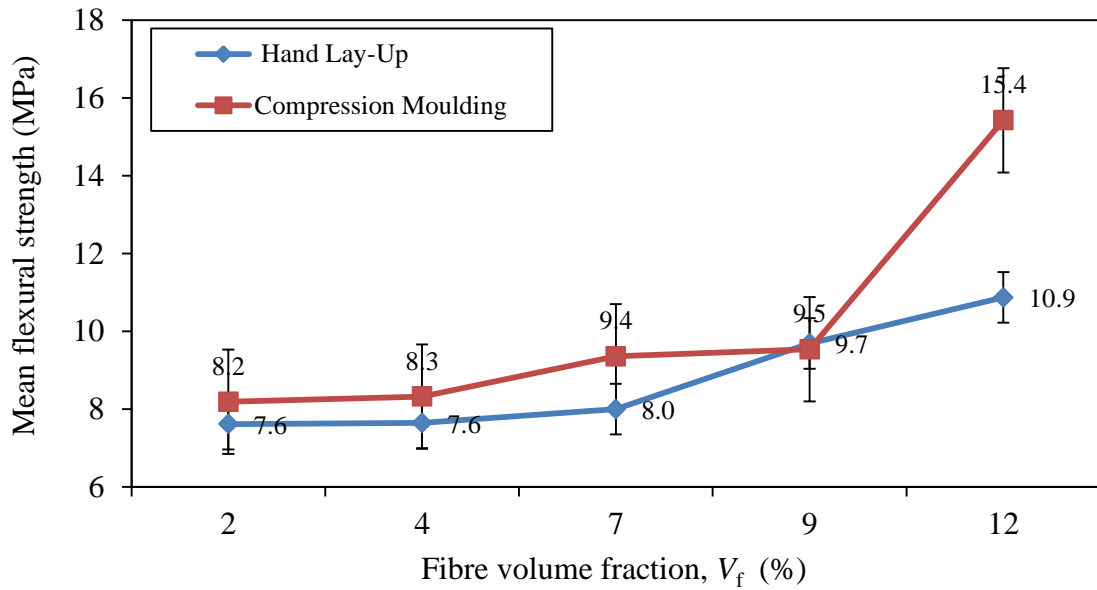


Figure 6.4: Relationship between mean flexural strength and fibre volume fraction for the CF1 cementitious material.

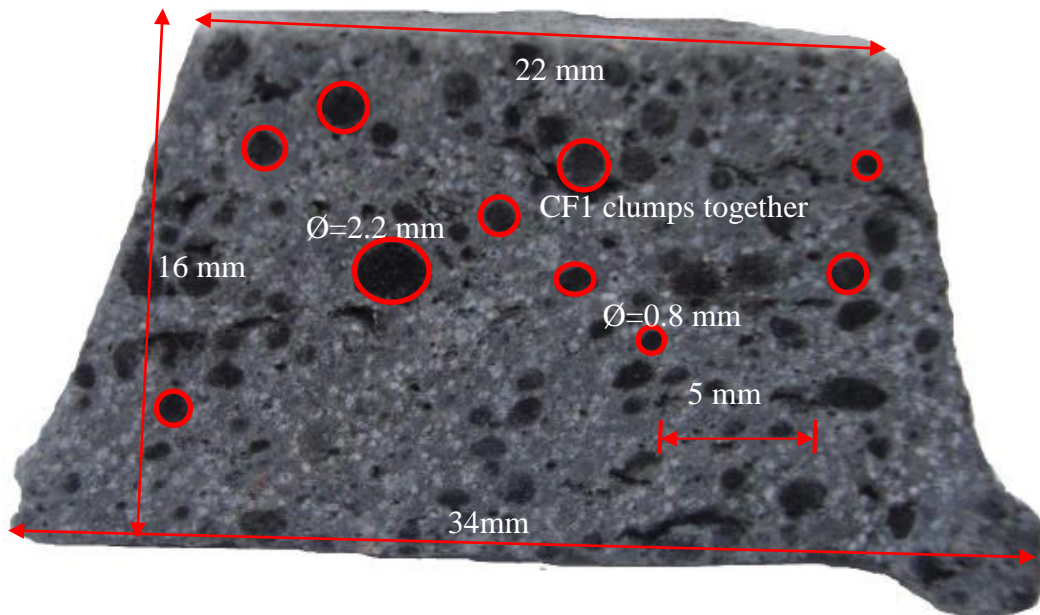


Figure 6.5: Cross-section of a material reinforced with CF1 fibre at $V_f = 2\%$ showing poor dispersion and clumping on the fibres into balls.

The author discovered that when V_f is higher than 2%, the mix was not workable with fibre types CF2, CF3, PP and PVA. This disadvantage was because of their longer lengths, in the range 3 to 25 mm. Moreover, it was found to be difficult with any of these four

fibres to uniformly distribute them throughout the mix. The outcome was that these materials exhibited poor compaction, poor surface finish and strength decreases. An example of CF2 FRC with V_f of 7% is shown in Figure 6.6(a). Castings were unsuccessful, as specimens often broke-up a few minutes after demoulding. Although apparently viable, the green form could be demoulded, but specimens suffered from severe delamination a few hours after curing. It also observed with CF2 that when V_f is higher than 9% the matrix was deficient, as seen in Figure 6.6(b), and was unable to carry its own self-weight. Penetration of the cement particles between the fibres was too limited. For this reason, V_f at 9 and 12% were not investigated, and the three fibre loading of 2, 4 and 7% were investigated.

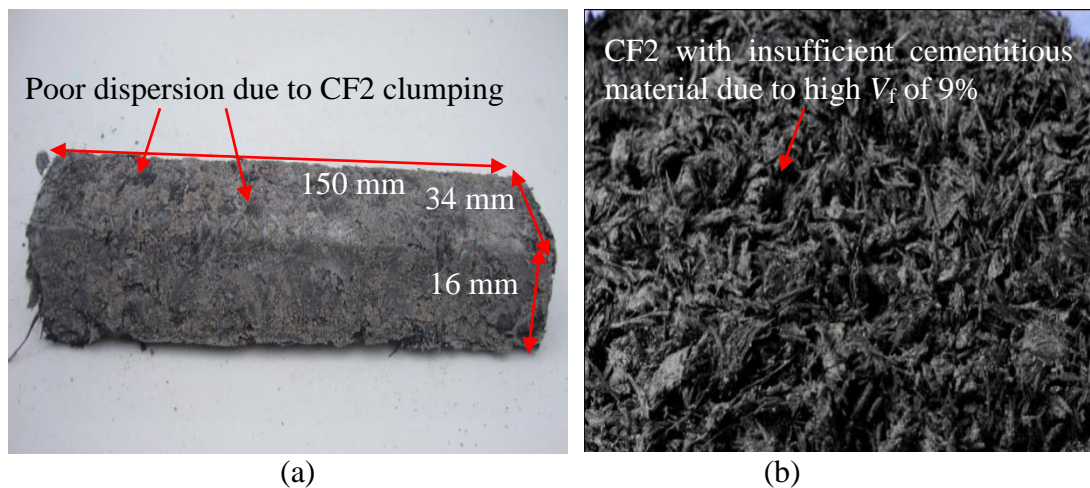


Figure 6.6: Matrix reinforced with CF2 fibres with a V_f : a) 7% and b) 9%.

The mean flexural strengths for CF2 batches in Figure 6.7 show that as V_f increases, towards its maximum of 7%, the flexural strength decreases. For compression moulding the 350% increase in fibre loading from 2 to 7% leads to a 72% strength decrease (from 12.2 to 3.4 MPa). In hand lay-up process, the flexural strength decreases at 65%, from 11.1 to 3.8 MPa. Results in Figure 6.7 show that for $V_f > 2\%$ the mean strength decreases for both FRC processing methods.

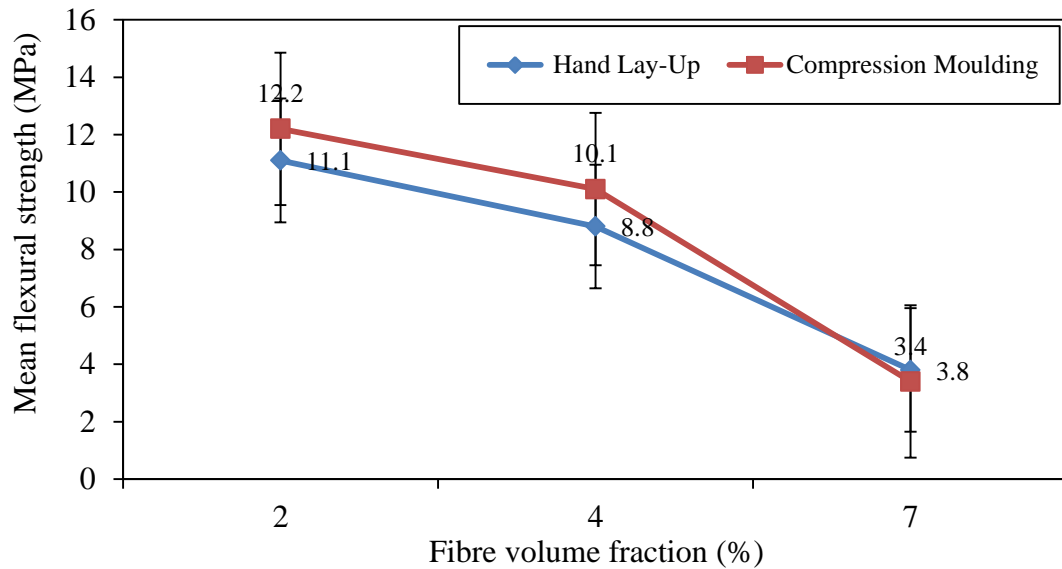


Figure 6.7: Relationship between mean flexural strength and fibre volume fraction for the CF2 cementitious material.

In general, the author discovered that when V_f is above 2% the mix was not workable, and it was found to be difficult to get uniformity in the distribution of the short fibres. This finding agrees with what was found by Kullaa (1998), Li (2003), Hanjari (2006), Purnell (2007), Farahi (2009) and Khorami (2011). These researchers concluded that V_f is typically set at 2% or less for two practical reasons. The first is that a higher V_f results in mixing and compaction problems, with the fibres clumping together and creating balls that create poor dispersion. This poor quality leads to a creation of weak points in the FRC. The second reason is related to the acceptance capacity of the cement matrix. This means there is a balanced condition between fibres and cement particles. Each fibre should be confined by enough hydrated cement particles. When the V_f is very high, the amount of C-S-H present is not enough to cover the external surfaces areas of the fibres. For this reason, it was decided to set V_f constant at 2% for CF1, CF2, CF3, PP and PVA fibres. It is relevant to know if this selected maximum V_f is greater than the critical fibre volume fraction (i.e. $V_f > V_{fcrit}$).

According to the ACK model of Section 2.13 and using the fibre orientation and fibre length factor (η) (Equations (2.22) and (2.23)), the minimum fibre volume fraction (V_{fcrit}) required to prevent brittle failure can be calculated using Equation (2.13). An example on how to obtain V_{fcrit} for fibre CF2 is given next by substituting parameters into Equation (2.13), to have:

$$V_{\text{fcrit}} = \frac{\sigma_{\text{mu}}}{\eta\sigma_{\text{fu}}} = \frac{6.4}{0.16 \times 2240} = 0.018 = 2\%$$

Table 6.6 presents the five calculated V_{fcrit} . It is noted that V_f of 2% with CF2 is also V_{fcrit} . It might therefore be expected that CF2 mixes are reinforced, and the fibres will support the transfer of force, provide multiple cracking behaviour and post-cracking capability. This beneficial post-cracking behaviour could be enhanced had it been practical to distribute the fibres uniformly. It can be seen from the results in Table 6.6 that the V_f loadings for CF3 (2% < 3%), PVA (2% < 6%) and PP (2% < 10%) are smaller than V_{fcrit} . When $V_f < V_{\text{fcrit}}$, the FRC will fracture immediately after matrix cracking, since the fibres are then unable to carry the additional tensile forces for the reasons given in Sections 2.10 and 2.14, and in this chapter.

As expected the V_{fcrit} of 143% from the first row of Table 6.6 shows a V_f of 2% for CF1 is negligible. In other words the mean length of the CF1 fibres is much smaller than l_c (see Section 6.3.2). This is more evidence to show that 2% is insufficient with CF1 to bridge the matrix cracks. In this case, failure is going to be governed by the fibre pull-out followed by matrix tensile fracture, as shown in Figure 2.6(a).

If it is assumed that V_{fcrit} has to be used for a FRC material, this loading will adversely affect the mix workability. Because of the extremely high V_{fcrit} with CF1 it could

be impractical, even impossible, to distribute the fibres uniformly to have a homogeneous FRC. This will lead to a negative effect on mechanical properties and cost will be higher. It can be concluded that fibre type CF1 cannot be used to produce a useful FRC material.

Table 6.6: Values of V_{fcrit} for, CF1, CF2, CF3, PP and PVA fibres.

Fibre Type	V_{fcrit} (%)
Recycle milled carbon fibre (CF1)	143
Recycle chopped carbon fibre (CF2)	2
Chopped carbon fibre 6 mm (CF3)	3
Chopped polyvinyl alcohol (PVA)	6
Chopped polypropylene (PP)	10

The effectiveness of fibre reinforcement depends on many factors, including the matrix properties, the quantity, length, shape, orientation, and adhesion properties of fibres. The fibres are fully effectively ($\eta = 1$) if they are unidirectional fibres (0°) and aligned in the direction of loading. The effective fibre volume fraction (V_f') for this specific case is equal to V_f (see Section 2.17). However, for short fibres V_f' is always $< V_f$. This is due to the 3D randomly distribution. Now V_f' is calculated for the five fibre types using Equation (2.24). An example on how to determine V_f' with CF2 fibres is:

$$V_f' = \eta V_f = 0.16 \times 2 = 0.32\%$$

Table 6.7 presents the five V_f' , and it is noted that it values for fibres CF2, CF3, PVA and PP are close, and in the range 0.2 to 0.32%. Noting that only 16% of V_f is found to be effective there is an agreement with the work of Farahi (2009) and Purnell (2007, 2010). Farahi (2009) found 11% of short glass fibres ($l = 12$ mm) were effective. Whereas Purnell (2007, 2010) estimated that the typical V_f' for 3D short-fibre FRCs would be 13%.

For the reasons known a V_f' for CF1 at 0.004% is considerably lower relative to the other four fibre types. Poor bond strength between fibres and matrix leads to an intrinsic requirement for the use of longer fibres.

Table 6.7: Values of V_f' for, CF1, CF2, CF3, PP and PVA fibres.

Fibre Type	V_f' (%)
Recycle milled carbon fibre (CF1)	0.004
Recycle chopped carbon fibre (CF2)	0.32
Chopped carbon fibre 6 mm (CF3)	0.20
Chopped polyvinyl alcohol (PVA)	0.26
Chopped polypropylene (PP)	0.30

6.3.4 Materials Reinforced With Milled Carbon Fibres (CF1)

The mix design, constituent materials and mixing procedure were the same as presented in Section 6.3. Before flexural testing the ten batches (twelve specimens per batch) were cured in hot water at 50 °C for 28 days, as discussed in Section 4.6. The Tables A.6.1 and A.6.2 in Appendix A present the four-point bending test results and statistical analysis for batches manufactured by the compression moulding and hand lay-up processes. Comparing results in the two tables is made to study the effect of CF1 fibres on the mechanical properties of flexural strength, strain at peak stress and toughness. Column (3) in Tables A.6.1 and A.6.2 show that LOP and the peak stress are the same ($\sigma_{mu} = \sigma_{cu}$), and they occur at ≈ 8 MPa. This is because only the matrix can carry tension and after matrix cracking (at the peak stress) the CF1 fibres are unable to carry additional load. This is attributed to the lack of sufficient fibre content (i.e. because $V_f < V_{f_{crit}}$) and insufficient bond between the cement matrix and CF1 fibres (i.e. because $l < l_c$).

Comparing the results of hand lay-up with compression moulding a slight difference is found in the overall mechanical behaviour with processing. Column (3) in Tables A.6.1

and A.6.2 show that the mean strength at 8.2 MPa by compression moulding is 7% higher than by hand lay-up. The variability between the two processes is found not to be significant. The lower variability on using compression moulding is due to the applied pressure that is known to reduce the capillary porosity, and thereby improves the flexural strength, as discussed in Section 4.5.5. Moreover, the mean strains and toughness at peak stress for hand lay-up and compression moulding in Tables A.6.1 and A.6.2 are almost the same at 0.03% and 0.001 J/m^3 , respectively. The SD of the results of flexural test for the CF1 fibres are seen to lie between 0.6 and 0.8 MPa, indicating that test results for specimens in a batch tend to be close to the mean. It is believed the lower variability with compression moulding is due to the consistency in mixing, curing and testing for the flexural specimens.

By comparing the test results from CF1 specimens reported in Tables A.6.1 and A.6.2 with the control results in Tables 6.1 and 6.2 only a slight difference in overall behaviour can be observed. Column (3) in Tables A.6.1 and A.6.2 show that the mean strength with CF1 is only 23% (7.9 vs 6.4 MPa) higher. Moreover, the mean strain and toughness at peak stresses are very low, and they are 15% (0.026 vs 0.03) and 33% (0.0009 J/m^3 vs 0.0012 J/m^3) higher. These findings further confirm the conclusion that CF1 fibres are unsuitable for making a FRC with mechanical properties significantly greater than the control matrix material.

Plotted in Figures 6.8 and 6.9 are the lower and upper bounds of stress-strain curves for FRC with 2% of CF1 fibres produced by compression moulding and hand lay-up. There is also plotted the lower bound curve for the control material. In such plots the black curve is for the upper bound and blue curve for the lower bound, with the control curve coloured red. The stress-strain curves in the figures for the FRCs are observed to have similar shape

to the control curve. The curves exhibit strain-softening behaviour, as discussed in Section 2.3, and they start the same with a Region I. Failure is by way of a relatively brittle behaviour. The stress-strain curves are virtually linearly elastic up to the first cracking stress (σ_{mu}), the line OA in Figure 6.9. At point A in Figure 6.9 the matrix cracks. After the LOP the FRC exhibits catastrophic failure by a single crack.

Using the ACK model from Section 2.13 the pre-cracking (Region I) and failure (Region IV) are observed in Figure 6.9. There is neither strain-hardening nor multiple cracking in the response (see Section 2.3). According to the classification of FRC materials by Naaman (2008) (see Section 2.3), both CF1 and control materials exhibited strain-softening behaviour. In other words, once the first cracking stress (σ_{mu}) has been reached, the specimens failed quickly. This demonstrates that the influence of bridging fibres for load sharing in the post-cracking zone (ACK model Regions II and III) is very weak, if non-existent. In this case there is clearly some post-peak region IV behaviour. It is small, but it is present as shown in Figure 6.9.

Pull-out fibre failures were observed in all CF1 specimens that were produced either by hand lay-up and compression moulding. This again can be associated with $V_f < V_{f,crit}$, $l < l_c$ and poor fibre dispersion. Regarding how the short fibres are distributed throughout the matrix it is known that advantages of uniform fibre dispersion are reduced shrinkage cracks and the improved post-crack strength. Li and Li (2012) reported that the fibre dispersion was found to have a strong effect on the strain capacity of FRC materials. Poor fibre dispersion reduces the strain capacity and ultimate tensile strength and can switch a FRC from a strain-hardening material to a strain-softening material. As presented in Section 2.7 and discussed in this chapter the dispersion of fibres is adversely affected by the fibre length (Banthia *et al.*, 1998).

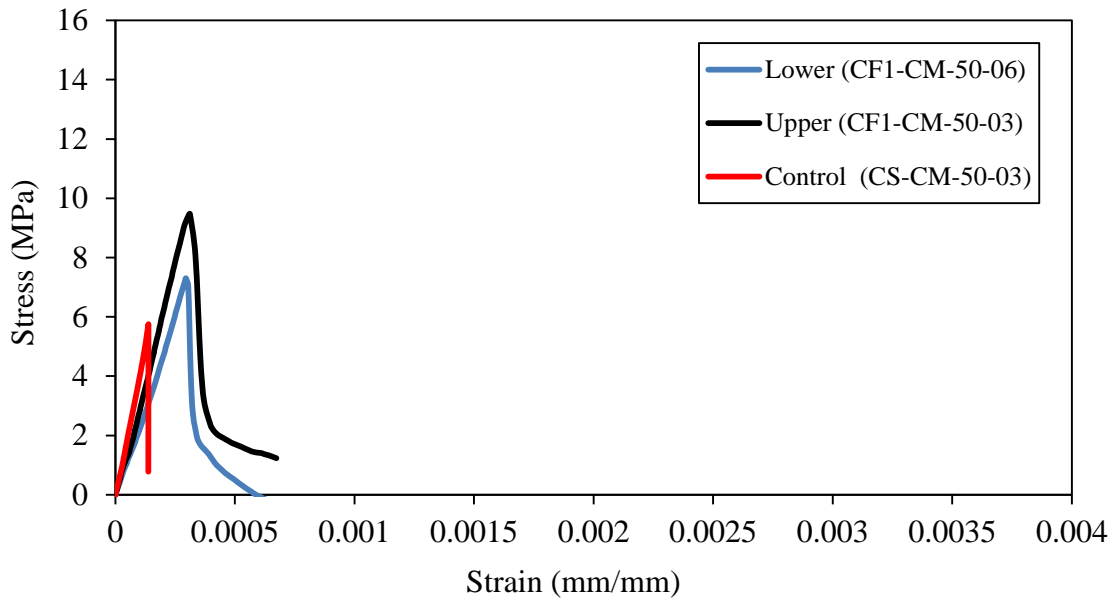


Figure 6.8: Comparison of the lower and upper bound stress-strain curves for CF1 cementitious specimens ($V_f = 2\%$) produced with compression moulding with lower bound curve from the control specimens.

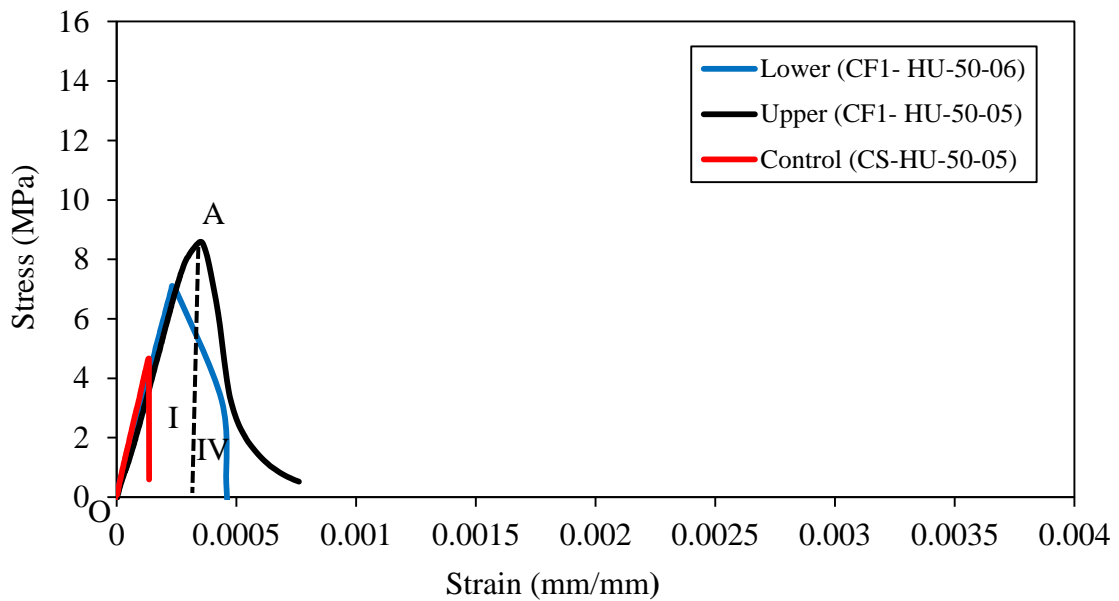


Figure 6.9: Comparison of the lower and upper bound of stress-strain curves for CF1 cementitious specimens ($V_f = 2\%$) produced with hand lay-up with lower bound curve from the control specimens.

It was observed in the experimental works that due to static electricity, the CF1 fibres clumped together and make balling or fibre clumping, as discussed in Sub-section 6.3.3. This usually occurred well before the fibres could be added into the mix and it was found they would remain grouped together throughout the mixing process. These balls had 5 to

30 mm diameter before grinding (see Sub-section 4.2), which was able to reduce the size to 1 to 2 mm diameter as seen in Figure 6.5 (see Sub-section 6.3.3). As a result, the reinforcing unit with CF1 is not a single filament dispersed in a matrix, but rather a ball (containing a few thousands of filaments) with each filament having freedom of movement relative to the others surrounding it. Only the outer filaments that can have direct contact with the matrix had the potential for a good bond performance. The inner filaments (core filaments) can transfer forces only by friction, resulting in less bond for the FRC. This feature with CF1 is because the matrix cannot penetrate into the balls or completely surround filaments, as discussed in Section 2.16.

Figure 6.10 is for four SEM photos of material with CF1 that can be analysed to see how the fibres are dispersed. It can be seen in Figure 6.10(a), as expected, that CF1 fibres are not well distributed, as shown by the voiding in the bottom left of the image. Fibre clumping is seen in Figure 6.10(b), and is known to be due to static electricity forcing the fibres to attract each other. Under higher magnification, Figure 6.10(c) shows the fibres are clean, smooth and not coated with cementitious material. These are features for why there is a weak bond between CF1 fibres and matrix. Another reason is the hydrophobic nature of carbon fibre. Figure 6.10(d) shows an area of matrix with 'no' fibres projecting through. When fibres clump together there has to be an increase volume in 'fibre-free' matrix. Now the initiation of a matrix crack requires less strain energy. This is further evidence not to add CF1 fibres to produce a FRC.

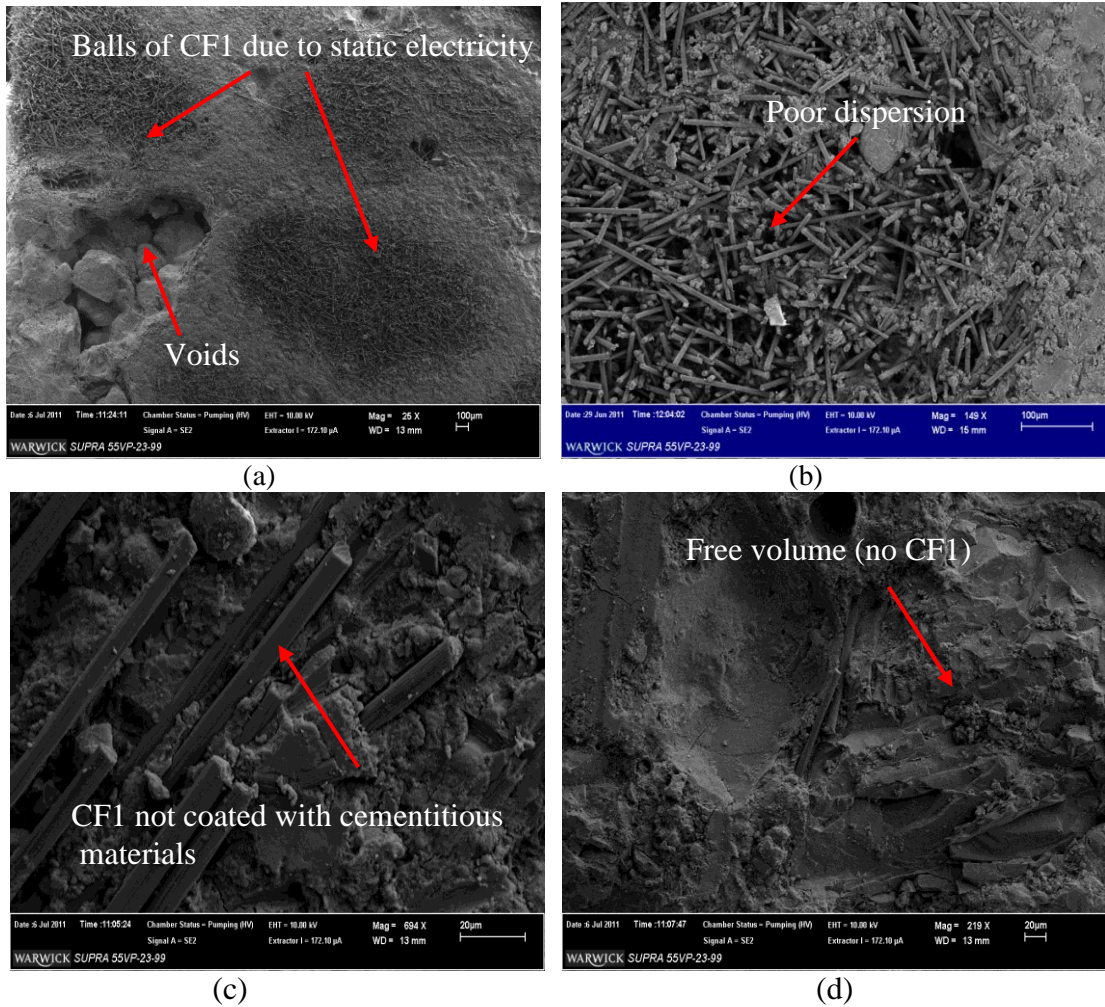


Figure 6.10: SEM photo for CF1 material made by compression moulding, (a) fibres stick together to form balls, (b) poor dispersion, (c) filaments are not coated with cementitious materials, (d) area of pure mortar with too few fibres.

A fractured CF1 specimen is shown in Figure 6.11 to confirm that, under flexure, the material experiences the same of brittle pull-out failure having a single crack, as did the control material (see Figure 6.3). After analysing the broken pieces it was observed that the CF1 fibres had not distribute uniformly and quantities had clumped together, and these balls can be found located anywhere in the volume. This meant that some regions in a specimen were without fibres. This could lead to initiation and growth of initial matrix cracks. This may be due to, the specific CF1 characteristics of short length (i.e. $l \ll l_c = 0.085 \ll 4 \text{ mm}$), small l/d ratio (i.e. $85/7 = 12$), smooth surface and no fibril and $V_f \ll V_{f_{crit}}$ (i.e. $2\% \ll 143\%$). It should be noted that the characteristics of CF1 fibres must be due to

the combination of all parameters and this implies that changing some of them is likely to lead to a FRC having different even acceptable flexural properties.

Because the use of CF1 fibre in FRCs is novel there are no other results in the literature to compare with the test results in this study. Based on the information obtained CF1 fibres at $V_f = 2\%$ cannot offer an acceptable FRC material for a building material.

Compared to asbestos fibres, very little work has been done on the inhalation toxicology of carbon fibres. The most common health hazards experienced when handling milled carbon fibres (CF1) are irritation and development of a skin rash, mechanical irritation to the mucus membranes of the nose and eyes, throat and upper respiratory tract and the potential for laceration and impregnation of fibre splinters into the skin. Adequate ventilation should be provided at points where CF1 is handled. Skin contact should be minimised through process design or protected with the use of protective clothing, eye protection and work gloves. Storage of wastes in sealed containers and disposal in a secured landfill are recommended.

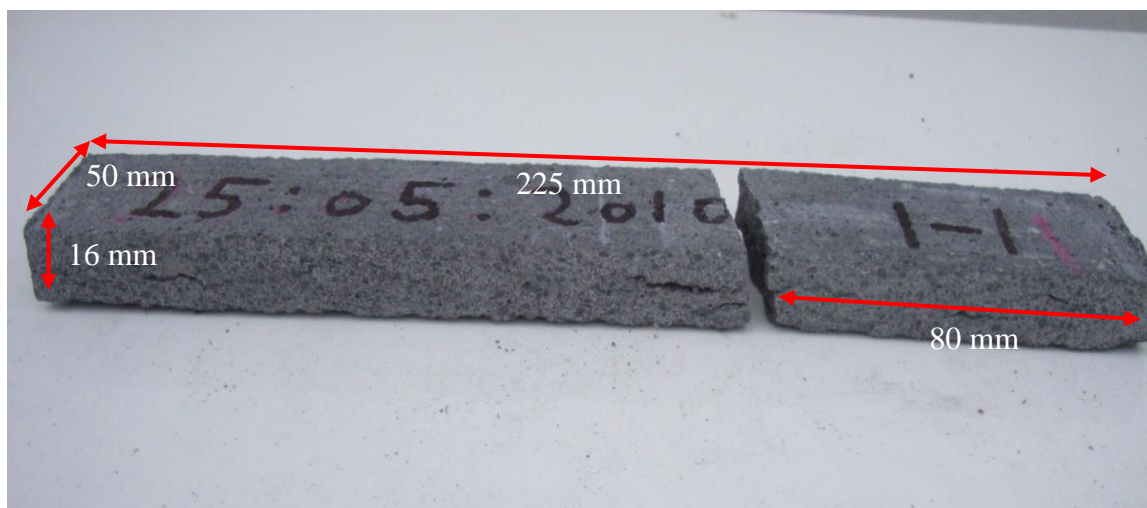


Figure 6.11: Brittle fracture of CF1 cementitious specimen after four-point bending test.

6.3.5 Materials Reinforced With Short Carbon Fibres of Types CF2 and CF3

The mix design, constituent materials and mixing procedure were the same as presented in Section 6.3. Before flexural testing the ten batches (twelve specimens per batch) were cured in hot water at 50 °C for 28 days, as discussed in Section 4.6. Appendix A Tables A.6.3 to A.6.6 present the four-point bending test results and statistical analysis for CF2 and CF3 specimens that had been manufactured by compression moulding and hand lay-up. Comparing the results it is found that there is a slight difference in the overall mechanical behaviour between the CF2 and CF3 batches produced by hand lay-up and compression moulding. Column (3) in Tables A.6.3 and A.6.5 show there to be a slight improvement in the mean peak stresses for both CF2 and CF3 FRCs produced by compression moulding. They are 11% (10.2 vs 11.4 MPa) and 13% (8.2 vs 9.4 MPa) higher than those by hand lay-up (see Section 6.5). As discussed in Section 4.5.5 the increase is because the application of pressure in compression moulding will reduce the capillary porosity and thereby improves flexural strength. Moreover, from Tables A.6.5 and A.6.6 the mean strain at peak stress for CF3 material by hand lay-up is 14% (0.058% vs 0.051%) higher than by compression moulding and the difference is almost the same for CF2 material (0.046% vs 0.045%). While the mean toughness at 0.003 J/m³ for CF2 and CF3 batches by compression moulding and hand lay-up is the same. The SD of the results of flexural test for the two CFs are seen to lie between 0.7 and 1.0 MPa, as presented in Appendix A Tables A.6.3 to A.6.6, indicating that individual results for specimens in a batch tend to be close to the mean.

By comparing the results in Tables A.6.3 to A.6.6 with the control materials in Tables 6.1 and 6.2 there is an improvement in overall properties for the CF2 and CF3

FRCs. Column (3) in Table A.6.3 show that the mean peak stress with CF2 is 70% (6.4 vs 10.8 MPa) higher. Similarly from to Table A.6.4 the CF3 material is seen to be (only) 40% (6.4 vs 8.8 MPa) higher. The mean strain and toughness at peak stress from the CF2 batch are 70% (0.026% vs 0.045%) and 250% (0.0009 J/m³ vs 0.0032 J/m³) higher. It is found that these two properties for the CF3 material are 110% (0.026% vs 0.055%) and 250% (0.0009 J/m³ vs 0.0032 J/m³) higher than for the control matrix. It is noted from Appendix A Tables A.6.3 and A.6.4 that an improvement in LOP strength was observed with CF2, and it is 40% (6.4 vs 9.2 MPa) higher. This is attributed to $V_f \geq V_{f_{crit}}$, uniform CF2 dispersion, and the mean fibre length $> 2l_c$ (14 mm $>$ 8 mm); this leads to increase the friction bonding area between the fibre and matrix.

Plotted in Figures 6.12 to 6.15 are the lower and upper bounds of stress-strain curves for the FRCs with CF2 and CF3 fibres at $V_f = 2\%$. The presentation is the same as for the CF1 FRCs in Figures 6.8 and 6.9. The shape of stress-strain curves in the four figures is seen to be similar to that labelled shape (b) in Figure 2.3(b) of Section 2.10. This form of curve commonly occurs when $V_f \leq V_{f_{crit}}$. The curves start in the same way with Region I, as does the control material. They are linearly elastic up to the first cracking stress (σ_{mu}), or LOP, as defined by line OA in, say Figure 6.13. After LOP has been reached, the stress continues to increase up to peak stress at point B in Figure 6.13, i.e. the load that was mainly carried by the matrix has been transferred to the fibres bridging across vertical cracking. This response is due to $V_f \geq V_{f_{crit}}$. Thus, the matrix cracking will not be catastrophic, and the FRC sustains additional loads and deformations and the reinforced material might be imbued with some post-cracking capacity. Failure in CF2 and CF3 materials was the same. Beyond point B the stress decreased gradually as the flexural fracturing progressively developed until the four-point bending specimen had no stiffness.

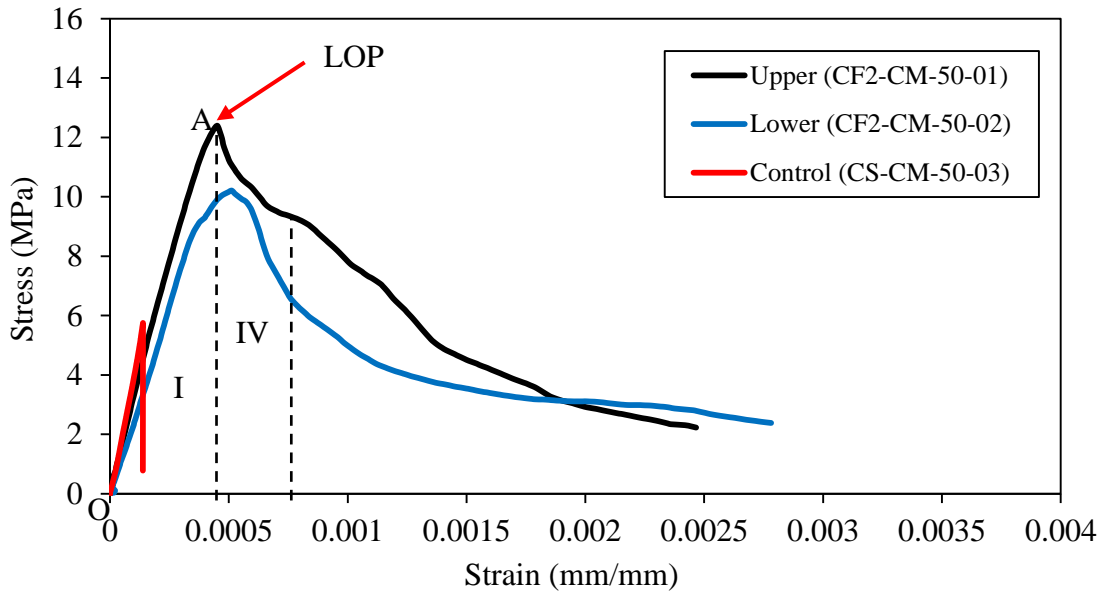


Figure 6.12: Comparison of the lower and upper bound of stress-strain curves for CF2 cementitious specimens ($V_f = 2\%$) produced by compression moulding with lower bound curve from the control specimens.

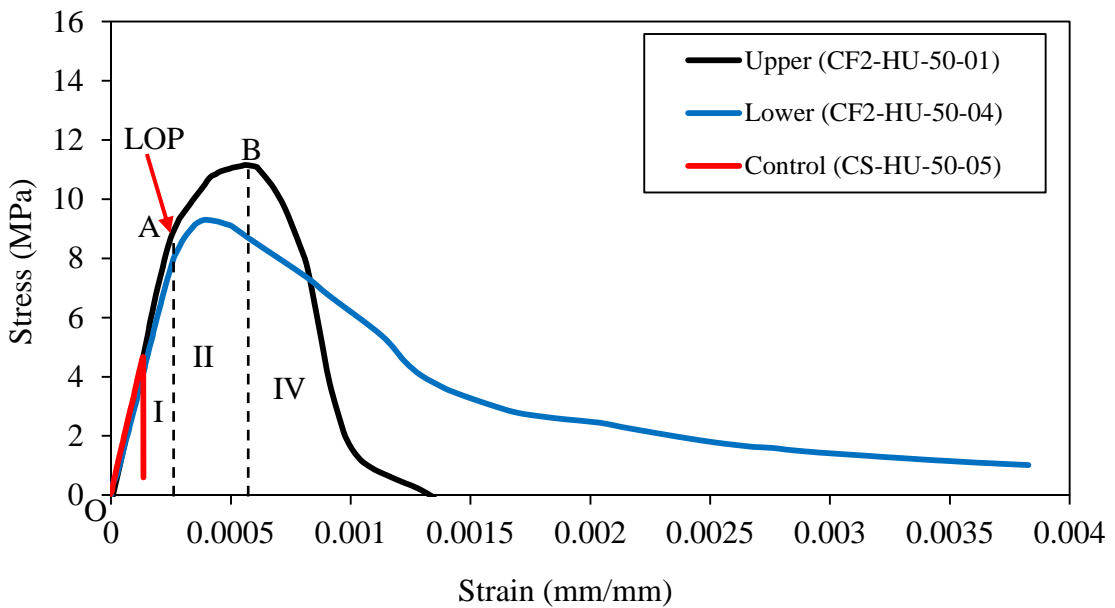


Figure 6.13: Comparison of the lower and upper bound of stress-strain curves for CF2 cementitious specimens ($V_f = 2\%$) produced by hand lay-up with lower bound from the control specimens.

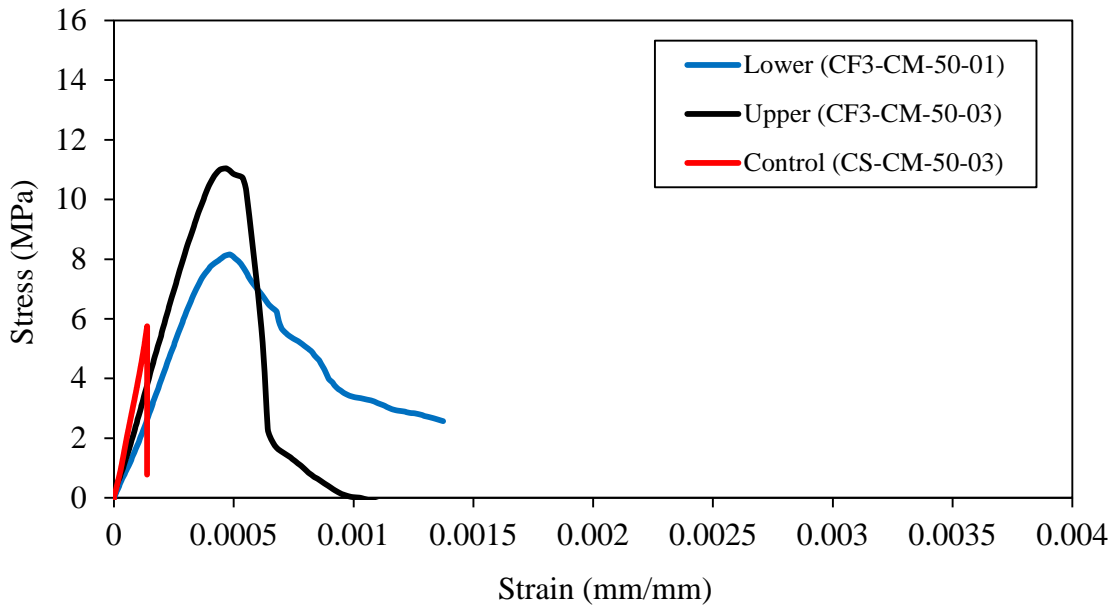


Figure 6.14: Comparison of the lower and upper bound of stress-strain curves for CF3 specimens ($V_f = 2\%$) produced by compression moulding with lower bound of control specimen.

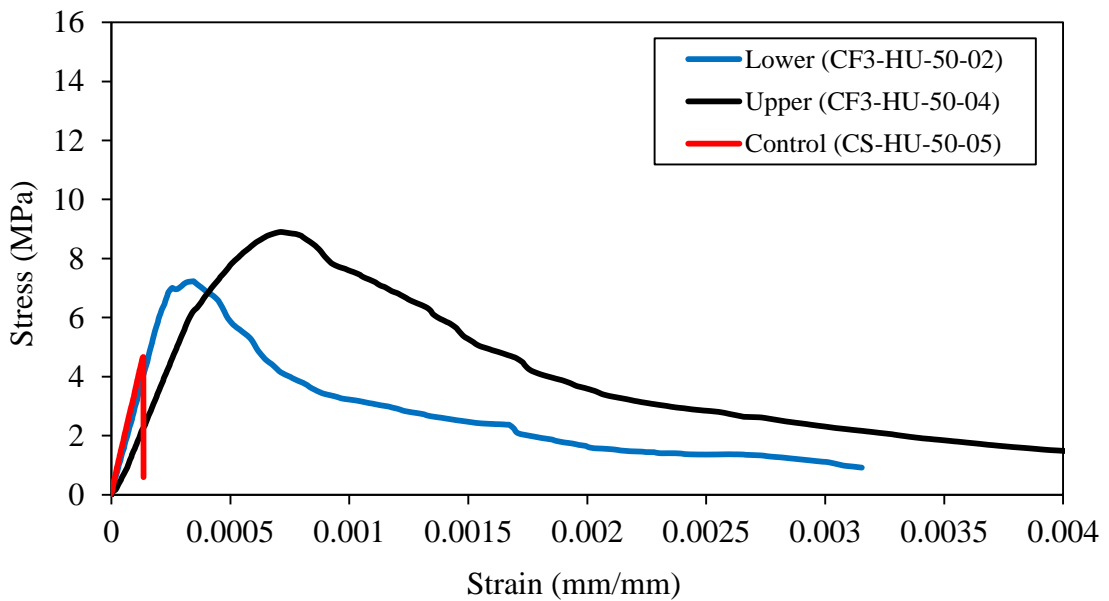


Figure 6.15: Comparison of the lower and upper bound of stress-strain curves for CF3 specimens ($V_f = 2\%$) produced by hand lay-up with lower boundary from the control specimens.

According to ACK model the two Regions I and IV exist and they are labelled in Figure 6.12. The multiple cracking and post-cracking Regions (II & III) are absent from the stress-strain curves (there is a Region II in Figure 6.13 that is relatively small). This finding

can be linked to some fibres not being full effectively and confirms the results presented in Sub-section 6.3.3 that the calculated V_f' suggests only 10% and 16% of the CF2 and CF3 fibres are likely to be effective for composite action. Failure caused by fibre pull-out was observed in CF2 and CF3 FRCs produced either by hand lay-up and compression moulding processes, and can be identified in Figures 6.12 to 6.15 by the long tail in the stress vs strain curves. To investigate if this behaviour is associated with either $V_f < V_{f_{crit}}$ and/or insufficient bond, via $l < l_c$, this will be explained the following.

The combined efficiency factor η was determined for CF2 and CF3 fibres using Equations (2.22) and (2.23), and it is used to calculate l_c and $V_{f_{crit}}$. The results of η are presented in Table 6.4 and discussed in Section 6.3.2. As explained in Sections 2.15 and 6.3.2, for effective reinforcement the minimum l has to be $2l_c$. It can be seen from the l_c values in Table 6.3 that l for CF2 fibres is $> 2l_c$ (i.e. 14 mm $>$ 8 mm). However, the situation with CF3 fibres is different as $l < 2l_c$ (i.e. 6 $<$ 9 mm). With CF3 FRCs it is therefore not possible for all the fibres to break in tension before there is pull-out failure. As explained in Section 2.3 this leads the stress-strain curve to exhibit a strain-softening behaviour after the initiation of matrix cracking (σ_{mu}). If the bond is relatively strong the strain-hardening behaviour can be obtained, providing there are sufficient fibres to bridge the cracks (i.e. $V_f \geq V_{f_{crit}}$), and they are well dispersed throughout the matrix.

For this reason $V_{f_{crit}}$ for CF2 and CF3 was calculated using Equation (2.13) with the results presented in Table 6.6. It is found that $V_f = V_{f_{crit}} = 2\%$ for CF2 and $V_f < V_{f_{crit}}$ (i.e. 2 $<$ 3%) with CF3. This means that V_f 2% of CF3 fibre is insufficient to provide adequate bridging to prevent matrix crack progression, i.e. CF3 fibres have insufficient length ($l = 6$ mm $<$ $2l_c = 9$ mm). It can be concluded that the experimental curves clearly show that it is not a brittle failure as there is a very long tail of post-peak region.

As we know the transmission of tensile forces required an interfacial bond. In order to evaluate the influence of this bond in FRCs with CF2 and CF3 fibres it is noted that these carbon fibres do not have fibrils and surface pores, and that they are weak in terms of wettability (Brandt, 2009). As a consequence of these poor fibre properties we can expect bonding between fibres and the matrix to be weak. Moreover, their hydrophobic nature and low affinity for the cement paste makes the transfer of tension between fibres and matrix even more unreliable and discontinuous. This background information has been discussed in Section 2.4.4.

On the other hand, CF2 fibres have positive properties (as given in Table 3.2) that are useful for FRCs. The bonding between CF2 fibres and matrix is not strong, but their longer lengths ($l > 2l_c$) and small diameters ($\approx 7 \mu\text{m}$) lead to a relative high aspect ratio ($l/d = 2000$) (see Table 6.3) that increases the friction bonding surface area between the CF2 and matrix. In other words, these longer carbon fibres are effective after the FRC reaches its strength, because they act as ties between the two fractured interfaces to prevent a sudden and brittle failure. As discussed in Section 2.7 the mechanical properties of FRCs, such as flexural strength and toughness, are very sensitive to fibre dispersion, which includes both how the short lengths are oriented and positioned within the matrix. For this reason SEM observations for materials with CF2 and CF3 fibres are considered, and images are presented in Figures 6.16 and 6.17. Figures 6.16(a) and 6.16(b) show that both fibre types are well dispersed and are coated with matrix as shown by red arrows. The close-up in Figure 6.17 shows particles of cementitious material on CF2 filaments. This image suggests that well under 50% of the surface area is coated (see red arrows). From these images in Figures 6.16 it can be said that there was the required dispersion of CF2 and CF3 fibres.

As seen from the results in Figures 6.12 to 6.15 specimens with CF2 and CF3 showed an improvement in flexural strength, maximum strain and toughness (c.f. with control presented in Figures 6.1 and 6.2). All FRCs with carbon fibres gave the strain-softening behaviour (see Section 2.3) with no multiple cracks formed. In other words, once the peak stress has been reached, all specimens were found to fail quickly or gradually via a single crack opening-up. This shows that the influence of bridging fibres for ACK Regions II and III is weak. As we have established this is because V_f is insufficient and there is poor interfacial bond. Another contributing factor could be the brittle nature of carbon fibres.

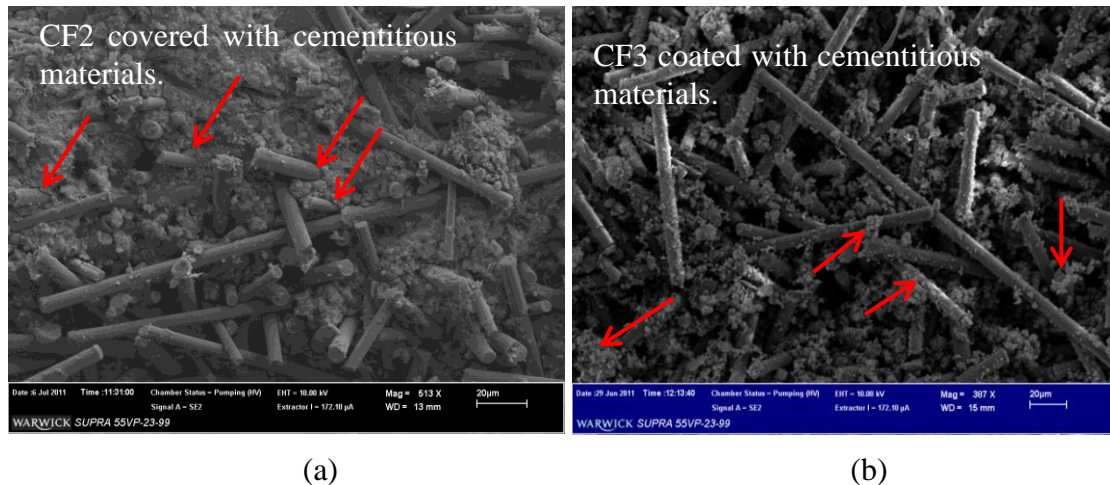


Figure 6.16: CF2 and CF3 materials were made by hand lay-up; a) CF2 dispersed well throughout the matrix; b) CF3 covered with cementitious materials.

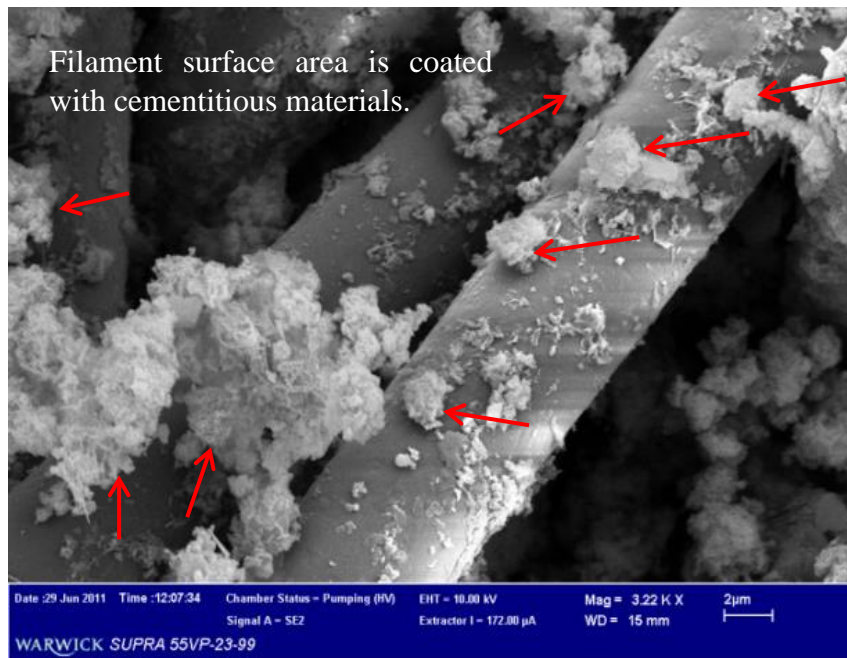


Figure 6.17: CF2 filaments are coated with cementitious materials.

6.3.6 Materials Reinforced With Polypropylene Fibre (PP)

The mix design, constituent materials and mixing procedure were the same as given in Section 6.3. Before flexural testing, ten batches (twelve specimens per batch) were cured in hot water at 50 °C for 28 days, as discussed in Section 4.6. Tables A.6.7 and A.6.8 present the four-point bending test results and statistical analysis for the PP FRCs manufactured by compression moulding and hand lay-up. Comparing the results in terms of processing it is seen that there is a slight difference in the overall mechanical behaviour. From the mean peak stresses reported in Column (3) in Tables A.6.7 and A.6.8 it is seen that there is a slight improvement with hand lay-up at 9.9 MPa from the 9.1 MPa with compression moulding. It could be said that a 9% difference does not necessarily suggest a difference in the two FRCs. Moreover, the mean maximum strain and mean toughness at peak stress with compression moulding are 30% (0.033% vs 0.044%) and 40% (0.0015 J/m³ vs 0.0021 J/m³) higher than by hand lay-up. The SD of the results of flexural test with

PP fibres are seen to lie between 1 and 1.2 MPa, as presented in Tables A.6.7 and A.6.8, indicating that test results for specimens in a batch tend to be close to the mean.

Figures 6.18 to 6.19 are for the lower and upper bounds of stress-strain curves, presented with the control material curve. With 2% PP fibres the FRC has a deformation curve that is behave similarly to shape (b) in Figure 2.3(b) of Section 2.10. Again a brittle fracture is obtained. This observation is the same as for the control materials and the FRCs with CF1 (see Section 6.3.4). However, according to the classification of FRCs by Naaman (2008) (see Section 2.3) the stress-strain curves in Figures 6.18 to 6.19 inform us there is a strain-softening behaviour. Using the ACK model the two regions of pre-cracking (Region I) and failure (Region IV) can be identified, and in Figure 6.18 they are labelled. One finding is that the multiple cracking and post-cracking regions (Regions II and III) are absent from the stress-strain curve. The elastic portion of the curves is linearly elastic up to the first cracking (LOP) ($\sigma_{c,A}$), being point (A) in Figure 6.18. In this case $\sigma_{c,A} = \sigma_{cu}$, which is the same brittle outcome found with CF1 and control materials. At point (A) the matrix fails and fracturing occurs at a single crack that was the first to initiate.

By comparing the results in Figures 6.18 and 6.19 it can be observed that with both processes the PP specimens exhibited fibre pull-out failure, i.e. there is a steep curve (falling branch), which is evidence for the pull-out mechanism of ‘fibre’ failure. Because this failure occurs suddenly it can be expected this PP FRC will be unable to carry additional load after the matrix started to crack under tension.

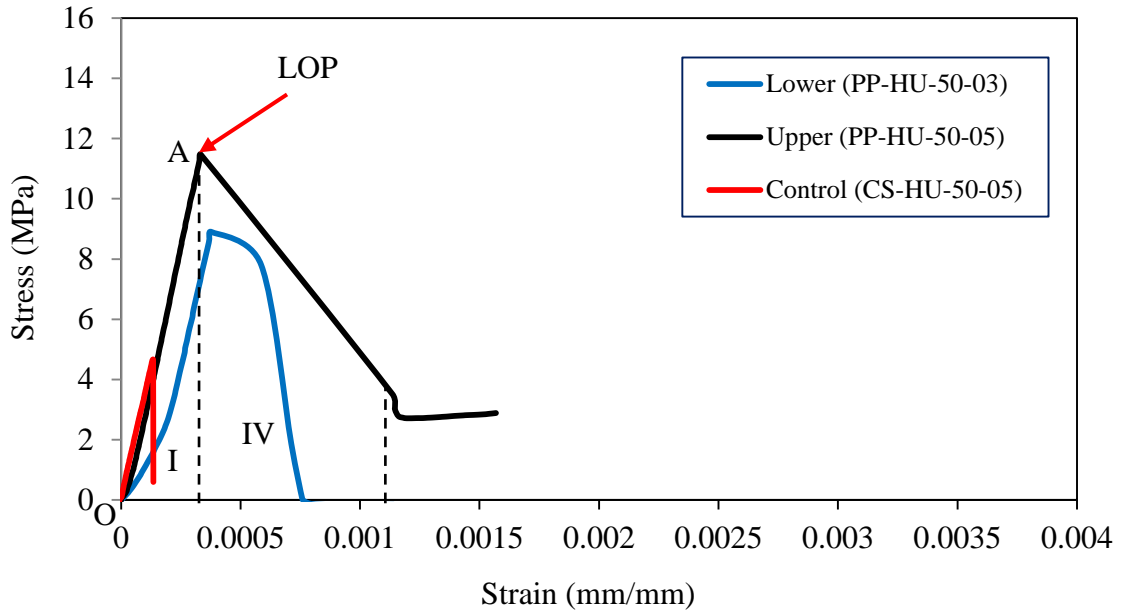


Figure 6.18: Comparison of the lower and upper bound of stress-strain curves for PP specimens ($V_f = 2\%$) produced by hand lay-up with lower bound curve from the control specimens.

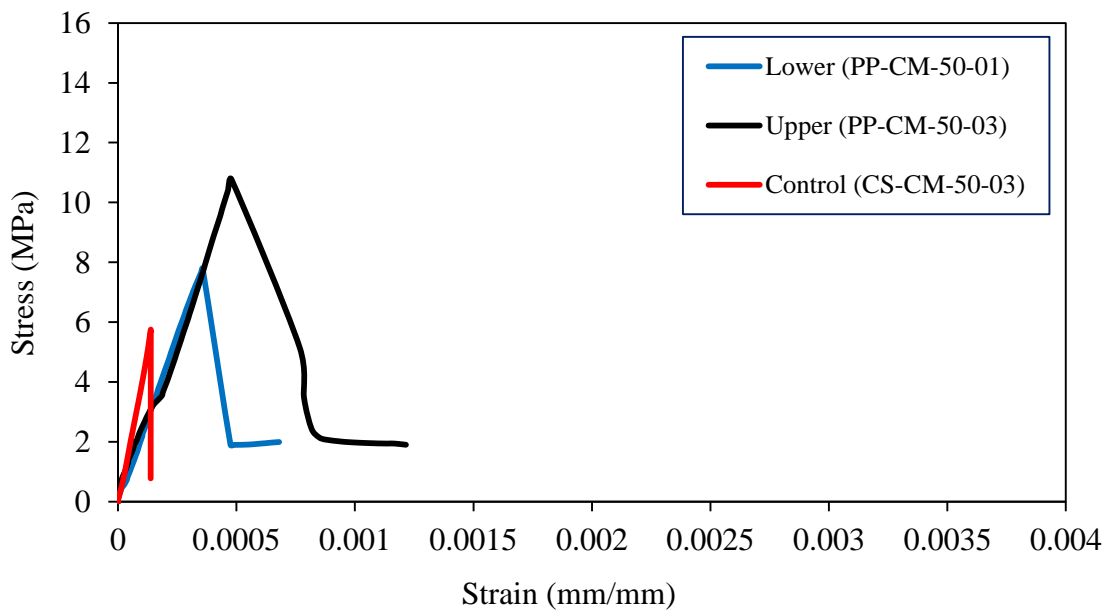


Figure 6.19: Comparison of the lower and upper bound of stress-strain curves for PP specimens ($V_f = 2\%$) produced by compression moulding with lower bound curve from the control specimens.

We now investigate if pull-out failure of PP fibres is associated with, lack of sufficient fibre content (i.e. $V_f < V_{f_{crit}}$), $l < l_c$ and/or insufficient bond between the cement matrix and PP fibres. The value of $2l_c$ for PP fibres is given Table 6.3 as 8 mm and l is 12

mm. For this fibre its strength should therefore be reached before pull-out failure. However, it is not only l that affects the mechanical properties, other contributing properties are: V_f ; orientation of fibres; bond strength (τ). In other words, brittle failure does not happen if PP fibres of length 12 mm are uniformly distributed and have sufficient numbers to bridge the cracks ($V_f > V_{f_{crit}}$). $V_{f_{crit}}$ for the PP fibre is listed in Table 6.6 and because $2\% \ll 10\%$ we find $V_f \ll V_{f_{crit}}$. This means 2% fibre loading is insufficient for a ductile FRC.

Furthermore, there are other two reasons that might cause the brittle failure in the PP FRCs. Firstly, the fibre modulus of elasticity (E) at 5 GPa is about 40 times lower than for the three carbon fibres (200 GPa). Secondly, as mentioned above the bond strength is one of the main parameters controlling mechanical properties. For PP fibres it is weak because of their hydrophobic nature (see Sub-section 2.4.3). To overcome the wettability problem a surface treatment can help. This observation agrees with the findings by Hannant (1978), Currie and Gardiner (1989), Bentur and Mindness (2007), Felekoglu *et al.* (2009), Peled (2009), Sadrmomtazi and Fasihi (2010), Ezeokonkwo and Nwoji (2011), and Khorami (2011). They all reported that τ for PP fibres is extremely poor. Moreover, Table 2.3 reports from Li and Stang (1997) and Redon *et al.* (2001) PP bond strengths that are from 0.1 MPa to 1.6 MPa.

Figure 6.20 has a single SEM image to show PP fibres in the matrix. From the image it can be seen that fibres are clean, smooth and not coated with the cementitious material, certainly when compared to the carbon fibres (see Figure 6.17). These features mean there is a going to be a poor bond in the FRC. From the findings on evaluating the PP test results it can be concluded that pull-out failure dominates. This weakness is associated with a combination of having $V_f < V_{f_{crit}}$, a poor bond and non-uniform fibre distribution. Change

to these parameters is required to improve the PP fibre properties so that its FRCs could possess the desired strain-hardening behaviour.



Figure 6.20: PP material was made by compression moulding and is clean, smooth and not coated with cementitious materials.

6.3.7 Materials Reinforced With Polyvinyl Alcohol Fibre (PVA)

The mix design, constituent materials and mixing procedure were the same. Before flexural testing, ten batches (twelve specimens per batch) were cured in hot water at 50 °C for 28 days. Figures 6.21 and 6.22 present plots for the lower and upper bound stress-strain curves for the two PVA FRCs with the lower bound curve from the control batch of specimens. In contrast to the previous four short fibre FRCs these stress-strain curves are seen to correspond to shape (e) in Figure 2.3(e) of Section 2.10. Such curves can exist when $l > l_c$ and/or the bond strength is strong enough. The mode of failure will be governed by fibre fracture and not fibre pull-out. Only the PVA fibres at 2% loading gave this very different flexural response. As we have seen with the other short fibre FRCs their stress-strain curves are of shape (b).

The initial portion of the curves in the figures is linearly elastic, up to the stress at first cracking (LOP), which is label point A in Figure 6.22. With PVA the LOP occurred in

the stress range of 6.8 to 12.6 MPa, which is between 50% and 98% of the peak stress. When the first matrix crack has formed, tensile force is transferred across the opening by the fibre-matrix bonding. The plots show that after point A there can be a fairly constant, if not slightly increasing, stress with a significant increase in strain. The instances when stress is seen to suddenly be relieved do suggest the development of new matrix cracks. Eventually, within the constant moment volume of the four-point bending specimens, there will be a network of closely-spaced (vertical) cracks. The mean peak stress (strength) for the FRC by compression moulding of 12.8 MPa showed progressive increases 44% over those by hand lay-up of 8.9 MPa as presented in Tables A.6.9 and A.6.10 in Appendix A (see Section 6.5). Once the strength has been reached the stress is seen to decrease very gradually as the flexural specimen continues to fracture and loses stiffness. Because the PVA fibres give the FRC the ability to carry more stress after matrix cracking the reinforcement has imparted the material with post-cracking strength.

In Figure 6.22 the four regions (I, II, III and IV) in the ACK model are readily defined. Only this short fibre is found to offer a flexural response with the desirable post-cracking Region III. This positive performance means that PVA fibre type used possesses the ability to absorb energy. Also reported in Tables A.6.9 and A.6.10 are the strains at peak stress. At 0.31% they are found to be almost identical for the batches by hand lay-up and by compression moulding. The toughness at peak stress using the lower and upper bound curves for compression moulding are 0.027 and 0.031 J/m³, whilst the upper bound toughness of hand lay-up material is 0.027 J/m³. These three energy absorptions are nearly the same and are doubled 0.013 J/m³ that is determined from the lower bound curve and hand lay-up. The mean strain and toughness at peak stresses has been improved by a factor of 11 (0.026% vs 0.31%) and 30 (0.0009 J/m³ vs 0.028 J/m³) times of that measured using

the control matrix. The author has shown, for the first time in this chapter, that short PVA fibres at 2% V_f can significantly increase the flexural strength, strains and toughness of FRC material.

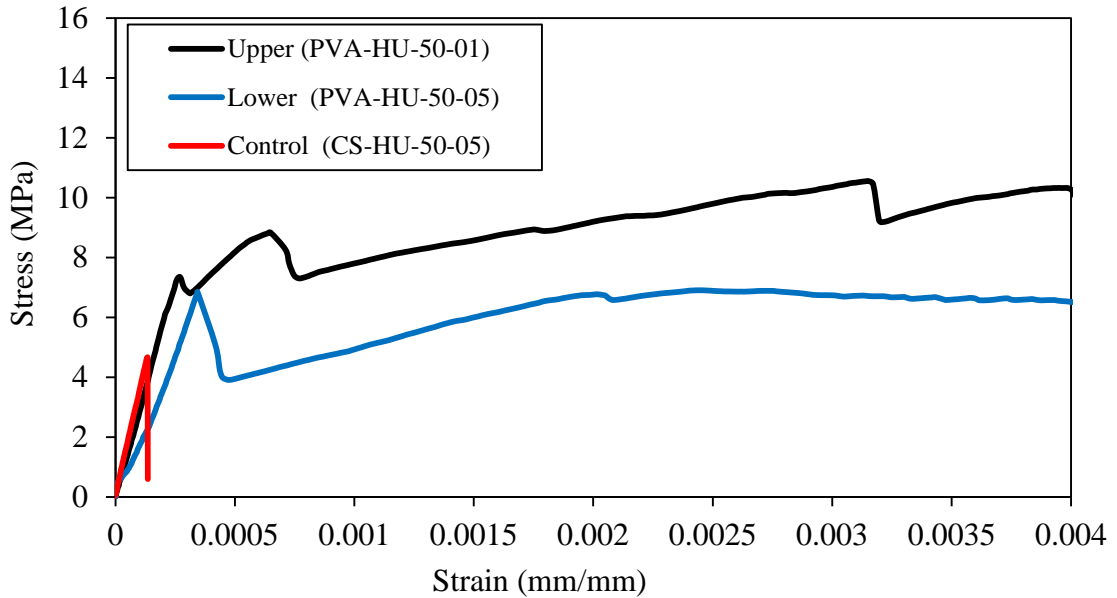


Figure 6.21: Comparison of the lower and upper bound of stress-strain curves for PVA specimens ($V_f = 2\%$) produced by hand lay-up with lower bound from the control specimens.

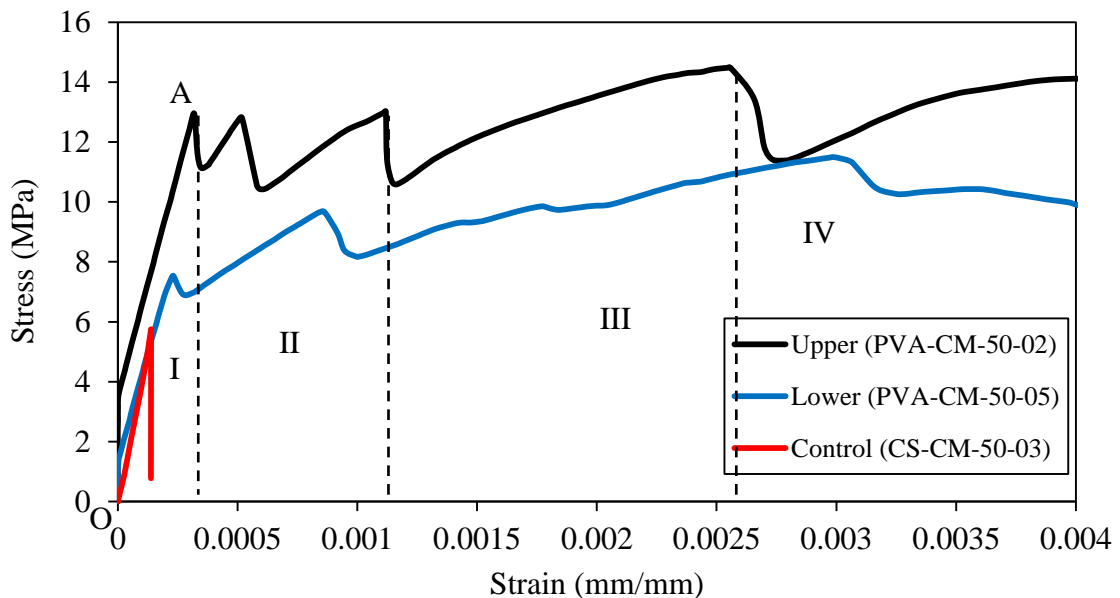


Figure 6.22: Comparison of the lower and upper bound of stress-strain curves for PVA specimens ($V_f = 2\%$) produced by compression moulding with lower bound from the control specimens.

The strain-hardening behaviour (see Section 2.3), which is for an increase in strain under increasing load is present in the stress-strain curves of Figures 6.21 and 6.22. This leads to a high failure strain capacity without a brittle failure. An earlier discussion in Section 2.16 explains that the bonding strength will control the failure mechanism. The SEM image in Figure 6.23(a) shows PVA fibre to have a rough surface. In image in Figure 6.23(b) shows a PVA fibre coated with cementitious material. It can be inferred that both features observed by SEM means there is an effective bond. As discussed in Section 2.4.2 this finding agrees with what other researchers have reported. Refer to the contributions by Zheng and Feldman (1995), Lin and Kanda (1999), Wang and Li (2006), Bentur and Mindess (2007), Peled *et al.* (2008) and Shen *et al.* (2008).

There follows the four reasons that explain why the PVA FRCs have given a better performance than FRCs with any of the four fibre types of CF1, CF2, CF3 and PP:

- The good bond strength (τ) means, the PVA fibres are likely to fracture, rather than to be pulled-out. It is believed the relatively high τ is due to the hydrophilic nature of PVA and the fibres' surface roughness (Figure 6.23(a)). Fibrils and rough surfaces indicate there can be a relatively high friction mechanism between fibres and matrix. The fibrils are evidence of direct contact between the two phases that could enhance interface strength, by providing mechanical anchorage to improved bond strength. Such fibrils and a rough fibre surface were not observed with the other four short fibres. As presented in Table 2.3 of Section 2.16 Li *et al.* (1990); Lin *et al.* (1999) and Peled *et al.* (2006) reported that τ with PVA fibre lies in the range 3 to 5 MPa. The bond strength for the four short fibres is believed not to exceed 2 MPa.

- The $l = 2l_c = 8 \text{ mm}$ (Table 6.3), this leads to an increase in the surface area of the fibres contacting with the cement, hence bonding between the cement and the fibres increases.
- PVA fibres were observed to be distributed uniformly and this increases their ability to bridge and arrest where microcracks initiate and grow.

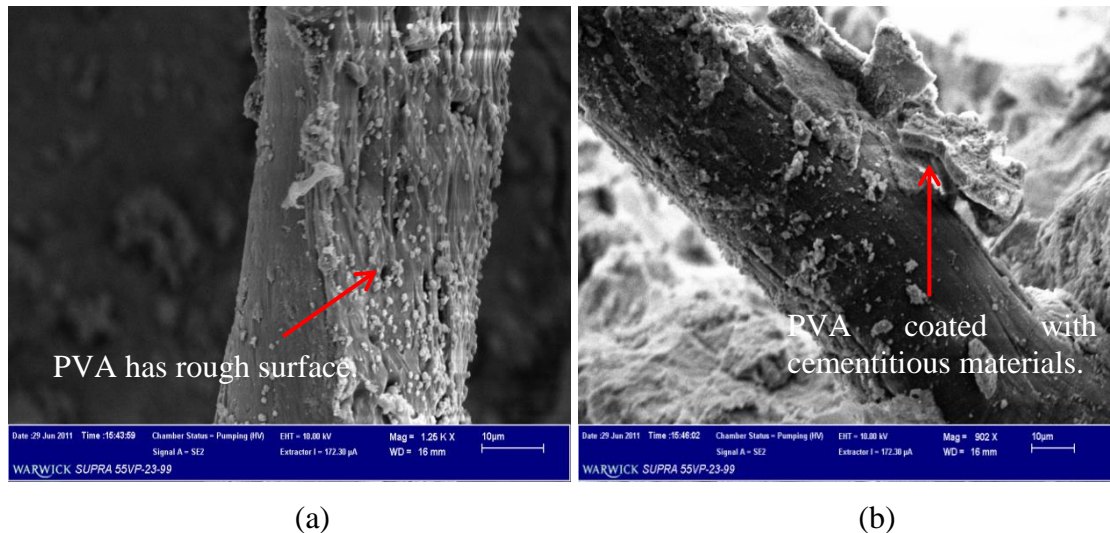


Figure 6.23: PVA material was made by compression moulding: a) PVA has rough surface and; b) PVA coated with cementitious materials.

6.3.8 Summary of Mechanical Test Results with Short Fibres

Using bar charts, Figures 6.24 to 6.27 give, respectively, the means of LOP strength, the means of flexural strength, toughness (energy absorption) and strains at the peak stresses for the five short fibres and control materials. Results for the two processing methods are given side-by-side, with hand lay-up on the left-side. Comparing the results in Figure 6.24 it is found that an improvement in LOP strengths was observed with all FRC specimens, and they are 19 to 59% higher than the control specimens. It can be seen that compression moulding and CF2 fibres specimens gave the highest mean LOP stress of 10.2 MPa, being 52% (6.7 MPa), 24% (8.2 MPa), 28% (8 MPa), 12% (9.1 MPa), and 6% (9.6 MPa) higher than for the other cementitious materials (going from left to right across the

bar chart in Figure 6.24). Comparing the hand lay-up LOP strengths in Figure 6.24 it is found that the PP batch gave the highest mean strength of 9.7 MPa, and that only the PP fibre material gave hand lay-up strength at 9.7 MPa higher than 9.1 MPa by compression moulding. These improvements in LOP strengths with CF2 and PP specimens might be attributed to their long length ($l > 2l_c$), this increases the friction bonding surface area between the fibres and matrix as discussed in Sections 6.3.5 and 6.3.6, resulting to increase the bond strength and can be effective after the FRC reaches its strength.

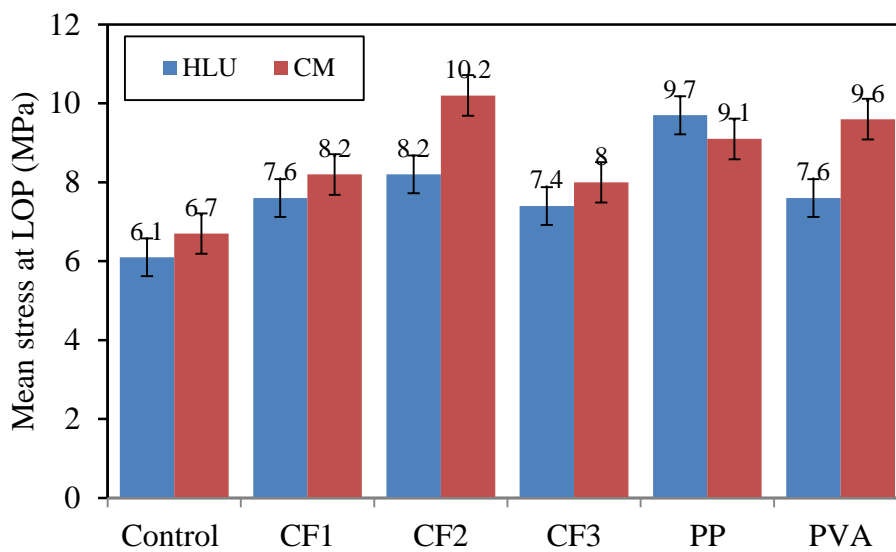


Figure 6.24: Mean LOP stress from flexural testing for control and short fibres materials.

It can be seen in Figure 6.25 that compression moulding and PVA fibres specimens gave the highest mean peak stress of 12.8 MPa, being 91% (6.7 MPa), 56% (8.2 MPa), 12% (11.4 MPa), 36% (9.4 MPa), and 40% (9.1 MPa) higher than for the other cementitious materials (going from left to right across the bar chart in Figure 6.25). Comparing the hand lay-up strengths in Figure 6.25 it is found that the CF2 batch gave the highest mean strength of 10.2 MPa, and that only the PP fibre material gave hand lay-up strength at 9.9 MPa higher than 9.1 MPa by compression moulding. Of the five fibre types only PVA gave, at 44%, a significant change in mean flexural strength between the hand

lay-up and compression moulding processes. On the assumption that 15% is not significant (see Sections 6.3.1 and 6.5), the two processing methods gave similar mean strength for the other four types; that is CF1 at 8%, CF2 at 12%, CF3 at 15%, and PP at 9%. The standard deviations of the results of flexural testing, presented in Tables A.6.1 to A.6.10, indicate the measurements per batch tend to be close to the mean and so the material is not significantly variable. Error bars in the Figure 6.25 are used to show the variability in batch results.

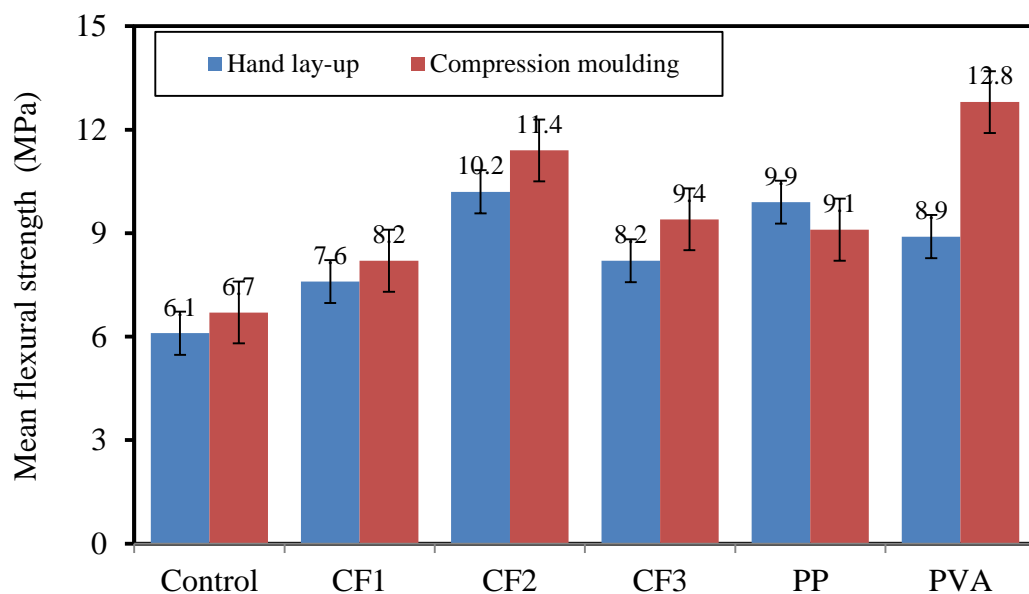


Figure 6.25: Mean peak stress from flexural testing for control and short fibres materials.

Figure 6.26 shows that, at 0.33%, the mean strain capacity at peak stress for PVA by compression moulding is the highest; the hand-lay capacity for this FRC is 0.29%. The highest strain is seen to be higher by a factor of 11 (0.029%), 7 (0.046%), 6 (0.051%), 8 (0.044%), and 15 (0.022%) by compression moulding with fibre types CF1, CF2, CF3, PP and for the control material, respectively, and by a factor of 9 (0.031%), 7 (0.044%), 5 (0.058%), 9 (0.033%), and 10 (0.03%) for the equivalent batches made by hand lay-up. As would be expected for the two PVA materials, Figure 6.27 shows these FRCs gave

relatively very high toughness values at 33 and $28 \times 10^{-3} \text{ J/m}^3$. The higher compression moulding value is higher by a factor of 28 (0.0012 J/m^3), 10 (0.0032 J/m^3), 10 (0.0032 J/m^3), 16 (0.0021 J/m^3), and 41 (0.0008 J/m^3) for the other compression moulding materials. It is also higher by a factor of 18 (0.0012 J/m^3), 7 (0.0033 J/m^3), 7 (0.0031 J/m^3), 15 (0.0015 J/m^3), and 22 (0.001 J/m^3) when the FRCs are made by hand lay-up.

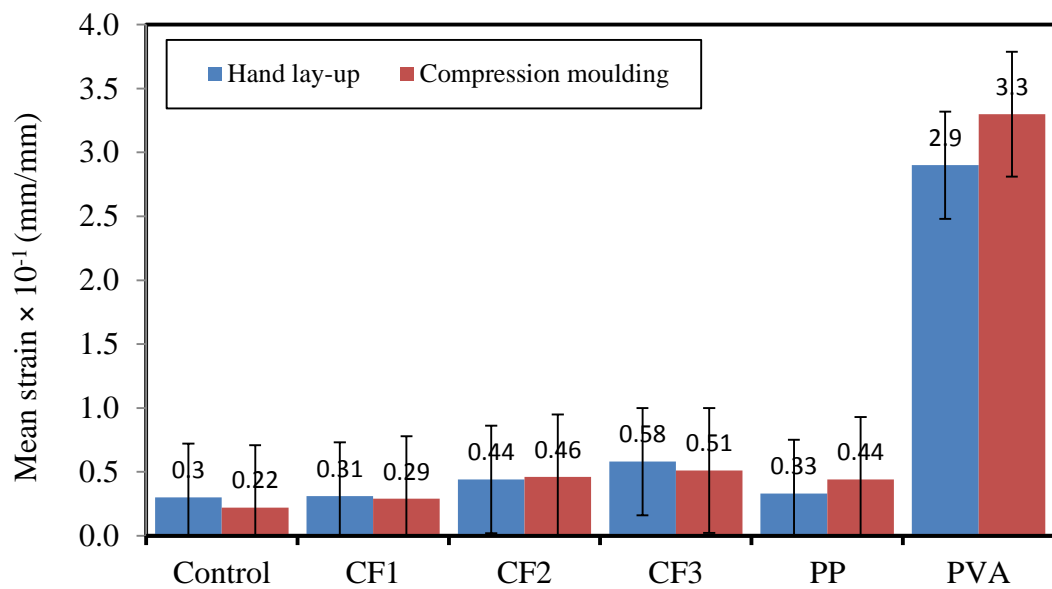


Figure 6.26: Mean strain at peak stress for control and short fibres materials.

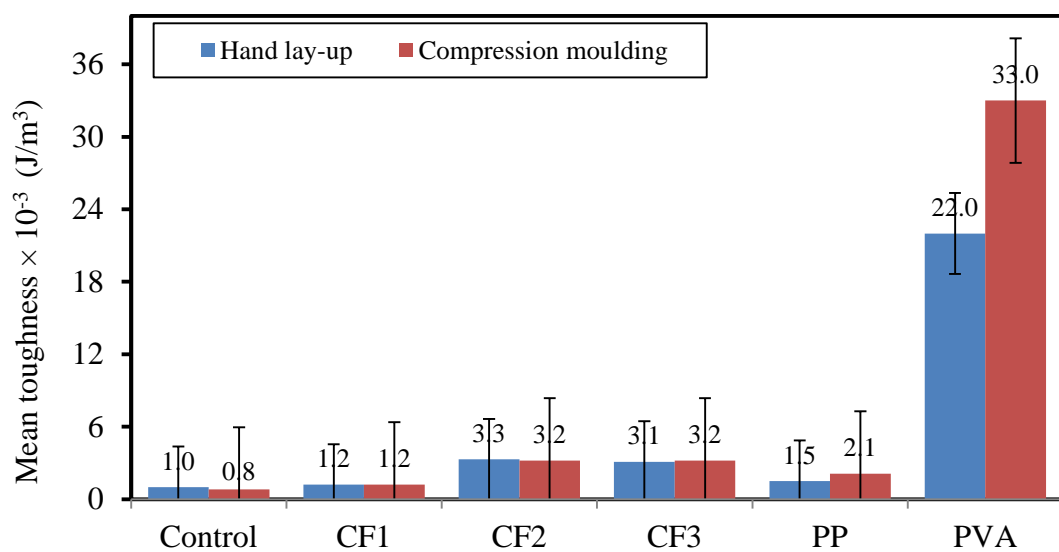


Figure 6.27: Mean toughness at peak stress for control and short fibres materials.

One key change to the cementitious matrix on applying compression moulding is a change in the w/b ratio. Figure 6.28 reports the excess water in the processed materials. The results indicate that the mean differences from the original w/b of 0.4 are 29% (0.29 after pressing), 31% (0.27 after pressing), 30% (0.28 after pressing), 34% (0.26 after pressing), 31% (0.27 after pressing), and 41% (0.24 after pressing) with CF1, CF2, CF3, PP, PVA, and for the control material. For the hand lay-up method of preparing flexural specimens the w/b ratio in the matrix material was always a constant.

A significance reduction in w/b from 29% to 41% on using compression moulding was found. This change is due to the applied pressure of 9 MPa used to minimise capillary porosity by removing excess water, and thereby increasing flexural strength, as discussed in Sub-section 4.5.5. This finding confirms and supports outcomes from the previous studies by Neville (1995), Kalliopi (2006), Bentz and Aitcin (2008). These researchers all considered the w/b ratio as a major variable that influences matrix strength and that has an important influence on the quality of hardened cement, knowing that as the w/b ratio increases the strength decreases. As the w/b ratio increases, so does the volume of capillary porosity and this change has a strong negative influence on matrix strength and permeability. It is therefore beneficial to use the compression moulding process to produce short FRCs with higher strengths.

In general, the improvements in flexural strength, maximum strain and toughness are associated with an effective bond for PVA fibres at 2% loading. Owing to favourable fibre properties there is sufficient composite action to transfer tensile forces across opening matrix cracks by fibre bridging without earlier loss in resistance due to fibre pull-out or fracture because distribution is non-uniform.

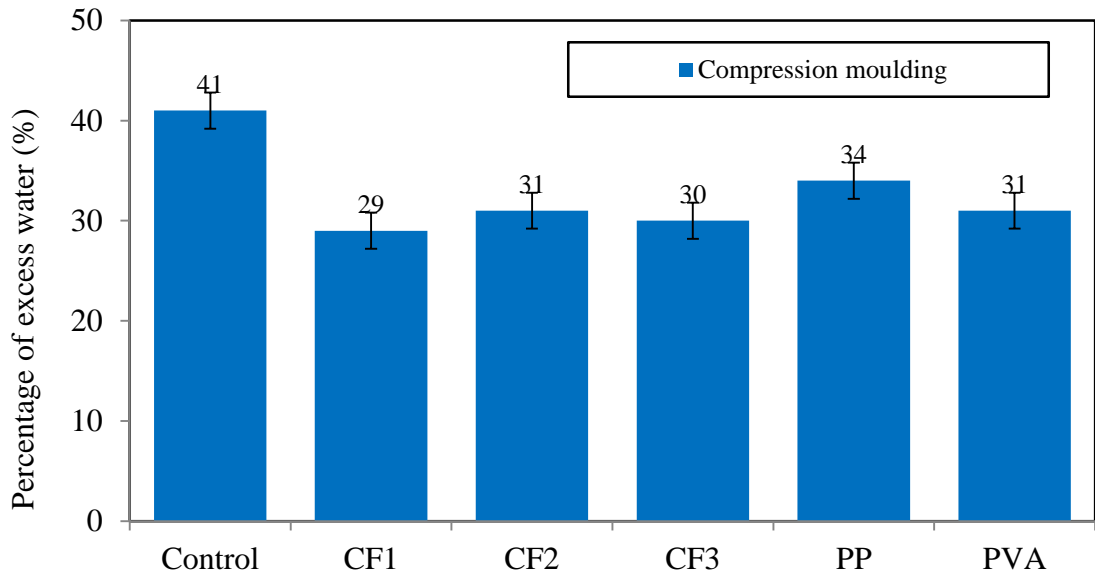


Figure 6.28: Excess water removed by using compression moulding process for control and short fibres materials.

6.4 Porosity Measurement

As discussed in Section 2.4.5 strength of FRCs is adversely affected by the level of porosity. Therefore, the effect of adding short fibres on the porosity was investigated. Measurements were made to establish porosity volumes in the five FRCs with 2% of CF1, CF2, CF3, PP and PVA fibres, and for the control matrix. Helium Pycnometry (HP) (model AccuPyc 1330 made by Micromeritics) was used to measure porosity following the test procedure given in Section 3.5.1. All specimens were produced with the same mix design of 1 C: 2 A: 0.66 W. Figure 6.29 presents the average percentage porosities from five specimens produced by hand lay-up and by compression moulding. In the figure the two processing methods are given side-by-side, with compression moulding (blue bars) on the left-side and hand lay-up (red bars) on the right-side. The results in Figure 6.29 indicate that materials produced by compression moulding have a lower porosity, which will be due to the applied compressive stress of 9 MPa; the processing method is explained in Section 4.5.5. The control material has a mean porosity of 13%, and this increases to between 16

and 28% after the addition of one of the five fibre types. Results show that the FRC with CF1 has higher porosity than those with CF2, CF3, PP, and PVA fibre. This finding is because of the tendency of CF1 fibres to form balls (that cannot easily be broken down). It is seen that the control material and CF3 FRC have the least porosity at 13 to 16%. The use of SF which has a diameter less than 1 μm and as such is able to penetrate into the spaces between the cement particles, reducing porosity and thus achieving very dense packing system as discussed in Section 2.8.1. Another observation is that PVA and CF2 materials by compression moulding have, at 16%, similar percentages of porosity and they have lower porosity than those with CF1, CF3 and PP fibre. Figure 6.30 shows the relationship between the mean strength (data from Figure 6.25) versus the mean porosity (data from Figure 6.29) for FRC materials with five short fibres produced by hand lay-up and compression moulding to see if an inverse relationship appears. It is found from Figure 6.30 that the lower the porosity is the higher the FRC strength. In other words, this is evidence that the strength has an inverse relationship with the porosity, as the porosity increases the strength decreases.

To see if there is a linear relationship, Figure 6.31 is a plot for the relationship between the mean flexural strength (data taken from Figure 6.25) versus the mean water loss (with data in Tables A.6.1, A.6.3, A.6.5, A.6.7 and A.6.9) for the FRC materials with five short fibres produced by compression moulding. It is clear from the results (blue diamond symbols) in the figure that the higher the water loss is the higher is the mean flexural strength. A linear trend line, coloured red, is added to show that strength increase could have a linear relationship with the water loss.

From the discussion above, it is concluded that there is evidence that compression moulding was successful in reducing porosity. It can be concluded that there is a direct

influence between the level of porosity and strength; the FRC with PVA fibres, produced by compression moulding, has the highest mean flexural strength at 12.8 MPa. This finding agrees with the work by Xu and Chung (1999) and Banfill *et al.* (2006), which is introduced in Section 2.4.5.

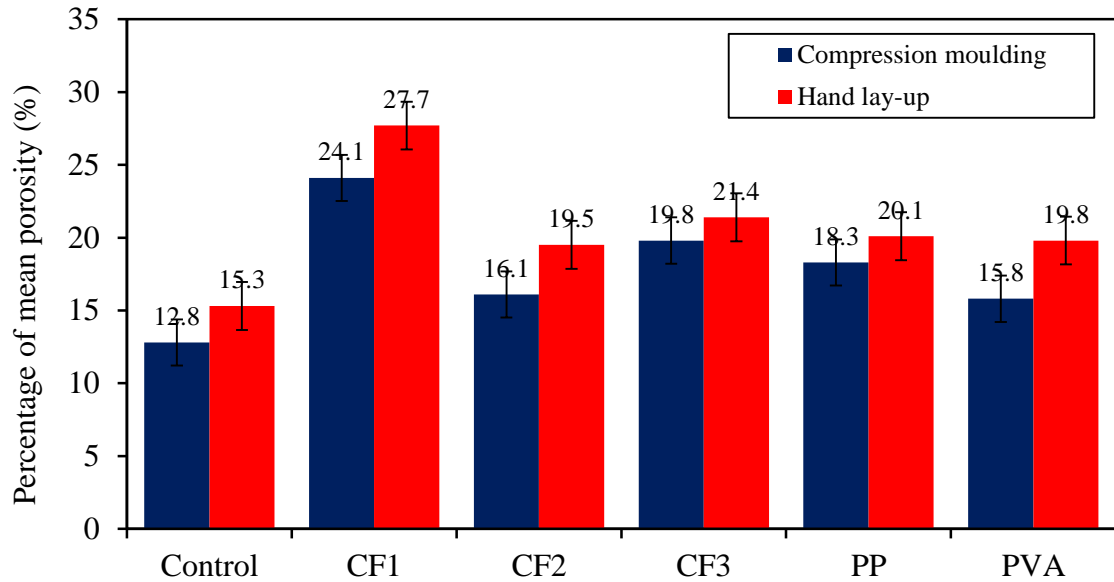


Figure 6.29: Percentage of mean porosity for control and five short fibre materials at $V_f = 2\%$ made by hand lay-up and compression moulding.

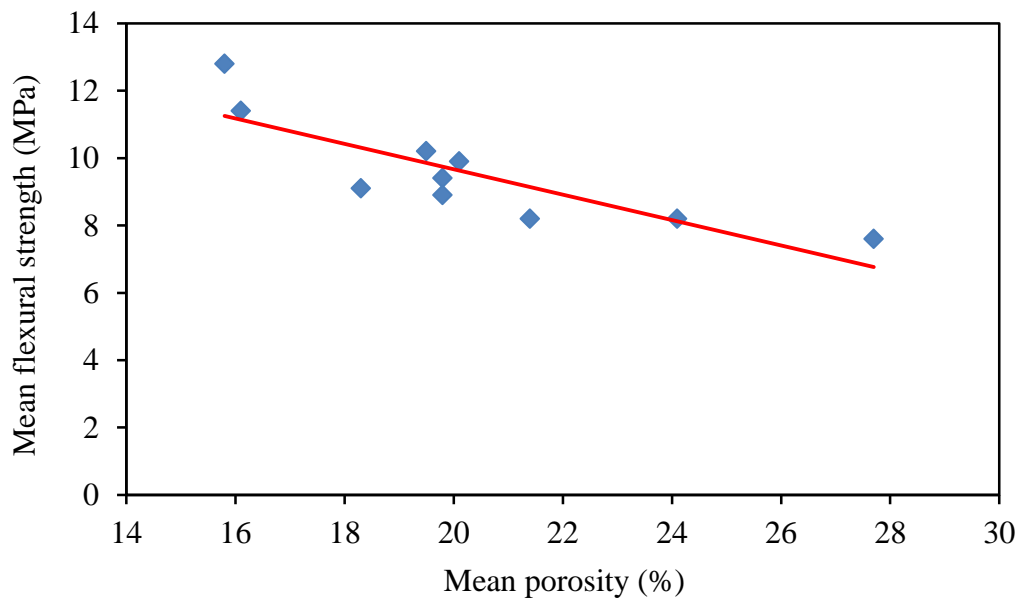


Figure 6.30: The mean peak strength versus mean porosity for five FRC materials with CF1, CF2, CF3, PP and PVA fibres made by hand lay-up and compression moulding.

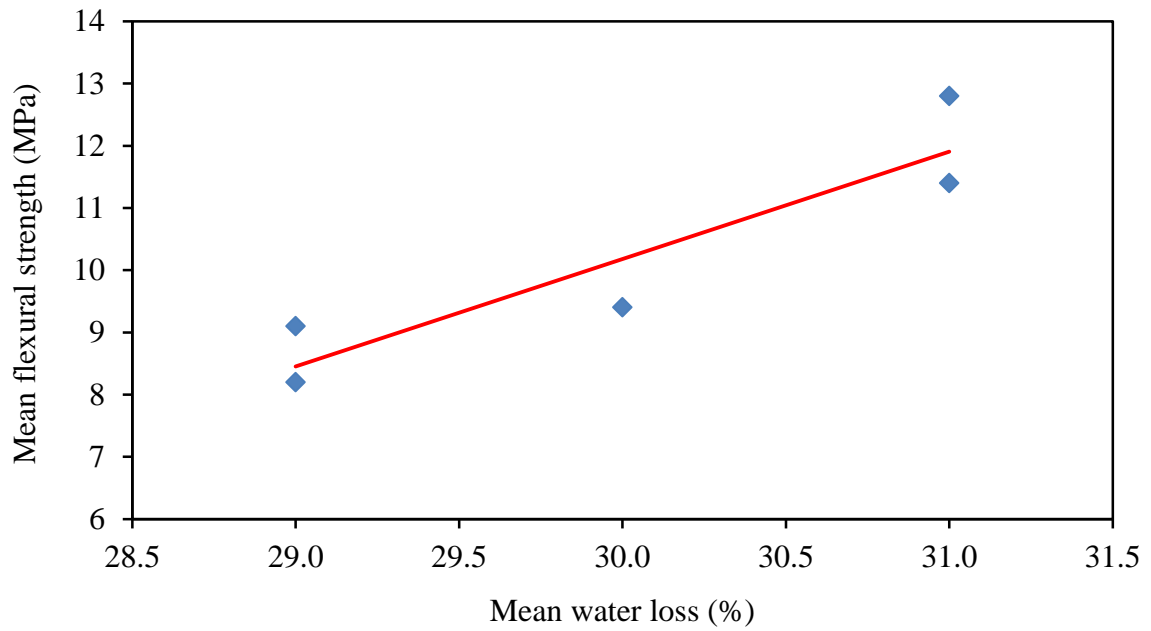


Figure 6.31: The mean peak strength versus mean water loss for five FRC materials with CF1, CF2, CF3, PP and PVA fibres made by compression moulding.

6.5 Statistical Analysis

The abbreviation ANOVA refers to analysis of variance, and is a statistical test used in order to analysis the differences between data sets and determines whether any of those data sets are significantly different from each other. The ANOVA test does not indicate which specific groups are significantly different from each other, it only informs, in a statistical sense, that at least two groups are different. The P -value is defined as the probability of obtaining values of the test statistic that would be equal or greater evidence against null hypothesis (H_0), if the null hypothesis is actually true. The P -value is used in the context of null hypothesis testing in order to quantify the idea of statistical significance of evidence. If there is a significant difference between the samples this will be identified by the P -value. In many areas of research, the critical P -value is usually set at 0.05. In other words, if the value of P -value is lower than 0.05 it is statistically significant, while a P -value > 0.05 is not giving statistically significant (Gelman, 2013).

In this study, ANOVA testing was carried out using Microsoft Excel software to determine if there is a significant difference between the flexural peak stress results from the two processes of hand lay-up and compression moulding. Presented in Appendix D Tables D.1 to D.6 are the ANOVA test results for the FRCs batches reinforced with the five short fibres (CF1, CF2, CF3, PP and PVA) at $V_f = 2\%$, and the control materials. For each reinforced material there are two parts (top and bottom) in each table. The top part provides familiar descriptive statistics for the individual group (e.g., groups, number of samples, sum of each group and variance (standard deviation squared)). Whereas the bottom part of a table is for the ANOVA analysis and has the following content. Column (1) is for the source and the name of the property that has entries in the row of columns to the right of it. Column (2) is the sum of squares (SS) and Column (3) is for the degrees of freedom (DF). Column (4) gives the calculation of the mean square (MS) with Column (5) for the F-statistic, sometimes referred to as F-ratio for the ratio of MS (between groups and within groups). Column (6) reports the P -value. The two rows for the ‘Between Groups’ and ‘Within Groups’ are for their variation. The final row in Tables D.1 to D.6 is for the ‘Total’ values. The information for the ANOVA testing was taken from Column (3) in Tables 6.1 and 6.2 for the control batches and from Tables A.6.1 to A.6.10 for the five short FRCs.

Table 6.8 summarises the P -values for the peak stress for the six materials. By inspecting the table the reader will be able to establish the relative differences. P -values for FRCs with CF1, CF2, CF3, PP reinforcement and the control material are found to be > 0.05 . This means that there is evidence that there is no significant statistically difference between the two methods of processing, compression moulding and hand lay-up. Furthermore, it is observed that only the peak stress for the PVA material is seen to have

been significantly affected by manufacture as the P -value is 0.004; considerable lower than for the other materials. This finding confirms, and supports, what was discussed in Sub-section 6.3.8 that the PVA specimens gave, at 44%, a significant change in peak stress between the hand lay-up and compression moulding processes.

Table 6.8: Values of P -value for, CF1, CF2, CF3, PVA, PP fibres and control specimens.

Material type	P -value	Significance
Control specimens	0.17	No
CF1 specimens	0.14	No
CF2 specimens	0.075	No
CF3 specimens	0.094	No
PVA specimens	0.00046	Yes
PP specimens	0.27	No

Based on the results in Table 6.8 it can be concluded that the statistical ANOVA test confirms and agrees with the author's proposal, introduced in Sub-section 6.3.1 that a difference of 0 to 15% between any two mean properties is not considered to be significant. Moreover it supports the findings given in Sub-sections 6.3.1 and 6.3.8 that, except for PVA batches, there is no significant difference between the two manufacturing processes. For the record the differences in peak stress between hand lay-up and compression moulding batches are: CF1 at 8%; CF2 at 12%; CF3 at 15%; PP at 9% and control specimens at 10%.

6.6 Findings from Mechanical Testing of Materials with Short Fibres

The main findings of the series of four-point bending tests reported in this chapter are:

- 1- The workability is too poor and too difficult to uniformly distribute the short fibres throughout the mix when V_f is $> 2\%$, especially with conventional mixing methods.

- 2- The strain-hardening response accompanied by multiple cracking stage can be achieved with short fibres even with low fibre volume fraction (2%) if the fibres: are long enough to transfer the stresses; are well dispersed throughout the matrix; have enough bond strength.
- 3- No benefit in mechanical properties for a FRC is to be had from adding the recycled milled carbon fibre (CF1). This is due to insufficient fibre length and lack of uniform dispersion.
- 4- Batch test results show that the FRCs processed by compression moulding generally have the highest mean peak stress. This mean flexural strength was however higher with a type of PP fibre when the processing was by hand lay-up.
- 5- Of the five materials reinforced with short fibres those with 2% by volume the PVA fibres exhibited strain-hardening behaviour and fibre fracture failure at ultimate failure. PVA fibres gave an FRC with greatly improved mechanical properties. PVA specimens produced by compression moulding gave the highest mean peak stress, highest mean maximum strain and largest toughness at peak stress. These properties were determined to be higher, by a factor of 2 (6.7 vs 12.8 MPa), 15 (0.022 vs 0.33%) and 41 (0.0008 vs 0.033 J/m³) over the mean from testing control specimens. This is attributed to the PVA fibres being hydrophilic (absorb water), possessing a rough surface (with fibrils) and high aspect ratios. From previous studies this fibre type is known to have a relatively high bond strength (note that mean length of PVA fibres is 8, which is = $2l_c$).

Chapter 7

7. Test Results for Cementitious Materials Reinforced With Continuous Fibres

7.1 Introduction

In this chapter the author presents, evaluates and discusses the characterisation of cementitious materials reinforced with the continuous fibre types introduced in Sub-section 3.2.4. To investigate different processing methods for the manufacture of green forms, compression moulding and hand lay-up are used. The processing findings presented in Chapter 5 were adopted to produce FRCs for this part of the work. Six of the seven continuous fibre reinforcements are of carbon and are allocated the labels CF4, CF5, CF6, CF7, CF8, and CF9. Of this group, three are unidirectional (CF4, CF5, and CF6), two are biaxial (equal fibre loading in weft and warp directions) (CF7 and CF8), and one is a multi-axial fabric (CF9). The seventh reinforcement is a biaxial fabric and of E-glass fibre, and is allocated the label GF. The reason for having E-glass fibre was explained in Sub-section 2.4.1. The fabrics were briefly introduced in Section 3.2.4 and the manufacturer's properties given in Table 3.3.

7.2 Specimen Labelling Code

It is important to have a labelling system that clearly identifies each specimen/batch of specimens. The four parts in the system are: fibre type; manufacturing method; curing regime; specimen number. The various entries in the four parts are as follows. Fibre type is 'CF4', 'CF5', 'CF6', 'CF7', 'CF8', 'CF9' or 'GF'. To avoid confusing the reader, the code for the control material (the matrix) changes from CS in Chapter 6 to CS1 in this chapter. The justification for this change is because the w/b ratio, at 0.35, is 0.05 lower

than in Chapter 6. Letter T denotes a surface treatment, S is for strips form, and H for the hybrid FRC having the three fibres, CF3 + PVA+ CF8. The type of manufacturing process is 'HU' for hand lay-up and 'CM' for compression moulding. For the curing regime, the coding is either: '50' for 50°C hot-water ageing or 'RH' for Relative Humidity condition of 100%. To help the reader to understand the labelling system, examples are given next:

- CF4-CM-RH-01. This FRC has unidirectional carbon fibre (200 g/m²), in sheets form, produced by compression moulding and cured in 100% RH. The specimen is number 1.
- CF4T-HU-50-02. The FRC has treated unidirectional carbon fibre (200 g/m²), immersed in Ethanol alcohol, produced by hand lay-up and cured in hot water at 50°C. The specimen is number 2.
- CF4S-CM-50-01. The FRC has unidirectional carbon fibre (200 g/m²) in strips form, produced by compression moulding and cured in hot water at 50°C. The specimen is number 1.
- H-CM-50-01. This FRC has hybrid fibre reinforcement from a combination of CF3, PVA and CF8, produced by compression moulding and cured in hot water at 50°C. The specimen is number 1.

7.3 Test Results and Discussion

Four-point bending testing was performed as per the procedure presented in Sub-section 3.8.1. The same data reduction method as for Chapter 6 results is employed to convert load vs. deflection data into stress vs. strain results. Comparisons for flexural response are developed graphically, and at the end of Section 7.3 a bar chart graph presents the flexural strengths for the seven FRCs. For all materials reinforced with continuous

fibres the strain is recorded at first cracking stress (for Loss of Proportionality (LOP)) and at peak stress. The toughness (energy absorption) is calculated for the specimen at LOP and peak stress.

Based on the outcomes of Chapter 5, a single mix design was chosen to manufacture the cementitious materials with both compression moulding and hand lay-up processes. This enables a direct comparison to be made. The mix proportions for constituent parts are 1 C: 2 A: 0.58 W, as introduced in Section 5.9. For the aggregate (Section 5.5), only fine aggregate (100% sand) with SPD < 1.18 mm is used. The best combination of binder materials, in terms of their weight percentage is 60.6% C+9.1% SF+12.1% PFA +18.2% GGBS. By weight of cement the other binder constituent percentages are: SF at 15%; PFA at 20%; GGBS at 30%. These proportions were selected by the author based on the processing investigations presented in Section 5.4, with 3% by weight of cement of the superplasticiser type SP_B (Glenium 51) (see Sub-section 3.6.1). The binder's proportions confirmed and agreed with results of the previous studies presented in Table 5.2. Preliminary experiments in Section 5.7 showed that the w/b ratio used is to be kept constant at 0.35 (i.e. 0.58W). This choice is needed to maintain matrix workability before curing. Preparation of the specimens is developed in Section 4.4 for the hand lay-up process and Section 4.5 for compression moulding. All mix proportions are given by the weight of cement in Tables 5.6 and 5.7 in Section 5.9. Seven reinforcements of CF4 to CF9 and GF are studied. In this series of flexural tests, the number of nominally identical specimens per batch is six, with four or five for a few of the batches. A comparison is made between the measured properties of the FRCs and the control materials.

Presented in Appendix B and Tables B.7.1 to B.7.42 are the test results and statistical analysis for the batches of specimens. For each reinforced material there are two tables in

Appendix B. The first table has the following content. Column (1) gives the specimen label and the top row follows with the names of the properties having entries in the columns below. Column (2) is for w/b ratios with hand lay-up and compression moulding, before and after pressing (and the difference between them). Column (3) is for LOP and peak stresses. Column (4) reports the strains at LOP and peak stresses. For each batch, the statistical analysis gives mean, standard deviation (SD) and characteristic value (in rows seven to nine). The final two rows report the maximum and minimum test values. The second table in Appendix B is used to present the toughness (energy absorption) determined at LOP and peak stress.

Figures 7.1 to 7.27 present the new results in form of bar charts, graphical plots for stress and strain (outer surface) relationships, photograph of specimens under flexure and failed, and Scanning Electron Microscopy (SEM) images for microstructural features. Plots in Figures 7.4 to 7.11, 7.16 to 7.21 and 7.25 and 7.26 are used to present the lower and upper bound stress-strain curves from the sixteen batches produced either by compression moulding or hand lay-up. Two of the figures are for control materials and fourteen figures for the FRCs with the seven fabrics CF4 to CF9 and GF. To allow each pair (compression and hand lay-up) of curves to be easily compared with each other the plotting has the same ordinate and abscissa axis scales. By inspecting the curves, the reader will be able to establish the relative differences in upper and lower test results from within a batch of six (or four or five) specimens, and can evaluate the energy absorption capacities of the different FRCs.

As one of the objectives of the work is to study the microstructure, SEM was used to observe the interaction between fibres and matrix and to examine matrix penetration into

the filament tows. Both the preparation process and the SEM technique are discussed in Section 3.4.

7.3.1 Curing Regimes

To investigate the curing regimes on flexural strength specimens with CF at 5% V_f were cured either in 100% Relative Humidity (RH) or by fully immersing specimens in hot water at 50°. As discussed in Section 4.6 the second of the two curing condition is based on the findings of previous studies by Marikunte *et al.* (1997), Purnell (1998), Peled *et al.* (2005) and Purnell and Beddows (2005). In the two CF5 batches the reinforcement is in sheet form, which is as supplied by the manufacturer. One batch was produced by a hand lay-up process and the other batch by compression moulding. The number of nominally identical specimens is twelve for compression moulding and ten for hand lay-up. 50% of the specimens were cured in 100% RH and the other 50% were cured by fully immersing specimens in hot water at 50° until the day before flexural strength testing. Curing and four-point bending test were carried out using the standard methods given in Sections 3.8 and 4.6.

The bar chart in Figure 7.1 reports the mean peak flexural strengths from this test series. It is observed that the strength of an CF5 FRC is always higher, at 27% for compression moulding and 24% for hand lay-up when cured in hot water at 50°. The author used this finding to make the decision not to use the other curing condition when preparing the specimens for characterising the FRC with continuous reinforcement. This finding is supported by results of previous studies by Marikunte *et al.* (1997), Purnell (1998), Peled *et al.* (2005) and Purnell and Beddows (2005). As explained in Section 4.6 they all found the full immersion method of curing to be successful when studying the durability of GFRC materials.

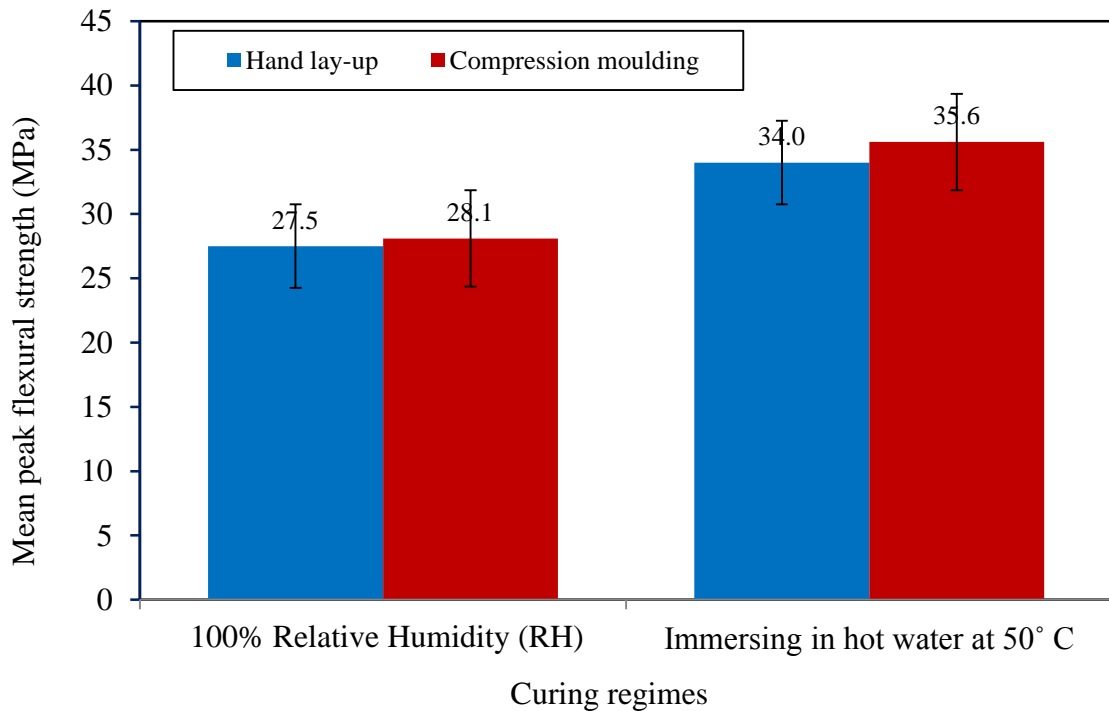


Figure 7.1: Mean peak flexural Strength with two curing regimes; cured in hot water at 50°C and Relative Humidity condition of 100% for CF5 materials in sheet form that were produced by hand lay-up and compression moulding processes.

7.3.2 Combined Efficiency Factor (η)

Investigated next are factors η_1 and η_θ , via combination factor $\eta = \eta_1 \eta_\theta$ for the FRCs with reinforcements CF4 to CF9 and GF. As discussed in Section 2.17 η with unidirectional fibres (0°) is 1.0. Because this is not a common reinforcement arrangement for most applications $\eta < 1$, and so it is to be calculated. Values for η_1 and η_θ are taken from Figure 2.10 in Section 2.17. As shown in Figure 2.10 $\eta_1 = 1.0$ for all cases of continuous fibres; this is due to the continuous fibre length condition. Now $\eta_\theta = 1.0$ for fabrics CF4 to CF6 because they are unidirectional and their filaments are aligned with the flexural deformation.

For the other two fibre arrangements, the balanced biaxial (0° and 90°) fabric (CF7, CF8 and GF) has $\eta_\theta = 0.5$. In case of CF9, which is a multi-axial fabric (equal 0° , 90° and $\pm 45^\circ$), η_θ is established to be 0.38. η is calculated for the seven fabrics; and presented in Table 7.1. From table the CF9 fabric with $\eta = 0.38$ will require ≈ 3 times the V_f to achieve the same effective V_f (for ‘same’ FRC stiffness and strength) as does the unidirectional fabrics of CF4, CF5 and CF6.

Table 7.1: Values of combined efficiency factor (fibre length and orientation) for seven fabrics, CF4, CF5, CF6, CF7, CF8, CF9 and GF.

Fibre type	Length factor, η_l	Orientation factor, η_θ	Combined efficiency factor, $\eta = \eta_l \eta_\theta$
Unidirectional carbon fibre 200 g/m ² (CF4)	1	1	1
Unidirectional carbon fibre 300 g/m ² (CF5)	1	1	1
Unidirectional carbon fibre 450 g/m ² (CF6)	1	1	1
Biaxial glass-carbon fibre (CF7)	1	0.5	0.5
Biaxial carbon fibre (CF8)	1	0.5	0.5
Multiaxial carbon fibre (CF9)	1	0.38	0.38
Glass fibre (GF)	1	0.5	0.5

It is not only the length and orientation of fibres that are responsible for improving the properties of an FRC that will exhibit the beneficial and desirable strain-hardening behaviour. V_f is another key variable that will be investigated in Sub-section 7.3.3. Values for η in Table 7.1 will be used later to determine the critical fibre volume fraction ($V_{f,crit}$) by Equation (2.13) and to determine the effective fibre volume fraction (V_f') of an FRC using Equation (2.24).

7.3.3 Fibre Volume Fraction (V_f)

Given that one of objectives of the research is to have the highest practical V_f fabric, CF4 was selected for a study to produce a relatively highly loaded material. This unidirectional fabric was chosen because its structure has the majority of the filaments

aligned in the principal loading direction (i.e. for 100% effectively), and because it has a small voids (holes) between every two adjacent fibre bundles. The voiding provides can improve the cement penetration between bundles or filaments, as discussed in Sections 2.5 and 2.16. Four different V_f of 5% (7 sheets), 11% (15 sheets), 13% (17 sheets), and 15% (21 sheets) were used to obtain test results from low to high V_f . The author selected these four V_f because it is more practical to compare the results between two processing methods, hand lay-up with compression moulding. The mix design, constituent materials, and mixing procedure were the same as previously mentioned in Section 7.3.

The influence of V_f on the mean flexural strength is plotted in Figure 7.2. Before flexural testing, the ten batches of twelve specimens (six each for compression and hand lay-up) were cured in hot water at 50 °C for 28 days. Test results for hand-lay are given in blue with a square symbol and for compression moulding in red with a circular symbol. Straight lines are used to join the individual mean results to give an indication of the likely change in mean strength with V_f . It can be seen from the results in Figure 7.2 that, for V_f of 11%, and higher, means are similar or lower than the control materials (averaging at 7 MPa), irrespective of the processing. It can be observed that the tendency is towards an adverse effect on the flexural strength when $V_f > 5\%$ and this effect increases towards its maximum of 15%. Nevertheless, given the V_f examined (7-15%) it may be concluded that the trend is showing that a higher flexural strength cannot be achieved with $V_f > 15\%$. It is more difficult to conclude that a higher flexural strength can be achieved with $V_f < 5\%$ or (slightly) higher. The author observed that when V_f is $> 5\%$ the CF4 FRC exhibited poor compaction and poor surface finish, and the flexural strength decreases. An example of one of these specimens is shown in Figure 7.3. Although apparently viable, as the green form could be readily demoulded, it was found immediately afterwards that specimens suffered

from severe delamination failure. Note that in Figure 7.3 the presence of major longitudinal cracks along, and in line, with the position of the CF4 fabric layers. The failure is mainly due to the inadequate penetration of the matrix resulting in a weak overall bond (interconnection) between reinforcement and matrix.

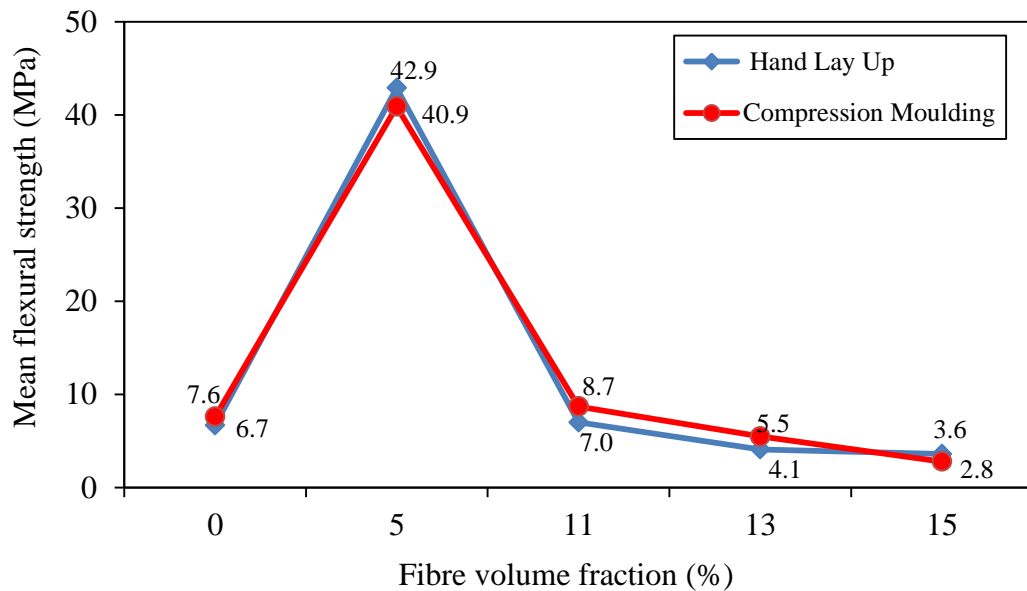


Figure 7.2: Relationship between mean flexural strength and fibre volume fraction for the CF4 cementitious material that produced by hand lay-up and compression moulding.

The key finding from this preliminary study is that mean strength at +40 MPa is nearly six times higher than control specimens when V_f is 5%, and for the next, and subsequent, number of fabric layers the strength disappears. The change in strength with V_f is seen to be independent of processing method. Using this important test series results it was therefore decided to set V_f constant at 5% for the FRCs having the other fabrics of CF5 to CF9 and GF. It is relevant to know if this selected maximum V_f is greater than V_{fcrit} .

Using the ACK model in Section 2.13 and the η listed in Table 7.1, the minimum fibre volume fraction (V_{fcrit}) required to prevent brittle failure is calculated using Equation (2.13). In the equation σ_m is the mean failure stress of the control materials and is given in

Table B.7.1 as 7.4 MPa for hand lay-up and in Table B.7.2 as 7.6 MPa for compression moulding. Taking the mean of the two processing batches we can assume σ_{mu} is 7.5 MPa. σ_{fu} is the single fibre tensile strength, and this property from single fibre tensile tests with the continuous fibres CF4, CF5, CF6, CF7, CF8, CF9 and GF are reported in Table 3.7.

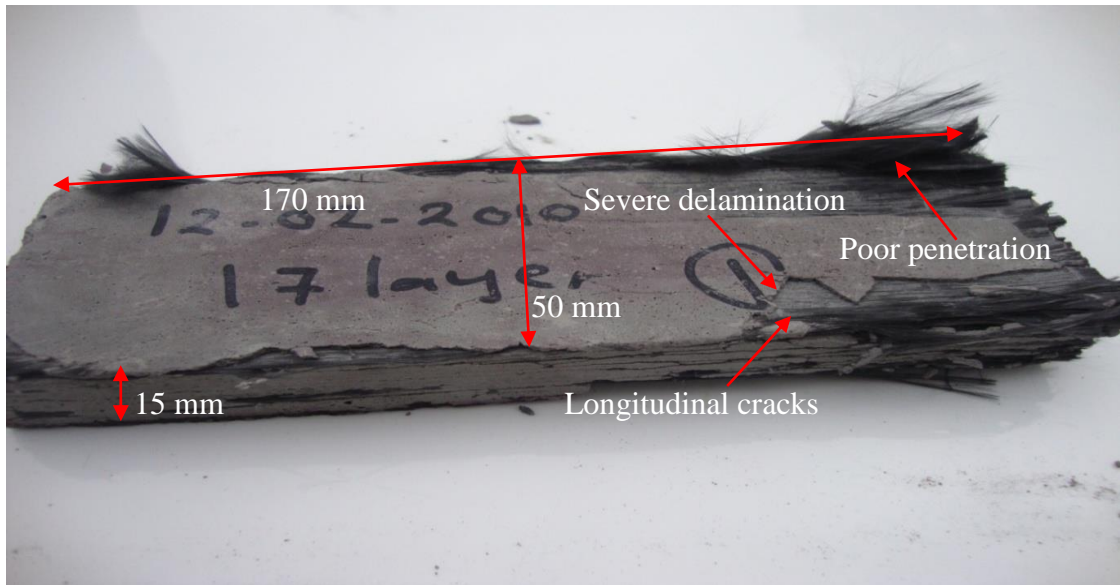


Figure 7.3: CF4 specimen having V_f equal to 13% has poor surface finish and delamination cracks throughout its thickness.

An example on how to calculate V_{fcrit} for CF8 is given next. Substituting known and estimated parameters into Equation (2.13) we have:

$$V_{fcrit} = \frac{\sigma_{mu}}{\eta \sigma_{fu}} = \frac{7.5}{0.5 \times 2240} = 0.006 = 0.6\%$$

By applying Equation (2.13) in turn, Table 7.2 presents the calculated V_{fcrit} , which are found to be in the range of 0.3% to 1.0%. This 1/5th or less than the reinforcement level of 5%. It is found to be seventeen times higher for the three fabrics CF4, CF5 and CF6, eight times higher for CF8 and CF9 and five times higher for CF7 and GF fabrics. It can therefore be expected that the seven FRCs with continuous fibre reinforcement will support the transfer of force after LOP, and provide the material with multiple cracking behaviour

and post-cracking capability. This finding confirms what has been reported in a previous study by Purnell (2010). We can expect the FRCs to have a with a stress-strain curve similar to that presented in Figure 2.3(a), i.e. the materials exhibit strain-hardening behaviour.

Table 7.2: Values of $V_{f,crit}$ for CF4, CF5, CF6, CF7, CF8, CF9 and GF fabrics.

Reinforcement type	$V_{f,crit}$ (%)
Unidirectional carbon fibre 200 g/m ² (CF4)	0.3
Unidirectional carbon fibre 300 g/m ² (CF5)	0.3
Unidirectional carbon fibre 450 g/m ² (CF6)	0.3
Biaxial glass-carbon fibre (CF7)	1.0
Biaxial carbon fibre (CF8)	0.6
Multiaxial carbon fibre (CF9)	0.6
Glass fibre (GF)	1.0

Based on the ACK model the effective fibre volume fraction (V_f') for the specific case of unidirectional reinforcement is equal to V_f (see Section 2.17). For other types of continuous reinforcement, such as biaxial or multi-axial, we find that V_f' is always $< V_f$. For this reason, V_f' is calculated for the seven fabrics using Equation (2.24). An example of how to determine V_f' for the CF8 fabric is given by:

$$V_f' = \eta V_f = 0.5 \times 0.05 = 0.025 \approx 2.5\%$$

Table 7.3 presents the V_f' , and because CF4, CF5 and CF6 fabrics are effectively unidirectional their V_f' are 5%. These FRCs are therefore expected to be 100% effective. V_f' for the multi-axial fabric CF9 is determined to be 1.9%, and so we observe that this reinforcement is 38% effective. It requires ≈ 3 times the V_f to achieve the same effective V_f (for an equivalent increase in FRC stiffness and strength) as does the three unidirectional fabrics.

Table 7.3: Values of V_f' for CF4, CF5, CF6, CF7, CF8, CF9 and GF fabrics.

Reinforcement type	V_f' (%)
Unidirectional carbon fibre 200 g/m ² (CF4)	5
Unidirectional carbon fibre 300 g/m ² (CF5)	5
Unidirectional carbon fibre 450 g/m ² (CF6)	5
Biaxial glass-carbon fibre (CF7)	2.5
Biaxial carbon fibre (CF8)	2.5
Multiaxial carbon fibre (CF9)	1.9
Glass fibre (GF)	2.5

7.3.4 Control Materials

Control specimens were produced with the same dimensions as the FRC specimens and same matrix composition. The mix design, constituent materials, and mixing procedure are those introduced in Section 7.3. These specimens were identified as series CS1-CM-50-01 to CS1-CM-50-06 by compression moulding and CS1-HU-50-01 to CS1-HU-50-06 for hand lay-up. Presented in Appendix B Tables B.7.1 and B.7.2 are results and statistical analysis for the two batches. Twelve specimens were cured in hot water at 50°C for 28 days. Inspecting column (3) in Tables B.7.1 and B.7.2 it is seen that σ_{mu} equals σ_{cu} because first cracking and ultimate failure coincide. Column (3) shows that the mean peak stress by compression moulding and by hand lay-up is, at 7.4 and 7.6 MPa, similar.

The strains and toughness reported in columns (4) and (5) are at peak stress. A significant difference in this strain and toughness measure is observed between the batches produced with hand lay-up and compression moulding. The results show an increase in the mean strain and toughness when FRC is by compression moulding. They are found to be up to a factor of 5 to 6 times higher than obtained from the hand lay-up batch. SD is 0.9 MPa for both processes. As might be expected from material consolidation using

compression moulding, the characteristic strength of the hand lay-up control batch is slightly lower by 5%.

Figures 7.4 and 7.5 show the lower and upper bounds of the stress-strain curves for compression moulding and hand lay-up of the control materials. It can be observed from these figures that all four stress-strain curves show the same relatively brittle behaviour, having linearly elastic up to LOP and ultimate failure. The peak stress range from hand lay-up of 5.8 and 8.5 MPa and from compression moulding of 6.0 and 8.8 MP are similarly. As shown in the figures control specimens always fail immediately the maximum load is reached; the curves exhibited sharp and sudden failure. Using the ACK model the region observed is for pre-cracking Region I. A flexural specimen fails with a single vertical (tension) crack, located directly below one of the two loading pins. This is equivalent to what has already been reported in Sub-section 6.3.1 when the control materials for the short fibre study were similarly characterised.

Generally, the overall performance of the control materials is similar, as they exhibit the strain-softening behaviour introduced in Section 2.3. There will be no strain-hardening or multiple cracking (no regions II and III as shown in Figure 2.2(b)). Following on from the discussion for the control materials the effect of adding different types of continuous fibres will be investigated in Sub-sections 7.3.5 to 7.3.7. In particular the study will look at how best to achieve strain-hardening behaviour accompanied by multiple cracking, as this leads to a high failure strain capacity a less catastrophic/brittle mode of failure.

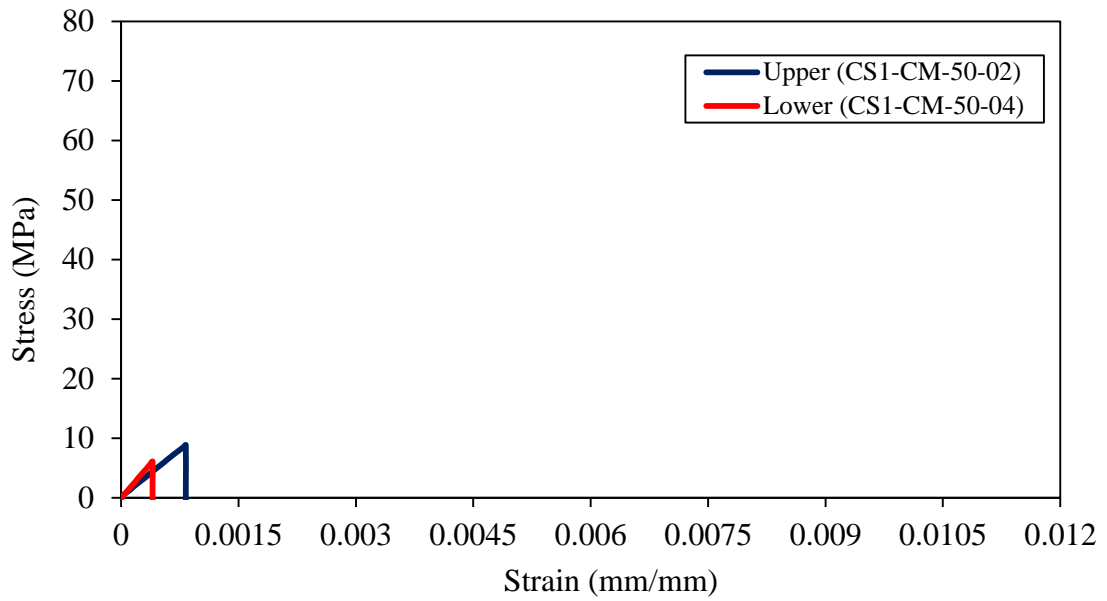


Figure 7.4: Lower and upper bound stress-strain curves for control specimens produced with compression moulding.

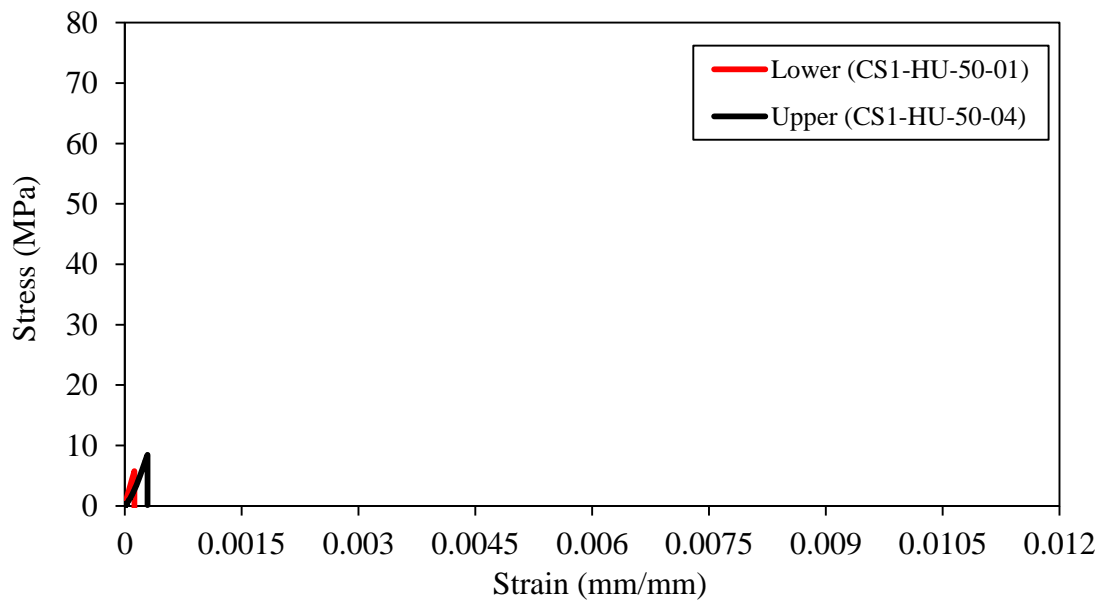


Figure 7.5: Lower and upper bound stress-strain curves for control specimens produced with hand lay-up.

7.3.5 Materials Reinforced With Unidirectional Fabrics; CF4, CF5 and CF6

The author divides the form of the stress-strain curves in Figures 7.6 to 7.11, 7.16 to 7.21 and 7.25 and 7.26 into three categories. The first category is for FRC materials reinforced with the unidirectional fabrics CF4, CF5 and CF6. The second category is for FRC materials reinforced with the biaxial fabrics CF7, CF8 and GF, with V_f' equal to 2.5%. The final category is for the single FRC material reinforced with the multi-axial fabric CF9, with V_f' equal to 1.9%. The first category is discussed in this sub-section, and the other two categories are discussed in the following two sub-sections.

The mix design, constituent materials and mixing procedure were the same as previous. Figures 7.6 to 7.11 show the lower and upper bounds for the stress-strain curves for the CF4, CF5 and CF6 FRCs (with $V_f = 5\%$) produced by the two manufacturing processes. Also plotted in the six figures is the lower bound curve for the FRC's control material. The black coloured curve is for the upper bound and blue for the lower bound, with the control curve coloured red. By comparing the curves in these figures it is seen that the materials deform and respond differently from the five common FRC materials defined by curves (a) to (e) in Figure 2.3 of Section 2.10. It is found that the shape of the curves in Figures 7.6 to 7.11 closely resembles the shape of curve (f). This form of curve with FRC materials has rarely been encountered in the past when $V_f \gg V_{f_{crit}}$, for the reasons discussed in Section 2.10.

The elastic portion of the curves in Figures 7.6 to 7.11 shows linearity up to the peak stress, occurring in the range 20 to 45 MPa (see Tables B.7.3 to B.7.14). For FRCs with fabrics CF4 to CF6 the first crack stress and the peak stress are the same (i.e. $\sigma_{mu} = \sigma_{cu}$). It

will later be shown in Sub-section 7.3.6 that σ_{mu} is at least three times higher than for FRCs with fabrics CF7, CF8 and CF9. Beyond the peak stress, the stress first drops some 10% to 25% before decreasing gradually until there is ultimate failure. As shown in Figure 7.6 the ACK model provides two distinct regions for the stress-strain curve for the pre-cracking Region I and gradual failure (for Region IV).

As seen from the curves in Figures 7.6 and 7.11 the 5% V_f of unidirectional continuous fibres dramatically improves the flexural strength, strains and toughness at peak stresses when compared to the control materials results in Figures 7.4 and 7.5. Furthermore, an effectively monotonic curve up to peak stress is observed, rather than the usual two or three-stage (ACK model) curve of the classic primary FRC as shown in Figure 2.3(f) and discussed in Section 2.10. This beneficial behaviour is a rarely observed with FRC materials and is interesting to discuss. It is associated with the following reasons:

1. $V_f = 5\% \gg V_{crit} = 0.3\%$, it is seventeen times higher (see Table 7.2). The cracking strength becomes significantly higher than the strength of matrix ($\sigma_{cu} > \sigma_{mu}$), and this response is generally attributed to the suppression and/or modification of crack growth (Purnell, 2010). Furthermore, as presented in Table 7.3, the values of V_f' for CF4 to CF6 fabrics are the same, and the reinforcement is 100% effective since $V_f' = V_f = 5\%$.
2. The combined efficiency factor $\eta = 1.0$, as given in Table 7.1. Since the FRC specimens were made with unidirectional carbon fabrics all the continuous fibres ($l \gg l_c$) can be aligned in the loading direction. Assisting with the 100% efficiency is the increased effective friction bonding area and the very large number of fibres available to bridge matrix cracking. Fibres will therefore be able to carry additional force after the matrix cracks.

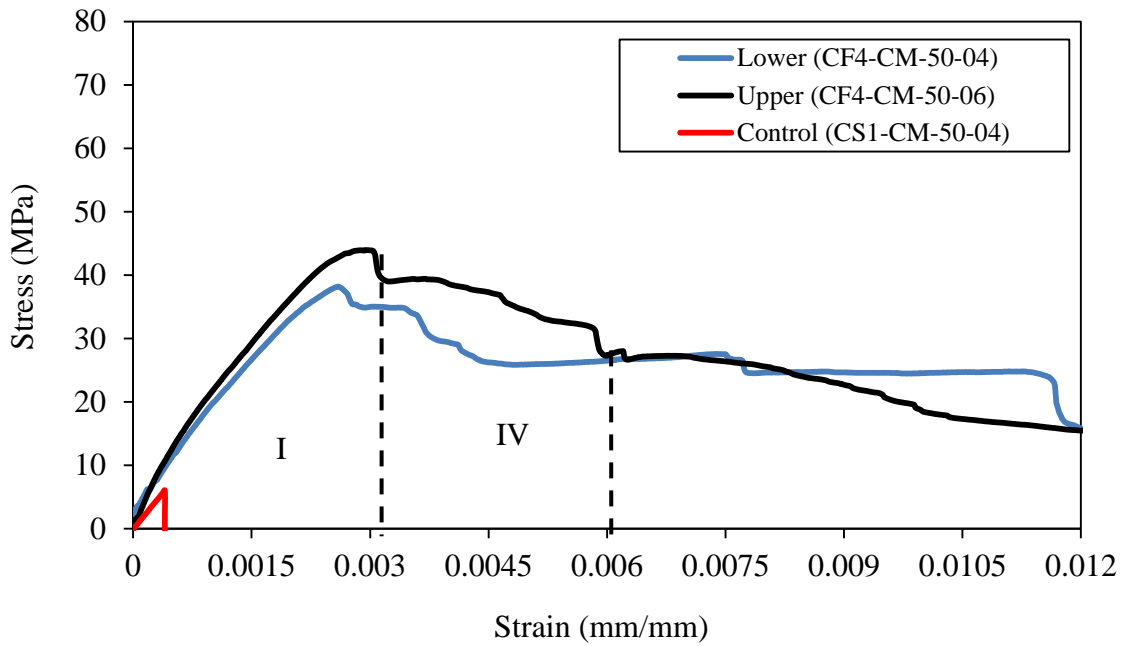


Figure 7.6: Comparison of the lower and upper bound stress-strain curves for CF4 cementitious specimens ($V_f = 5\%$) produced with compression moulding with lower bound curve from the control specimens.

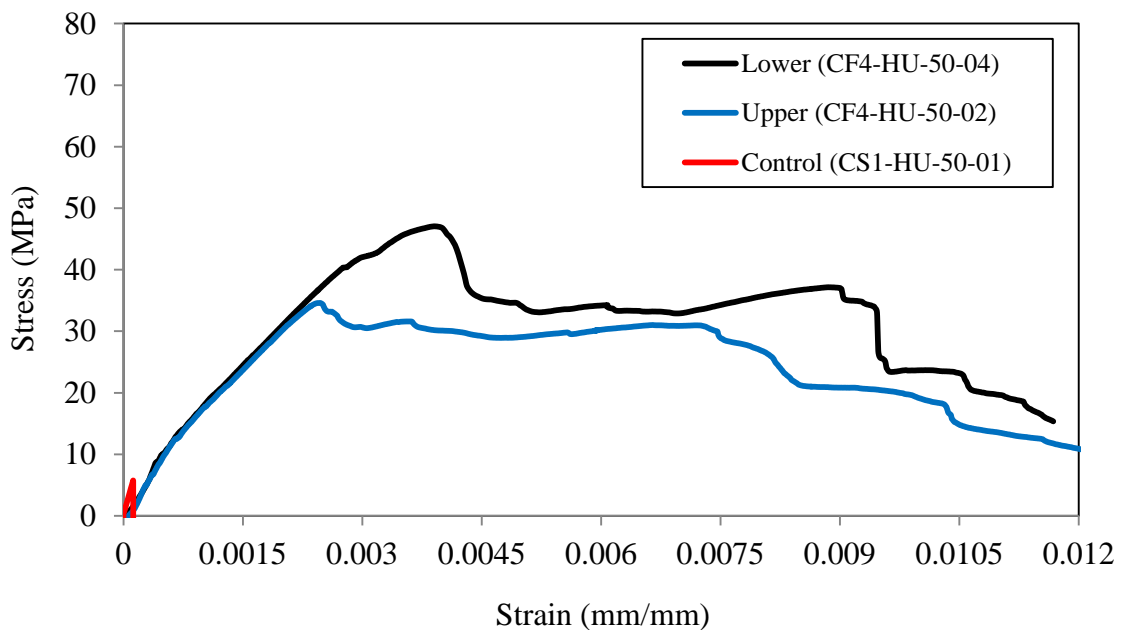


Figure 7.7: Comparison of the lower and upper bound stress-strain curves for CF4 cementitious specimens ($V_f = 5\%$) produced with hand lay-up with lower bound curve from the control specimens.

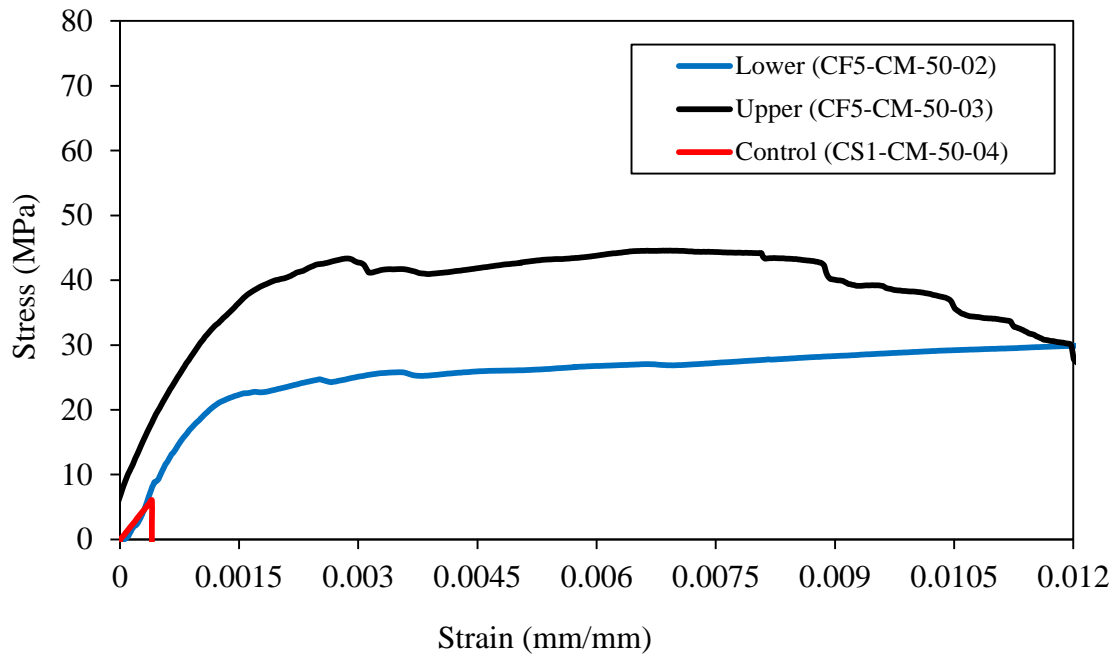


Figure 7.8: Comparison of the lower and upper bound stress-strain curves for CF5 cementitious specimens ($V_f = 5\%$) produced with compression moulding with lower bound curve from the control specimens.

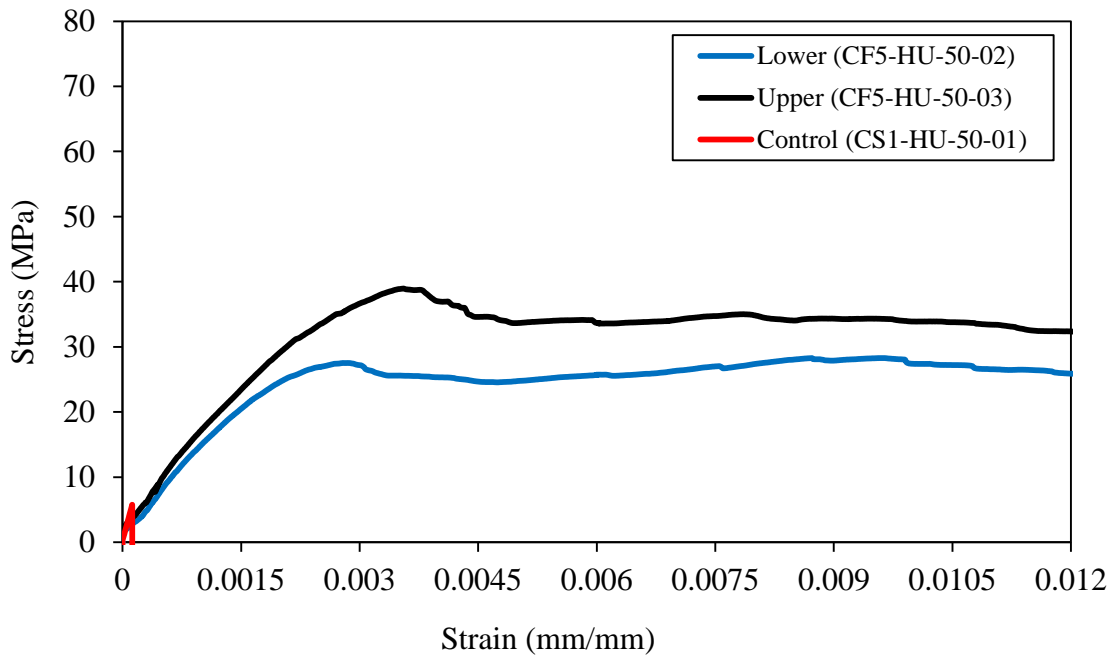


Figure 7.9: Comparison of the lower and upper bound stress-strain curves for CF5 cementitious specimens ($V_f = 5\%$) produced with hand lay-up with lower bound curve from the control specimens.

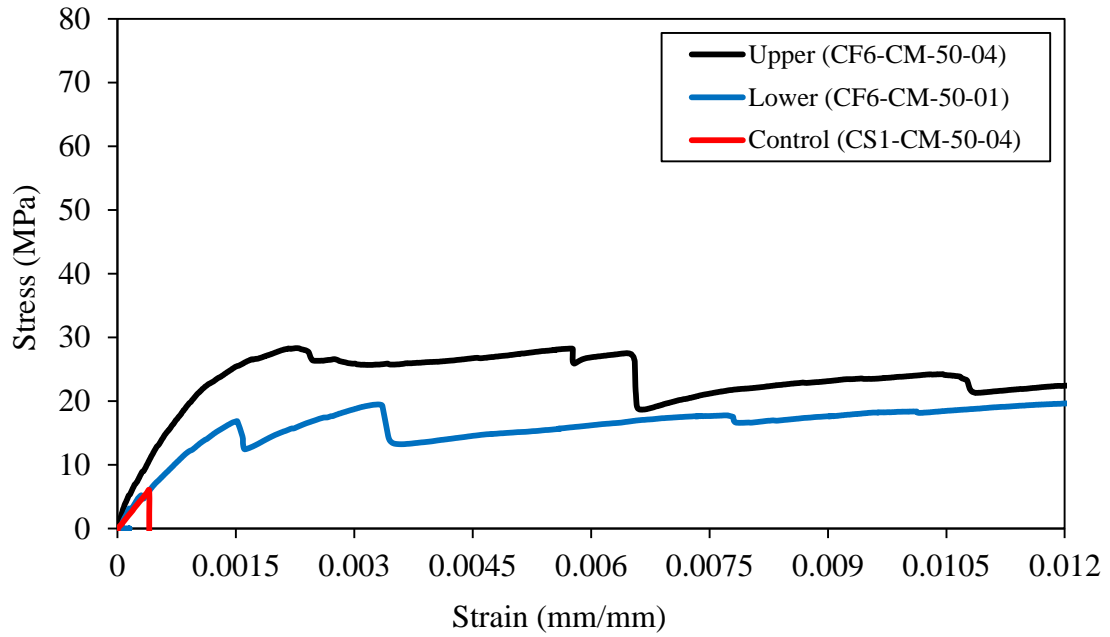


Figure 7.10: Comparison of the lower and upper bound stress-strain curves for CF6 cementitious specimens ($V_f = 5\%$) produced with compression moulding with lower bound curve from the control specimens.

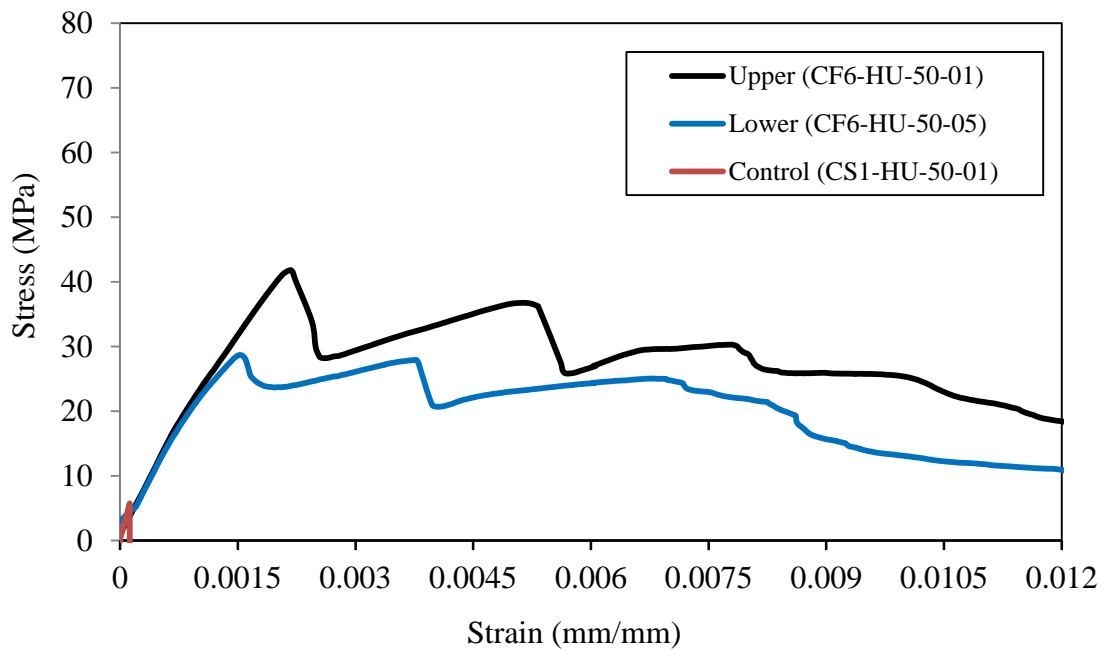


Figure 7.11: Comparison of the lower and upper bound stress-strain curves for CF6 cementitious specimens ($V_f = 5\%$) produced with hand lay-up with lower bound curve from the control specimens.

Figure 7.12 shows that a flexural specimen of CF4 (made by hand lay-up), failed with multiple delamination cracks, which will have initiated directly below a loading pin and propagated to the nearest free end. This type of failure mechanism is normally not related to the failure of slender rectilinear specimens under flexural, and is usually observed in ‘stocky’ specimens when failure is in shear. In continuous FRCs the shear mode of failure only happens when V_f is much higher than V_{crit} and the overall bond (between reinforcement and matrix) is high enough to enable the fibres to resist deformation.

As discussed in Section 2.16, the cement penetrability is a key factor in multifilament cement based composites. The bond between CFs and cement matrix is relatively low due to the hydrophobic nature of the fibre, which is opposite to the hydrophilic nature of the matrix itself, as discussed in Section 2.4.4. Because fibres have a poor chemical affinity, it can be essential to find a way to improve the bond in order to maximise the reinforcing efficiency, thereby achieving the highest FRC strength. This is particularly important when dealing with multifilament reinforcement as the penetrability of the cement between the filaments can be limited by the fabrics form, and only filaments near a bundle’s perimeter will be in direct contact with the hardened cement matrix. This physical situation will result in a relatively low fibre/matrix bond strength (τ).

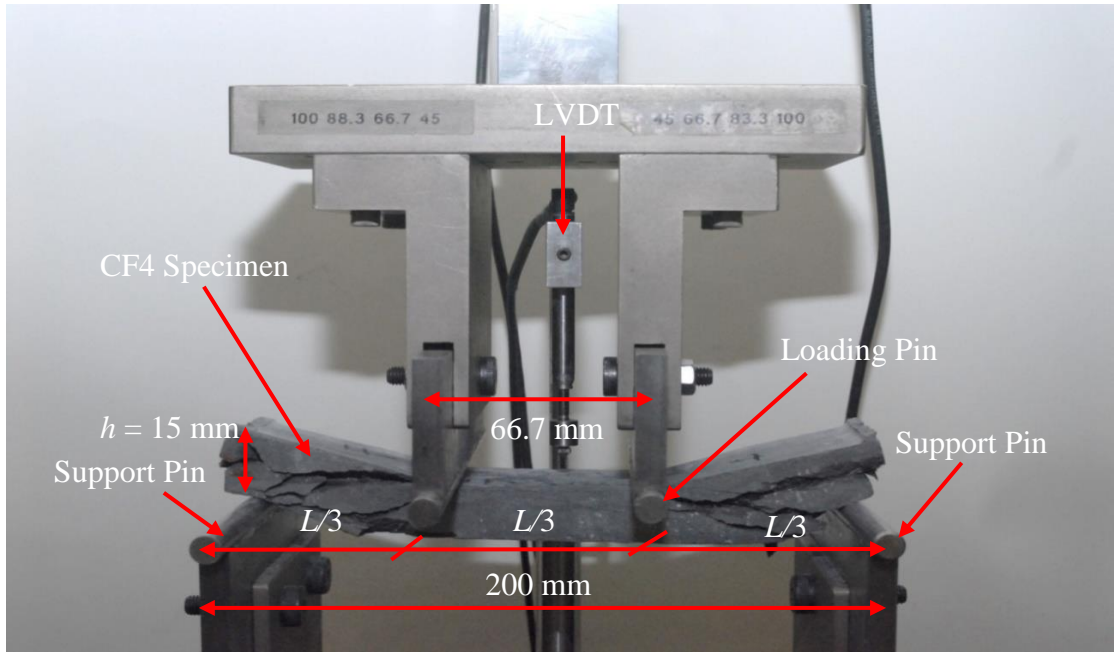


Figure 7.12: Fracture of CF4 specimen after four-point bending test.

SEM photos in Figures 7.13 to 7.15 for FRCs of fabrics CF4 to CF6 are from an investigation to examine cement penetrability. The consolidation pressure in compression moulding promotes penetration of the matrix between openings in the fabric, by squeezing the cement particles into them. This feature is observed for CF4 material in Figure 7.13.

It can be seen in Figure 7.14 that there is a low level of penetration of the matrix into the voiding between the CF5 fibres. This is due to the presence of the bulky stitches themselves, as well as the tightening effect of the stitches that forces every bundle of fibres to remain closely packed. The matrix has particle sizes that cannot enter the voiding between the ‘touching’ carbon fibres. Because the fibre architecture inherently leads to poor matrix penetration it is not possible for the full reinforcement potential to be materialised. Fabric CF5 (like all others investigated) was woven to manufacture FRP composite laminates with a polymer resin for the matrix, and this matrix material is readily able to fill the voiding.

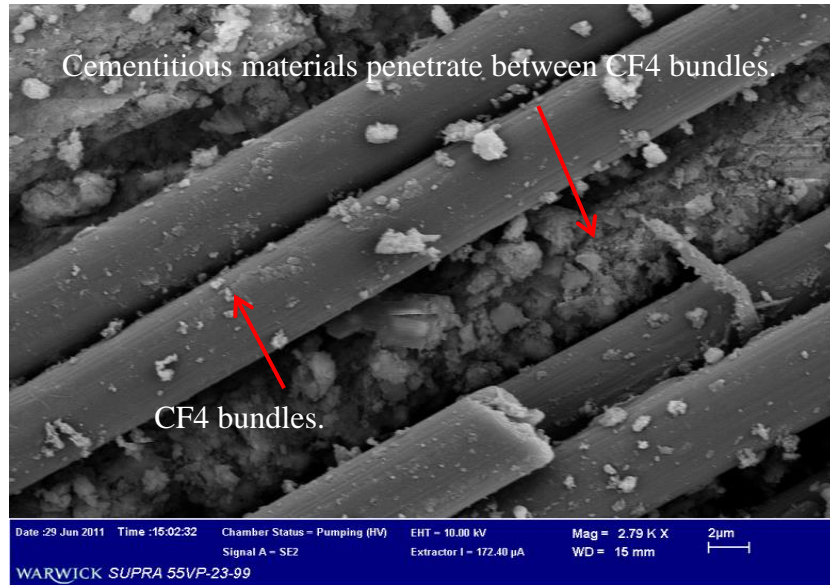


Figure 7.13: Cementitious material penetrate CF4 fabric between the openings of the bundles by compressive pressure in compression moulding process.

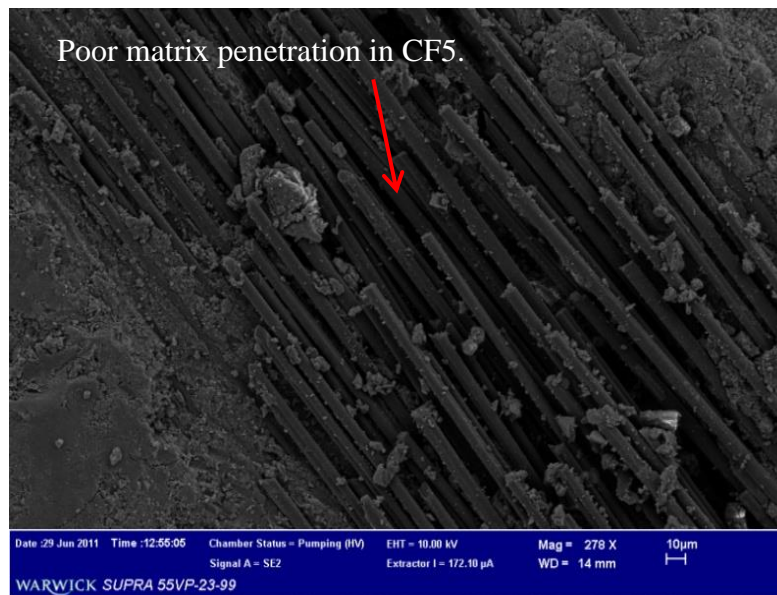


Figure 7.14: SEM image showing poor matrix penetration in CF5 (sheets form).

The CF6 material in Figure 7.15 shows the outer filaments (left side) are in direct contact with the matrix and the inner filaments (top right) are free of the hydration products. This is evidence for a poor penetration towards the centre of the tow or bundle. Another feature for why there is a weak overall bond with CF6 fabric is the voiding seen in the SEM image.

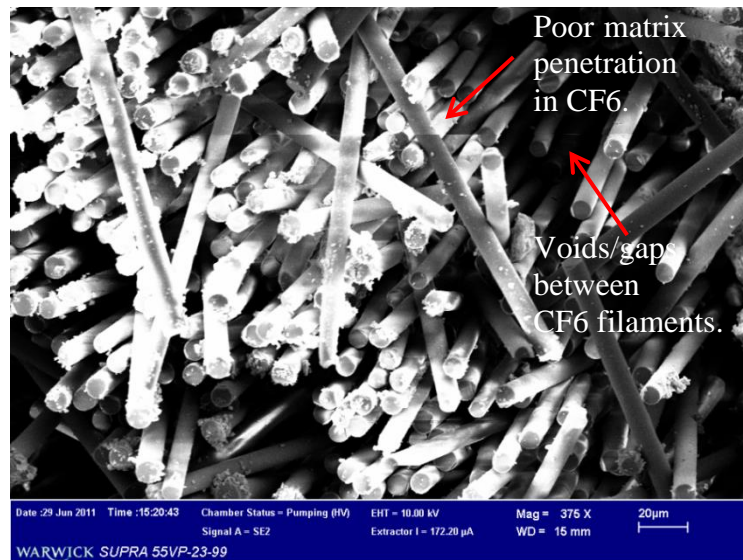


Figure 7.15: SEM image showing voiding and poor matrix penetration in CF6 fabric.

In order to achieve a higher degree of composite action and increased overall bond strength it is necessary for a surface treatment that will aid the matrix to penetrate between fibres and to create continuous regions of unreinforced matrix that bridge across layer of fabric. Previous studies by Briggs (1977), Fu *et al.* (1996), Wiberg (2003), and Bentur and Mindess (2007) reported that the treatment of fibre surfaces changes properties of the carbon filament, including wettability and chemical affinity between the hydrophobic CF and the hydrophilic cement matrix. Both of these surface changes can support an increase in the fibre and overall bond strength. For this beneficial reason the effect of a surface treatment to CF4 and CF5 fabrics will be investigated in Section 7.5.

7.3.6 Materials Reinforced With Biaxial Fabrics; CF7, CF8 and GF

We now discuss the test results of the second category for FRCs reinforced with the three biaxial fabrics. The mix design, constituent materials and mixing procedure are the same as before. As discussed in Section 7.3.2, η is estimated to be 0.5 (it is presented in Table 7.1). V_{crit} is found to be 0.6% for fabric CF8 and 1.0% for fabrics CF7 and GF (see

Table 7.2 in Section 7.3.3). From Table 7.3 V_f' for the three biaxial fabrics is 2.5%, which is at least two times greater than $V_{f_{crit}}$ (2.5% > 1.0%).

Tables B.7.15 to B.7.26 present the four-point bending test results and statistical analysis for CF7, CF8 and GF batches manufactured by compression moulding and hand lay-up. Comparing the results it is found that there is a difference in the overall mechanical behaviour between the FRC materials. Column (3) in Tables B.7.17 and B.7.21 show there to be a significant improvement in the mean peak stresses for both CF7 and CF8 FRCs produced by hand lay-up. They are higher at 112% (16.5 MPa to 35.0 MPa) and at 69% (21.2 MPa to 35.8 MPa) than those by the other processing method.

It is noted that only the GF fabric FRC gave a mean strength, by compression moulding, at 24.6 MPa that is higher than the 13.7 MPa by hand lay-up, a significant 80% difference. As discussed in Section 4.5.5 the increase can be due to the application of the consolidation pressure that can reduce the capillary porosity and then improves flexural strength. Moreover, from Appendix B Tables B.7.19 and B.7.23 the mean strain at peak stress for CF7 and CF8 materials by hand lay-up are higher by 26% (0.59% to 0.47%) and by 15% (0.47% to 0.54%) than by compression moulding. While the mean strain at peak stress for the CF7 material by compression moulding is higher by 146% (0.39% to 0.96%) than by hand lay-up. It is noted from the data given in Tables B.7.18 and B.7.22 that the mean toughness at peak stress for CF7 and CF8 materials by hand lay-up are higher by 146% (0.057 J/m³ to 0.14 J/m³) and by 90% (0.10 J/m³ to 0.19 J/m³) than by compression moulding. While the mean strain at peak stress for GF material by compression moulding is higher by 241% (0.041% to 0.14%) than by hand lay-up.

By comparing the FRC results listed in Tables B.7.15 to B.7.26 with the control materials in Appendix B Tables B.7.1 and B.7.2 there is a measureable improvement in

overall properties using fabrics CF7, CF8 and GF at 2.5% V_f . Column (3) in the tables show that the mean peak stress with CF7 and CF8 materials is higher by 367% (7.5 MPa to 35 MPa). Similarly, from Table B.7.23 the GF material is seen to be 228% higher (7.5 MPa to 24.6 MPa) than control materials. Compared to the control batch the mean strain at peak is found to be 17 times higher for CF7 (0.034% to 0.59%), 14 for CF8 (0.034% to 0.47%) and 28 for GF (0.034% vs 0.96%). It is noted that the mean toughness at peak stress for the CF7 and GF FRCs are the same, and the value is 140 times that determined for the control (0.001 J/m³ to 0.14 J/m³). It is seen from Table B.7.22 that this property with CF8 fabric has increased by an enormous factor of 190 times (0.001 J/m³ to 0.19 J/m³).

In the usual way, Figures 7.16 to 7.21 present plots for the lower and upper bounds for FRCs with fabrics CF7, CF8 and GF and for the equivalent lower bound control materials. It is seen that the FRC curves exhibit the desirable strain-hardening behaviour. This response to flexure leads to a high failure strain capacity without brittle failure. All curves start with a Region I and show a linearly elasticity response up to the first cracking stress (σ_{mu} for LOP), as defined by line OA in Figure 7.17. The loss of linearity happens at a stress in the range 2 to 15 MPa, which is 16% to 34% of the peak stress. Once tensile cracks are initiated in the matrix the shape of the curves deviates to become non-linear, and it is seen stress increases up to the peak stress (σ_{cu}), which is labelled as point B in Figure 7.17. The presence of post-cracking strength shows that stress is being transferred by fibre bridging across the vertical cracking. For these FRCs the peak stresses are determined to be in the range 12.8 to 43.5 MPa (see Tables B.7.3 to B.7.18). Beyond the peak, the stress being resisted first drops some 10% to 20%, before continuing to decrease gradually, until ultimate failure occurs.

The shape of stress-strain curves in the six figures is seen to be similar to that labelled (d) in Figure 2.3(d) of Section 2.10. This form of curve commonly occurs when $V_f \geq V_{\text{crit}}$. Thus, the onset of matrix cracking is not catastrophic, and the FRC sustains additional deformations as the reinforcement can imbue some post-cracking capacity. The six plots show for these FRCs significant increase in the strains and toughness at peak stresses when compared to their control material. This positive outcome means that these fabric types in an FRC possess the ability to absorb energy. In the ACK model there are four distinct regions to a stress-strain curve. Labelled in Figure 7.17 is the pre-cracking Region I, with post-cracking Regions II/III overlapping and failure Region IV is distinctive too. It is observed that fabrics impart the FRC with a post-cracking strength. It is believed this could, in part, be due to an increase in friction between the fibres and matrix from improved cement penetration.

An earlier discussion in Section 2.16 explains why the value of (overall) bond strength controls the failure mechanism. Fractured fibres were observed in biaxial specimens produced by both hand lay-up and compression moulding. This observation means that the composite cracking strength (σ_{cu}) must be significantly higher than the strength of matrix (σ_{mu}). This finding can be associated with $V_f > V_{\text{crit}}$ and the continuous fibre length. It might be due to good matrix penetration. For this reason the microstructure of the biaxial fabrics was investigated by SEM. The preparation of specimens and the SEM technique are discussed in Section 3.4.

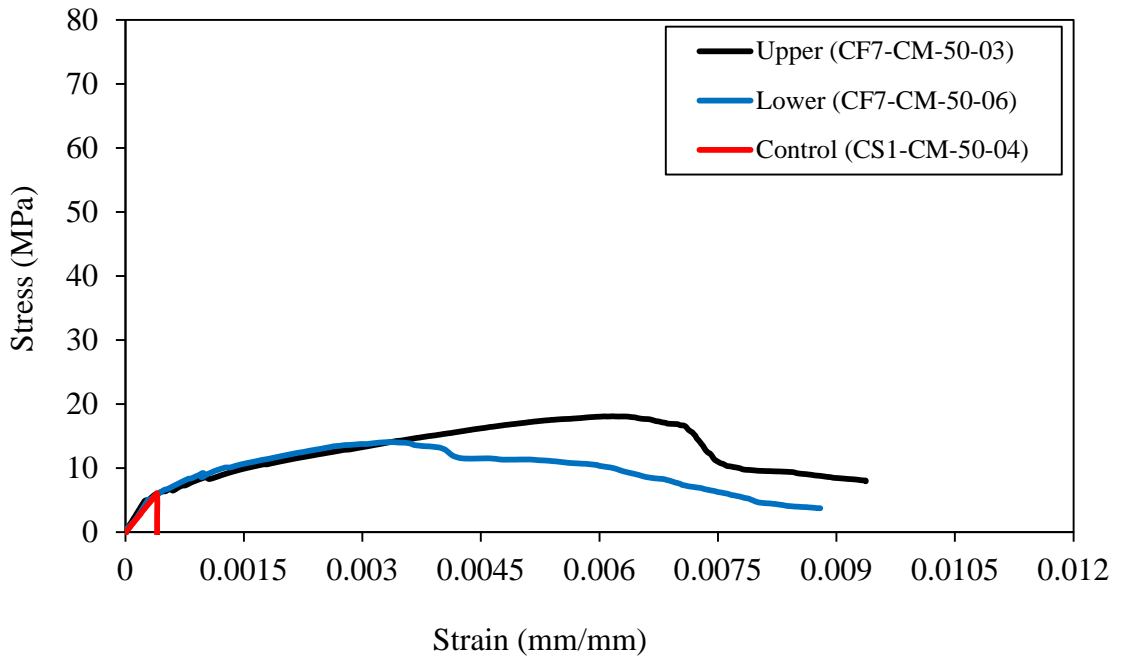


Figure 7.16: Comparison of the lower and upper bound stress-strain curves for CF7 cementitious specimens ($V_f = 5\%$) produced with compression moulding with lower bound curve from the control specimens.

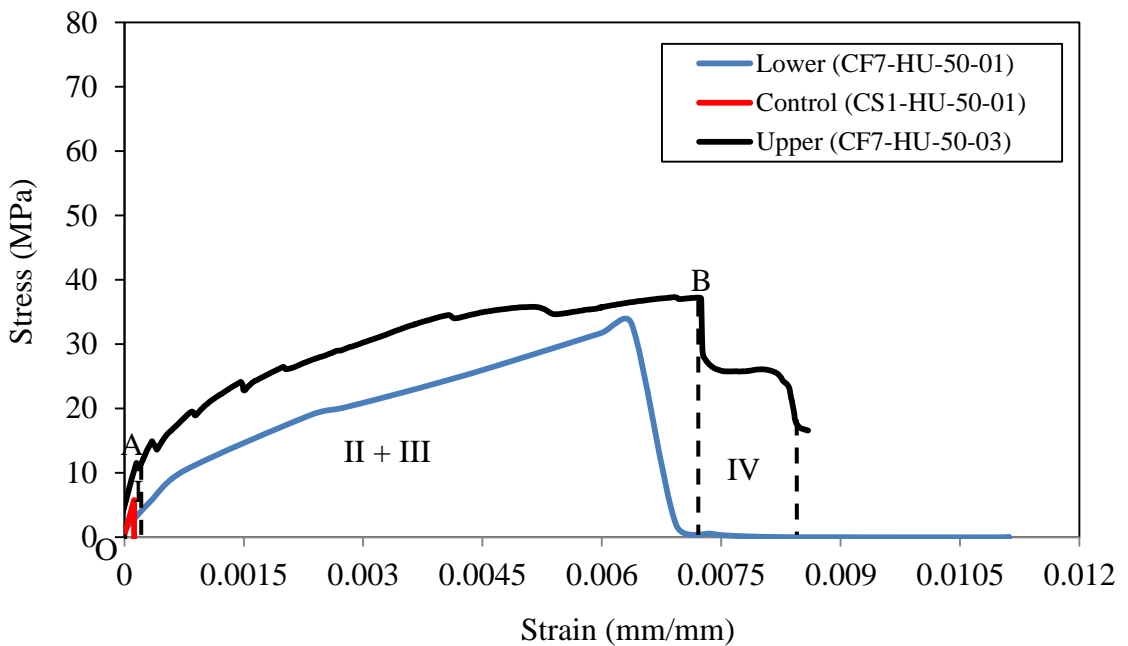


Figure 7.17: Comparison of the lower and upper bound stress-strain curves for CF7 cementitious specimens ($V_f = 5\%$) produced with hand lay-up with lower bound curve from the control specimens.

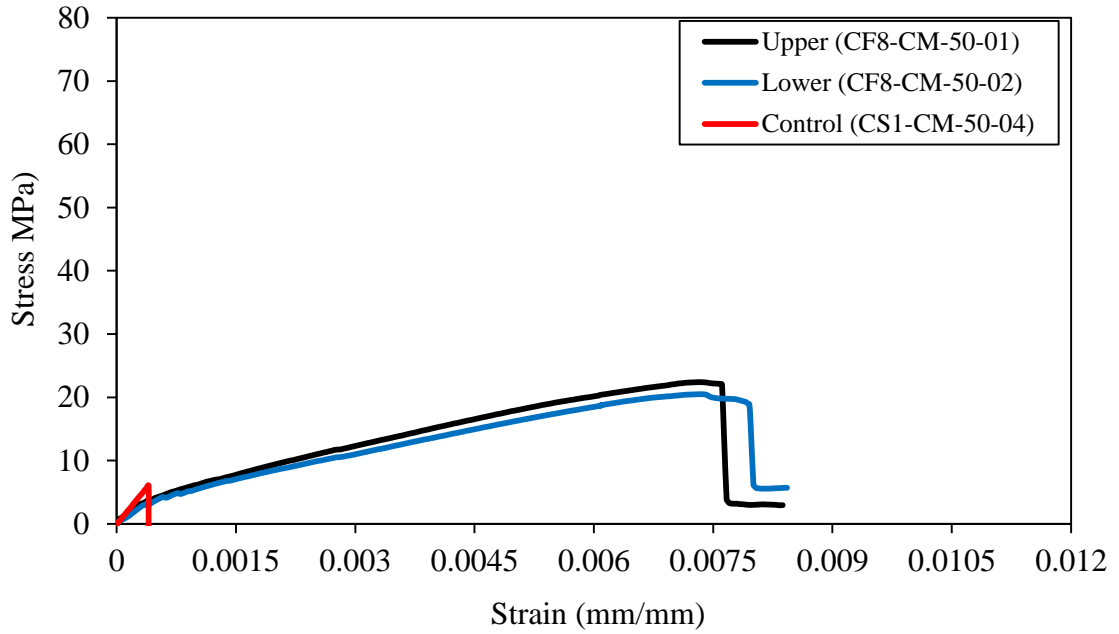


Figure 7.18: Comparison of the lower and upper bound stress-strain curves for CF8 cementitious specimens ($V_f = 5\%$) produced with compression moulding with lower bound curve from the control specimens.

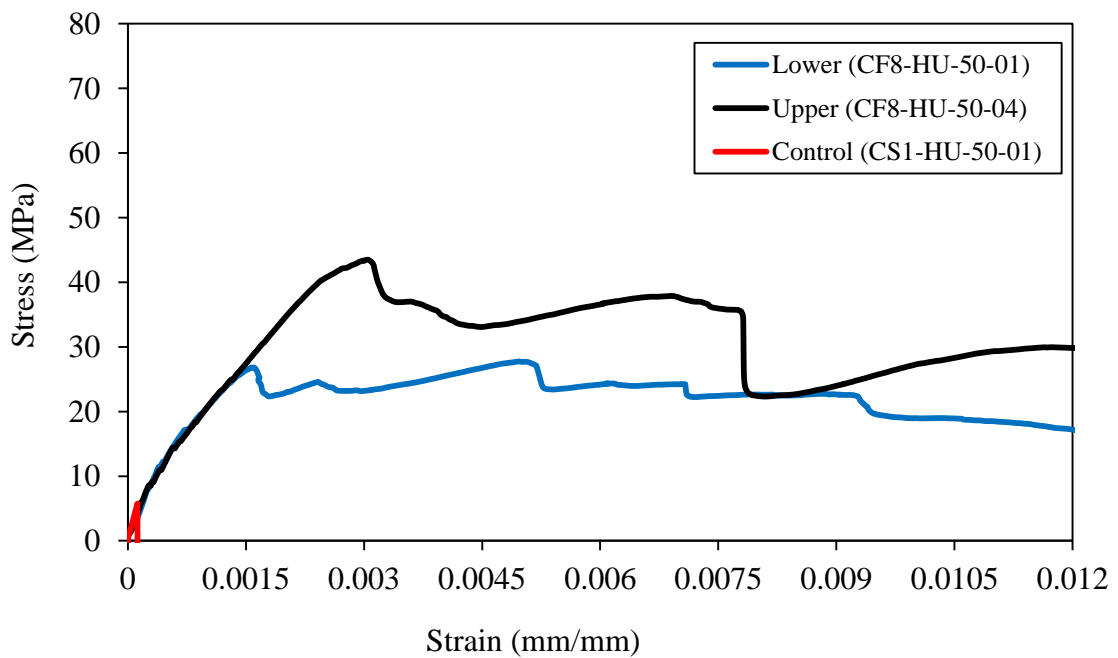
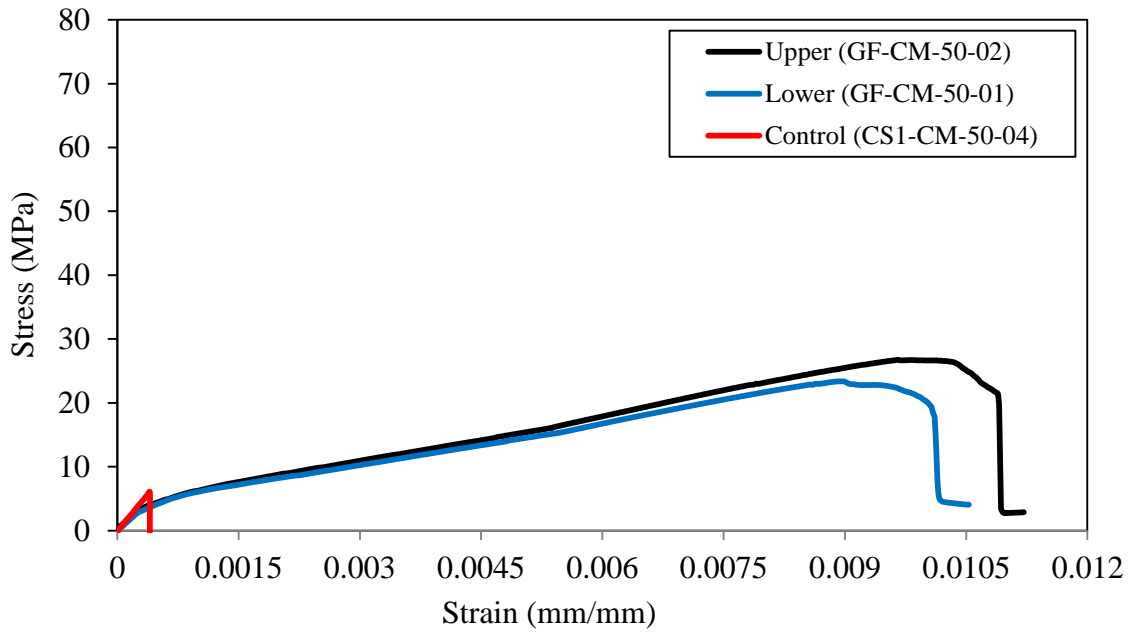
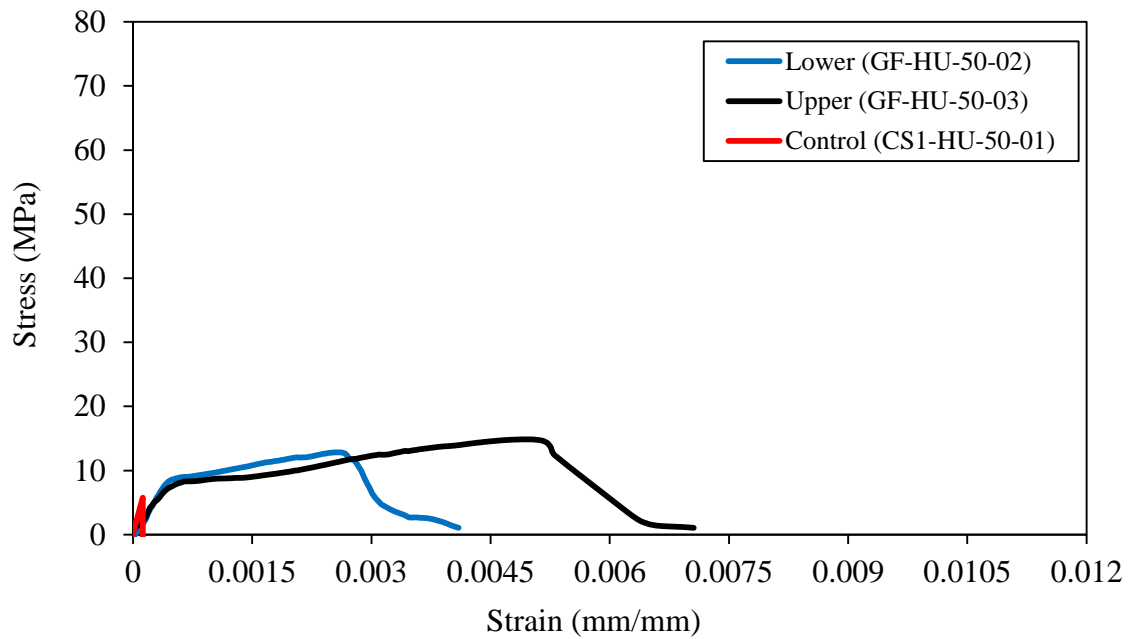


Figure 7.19: Comparison of the lower and upper bound stress-strain curves for CF8 cementitious specimens ($V_f = 5\%$) produced with hand lay-up with lower bound curve from the control specimens.



Figures 7.20: Comparison of the lower and upper bound stress-strain curves for GF cementitious specimens ($V_f = 5\%$) produced with compression moulding with lower bound curve from the control specimens.



Figures 7.21: Comparison of the lower and upper bound stress-strain curves for GF cementitious specimens ($V_f = 5\%$) produced with hand lay-up with lower bound curve from the control specimens.

Figures 7.22(a) to 7.22(c) are for three SEM images of the CF7 material. It can be seen in Figure 7.22(a), that there are indications of very good matrix penetration between

fibres; even the filaments at the centre of the tow are covered with cement hydrates. Figure 7.22(b) shows the voiding between two neighbouring filaments is filled with 9 to 11 micron sized hydration products as shown by yellow arrow. With the CF7 reinforcement large quantities of the matrix coating the fibres is observed. Figure 7.22(c) is included to show evidence for fibre rupture that occurs at ultimate failure.

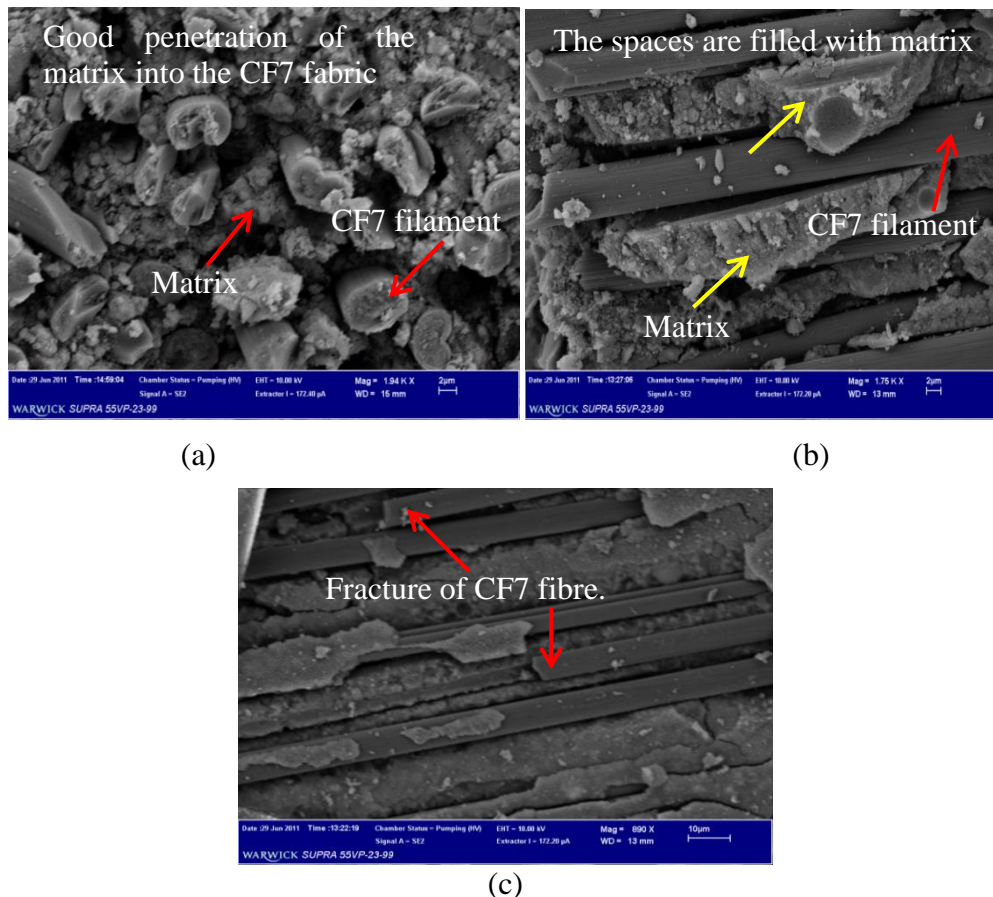


Figure 7.22: SEM Photo for CF7 material was made by compression moulding; (a) good penetration of the matrix into the fibre tow, (b) opening spaces between the two filaments neighbours are filled with cementitious materials, (c) evidence of fracture fibre failures.

For CF8 material Figure 7.23(a) shows the interface between fibres and matrix is intimate as shown by red arrows. The close-up in Figure 7.23(b) shows the outer filaments (left side and bottom) are in direct contact with the matrix, whereas the inner filaments (right side and top) are free of hydration products. Matrix penetration to the centre of the tow is seen to be poor. Zooming-in the image in Figure 7.23(c) shows that filaments of

CF8 can be covered with binder material. The SEM picture also shows there is voiding in the bottom left of the field of view. The SEM investigation shows that for CF8 the outer filaments in a bundle are in contact with the cement matrix and will be well bonded, whereas internal filaments will have low bonded because of the absence of the matrix there. This leads to a telescopic type of failures mode, where outer filaments can fracture and the inner filaments simply pulled-out. These are features for why overall there is a weak bond between the CF8 fibres, fabric and matrix. It was discussed in Section 2.16 that the independent researchers of Majumdar (1974), Fu *et al.* (1996), Purnell *et al.* (2000), Bentur and Mindess (2007), and Purnell (2010) reported that bond strength can change significantly as the matrix ages and hydration continues, leading to the contact area growing.

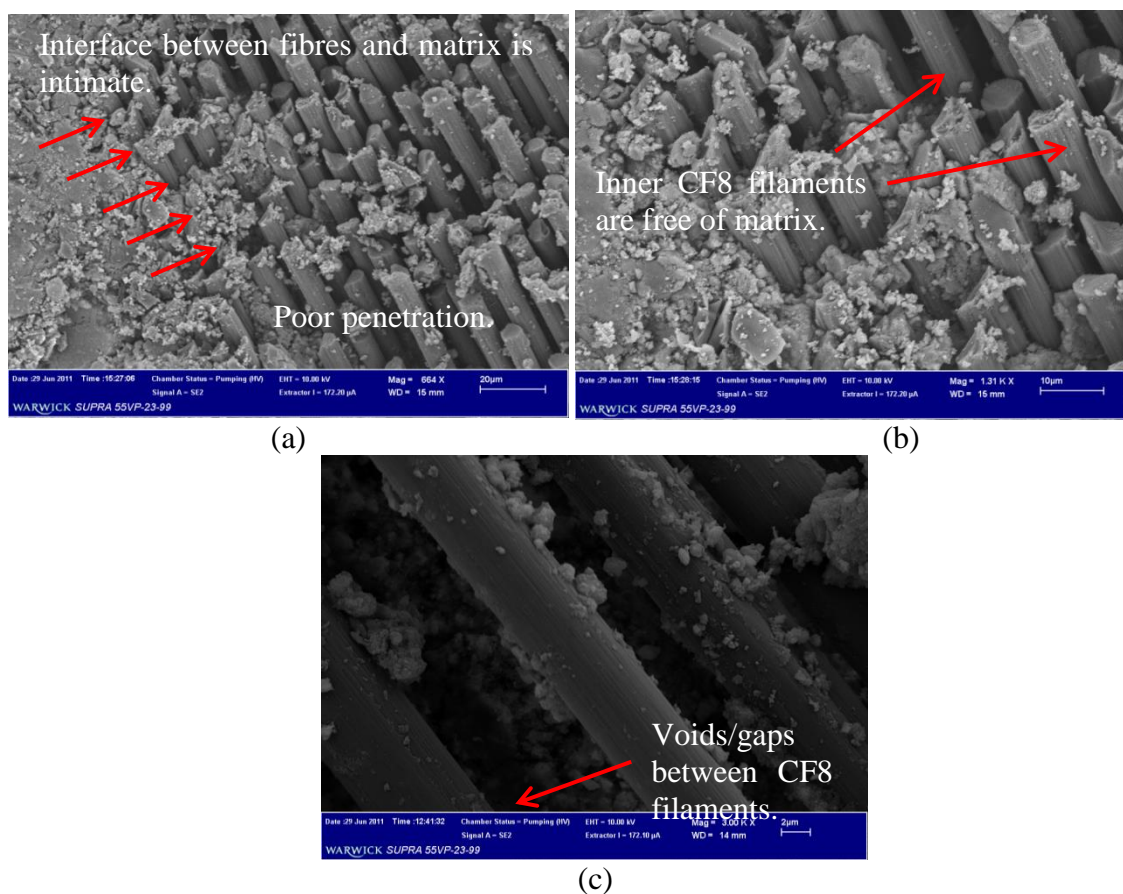


Figure 7.23: SEM Photo for CF8 material was made by compression moulding; (a) interface between fibres and matrix is intimate, (b) poor penetration of the matrix into the fibre tow, (c) evidence of voiding and few filaments are covered with binder materials.

On the other hand, GF fabric (with coated yarns) has limited potential for mortar penetration, and so an overall bond for composite action is mainly developed between the bundle perimeter and the matrix. The fabric was treated by the supplier with a proprietary mineral filled organic binder system that effectively glued the filaments together and filled voiding between them, as shown in Figure 3.2(g). Only a bundle's perimeter can therefore be in direct contact with the matrix. Matrix penetration will exist within the open holes in the fabric's construction. This beneficial feature of the GF fabric (with its 2 x 2 mm grillage) can be seen in Figure 7.24. As a consequence of the pre-treatment the material consolidation offered by compression moulding is made redundant. This weakness is associated with a poor fibre-matrix bond. If this part of the overall bond strength is to be enhanced a surface treatment is needed to remove the sizing for matrix penetration to be developed within GF bundles.

Generally, as seen from the stress-strain curves in Figures 7.16 to 7.21 (results reported in Tables B.7.15 to B.7.26) a 2.5% V_f in the loading direction does produce an FRC that has higher flexural strength, strain and toughness at peak stress compared to the control materials (see Figures 7.4 and 7.5), for the same reasons developed in Sub-section 7.3.5

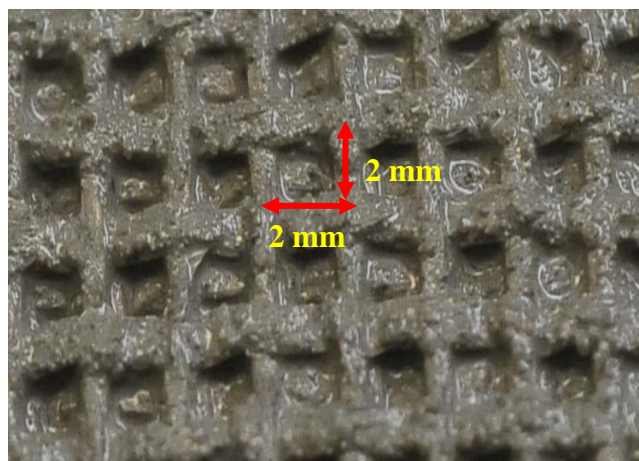


Figure 7.24: Cementitious material cannot penetrate the GF filaments due to sizing.

All six FRCs with biaxial fabrics gave the strain-hardening behaviour with multiple cracks formed along the length of the constant moment zone for four-point bending. In other words, once the matrix cracks, the fibres/fabric are/is bonded sufficiently to carry additional flexural deformation. Thus, we find that initiation of matrix cracking is not catastrophic, and the FRC specimen sustains more load and deformation; there is a post-cracking capability (see Section 2.10). The results show the influence of fibre bridging is effective for ACK model Regions II and III. One possible explanation for what creates the overall bond strength with biaxial fabrics is the benefit from the orthogonal yarns in the warp (0°), and weft directions (90°). The fabric's construction has openings (holes) between the bundles which matrix can readily fill as shown in Figures 3.2(d), 3.2(e) and 3.2(g). When cured there will be volumes of continuous matrix across fabric layers that provide mechanical interlocking with the fibre reinforcement.

Based on the above discussion it is concluded that proper penetration of the cement matrix between filaments is desirable in order to maximise the reinforcing efficiency of the fabrics and to maximum the overall bond strength.

7.3.7 Materials Reinforced With Multi-axial Fabric, CF9

Reported next are results for the third category for FRC materials that is reinforced with a multi-axial fabric having fibre orientations of 0° , 90° and $\pm 45^\circ$. The mix design, constituent materials and mixing procedure are as previous. η for the CF9 FRC has been estimated to be 0.38 (see Table 7.1). V_{crit} is predicted to be 0.6% (see Table 7.2) and V_f' is 1.9% (see Table 7.3), this fibre volume fraction is three times V_{crit} (i.e. $1.9\% > 0.6\%$). In the FRC material 38% of the V_f of 5% is aligned with the loading direction. Tables B.7.27 to B.7.30 present the flexural test results and statistical analysis as for the previous fabrics studied. Figures 7.25 and 7.26 are for the usual stress-strain curves. It is found that there is

a slight difference in the overall mechanical behaviour of the CF9 batches produced by hand lay-up and compression moulding. Column (3) in Tables B.7.27 and B.7.29 show that the mean peak stress by compression moulding and hand lay-up, at 44.9 and 47.8 MPa, possess a 6% difference, which is not significant. There is however a considerable difference in the mean maximum strain at peak stress and mean toughness at peak stress with hand lay-up higher by 88% (0.40% to 0.75%) and by 77% (0.13 J/m³ to 0.23 J/m³), respectively.

By comparing the results in Tables B.7.27 to B.7.30 with the control materials properties in Tables B.7.1 and B.7.2 it can be seen that there is a significant improvement in properties. Column (3) in Table B.7.29 shows that the mean peak stress for the FRC has increased by factor of 6 times (7.5 MPa to 47.8 MPa). Similarly, the mean strain and toughness at peak stress is found to be higher by 22 times (0.034% to 0.75%) and by 230 times (0.001 J/m³ vs 0.23 J/m³).

The curves in Figures 7.25 and 7.26 exhibit strain-hardening behaviour for a high failure strain capacity. The shape of these stress-strain curves is seen to match the shape of the curves in Figures 7.17 and 7.19 for CF7 and CF8 FRCs (see Section 7.3.6), and they are similar to shape (d) in Figure 2.3(d) of Section 2.10. This form of curve commonly occurs when $V_f \geq V_{f,crit}$. From the ACK model the pre-cracking Region I, with Regions II/III overlapping and failure Region IV are illustrated in Figure 7.25.

CF9 comprised of four unidirectional fibre layers, one in each direction of 0°, 90°, -45°, and +45° (see Section 3.2.4). For this reason, the efficiency factor (η) of CF9 fabric is less than with unidirectional fabrics ($0.38 < 1.0$) as presented in Table 7.1. As discussed in Section 7.3.2 this is because only 38% of the fibre reinforcement is fully effective, whereas it is 50 to 100% for biaxial and unidirectional, respectively. It is not only the η affecting on

the overall mechanical properties of FRC composites. However, the bond strength is one of the main parameters controlling mechanical properties (see Section 2.16). As has been discussed the results plotted in Figures 7.25 and 7.26 show a significant increase in the flexural strength for the CF9 FRCs produced either by hand lay-up or compression moulding process. This positive finding means that these fabric types possess the ability to absorb energy. The reasons for this are the same as given previously for the unidirectional and biaxial fabrics in the Chapter 7 investigation. Furthermore, the best measured mean strength with CF9 fabric can be attributed to the good interfacial bond strength from good matrix penetration into the CF9 fibres and across the fabric. Because the cement penetration for higher overall bond take place only if the tows and fibres in a fabric are sufficiently open to allow for the penetration (see Section 2.16). The CF9 fabric has an important advantage over the other fabrics which is useful for FRCs. This particular fabric has 7 mm sized holes which are bigger than the 2 to 5 mm sized holes with fabrics GF, CF7 and CF8 (see Figure 3.2). These holes between their tows within the CF9 fabric provide for better cement penetrability, this could enhance interface strength (τ), by providing mechanical anchorage to improved bond strength, hence increasing the FRC's mechanical properties such as flexural strength (See Section 7.4.3).

The microstructure of the CF9 material is investigated by SEM and Figure 7.27(a) shows it has holes of ≈ 7 mm (in all direction) in its fabric construction. The SEM image in Figure 7.27(b) shows that there is matrix completely covering individual CF9 fibres. It can be expected that this level of matrix cover will aid in the overall bond strength of the FRC with CF9 reinforcement.

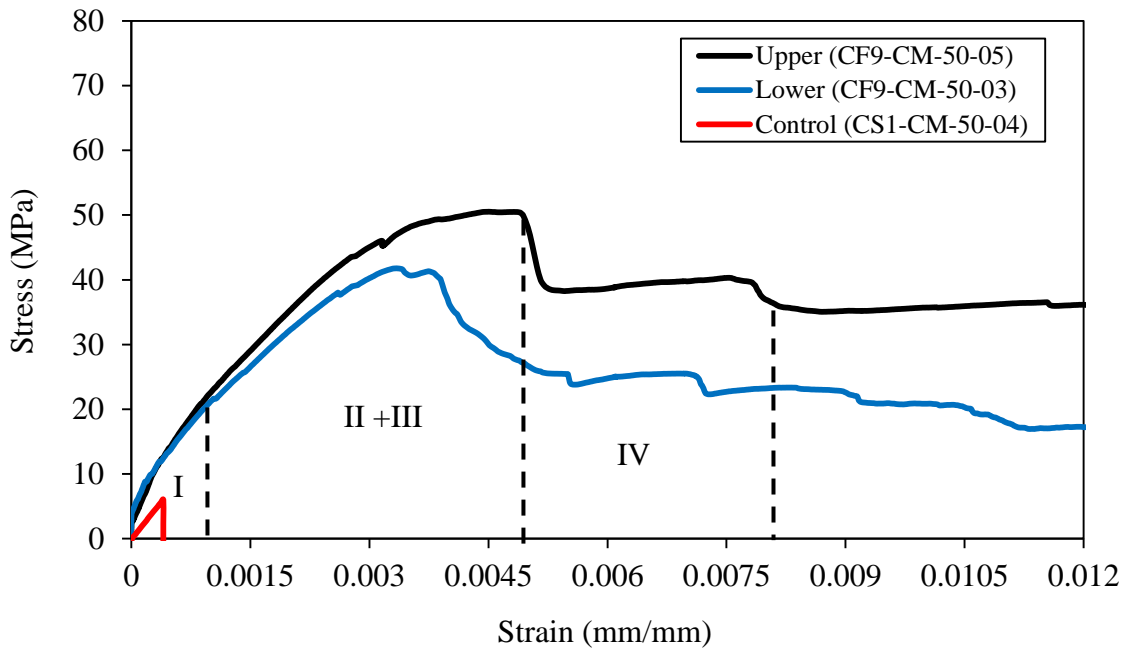


Figure 7.25: Comparison of the lower and upper bound stress-strain curves for CF9 cementitious specimens ($V_f = 5\%$) produced with compression moulding with lower bound curve from the control specimens.

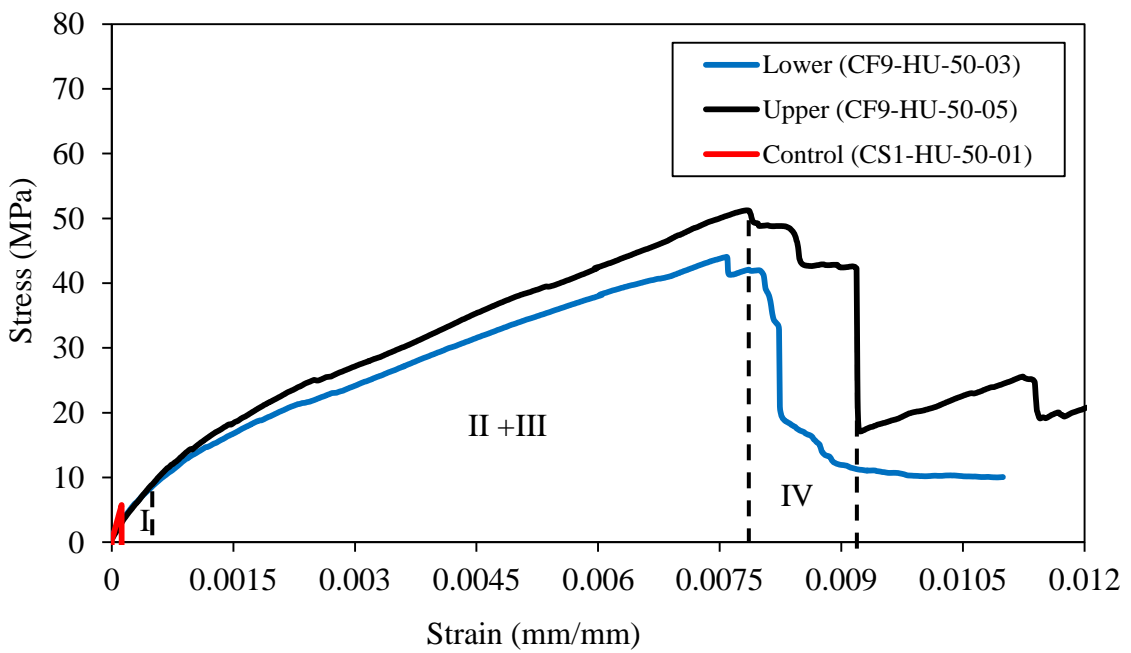
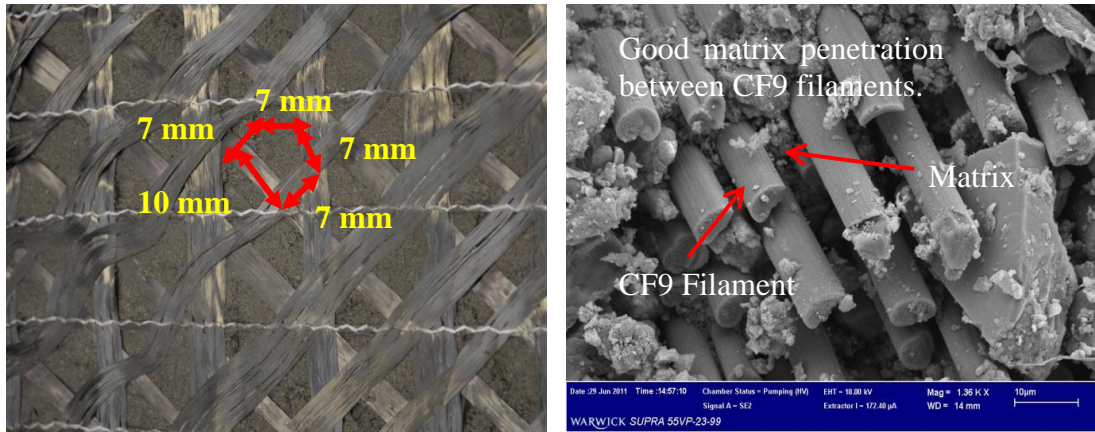


Figure 7.26: Comparison of the lower and upper bound stress-strain curves for CF9 cementitious specimens ($V_f = 5\%$) produced with hand lay-up with lower bound curve from the control specimens.



(a)

(b)

Figure 7.27: CF9 material was made by compression moulding; (a) spaces in all direction between the carbon tows. (b) cement matrix is seen to penetrate between the individual CF9 fibres.

7.4 Summary of Mechanical Test Results With Continuous Fibres

Cement penetrability is a key factor since it directly influences the mechanical properties by controlling how effective is the interfacial bond strength. A comparison of the four-point bending test results, effect of the manufacturing process and fabric type on the mechanical properties of the FRCs reinforced with seven fabrics is given in Sub-sections 7.4.1 to 7.4.3.

7.4.1 Mechanical Properties

From Sub-sections 7.3.5 to 7.3.7 it is found that the mean LOP is 2 to 15 MPa with fabrics CF7, CF8, CF9 and GF by hand lay-up and compression moulding processes. These low values are similar to the control materials at 6 and 9 MPa, respectively. For fabrics CF4, CF5 and CF6 it is seen that LOP is much higher at 20 to 45 MPa. As discussed in Sub-section 7.3.5, this increase is due to the presence of ‘unusual’ composite action (i.e. the material exhibits behaviour same as shape (f) in Figure 3.2(f)) for the reasons developed. Because $\eta = 0.5$ with the biaxial reinforcements of CF7, CF8 and GF we know that 50% of the filaments are aligned perpendicular to the deformation. Similarly

with the multi-axial fabric CF9 $\eta = 0.38$ only 38% of the filaments are effective in the loading direction.

Figures 7.28 to 7.30 are bar charts collating test results for, respectively, the means of flexural strength, of strain at peak stress and of toughness at peak stress. For each material the two processing methods are given side-by-side, with hand lay-up on the left-side. This presentation shows that the seven FRCs have significantly higher strength, strains and toughness than their equivalent control materials. For hand lay-up, Figure 7.28 shows that CF9 gave the highest mean flexural strength of 47.8 MPa, which is 555% (7.3 MPa), 11% (42.9 MPa), 41% (34.0 MPa), 33% (36.0 MPa), 37% (35.0 MPa), 34% (35.8 MPa) and 249% (13.7 MPa) higher from the other materials, going from left to right across the chart. This best measured mean strength can be attributed to the good interfacial bond strength from good matrix penetration into the CF9 fibres and across the fabric, as can be observed in Figure 7.27.

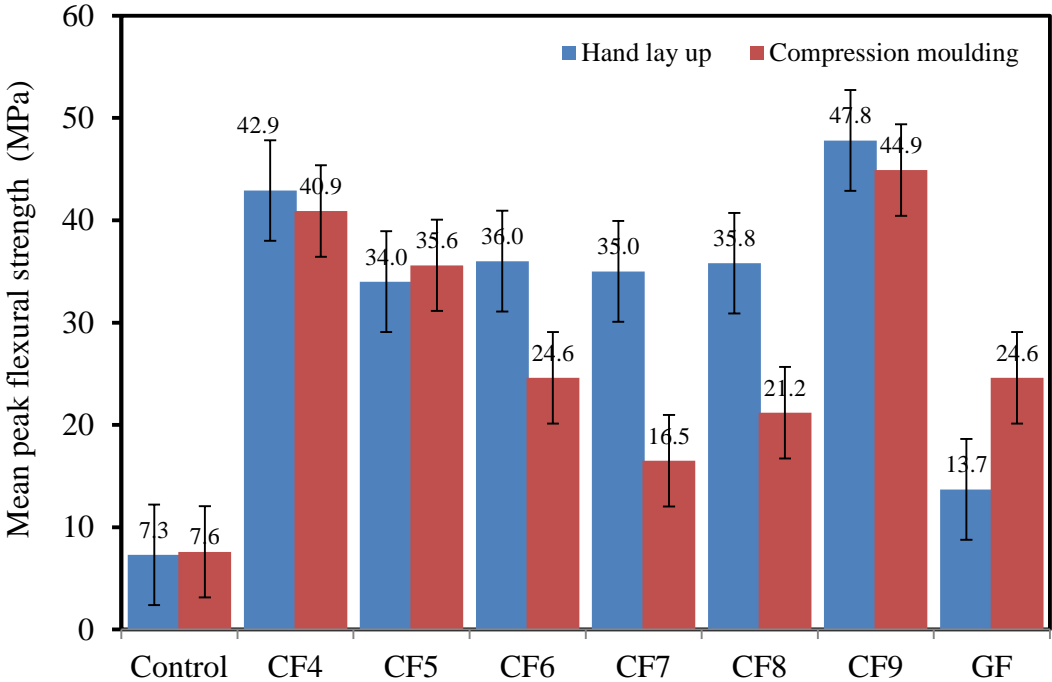


Figure 7.28: Mean peak flexural strengths for control and continuous fibres materials.

From Figure 7.29 the highest mean strain at peak strain is 0.96% with glass fabric and compression moulding. This batch mean is higher by 134% (0.41%), 96% (0.49%), 37% (0.70%), 104% (0.47%), 104% (0.47%) and 140% (0.40%) than the other seven materials going from right to left across the chart. It is increased by the factor of 17 times (0.056%) over the control material. Using hand lay-up it is CF9 fabric that achieves the highest mean strain at 0.75%. This is seen to be 114% (0.35%), 54% (0.37%), 142% (0.31%), 27% (0.59%), 39% (0.54%) and 92% (0.39%) higher than for the other FRCs. The increased against the control material is a factor of 63 times (0.012%).

Figure 7.30 shows that the mean toughness at peak stress by hand lay-up is highest at 0.23 J/m^3 for CF9 by a factor of 3 times (0.092 J/m^3), 1.6 (0.14 J/m^3), 3 (0.074 J/m^3), 1.6 (0.14 J/m^3), 1.2 (0.19 J/m^3), and 6 (0.041 J/m^3) higher than the other FRCs. The increase is an enormous 575 times (0.0004 J/m^3) over the control. For compression moulding the results presented in Figure 7.30 show that the CF5 batch gave at 0.15 J/m^3 the highest toughness.

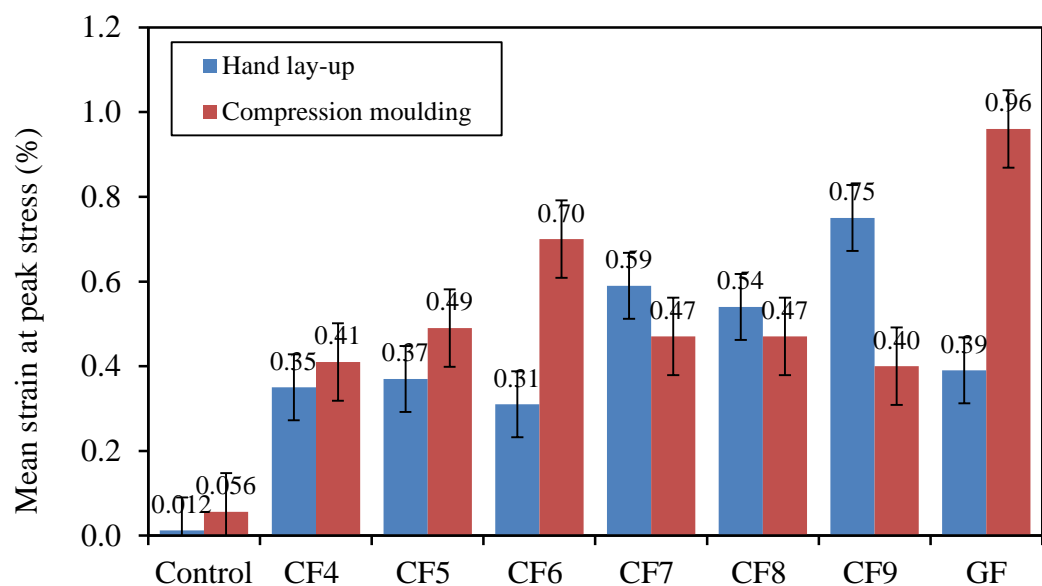


Figure 7.29: Mean strain at peak stress for control and continuous fibres materials.

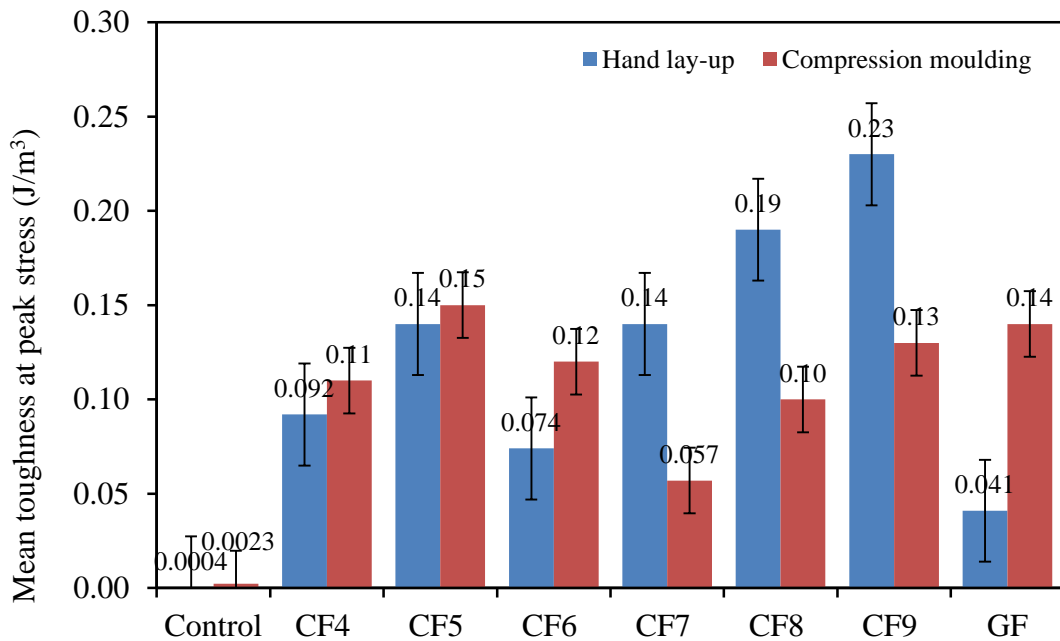


Figure 7.30: Mean toughness at peak stress for control and continuous fibres materials.

The lower mechanical properties are the consequence of an overall lower bond, leading to relatively poor composite response (Peled, 2009). To achieve the best structural performance the research has shown that there is the need to produce effective composite action that can uniformly transfer forces between the matrix and fibres, especially for stresses above LOP when the FRC is deformed in the post-cracking region.

7.4.2 Effect of Manufacturing Process on Mechanical Properties

The results obtained (Figure 7.28) in this study indicate that the CF7 fabric was most affected by the two processing methods. Of the seven fibre types, those with CF7, GF, CF8, and CF6 reinforcement gave, at 112%, 80%, 69%, and 46% respectively, a significant change in the mean flexural strength between the hand lay-up and compression moulding processes. On the assumption introduced in Section 6.3.1 that a 15% is not significant the two processing methods are equivalent for the other three reinforcement types (CF4 (5%), CF5 (5%), and CF9 (6%)).

By comparing the processing results in Figure 7.28 it is seen that five of the seven hand lay-up FRCs gave mean flexural strengths higher than by compression moulding. The two FRCs that did not are CF5 (35.6 MPa and 24.6 MPa) and GF (34.0 MPa and 13.7 MPa). One change to the cementitious mix on applying compression moulding is a change in the water/binder (w/b) ratio. From column (2) in Appendix B Tables B.7.3 to B.7.47 the mean differences from the original ratio of 0.35 is fairly constant at 30%. For the hand lay-up method of preparing flexural specimens the w/b ratio does not change, and it was 0.35.

The processing method of compression moulding is novel, except for a few FRC specimens produced in a study by Farahi (2009). This work is introduced in Sub-section 2.6.8. Farahi reported that the method was unsuccessful because Farahi's FRCs, reinforced with a fabric, severely delaminated, with cracks developing in the direction of the fibres. For this reason it is not feasible to compare the new results from the author with those reported by Farahi (2009). By suitably modifying the mix design the author has been able to overcome the processing issues in Farahi's work. As a result green processing with both short and continuous FRCs has been shown to be successful using the compression moulding process.

It is to be expected that compression moulding will improve matrix penetrability by squeezing the cement particles into a fabric. This should lead to improved fibre/matrix bonding and better stress transfer that can maximise the reinforcement efficiency. Consolidation aids the development of higher frictional forces between constituents that generates a high overall (material) strength. Based on the results in Sections 7.3.5 to 7.3.7 it can be concluded that either the hand lay-up or compression moulding process can be employed to produce a FRC, having continuous fibres with V_f' from 1.9 to 5%, exhibiting beneficial strain-hardening behaviour. However, it can be concluded that the benefit of

matrix consolidation by compression moulding over hand lay-up has not been found to significantly increase the mean mechanical properties.

Figure 7.31 reports the excess water in the processed materials after compression moulding. The original w/b of 0.35 is reduced after pressing to 0.21 (with 40% of excess water for the control materials) to 0.27 (with 24% of excess water for CF9). As discussed in Section 4.5, the reason for applying compression moulding was to minimise porosity by increasing the degree of consolidation and reducing the water/cement (w/c) ratio, thereby eliminating the problem of low workability. For the hand lay-up method of preparing specimens the w/b ratio in the matrix material was always a constant at 0.35.

As discussed in Section 2.16, the matrix penetrability is influenced by the fabric structure. Other parameters affecting the matrix distribution are voiding (holes) between the neighbour fibre tows, the levels of openings and voiding between filaments, fibre surface properties (including wetting and chemical affinity with the matrix), matrix viscosity and the FRC processing method.

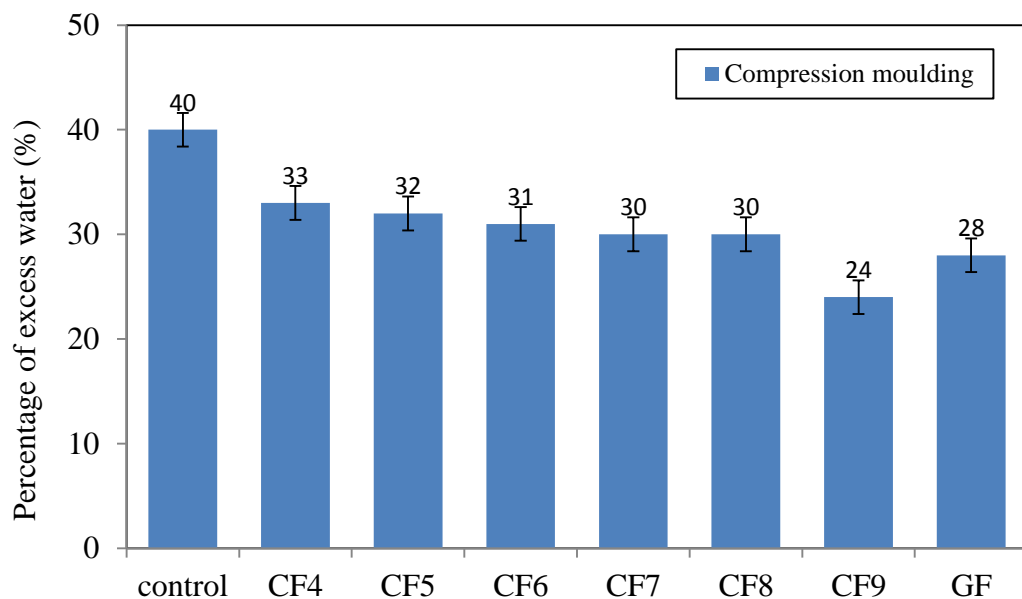


Figure 7.31: Excess water attained by using compression moulding process for control and seven continuous fibres materials.

7.4.3 Effect of Fabric Type

Three forms of fabric were used in this study and cement penetration for higher overall bond take place only if the tows and fibres in a fabric are sufficiently open to allow for the penetration. As an example of the processing challenge, fabrics with stitching may hold the tows or bundles too tightly for effective matrix penetration. An improvement in cement penetrability can be made by pushing the matrix into voids by external forces, such as applying pressure in compression moulding. Figure 7.13 shows this approach with the CF4 fabric FRC. The flexural test results confirm there is a stronger bond, leading to an improved structural performance.

When fabrics are biaxial or multi-axial the efficiency factor is less than with unidirectional fabrics ($0.38 < 1.0$). As discussed in Section 7.3.2, this is because only 25 to 50% of the fibre reinforcement is effective, whereas it is 100% for unidirectional. However, both biaxial and multi-axial fabrics do have an important advantage in that the openings (voiding or holes) between their tows or bundles allow the matrix to bridge between two matrix rich layers. This physical feature results in four-point bending specimens with higher flexural strength, as observed in Figure 7.28 for the CF9 FRC. This particular fabric has 7 mm sized holes which are bigger than the 2 to 5 mm sized holes with fabrics GF, CF7 and CF8 (see Figure 3.2). The voiding within the CF9 fabric provides for better cement penetrability (Figure 7.27(b)), which improves greatly the FRC's properties. The study finds that for the fabric with the smaller holes of 2 mm, the matrix cannot penetrate as deeply and this leads to lower composite properties.

With hand lay-up processing the FRCs with unidirectional fabrics CF4, CF5 and CF6 show a relatively low matrix penetration. This is due to fabric constructions having no gaps between the tows, which are sufficiently held together to limit matrix penetration for

bridging between the matrix rich layers. As shown in Figures 7.14 and 7.15 the presence of poor penetration prevents the reinforcement potential from being fully materialised. Compression moulding develops adequate filling to improve anchoring of the matrix to the fabric and thereby increases overall bond strength. This change in processing method leads to enhanced strain and toughness, as is clearly shown by the results for fabrics CF4 to CF6 in Figures 7.29 and 7.30.

Based on the above discussion it can be concluded that a fabric's structure (its fibre architecture) highly influences the structural properties of the FRC. It is seen that in the case of CF9, a good cement penetrability is essential in order to achieve the required overall bonding for higher mechanical properties. Surface treatment to CF4 and CF5 fabrics is investigated in the following section with the aim of improving the degree of matrix penetration and fibre 'wet-out'.

7.5 Improving Effectiveness of Unidirectional Reinforcements, CF4 and CF5

This study focuses on the influence of modifying fabrics CF4 and CF5 since they were produced specifically for processing fibre reinforced polymer composites and not for an FRC. As the characterisation work above has shown their fibre architectures (see Figure 3.2(a) and b) are not ideal for producing an FRC material because they lead to undeveloped matrix penetration. To obtain the full potential of carbon fibres as reinforcements for FRC composites, it is necessary to have an adequate fibre-matrix interface to ensure effective load transfer from the matrix to the fibre. However, carbon fibres are hydrophobic in nature (as discussed in Section 2.4.4) and therefore the lack of fibre 'wet-out' these fabric constructions allow means the FRCs have a relatively low overall bond strength. The surface treatment of fibres may either produce chemical bonds on their surface (leading

more interaction with the matrix) or roughen the surface (which provides better mechanical interlocking between the matrix and fibre) or do both, which improves the bond with the matrix.

To increase 'wet-out' the author created two novel processing steps for fabrics CF4 and CF5. One modification is cut the fabric (in sheets form) into small unidirectional strips of ≈ 4 to 5 mm width; each single strip has two carbon bundles or tows. When the strips are laid into the matrix a separation between them of 3 to 5 mm is introduced. This lay-up arrangement is shown in Figure 7.32. The rectangular shaped voids (holes) then provide continuity for the matrix across the reinforcement layer leading to an enhancement in structural performance. The second modification is by immersing sheets of CF4 and CF5 in Ethanol alcohol for 2 to 3 minutes before drying them for 24 hours. The Ethanol alcohol was selected based on the advice from Professor Jan Baeyens in Chemical Engineering Research Group at the University of Warwick. By applying this surface treatment the original fabric form seen in Figure 7.33(a) becomes like that shown in Figure 7.33(b), which has holes of similar size and shape to the spaces available by the first modification. Both processing steps create reinforcement openings that can be filled with matrix and give matrix bridging across the reinforcement layers and connects the matrix rich layers.



Figure 7.32: CF4 cut into strips to increase the penetration of the cement in between the tows and to improve the bond and enhance the mechanical performance.



(a)

(b)

Figure 7.33: Photo shows CF4 (a) before and (b) after surface treatment.

To investigate their influence new batches of flexural specimens were produced using hand lay-up and compression moulding with the same mix design, constituent materials and mixing procedure as previous. Presented in Appendix B Tables B.7.31 to B.7.46 are the test results and statistical analysis for the modified CF4 and CF5 FRCs produced by both hand lay-up and compression moulding, with $V_f = 5\%$. The number of nominally identical specimens per batch is five (in some cases six). It can be seen from the Appendix B Tables B.7.31 to B.7.46 that the modified (strips and treated) CF4 and CF5 FRC

specimens produced by compression moulding gave higher mean flexural strength of 66 MPa than those from the hand lay-up. By comparing the results in Table B.7.31 it is found that the compression moulding CF4 FRC with strip reinforcement gave the highest peak strength of 75.2 MPa. While the modified (strips and treated) CF5 and treated CF4 FRC specimens produced by hand lay-up gave higher mean strain at peak stress of 0.56% than those from the compression moulding (0.4%). By comparing the results in Table B.7.38 it is found that the hand lay-up CF5 FRC with strip reinforcement gave the highest mean toughness at peak stress of 0.20 J/m³.

Plotted in Figures 7.34 to 7.41 are the stress-strain curves for CF4 and CF5 reinforcements with Figures 7.34 to 7.37 for strip reinforcement and Figures 7.38 to 7.41 after the fabrics had been treated with Ethanol alcohol. It is seen from the curves in the five figures (7.34 to 7.36, 7.38 and 7.40) that the shape of the stress-strain curves is similar to that labelled shape (f) in Figure 2.3(f) of Section 2.10. They also have the same form as the FRCs with fabrics CF4, CF5 and CF6 without any fabric treatment. From the equivalent curves in Figures 7.6 to 7.11 it is observed that the original FRCs have lower mean flexural strength and mean toughness at peak stress. It has been revealed that unusual composite action (Figures 7.34 to 7.36, 7.38 and 7.40) is achieved in FRCs made using compression moulding process for both the Ethanol treated and with the strip form of reinforcement. As explained in Section 2.10 the shape of these stress-strain curves for a reinforcement with $V_f \gg V_{f_{crit}}$ has rarely been encountered in the past. While the curves in the three figures (7.37, 7.39, and 7.41) that the shape of the stress-strain curves is similar to that labelled shape (e) in Figure 2.3(e) of Section 2.10. By having regions of continuous matrix in the reinforcement layer plane this treatment study has demonstrated that very effective composite action can be activated, leading to higher reinforcement efficiency.

The elastic portion of the curves in Figures 7.34 to 7.36, 7.38 and 7.40 is fairly linear up to peak stress, occurring in the range 40 to 64 MPa (see Tables B.7.31 to B.7.35, Tables 7.39 and 7.43). It can be observed that the LOP of the treated FRCs are higher than the control materials and non-treated materials. Beyond the peak stress, the stress can first drops some 10% to 25%, before decreasing gradually until ultimate failure. As labelled in Figure 7.38, the ACK model gives two distinct regions along the stress-strain curve for the pre-cracking Region I and the failure Region IV. The ultimate strain reaches as much as 0.56%.

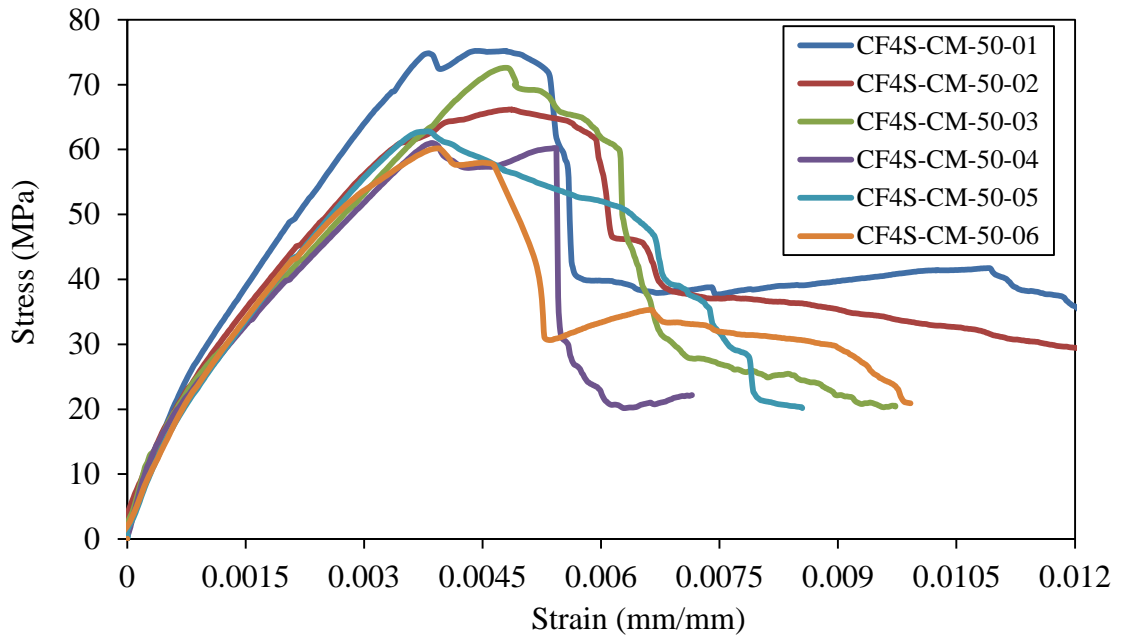


Figure 7.34: Stress-strain curves for CF4 cementitious specimens ($V_f = 5\%$) in strip form produced with compression moulding.

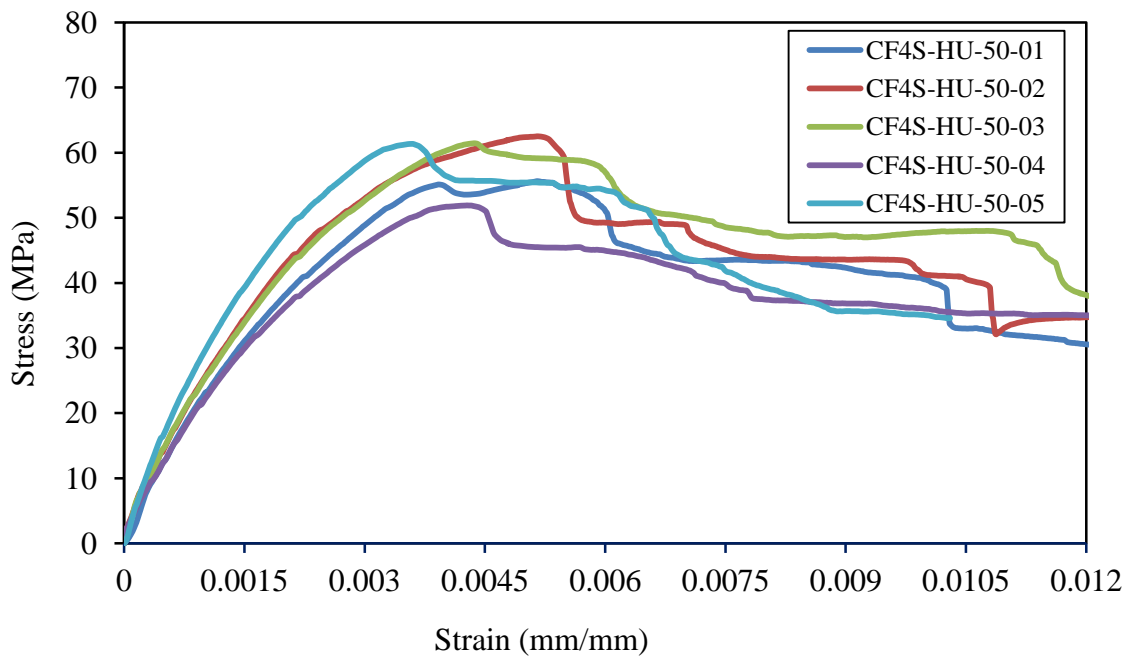


Figure 7.35: Stress-strain curves for CF4 cementitious specimens ($V_f = 5\%$) in strip form produced with hand lay-up.

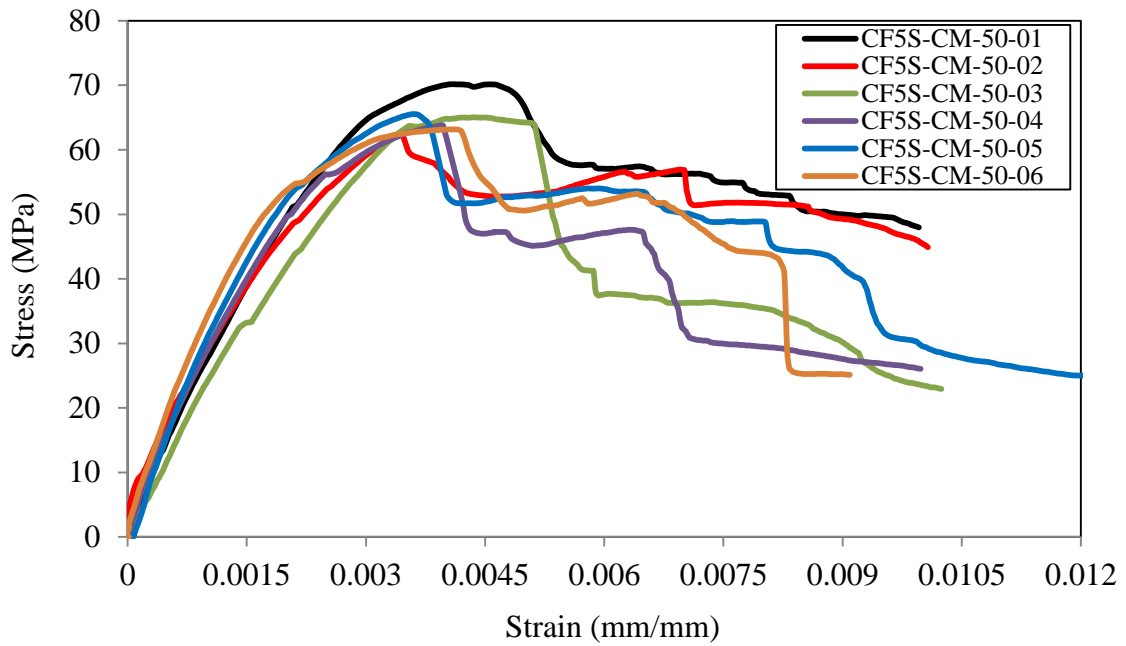


Figure 7.36: Stress-strain curves for CF5 cementitious specimens ($V_f = 5\%$) in strip form produced with compression moulding.

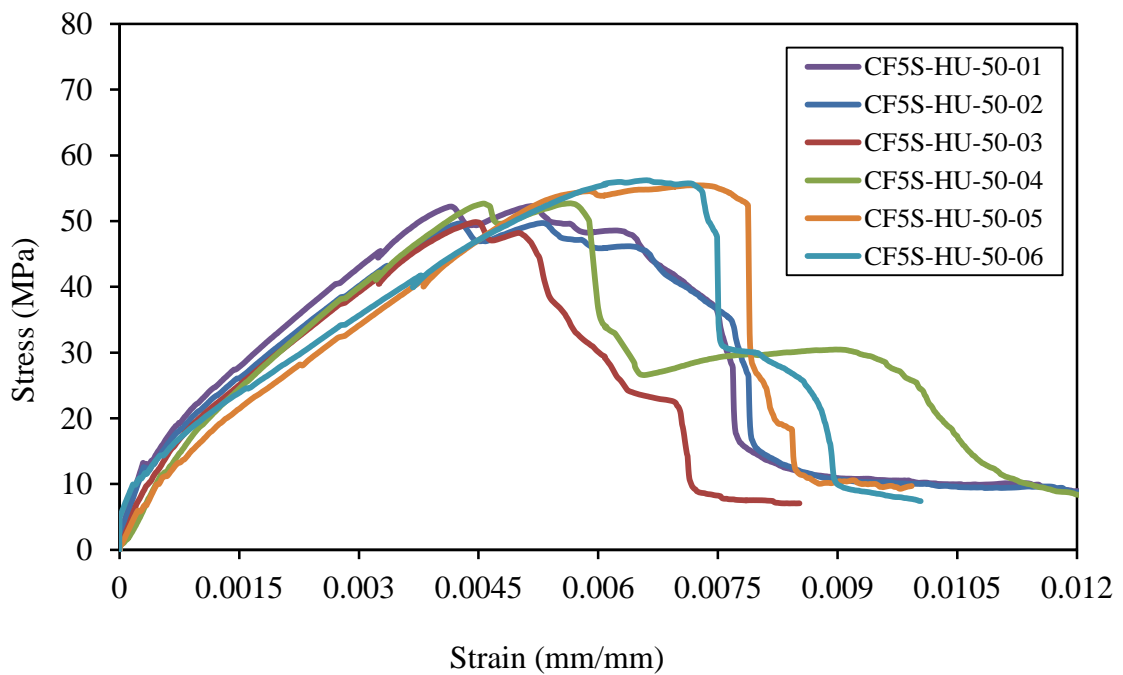


Figure 7.37: Stress-strain curves for CF5 cementitious specimens ($V_f = 5\%$) in strip form produced with hand lay-up.

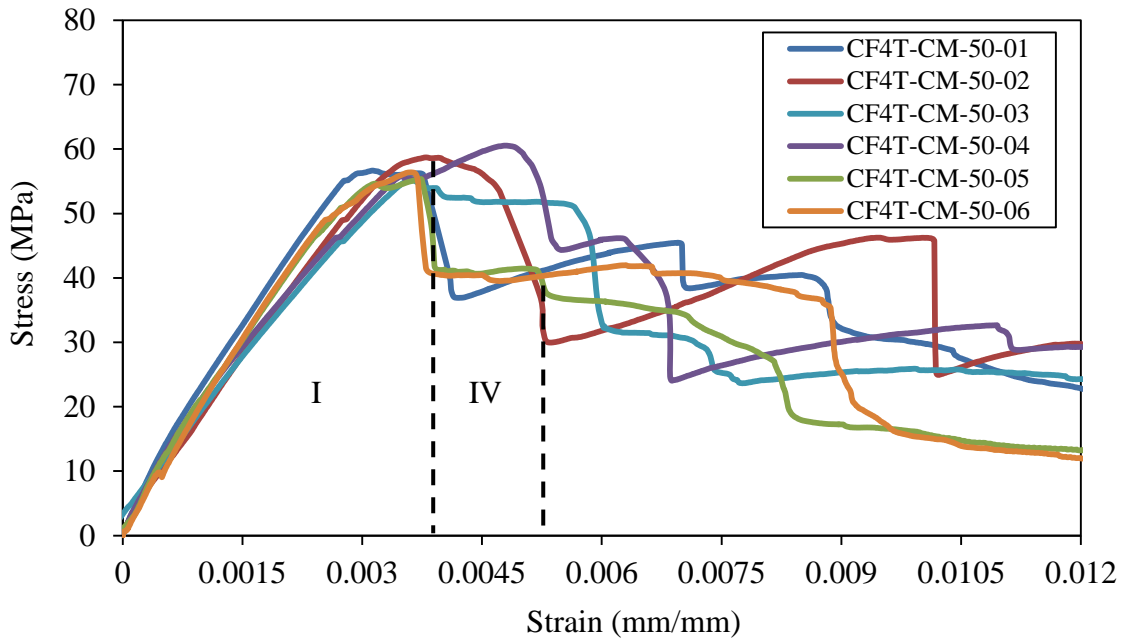


Figure 7.38: Stress-strain curves for Ethanol treated CF4 cementitious specimens ($V_f = 5\%$) produced with compression moulding.

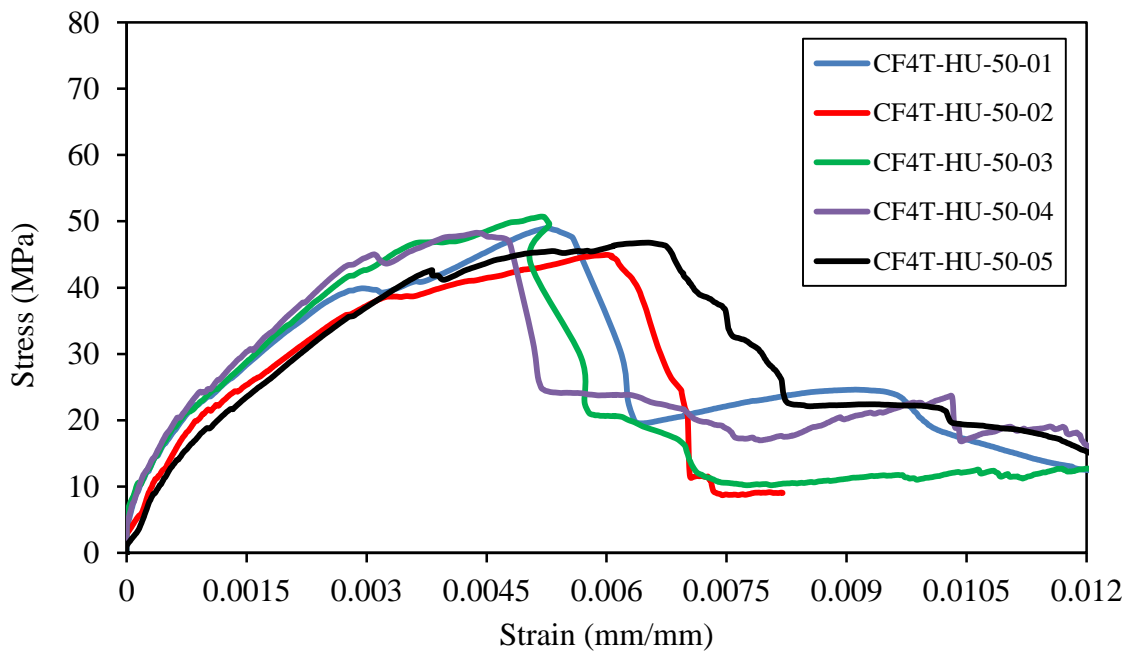


Figure 7.39: Stress-strain curves for Ethanol treated CF4 cementitious specimens ($V_f = 5\%$) produced with hand lay-up.

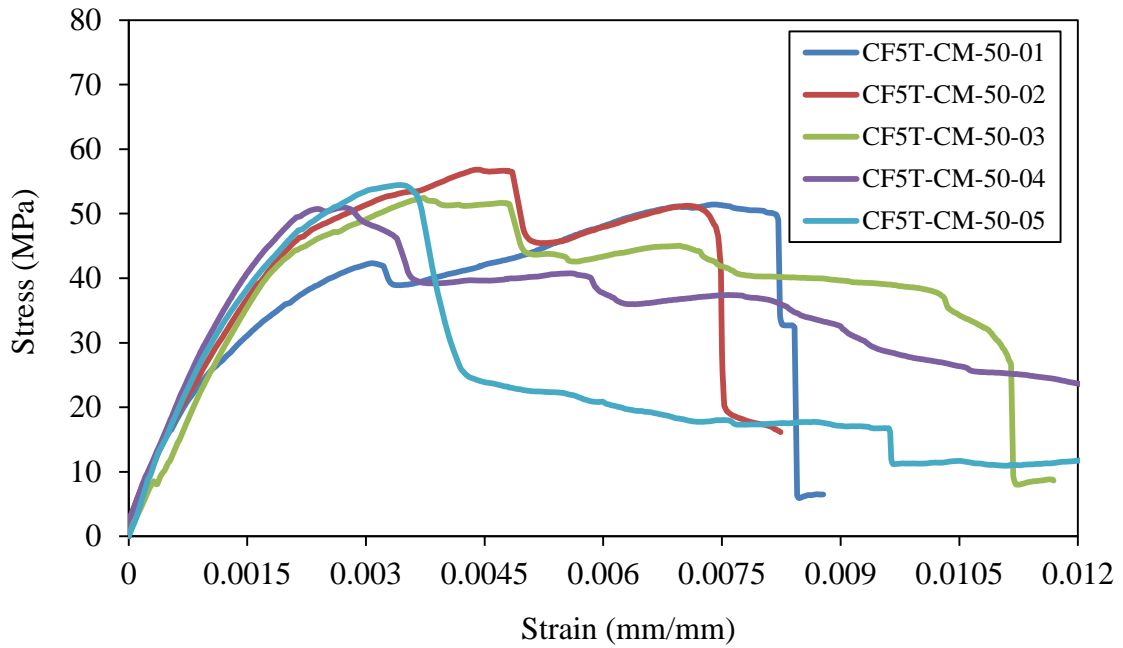


Figure 7.40: Stress-strain curves for Ethanol treated CF5 cementitious specimens ($V_f = 5\%$) produced with compression moulding.

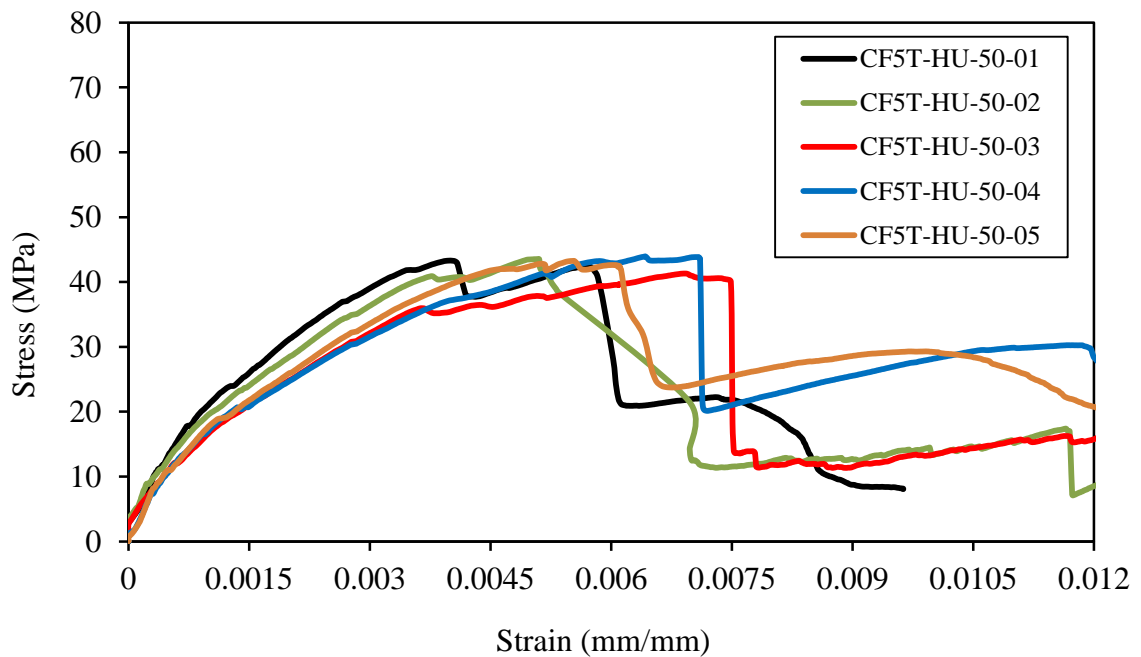


Figure 7.41: Stress-strain curves for Ethanol treated CF5 cementitious specimens ($V_f = 5\%$) produced with hand lay-up.

The improvement in overall bond strength after surface treatment can be explained by using SEM to analyse the microstructure. The SEM images in Figures 7.13 and 7.42 can

be used to confirm that there is an increased in cement penetration with the Ethanol treated CF4 fabric. Figures 7.42(a) and 7.42(b) shows treated CF4 fibres are completely covered with the hydration products that further fill the voiding between neighbour filaments. This benefit of modifying fabrics enhances the flexural properties.

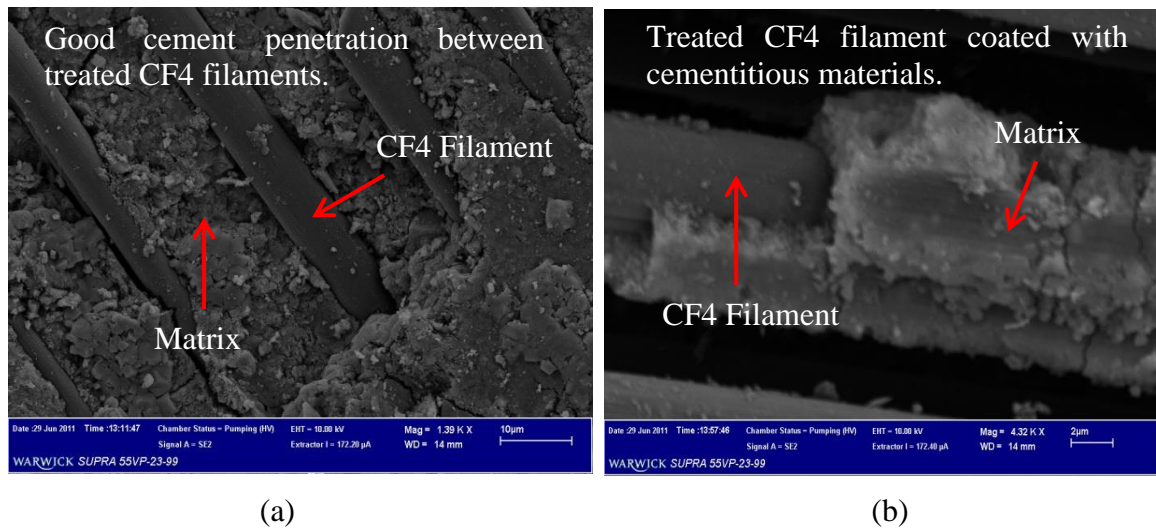


Figure 7.42: Photo shows surface treated CF4 fabric; (a) the matrix exists between fibres (b) and CF4 filament fully coated.

Using bar charts Figures 7.43 to 7.45 give, respectively, the means of flexural strength, strain at peak stress and toughness at peak stress for FRCs with CF4 and CF5 fabrics in three forms. For each material the two processing methods are given side-by-side, with hand lay-up on the left-side. The left most result is for sheets (as received from the supplier), the middle is for the strip form of modification and the right sided for surface treatment with Ethanol alcohol. The first bar is for the control material made by compression moulding. This presentation shows that the four FRCs have significantly higher strength, strains and toughness than their equivalent control materials. Batch test results show that the materials processed by compression moulding have the highest mean peak stress. This means flexural strength was higher only with CF4 (sheet form) fabric when the processing is by hand lay-up. The mean flexural strengths for CF4 and CF5

specimens, in strips form, are the same (65 MPa vs 66.3 MPa) and gave the strongest FRC. They are 772% (7.6 MPa), 62% (40.9 MPa), 16% (57.1 MPa), 86% (35.6 MPa) and 25% (53.2 MPa) higher than for the other twelve materials reading from left to right across the bar chart.

By comparing results of mean strain at peak stress in Figure 7.44, it is observed that the hand lay-up CF5 in strips form and treated specimens and treated CF4 specimens are the same and they gave the highest mean strain at peak stress of 0.56% for an increase by factor of; 56 (0.01%), 1.6 (0.35%), 1.2 (0.45%) and 1.5 (0.37%) on reading the hand lay-up bars from left to right. Furthermore, the results presented in Figure 7.45 showed that the mean toughness at peak stress for the hand lay-up CF5 FRC in the strips form gave the highest mean toughness at peak stress of 0.20 J/m³. This is an increase by a factor of 500 (0.0004 J/m³), 2.2 (0.092 J/m³), 1.1 (0.18 J/m³), 1.1 (0.19 J/m³), 1.4 (0.14 J/m³) and 1.2 (0.17 J/m³) over the other hand lay-up materials on reading the bars from left to right.

The reasons for the improvement in the flexural properties of the modified unidirectional CFRC materials are the same as given previously for the unidirectional fabrics in the Chapter 7 investigation (see Section 7.3.5). Furthermore, the best measured mean strength with unidirectional fabrics (i.e. treated and in strips form) can be attributed to the good interfacial bond strength from good matrix penetration into the modified unidirectional fabric and across the fabric.

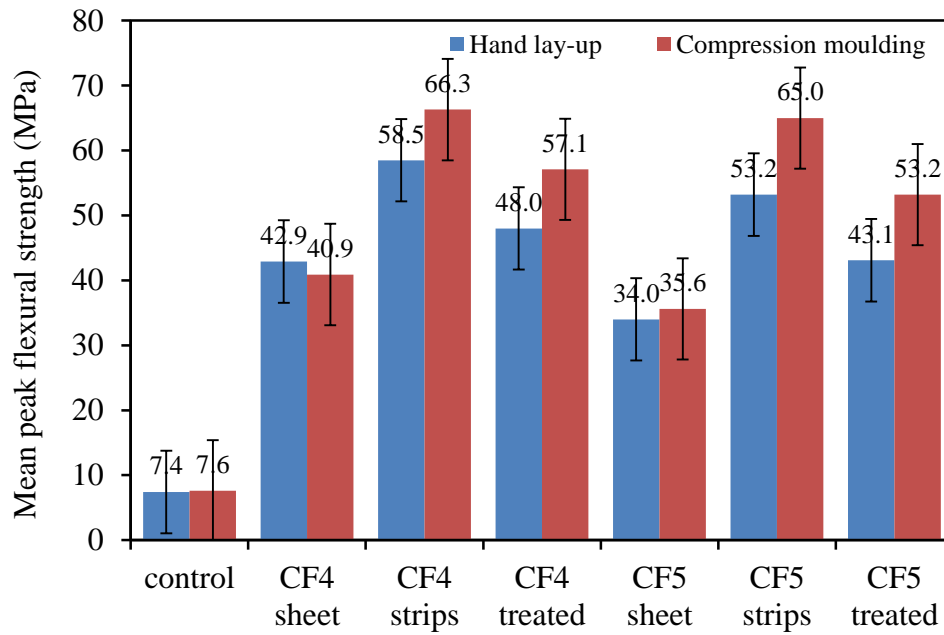


Figure 7.43: Mean peak flexural strengths for CF4 and CF5 in three forms (sheets, strips, and treated) and control materials.

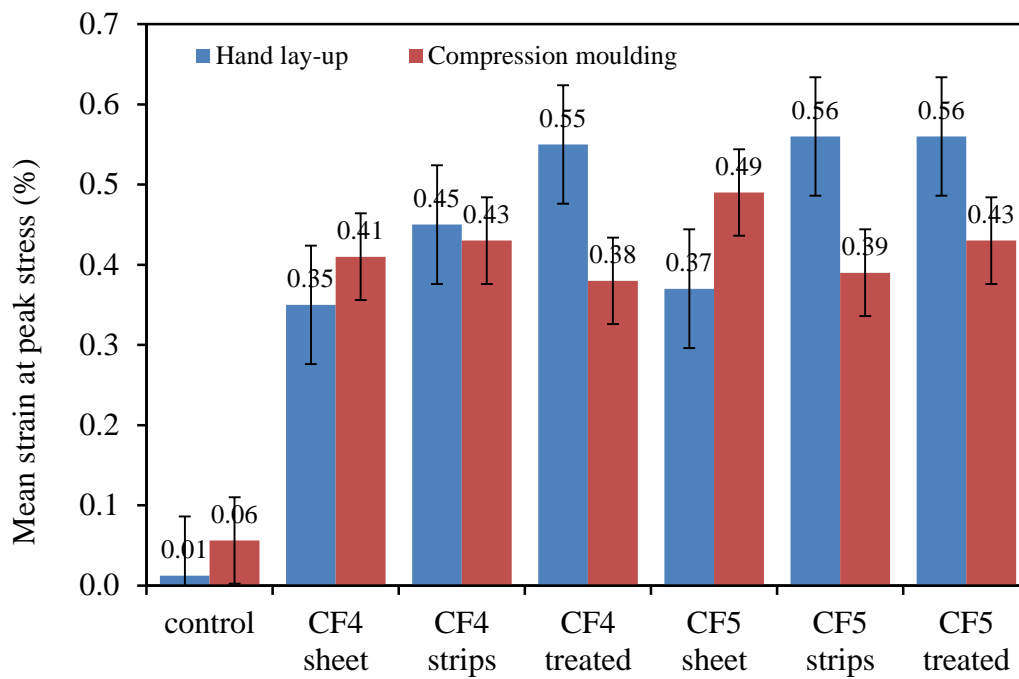


Figure 7.44: Mean strain at peak stress for CF4 and CF5 in three forms (sheets, strips, and treated) and control materials.

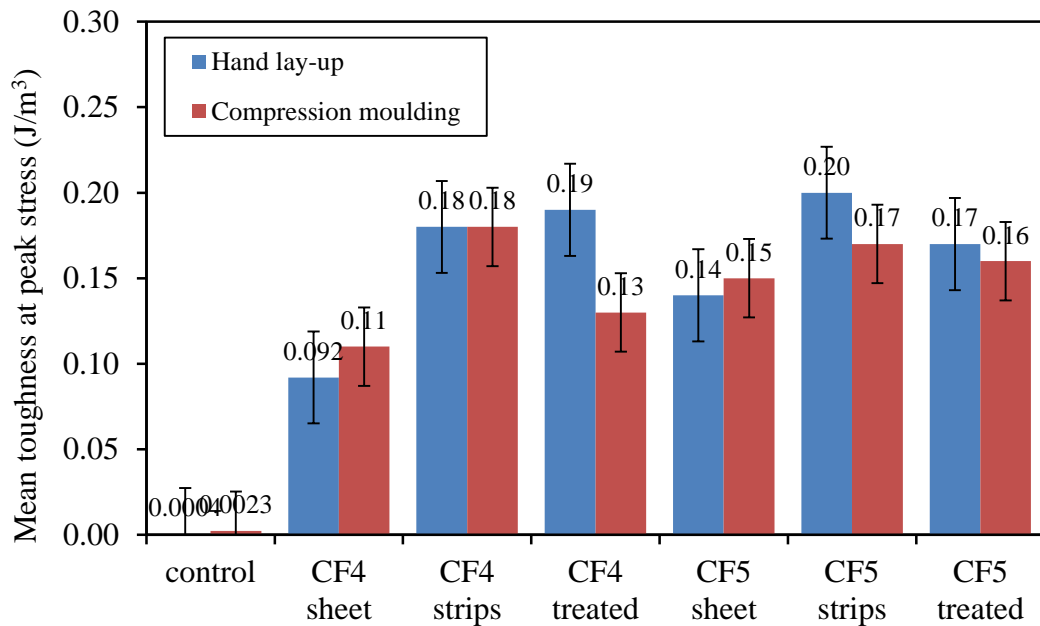


Figure 7.45: Mean toughness at peak stress for CF4 and CF5 in three forms (sheets, strips, and treated) and control materials.

To achieve the best overall bond strength it can be concluded that it is important that as many as possible of the fibre filaments are in contact with the cement matrix. Modification treatments are intended therefore to enhance the chemical affinity between the fibres and the matrix, to open ‘holes’ between the filaments for the matrix to readily penetrate and to create surface roughening that gives mechanical interlocking. As discussed in Section 1.2, one of the objectives of the PhD work was to maximise the flexural strength of FRC. This goal has been met as seen by the significant improvement in mean flexural strength for the four modified CF4 and CF5 FRCs given by the results in Figure 7.43. Findings and property changes obtained from the two processing changes agree and confirm results from previous studies by Fu *et al.* (1996), Peled *et al.* (1998), Bentur and Mindess (2007), Badanoiu and Holmgren (2003) and Ombres (2012). These researches have concluded that fibre surface treatment is an effective method in improving the overall bond strength in FRCs.

7.6 Influence of Hybrid Fibre on Mechanical Properties

Bentur and Mindess (2007) introduce that hybrid reinforcement consists of two or more types of fibre, rationally arranged in a common matrix to produce a composite material that derives benefits from each of the individual reinforcements and therefore exhibits a synergetic response. A single FRC is investigated having the 5% V_f of reinforcement as a combination of three reinforcements comprising the two short fibres PVA and CF3 (Chapter 6), and the biaxial fabric CF8.

These three reinforcements were selected for three reasons. Firstly, the CF8 fabric has mesh construction with distinctive openings of 6 mm between two adjacent roving bundles in both 0° and 90° directions. Figure 3.2(e) shows the construction of this fabric. It is known that holes in a fabric benefit the overall bonding strength by allowing matrix to bridge through a reinforcement layer. Secondly, the PVA fibre was selected because, from the work reported in Chapter 6, this short fibre FRC material had greatly improved flexural strength and toughness, refer to Section 6.3.7. Thirdly, the short CF3 fibre was selected due to high tensile strength (2240 MPa) and length of 6 mm (i.e. $l > l_c$), which is sufficient to provide reinforcement and not too long to prevent a uniform distribution throughout the mix.

Two batches of hybrid specimens were produced using compression moulding and hand lay-up with the same mix the design, constituent materials and mixing procedure as previous. The reinforcement arrangement comprised five layers of CF8 fabric, for $V_f = 3\%$ (1.5% in both warp and weft directions), and the two short fibres (PVA and CF3) at 1% V_f each. Four-point bending testing was carried out following the usual test procedure in Section 3.8. Figures 7.46 and 7.47 give the stress-strain curves in the usual way. Also plotted is the lower bound curve for the equivalent control material. By inspecting the

curves characteristics it is observed that the shape of stress-strain curves in the figures is similar to that labelled shape (f) in Figure 2.3(f) of Section 2.10. As previously mentioned this form of stress-strain curve is rarely encountered when $V_f \gg V_{f,crit}$.

The peak stress is found to lie in the range 44 to 74 MPa (from Tables B.7.47 and B.7.49). It can be observed in Figures 7.46 and 7.47 that the LOP is much higher than the control materials and higher than for the FRC reinforced either with short CF3 (Figures 6.14 and 6.15), short PVA (Figures 6.21 and 6.22) or CF8 fabric (Figures 7.18 and 7.19). This finding suggests that the composite action has been enhanced by having a combination of the three reinforcement types. For the hybrid FRCs the first crack stress and peak stress are the same ($\sigma_{mu} = \sigma_{cu}$). σ_{mu} is found to be at least five times higher than the FRCs of only CF3, PVA or CF8, and the loss of linearity happens when the average stress is 8 MPa. As seen in Figures 7.46 and 7.47 the curves show that after peak stress the stress resisted by the flexural specimen decreases gradually until there is ultimate failure. Because the strain at peak stress ranges from 0.2% to 0.9% there is evidence for the ability of the fabric reinforcement to control crack distribution and growth. The pre-cracking Region I and failure Region IV are present from the ACK model.

Why does the hybrid FRC have promise? First reason is that the short fibres CF3 and PVA will bridge hardened cement micro-cracks, and this leads to a higher tensile strength. Second reason is the mechanical anchoring developed by matrix bridging across a CF8 fabric layer results in a strong overall bond (see Section 2.16). The presence of the fabric also arrests the propagation of macro-cracks and substantially improves the toughness of the composite.

Generally, the overall performances of the hybrid batches are similar. It is however important to note that the FRC produced by compression moulding is significantly stiffer,

by about four times higher than those by hand lay-up, and gave the highest mean strength of 74.3 MPa (see Figure 7.46). This improvement must be due to the additional consolidation from the processing method.

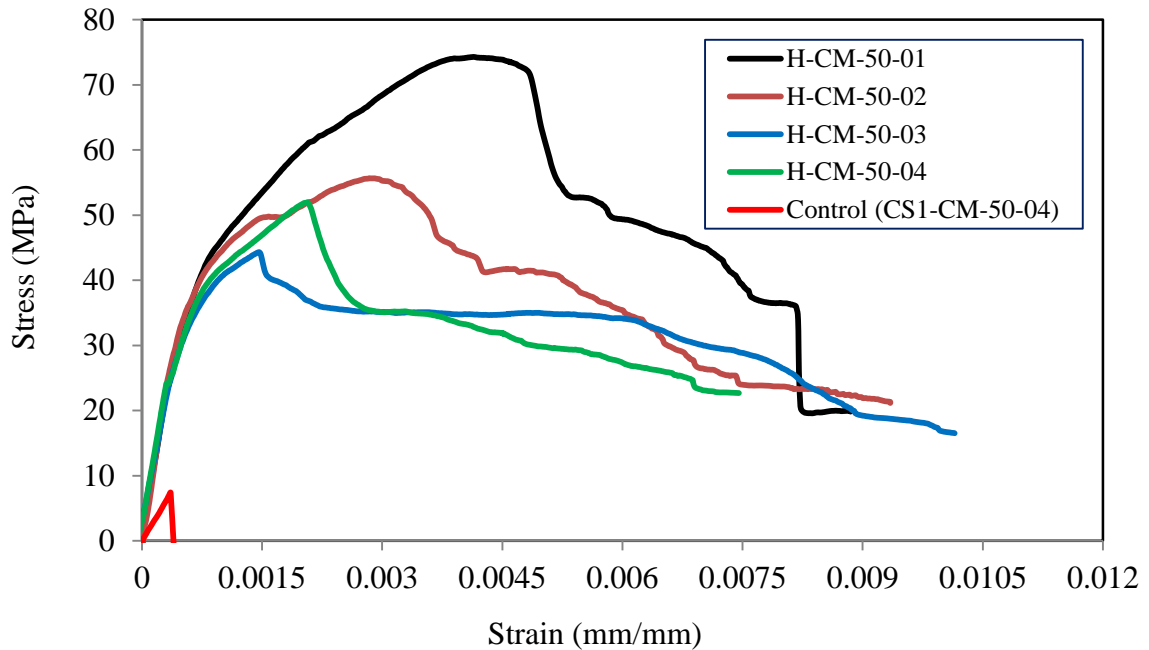


Figure 7.46: Stress-strain curves for hybrid (1%CF3+1%PVA+3%CF8) specimens ($V_f=5\%$) produced with compression moulding.

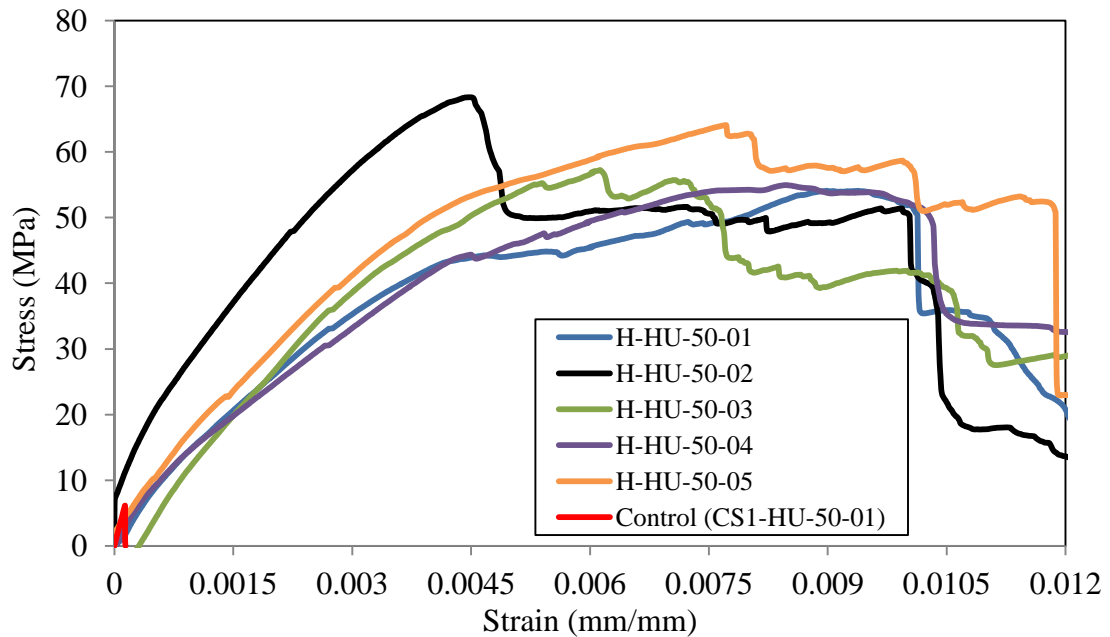


Figure 7.47: Stress-strain curves for hybrid (1%CF3+1%PVA+3%CF8) specimens ($V_f=5\%$) produced with hand lay-up.

Figures 7.48 to 7.50 present bar charts for the means of peak flexural strength, strain at peak stress and toughness at peak stress for the materials reinforced with individual fibres (i.e. CF3, PVA or CF8, having $V_f = 5\%$) and the hybrid FRCs (having 1% of CF3 and 1% of PVA and 3% of CF8). For a baseline comparison, the test results for the control material are given on the left-hand side of the charts. As usual the two processing methods are given side-by-side, with hand lay-up on the left. In each figure the hybrid's results are given on the right hand side with the individual reinforced FRCs in the middle. The strength results in Figure 7.48 show that the hybrid FRC produced by hand lay-up and compression moulding are similar giving the mean peak strengths of 56.6 MPa and 59.7 MPa. These means are higher by a factor of 1.7 to 8 times than determined for the other four materials (control, and FRCs of PVA, CF3 and CF8) reading from left to right across the bar chart.

By comparing the results of mean strain at peak stress in Figure 7.49 it is found that the hybrid FRC batches produced by compression moulding and hand lay-up are similar and gave the highest value of 0.62% and 0.69%. These means are higher by a factor of 1.3 to 58 times than determined for the other four materials (control, and FRCs of PVA, CF3 and CF8) reading from left to right across the bar chart. Furthermore, from Figure 7.50 it is seen that the hybrid FRC batches produced by compression moulding and hand lay-up gave the highest mean toughness at peak stress of 0.21 J/m^3 and 0.27 J/m^3 . The hybrid batches gave a mean toughness that is many time higher than the control materials and the other individual fibre FRCs.

From the test results in Tables B.7.47 and B.7.49 it is found that the hybrid material with the highest peak strength of 74.3 MPa was made by compression moulding. The maximum strength from the batch of specimens was slightly lower at 68.3 MPa by hand

lay-up. The maximum is an increase of nearly 900% over the control materials having a mean strength of 7.6 MPa. The reasons for the big improvement have been documented through this chapter, and in Chapter 6, and so there is no need to repeat them again. Needless-to-say there is evident from the present investigation that the hybridisation of the FRC reinforcement can offer better overall mechanical properties than could an FRC material reinforced by a single type of reinforcement.

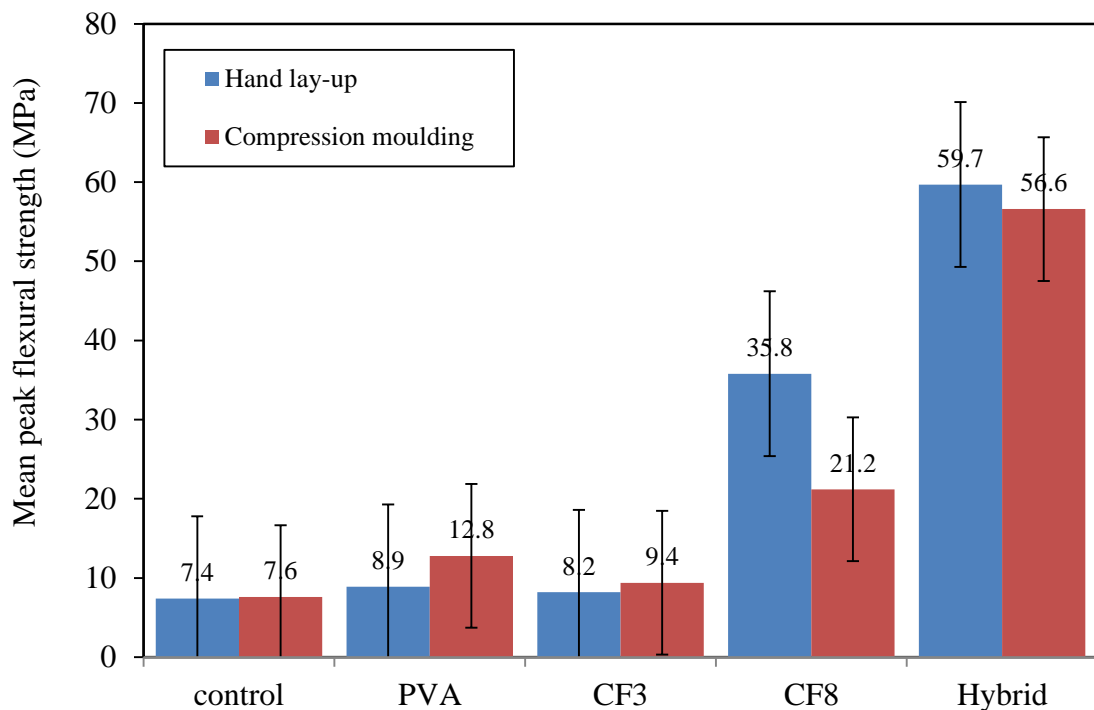


Figure 7.48: Mean peak flexural strength for materials reinforced with; CF3, PVA, CF8, hybrid (1% CF3+1% PVA+3% CF8) fibres and control materials.

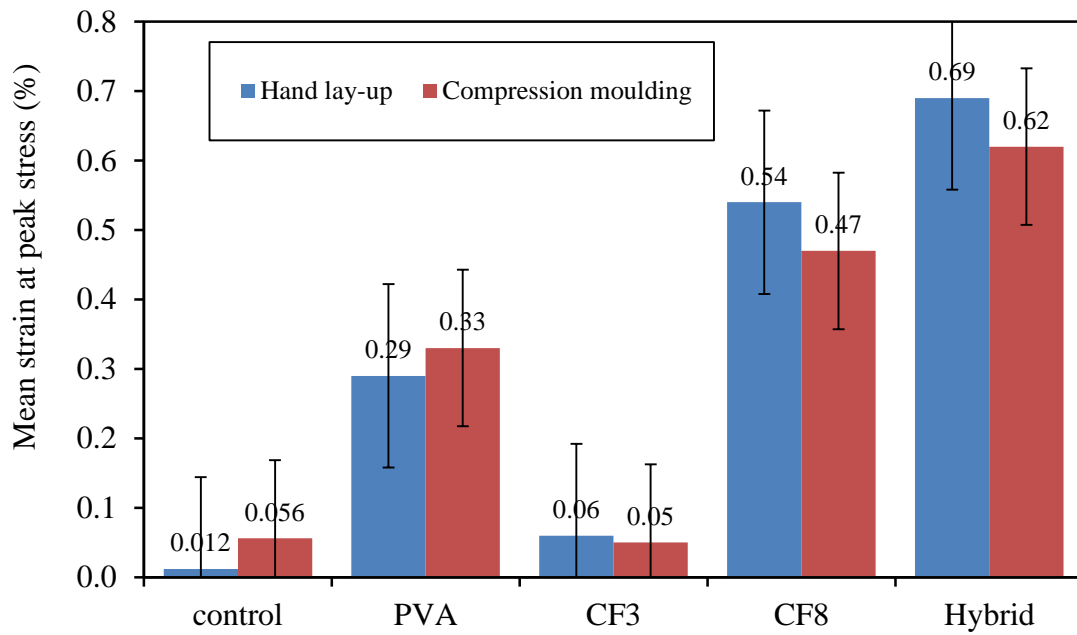


Figure 7.49: Mean strain at peak stress for materials reinforced with; CF3, PVA, CF8, hybrid (1% CF3+1% PVA+3% CF8) fibres and control materials.

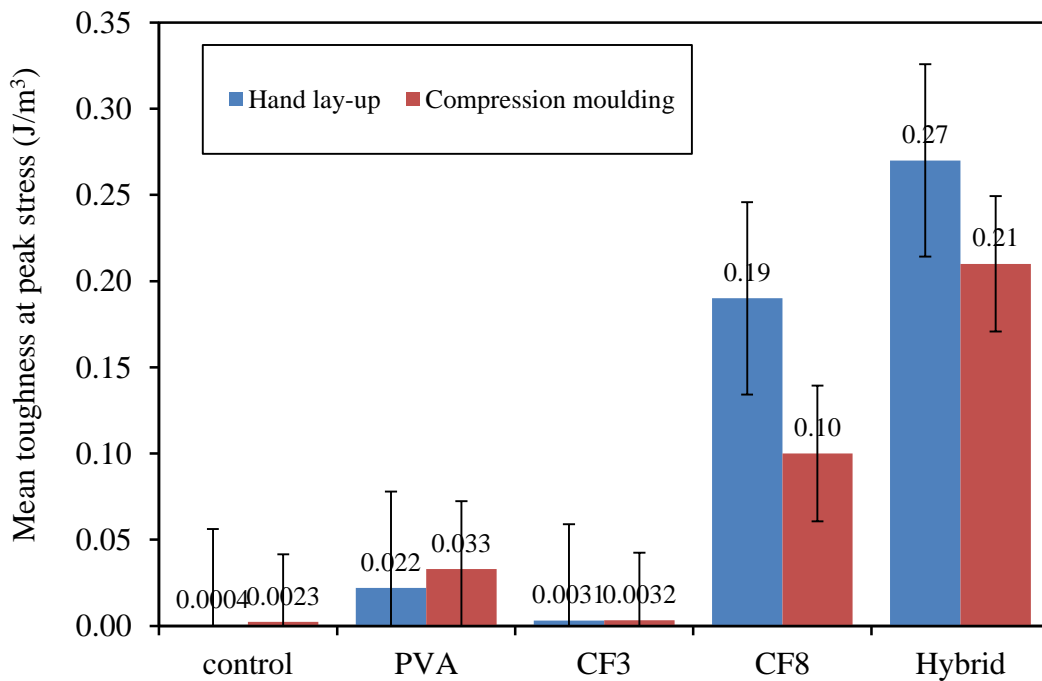


Figure 7.50: Mean toughness at peak stress for materials reinforced with; CF3, PVA, CF8, hybrid (1% CF3+1% PVA+3% CF8) fibres and control materials.

7.7 Porosity Measurement

As discussed in Sub-section 2.4.5, strength is adversely affected by a higher level of porosity. The change in porosity on having fabric reinforcement was therefore investigated. Measurement was made using Helium Pycnometry (HP) (model AccuPyc 1330 made by Micromeritics), following the test procedure given in Sub-section 3.5.1.

Specimens were produced by hand lay-up and compression moulding with the same mix the design, constituent materials and mixing procedure as previous. The bar chart in Figure 7.51 presents the average percentage porosities from five specimens per process method. In the figure the results for compression moulding (blue bars) are on the left-side and for hand lay-up (red bars) are on the right-side of the pairs.

Mean porosities and their range reported in Figure 7.51 indicate that the materials produced by compression moulding have, as expected, a lower porosity that averages 3.1%. This reduction shows that the applied processing pressure of 9 MPa does consolidate the materials. The control has a mean porosity of 12.5% (from 11 and 14%), which can be used as a baseline value. It is seen that porosity increases from 16 to 22% after the addition of one of the seven continuous reinforcements. Results also show that the FRC with GF fabric has a higher porosity, at 22%, than those with CF4 to CF9 fibre, which will be due to the specific geometry of this biaxial fabric. Because the sizing on the GF yarns (see Figure 3.2(g)) prevents cement matrix penetration between the filaments of the bundle. The stiff and strong junctions of the fabric contribute to the mechanical performance of the composite; however, the coating of the bundles may be detrimental from a bonding point of view, since only the perimeter of the bundle is in contact with the cement matrix, then the voids and porosity could be increased.

FRC with CF9 and CF4 fabrics give the lower porosities in range 15.5 to 19.5%, which are 5% higher than for the control material. Another observation from the results in the figure is that CF5, CF6 and CF7 FRCs by hand lay-up have similar percentages at 21%. From this study it can be concluded that the porosity content is increased by the addition of fibres and that the form of the fabric could have an influence too. This finding agrees with the previous work by Xu and Chung (1999) and Banfill *et al.* (2006), which is introduced in Sub-section 2.4.5. They all have said that the porosity was increased when fibres were added.

Figure 7.52 shows the relationship between the mean strength (data from Figure 7.28) versus the mean porosity (data from Figure 7.51) for FRC materials with seven continuous fabrics produced by compression moulding to see if an inverse relationship appears. It is found from Figure 7.52 that the lower the porosity is the higher the FRC strength. In other words, this is evidence that the strength has an inverse relationship with the porosity, as the porosity increases the strength decreases. From the discussion above, it is concluded that there is evidence that compression moulding was successful in reducing porosity.

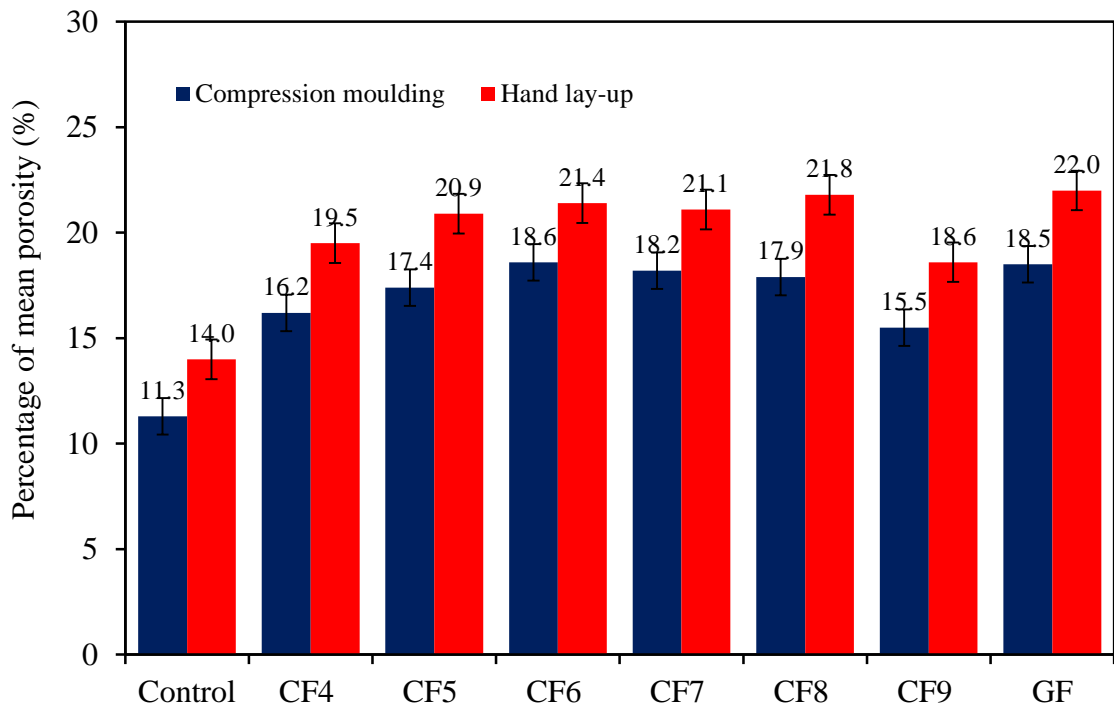


Figure 7.51: Percentage of mean porosity for control and continuous materials made by hand lay-up and compression moulding.

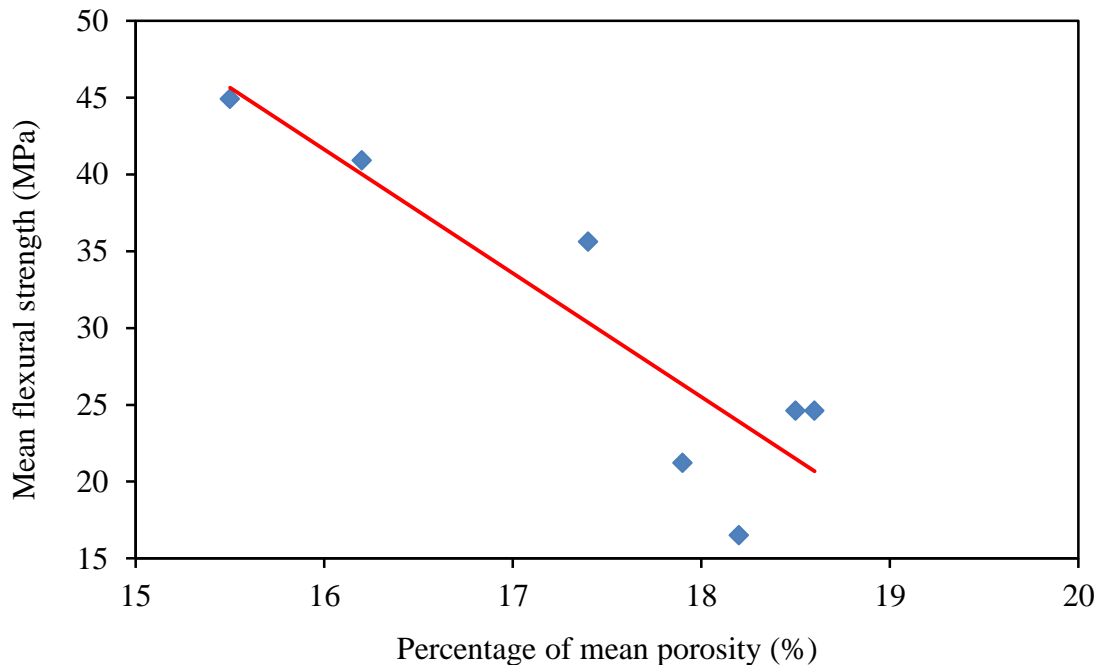


Figure 7.52: The mean peak strength versus mean porosity for seven FRC materials with CF4, CF5, CF6, CF7, CF8, CF9 and GF fabrics made by compression moulding.

7.8 Statistical Analysis

In this study, ANOVA testing was carried out using Microsoft Excel software to determine if there is a significant difference between the flexural peak stress results from the two processes of hand lay-up and compression moulding. As discussed in Section 6.5 the critical P -value is usually set at 0.05. In other words, if the value of P -value is lower than 0.05 it is statistically significant, while a P -value > 0.05 is not for a statistical significance.

Presented in Tables E.7.1 to E.7.8 in Appendix E are the ANOVA results for the FRCs batches reinforced with the seven continuous fibres (CF4, CF5, CF6, CF7, CF8, CF9 and GF) at V_f of 5%, 2.5% and 1.9% for unidirectional, biaxial and multi-axial reinforcements, respectively. The tables also have the analysis results for the control materials. For each reinforced material there are two parts (top and bottom) in each table. The contents and details of each part are introduced in Section 6.5. The data for the ANOVA testing was taken from Column (3) in Tables B.7.1 and B.7.29.

Table 7.4 summarises the P -values for the peak stress for the eight materials. By inspecting the table the reader will be able to establish the relative differences. P -values for FRCs with CF4, CF5, CF9 reinforcement and the control material are found to be > 0.05 . This means that there is evidence that there is no significant statistically difference between the two methods of processing. Furthermore, it is observed that the peak stress for the CF6 to CF8 and GF materials are seen to have been significantly affected by manufacture as the P -value is < 0.05 . This finding confirms, and supports, what was discussed in Sub-section 7.4.2 that the CF6 to CF8 and GF FRCs gave, at 46% to 112%, a significant change in peak stress when produced by the hand lay-up and compression moulding processes.

Table 7.4: Values of P-value for, CF4, CF5, CF6, CF7, CF8, CF9 and GF fabrics and control specimens.

Material type	P-value	Significance
Control specimens	0.64	No
CF4 specimens	0.38	No
CF5 specimens	0.60	No
CF6 specimens	0.0071	Yes
CF7 specimens	2.82×10^{-9}	Yes
CF8 specimens	0.00013	Yes
CF9 specimens	0.13	No
GF specimens	3.10×10^{-6}	Yes

Based on the results in Table 7.4 it can be concluded that the statistical ANOVA testing has confirmed the author's proposal in Sub-section 6.3.1 that a difference of 0 to 15% between any two mean properties shall not be considered as significant. Moreover, it supports the findings given in Sub-sections 7.4.2 that there is no significant difference between the two manufacturing processes for CF4, CF5, CF9 reinforcement and the control material. For the record the differences in peak stress between hand lay-up and compression moulding for these materials lie in the narrow range 5% to 6%.

7.9 Findings From Mechanical Testing of Materials With Continuous Fibres

The main findings from the series of four-point bending tests reported and analysed in this chapter are:

- 1- With continuous fibres increasing $V_f > 5\%$ showed a reduction in strength because of delamination failure between the fibre and matrix layers. For this reason all FRCs characterised had a constant V_f of 5%, as reported in Sub-section 7.3.3.
- 2- Evaluation of the preliminary, fact finding, test results show that 'unusual' composite action (shape (f) in Figure 2.3) is achieved with the continuous reinforcements of type

CF4, CF5, and CF6; treated and non-treated specimens in Sub-sections 7.3.5 and Section 7.5. When the FRC possesses unusual composite action (shape f in Figure 2.3(f)) the first crack stress (for LOP) coincides with the peak stress. This can be due to continuous fibres orientated in the principal loading direction (0°) giving a combined efficiency factor (η) of 1.0, as discussed in Sub-section 7.3.2.

- 3- Of the seven materials reinforced with continuous fibres the six having carbon fibres gave an FRC with much improved mechanical properties, in terms of post-cracking strength, strains and toughness (energy absorption). As discussed in Sub-sections 7.3.2 and 7.3.3 this is associated with continuous reinforcement having $l \gg l_c$ (for a fibre length efficiency factor, $\eta_l = 1.0$) and a $V_f > V_{f,crit}$. Improvement might also be attributed to an apparent increase in interfacial contact area between fibres and matrix and improved mechanical anchoring of the fabric and thereby, higher overall bond strength.
- 4- Test results show that the compression moulding FRCs with the modified fabrics containing strips of CF4 and CF5 were effective in maximising flexural strength. These FRCs give double the mean flexural strength at 75.2 and 70.2 MPa, respectively, compared to mean flexural strengths of 35 to 41 MPa for same materials in sheets form of CF4 and CF5, as reported in Section 7.5. This is attributed to the good cement penetration into the fabrics.
- 5- The most promising of the FRCs characterised in terms of strength is reinforced with hybrid fibres. This material has a relative high LOP and the best flexural performance in the post-cracking zone. Hybrid material produced by compression moulding gave the highest measured mean peak stress of 74.3 MPa. This property is found to be higher, by a factor of 8 (9.4 MPa), 6 (12.8 MPa) and 4 (21.2 MPa) than from the FRCs containing only the one type of reinforcement of CF3, PVA and CF8, respectively.

And as discussed in Section 7.6 this flexural strength is found to 10 times the mean of 7.5 MPa determined for the control material of matrix alone.

Chapter 8

8. Conclusions and Further Works

8.1 Conclusions

The conclusions of each aspect of the investigation have been collated and reported at the end of Chapters 3 to 7. This Chapter therefore provides a brief and succinct summary of the major conclusions from the research work. Main research findings, in context of the initial objectives, are given in what follows, together with cross reference to the relevant thesis section or sub-section where the new contribution is presented.

- 1) From the experimental results to optimise the pressing conditions in compression moulding process, it was found that increasing pressing parameters (pressure and duration) had a negligible positive effect (and in some cases even an adverse effect) on the strength of the FRC. Optimum pressing conditions were determined with a 9 MPa pressure applied for one minute (Sub-section 4.5.5).
- 2) One objective of the research had been to increase the maximum practically attainable fibre volume fraction (V_f) with either short or continuous fibre reinforcement. It proved impractical to overcome the poor workability of short fibre mixes when V_f is 4% or higher. It is concluded that to have a viable FRC material with the short fibre types used in this study, the maximum V_f is to be 2% (Sub-section 6.3.3). This limitation is due static electricity causing the short fibres to attract each other, thereby causing them to clump together into balls that lead to poor fibre dispersion (Sub-section 4.2). For this reason it was found to be difficult to get uniformity in the distribution of the short fibres throughout the matrix.

- 3) It is found from the literature that the processing method of compression moulding is novel for producing FRC materials and has not previously been thoroughly investigated. This method for processing short and continuous FRCs is shown to be successful in improving the quality of green form material. This is because it minimises porosity, by increasing the degree of consolidation and lowering the water/binder ratio compared to the hand lay-up process (Sections 6.4 and 7.7). This is attributed to the applied pressure of 9 MPa during processing. Furthermore, compression moulding improves the penetration of the cement matrix into the fabric of the continuous reinforcements, by squeezing/forcing the matrix particles into openings in the fabric. However, the results of flexural properties of FRC showed that the beneficial of the compression moulding process over the hand lay-up is not significant.
- 4) The results show that the contribution of short fibres to the mechanical properties of FRCs is likely to be smaller and less efficiency than for continuous fibres. Furthermore, the vast majority of the stress-strain curves for short fibre FRCs, except with the polyvinyl alcohol (PVA) fibre type, exhibited strain-softening behaviour. Their response can be attributed to; low fibre volume fraction; poor dispersion of fibres; fibre length not long enough for FRC to achieve maximum strength; poor bond strength between the fibres and matrix (Sub-section 6.3.8).
- 5) Because the use of recycled milled carbon fibre (CF1) is novel there are no other results in the literature to compare with new FRC test results. Based on the test results obtained no benefit in mechanical properties is found when adding recycled milled carbon fibre (Sub-section 6.3.4). The testing has shown that short fibres were unable to carry additional load after the matrix started to crack under tension from the flexural deformation. Brittle failure is present because of: insufficient fibre length (typically

0.085 mm) in the FRC for the stress to reach the maximum practical; a lower V_f than the critical volume value; a lack of uniform fibre dispersion for the reason given in 2 above. As a consequence of poor fibre properties, it can be concluded that the overall bond strength between fibres and the matrix is relatively weak. Moreover, the hydrophobic nature of the carbon fibres and their low affinity for the cement paste makes the transfer of stress between fibres and matrix even more unreliable and discontinuous.

- 6) Of the five FRCs having short fibres the application of polyvinyl alcohol (PVA) fibres with the compression moulding process gave the largest improvement in mechanical properties as determined by flexural testing. This material possesses post-cracking strength, and improved capacities in strain at peak stress and energy absorption. Furthermore, the PVA FRCs exhibited strain-hardening behaviour with multiple cracking and fibre fracturing was found at ultimate failure (Sub-section 6.3.7). This is because the PVA fibres give a FRC the ability to carry more stress after matrix cracking; this short fibre reinforcement imparts post-cracking strength. The three reasons for this favourable finding are that: there is a good dispersion of fibres (distributed uniformly); is a relatively good bond between the PVA fibres and matrix; the mean fibre length at 8 mm is at least two times the critical length for effective fibre reinforcement (Sub-section 6.3.7). It is believed the relatively high bond strength is due to a combination of the hydrophilic nature of PVA and the fibres' surface roughness. Fibrils and rough surfaces mean there can be a relatively high friction mechanism between fibres and matrix (Sub-section 6.3.7). It is concluded that the materials reinforced with short PVA fibres might have applications as a building

construction material in thin sheets, corrugated sheets, cladding, concrete pipes, facades, parapet sheets, water tanks, and industrial flooring.

- 7) In this study a V_f of 15% with continuous fibres was reached using hand lay-up processing. However, this FRC gave a significant reduction in flexural strength at 3.6 MPa and there were severe delamination failures between the reinforcement and matrix layers from a lack of matrix thickness between two layers of fabric. The key finding from the study in Sub-section 7.3.3 is that, with V_f equal to 5%, a mean flexural strength of 43 MPa is nearly twelve times higher than the FRC with V_f at 15%. It was decided to continue work with continuous reinforcement types having V_f set constant at 5%.
- 8) In continuous fibre FRCs the stress-strain curves can exhibit strain-hardening behaviour with multiple cracking (Section 2.3). This is due to higher fibre efficiency because; fibre length exceeds the critical length; orientation can be aligned parallel to the applied flexural stress load; 5% V_f is higher than the critical volume; there is increase strength from mechanical interlocking. These four features result in greater contact area between the fibres and matrix resulting in increase of bond strength.
- 9) Flexural test results in Chapter 7 with three FRCs having unidirectional continuous reinforcement types of carbon fibre (CF4, CF5 and CF6) (Sub-section 7.3.5) gave the desired 'unusual' composite action defined by stress-strain curve (f) in Figure 2.3(f). This behaviour has been rarely encountered in the past. It is found that there is effectively a linear curve up to peak stress, rather than the usual two or three-stage curve (with Regions II and III in the ACK model). Matrix tensile crack width/spacing is so small that it cannot be seen. The change in response makes it difficult to establish the first-crack stress (for Loss of Proportionality) from the shape of the stress-strain

curve. This desirable response may be attributed to the following five reasons of; the high stiffness of carbon fibres; the fibre length exceeding the critical length; a favourable fibre orientation allowing reinforcement to be fully effectively; V_f being 17 higher than the critical value (Sub-section 7.3.3); mechanical anchoring developed from matrix penetration into openings in a fabric.

- 10) Of the seven fabric reinforcements studied, the six having carbon fibres gave a FRC with greatly improved mechanical properties, in terms of the post-cracking strength and toughness (Section 7.4). This enhancement in mechanical properties determined by flexural testing is associated with good overall matrix penetration.
- 11) Given that the fabric reinforcements are primarily for reinforcement with polymer resin matrix the author decided to take two of the carbon fibre fabrics and, before FRC processing, either to cut them into strips or apply a surface treatment by immersing in Ethanol alcohol. The strip reinforced FRC made by compression moulding achieved a flexural strength of 75 MPa (Section 7.5), and this is nearly a doubling of what was determined with the same reinforcement without treatment. It is noteworthy that the flexural strength of this FRC material is 10 times that of the unreinforced matrix and might be attributed to the interfacial bond strength created from good matrix penetration into the modified unidirectional fabric and across the fabric due to enhancing the chemical affinity between the fibres and the matrix by creating surface roughening that gives mechanical interlocking for surface treatment proposal.
- 12) Reinforcements for the hybrid FRC comprised of the biaxial carbon fabric (CF8) and the two short fibres of PVA having mean length of 8 mm and of carbon (CF3) having mean length of 6 mm. This particular FRC is novel, and was found to give the highest stress at first matrix cracking and improved flexural performance in the post-cracking

zone compared with those containing only one type of reinforcement. The hybrid FRC achieved a mean flexural strength of 74 MPa by compression moulding and 68 MPa by hand lay-up process (Section 7.6). The improvement is attributed to the presence of shorter fibres being able to bridge the onset of micro-cracks, and when their bonding fails the CF8 fabric maintains the bridging for a flexural strength of about 70 MPa.

- 13) From the experimental results in Chapter 7 it can be concluded that the FRCs reinforced with continuous carbon fibre fabrics might have applications as a building construction material in thin sheets, cladding, concrete pipes, facades, parapet sheets, water tanks, and industrial flooring.

8.2 Further Works

Further investigations are recommended and should be carried out to characterise the portfolio of mechanical properties for having building products of FRC material. Several recommendations for further studies are mentioned below:

- 1) Only the flexural response of FRC materials has been investigated. New experimental tests with practical FRCs are needed to characterise pull-out, tensile strength and impact resistances.
- 2) Work is required at the interface level to understand the nature of the bond between cementitious matrices and the fibres. LOP and at peak stress?
- 3) Why we measure the toughness at
- 4) The PhD work has shown that the manufacturing processes of hand lay-up and compression moulding can be successfully used to manufacture FRCs having a fibre volume fraction of 5%. Further work is needed to find out if the maximum volume

fraction and mechanical properties can be higher with other manufacturing process, such as pultrusion or extrusion.

- 5) It will be necessary before any exploitation is feasible of a promising FRC material to conduct studies that will characterise the long-term durability. Without us knowing if a FRC will retain adequate mechanical and other properties over the service life the material cannot be used to manufacture building products.

9. Bibliography

AASHTO T26- 79 (2004), "Standard Method of Test for Quality of Water to be Used in Concrete", (Twelfth ed.), *American Association of State Highway and Transportation Officials, AASHTO Designation T 26-79*, Washington, USA.

Akihama, S., Suenaga, T. and Bann, T. (1986), "Mechanical Properties of Carbon Fibre Reinforced Cement Composites", *The International Journal of Cement Composites and Lightweight Concrete*, Volume 8, Issue 1, pp. 21-33.

Akkaya, Y., Peled, A. and Shah, S. (2000), "Parameters Related to Fibre Length and Processing in Cementitious Composites", *Materials and Structures*, Volume 33, Issue 232, pp. 515-524.

Aldea, C., Marikunte, S. and Shah, S. (1998), "Extruded Fibre Reinforced Cement Pressure Pipe", *Advanced Cement Based Materials*, Volume 8, Issue 2, pp. 47-55.

Aligizaki, K. (2006), "*Pore Structure of Cement Based Materials; Testing, Interpretation and Requirements*", Taylor and Francis, 1st Edition, 432 Pages.

Asano, K. and Kanakubo, T. (2012), "Study on Size Effect in Bond Splitting Behaviour of ECC", *High Performance Fibre Reinforced Cement Composites 6, RILEM State of the Art Reports*, Volume 2, pp. 137-144.

ASTM C143/C143M-10a (2010), "*Standard Test Method for Slump of Hydraulic Cement Concrete*".

Atis, C. (2003), "High-Volume Fly Ash Concrete with High Strength and Low Drying Shrinkage", *Journal of Materials in Civil Engineering*, Volume 15, Issue 4, pp. 153-156.

Atis, C. (2004), "Carbonation-Porosity-Strength Model for Fly Ash Concrete", *Journal of Materials in Civil Engineering*, Volume 16, Issue 1, pp. 91-94.

Aveston, J., Cooper, G. and Kelly, A. (1971), "Single and Multiple Fracture", *Proceeding of NPL Conference*", *The Properties of Fibre Composites*, UK, IPC Science and Technology Press, pp. 15-27.

- Aveston, J. and Kelly, A. (1973), "Theory of Multiple Fracture of Fibrous Composites", *Journal of Materials Science*, Volume 8, Issue 3, pp. 352-362.
- Aveston, J., Mercer, R. and Sillwood, J. (1974), "Fibre Reinforced Cements- Scientific Foundations for Speculations", *In: Proceedings of the Composites Standards Testing and Design, National Physical Laboratory Conference*, UK, IPC Science and Technology Press, Guildford, pp. 93-103.
- Awasare, V. and Nagendra, M. (2014), "Analysis of Strength Characteristics of GGBS Concrete", *International Journal of Advanced Engineering Technology*, Volume V, Issue II, pp. 82-84.
- Badanoiu, A. and Holmgren, J. (2003), "Cementitious Composites Reinforced with Continuous Carbon Fibres for Strengthening of Concrete Structures", *Cement and Concrete Composites*, Volume 25, Issue 3, pp. 387-394.
- Bagel, L. (1998), "Strength and Pore Structure of Ternary Blended Cement Mortars Containing Blast Furnace Slag and Silica Fume", *Cement and Concrete Research*, Volume 28, Issue 7, pp. 1011-1020.
- Balaguru, P. and Shah, S. (1992), "*Fibre Reinforced Cement Composites*", McGraw- Hill. New York, USA, 535 Pages.
- Banfill, P., Starrs, G., Derruau, G., McCarter, W. and Chrisp, T. (2006), "Rheology of Low Carbon Fibre Content Reinforced Cement Mortar", *Cement and Concrete Composites*, Volume 28, Issue 9, pp. 773-780.
- Banholzer, B. (2004), "*Bond Behaviour of a Multi-Filament Yarn Embedded in A Cementitious Matrix*", PhD thesis, RWTH Aachen University, Germany.
- Banthia, N. and Sheng, J. (1996), "Fracture Toughness of Micro-Fibre Reinforced Cement Composites", *Cement and Concrete Composite*, Volume 18, Issue 4, pp. 251-69.
- Banthia, N., Yan, C. and Sakai, K. (1998), "Impact Resistance of Fibre Reinforced Concrete at Subnorma Temperatures", *Cement and Concrete Composites*, Volume 20, Issue 5, pp. 393-404.

- Barnett, S., Soutsos, M., Millard, S. and Bungey, J. (2006), "Strength Development of Mortars Containing Ground Granulated Blast-Furnace Slag: Effect of Curing Temperature and Determination of Apparent Activation Energies", *Cement and Concrete Research*, Volume 36, Issue 3, pp. 434-440.
- Bartos, P. (1980), "Analysis of Pull-out Tests on Fibres Embedded in Brittle Matrices", *Journal of Materials Science*, Volume 15, Issue 12, pp. 3122-3128.
- Bartos, P. (1985), "Effects of Changes in Fibre Strength and Bond Characteristics Due to Ageing on Fracture Mechanism of GRC", In: *Proceedings of the 12th International Symposium on Durability of Glass Fibre Reinforced Concrete*, Edited by Diamond, S., PCI, Illinois, USA, pp. 136-146.
- Bartos, P. and Zhu, W. (1996), "Effect of Microsilica and Acrylic Polymer Treatment on the Ageing of GRC", *Cement and Concrete Composites*, Volume 18, Issue 1, pp. 31-39.
- Bascoul, A. (1996), "State of the Art Report- Part 2: Mechanical Micro-Cracking of Concrete", *Materials and Structures*, Volume 29, Issue 2, pp 67-78.
- Bazant, Z. (1976), "Instability, Ductility, and Size Effect in Strain-Softening Concrete", *Journal of Engineering Mechanics*, Volume 102, Issue 2, pp. 331-344.
- Bazant, Z. and Oh, B. (1983), "Crack Band Theory for Fracture of Concrete", *Materials and Structures*, Volume 16, Issue 93, pp.155-177.
- Bazant, Z. (2002), "Concrete Fracture Models: Testing and Practice", *Engineering Fracture Mechanics*, Volume 69, Issue 2, pp. 165-205.
- Beaudoin, J. and Feldman, R. (1978), "The Significance of Helium Diffusion Measurements in Studying the Removal of Structural Water in Inorganic Hydrated Systems", *Cement and concrete Research*, Volume 8, Issue 8, pp. 223-231.
- Benmokrane, B., Wang, P., Ton-That, T., Rahman, H. and Robert, J. (2002), "Durability of Glass Fibre Reinforced Polymer Reinforcing Bars in Concrete Environment", *Journal of Composite for Construction*, Volume, 6, Issue 2, pp. 143-153.

Bentur, A. (1989), "Fibre-Reinforced Cementitious Materials", in '*Material Science of Concrete*', The American Ceramic Society, OH, U.S.A. pp. 223-285.

Bentur, A. and Diamond, S. (1985), "Effects of Direct Incorporation of Microsilica into GFRC Composites on Retention of Mechanical Properties After Ageing", In: *Proceedings of the Durability of Glass fibre Reinforced Concrete Symposium*, Illinois, USA, pp. 337-351.

Bentur, A., and Mindess, S. (2007), "*Fibre Reinforced Cementitious Composites*", 2nd Edition. London, UK, 625 Pages.

Bentz, D. and Aitcin, P. (2008), "The Hidden Meaning of Water-Cement Ratio: Distance Between Cement Particles is Fundamental", *Concrete International*, Volume 30, Issue 5, pp. 51-54.

Betterman, L., Ouyang, C. and Shah, S. (1995), "Fibre-Matrix Interface in Microfibre-Reinforced Mortar", *Advanced Cement Based Materials*, Volume 1, Issue 2, pp. 53-61.

Biryukovich, K., Biryukovich, Y. and Biryukovich, D. (1964), "Glass Fibre Reinforced Cement" (Kiev, Budivelinik); Translated from the Russian by G.L. Cairns, *CERA translation No 12, Civil Engineering Research Association*, London (1965).

Blom, J., Van-Ackeren, J. and Wastiels, J. (2012), "Determination of Material Parameters of Textile Reinforced Cementitious Composite Exposed to High Temperatures Using an Inverse Method", In: *Proceedings of the 15th European Conference on Composite Materials*, Venice, Italy, pp. 24-28.

Blom, j. and Wastiels, J. (2013), "Modelling Textile Reinforced Cementitious Composites - Effect of Elevated Temperatures", In: *Proceedings of the 19th International Conference on Composite Materials (ICCM)*, Volume: 19, Montreal, Canada, pp. 1-10.

Brameshuber, W., Brockmann, T., Mobasher, B., Pachow, U., Peled, A., Reinhardt, H., Kruger, M. and Wastiels, J. (2006), "Production Technologies, Chapter 5, Textile Reinforced Concrete" - *State-of-the-Art Report of RILEM TC 201-TRC*, RILEM Publications SARL, pp. 57-81.

Brandt, A. (2008), "Fibre Reinforced Cement-Based (FRC) Composites after over 40 Years of Development in Building and Civil Engineering", *Composite Structures*, Volume 86, Issues 1-3, pp. 3-9.

Brandt, A. (2009), "*Cement-Based Composites: Materials, Mechanical Properties and Performance*", 2nd Edition, CRC Press, 535 pages.

Briggs, A. (1977), "Review: Carbon Fibre Reinforced Cement", *Journal of Materials Science*, Volume 12, Issue 2, pp. 384-404.

Brighenti, R., Carpinteri, A., Spagnoli, A. and Scorza, D. (2012), "Crack Paths in Unidirectional Fibre-Reinforced Brittle Matrix Materials through Two Computational Models", *In: Proceedings of the 4th International Conference on Crack Paths*, Gaeta, Italy, pp. 303-310.

Broek, D. (1989), "*The practical Use of Fracture Mechanics*", Kluwer Academic Published, The Netherlands, 522 Pages.

BS 3148-1980, (1980), "Method for Test for Water for Making Concrete", *British Standard Institution*.

BS 812-105.1:1989, (1989), "Testing Aggregates: Methods for Determination of Particle Shape", Flakiness Index, *British Standard Institution*.

BS 882-1992, (1992), "Specification for Aggregates from Natural Sources for Concrete", *British Standard Institution*.

BS 6699:1992, (1992), "Specification for Ground Granulated Blast Furnace Slag for Use with Portland Cement", *British Standard Institution*.

BS EN 197-1:2000, (2000), "Cement, Composition, Specifications and Conformity Criteria for Common Cements)", *British Standard Institution*.

BS 410-1:2000, ISO 3310-1:2000, (2000), "Test Sieves, Technical Requirements and Testing", *British Standard Institution*.

BS EN 1990:2002, (2002), "Eurocode, Basis of Structural Design: Annex D", *British Standard Institution*.

BS EN 1008:2002, (2002), "Mixing Water for Concrete -Specification for Sampling, Testing and Assessing the Suitability of Water, Including Water Recovered From Processes in the Concrete Industry, as Mixing Water for Concrete", *British Standard Institution*.

BS EN 15167-1:2006, (2006), "Ground Granulated Blast Furnace Slag for Use in Concrete, Mortar and Grout: Definitions, Specifications and Conformity Criteria", *British Standard Institution*.

BS EN 450-1:2005+A1:2007, (2007), "Fly Ash for Concrete: Definition, Specifications and Conformity Criteria", *British Standard Institution*.

BS EN 13263-1:2005+A1 2009, (2009), "Silica Fume for Concrete: Definitions, Requirements and Conformity Criteria", *British Standard Institution*.

BS EN 934-2:2009, (2009), "Admixtures for Concrete, Mortar and Grout - Part 2: Concrete Admixtures", *British Standard Institution*.

BS EN 12350-2:2009, (2009), "Testing Fresh Concrete- Part 2: Slump Test. Tensile, Flexural and Compression Types (Constant Rate of Traverse) - Specification", *British Standard Institution*.

BS ISO 5893:2002, (2002), "Rubber and Plastics Test Equipment", *British Standard Institution*.

Budiansky, B., Hutchinson J. and Evans, A. (1986), "Matrix Fracture in Fibre-Reinforced Ceramics", *Journal of Mechanics and Physics of Solids*, Volume 34, Issue 2, pp. 167-189.

Buendia, A., Sanchez, M., Climent, V. and Guillem, C. (2013), "Surface Treated Polypropylene (PP) Fibres for Reinforced Concrete", *Cement and Concrete Research*, Volume 54, pp. 29-35.

Carette, G. and Malhotra, V. (1983), "Mechanical Properties, Durability, and Drying Shrinkage of Portland Cement Concrete Incorporating Silica Fume", *Cement, Concrete, and Aggregates, CCAGDP*, Volume 5, Issue 3, pp. 3-13.

- Carette, G. and Malhotra, V. (1987), "Characterization of Canadian Fly Ashes and Their Performance in Concrete", *Canadian Journal of Civil Engineering*, Volume 14, Issue 5, pp. 667-682.
- Carpinteri, A. and Massabo, R. (1997), "Continuous vs Discontinuous Bridged- Crack Model for Fibre-Reinforced Materials in Flexure", *International Journal of Solids and Structures*, Volume 34, Issue 18, pp. 2321-2338.
- Carrasco, L., Claramunt, J. and Ardanuy, M. (2014), "Autoclaved Cellulose Fibre Reinforced Cement: Effects of Silica Fume", *Construction and Building Materials*, Volume 66, pp. 138-145.
- Chen, P. and Chung, D. (1993), "Concrete Reinforced With up to 0.2 Vol% of Short Carbon Fibres", *Composites*, Volume 24, Issue 1, pp. 33-52.
- Chen, P., Fu, X. and Chung, D. (1997), "Microstructural and Mechanical Effects of Latex, Methylcellulose, and Silica Fume on Carbon Fibre Reinforced Cement", *ACI Materials Journal*, Volume 94, Issue 2, pp. 147-155.
- Chuang, W., Ke-Zhi, L., He-Jun, L., Geng-Sheng, J., Jinhua, L. and Dang-She, H. (2008), "Effect of Carbon Fibre Dispersion on the Mechanical Properties of Carbon Fibre-Reinforced Cement-Based Composites", *Materials Science and Engineering A*, Volume 487, Issue 1-2, pp. 52-57.
- Chung, D. (1992), "Carbon Fibre Reinforced Concrete", *Report No. SHRP-ID/UFR 92605, Strategic Highway Research Program (SHRP), National Research Council Washington, No. 92, Washington, USA.*
- Chung, D. (2000), "Cement Reinforced With Short Carbon Fibres: A Multifunctional Material", *Composites Part B: Engineering*, Volume 31, Issues 6-7, pp. 511-526.
- Chung, D. (2002), "Improving Cement-Based Materials by Using Silica Fume", *Journal of Materials Science*, Volume 34, Issue 10, pp. 673-682.
- Chung, D. (2005), "Dispersion of Short Fibres in Cement", *Journal of Materials in Civil Engineering*, Volume 17, Issue 4, pp. 379-383.

- Cooper, J. (1998), "Particle size Analysis- The Laser Diffraction Technique", *Materials World*, Volume 6, Issue 1, pp. 5-7.
- Cox, H. (1952), "The Elasticity and Strength of Paper and Other Fibrous Materials", *British Journal of Applied Physics*, Volume 3, Issue 3, pp. 72-79.
- Currie, B. and Gardiner, T. (1989), "Bond Between Polypropylene Fibres and Cement Matrix", *The International Journal of Cement Composites and Lightweight Concrete*, Volume 11, Issue 1, pp. 3-9.
- Curtin, W. (1999), "Stochastic Damage Evolution and Failure in Fibre-Reinforced Composites", *Advances in Applied Mechanics*, Volume 36, pp. 163-253.
- Cuypers, H. (2002), "*Analysis and Design of Sandwich Panels with Brittle Matrix Composite Faces for Building Applications*", PhD thesis, Vrije University Brussel, Belgium.
- Cuypers, H. and Wastiels, J. (2006), "Stochastic Matrix-Cracking Model for Textile Reinforced Cementitious Composites under Tensile Loading", *Materials and Structures*, Volume 39, Issue 292, pp. 777-786.
- Cuypers, H., Wastiels, J., Van-Itterbeeck, P., De Bolster, E., Orlowsky, J. and Raoach, M. (2006), "Durability of Glass Fibre Reinforced Composites Experimental Methods and Results", *Composites: Part A*, Volume 37, Issue 2, pp. 207-215.
- Da Silva, A., Proenca, S., Billardon, R., and Hild, F. (2004), "Probabilistic Approach to Predict Cracking in Lightly Reinforced Microconcrete Panels", *Journal of Engineering Mechanics*, Volume 130, Issue 8, pp. 931-941.
- Daniel, J., Roller, J. and Anderson, E. (1998), "*Fibre Reinforced Concrete*", Portland Cement Association, Chapter 5, pp. 22-26.
- Deng, Z. (2005), "The Fracture and Fatigue Performance in Flexure of Carbon Fibre Reinforced Concrete", *Cement and Concrete Composites*, Volume 27, Issue 1, pp. 131-140.

- Denneman, E. (2011), "*Fracture in High Performance Fibre Reinforced Concrete Pavement Materials*", PhD Thesis, University of Pretoria, South Africa.
- Domone, P. and Illston, J. (2010), "*Construction materials: Their Nature and Behaviour*", 4th Edition, Spoon Press, 584 Pages.
- Duchesne, J. and Berube, M. (1994), "Available Alkalies from Supplementary Cementing Materials", *Aci Materials Journal*, Volume 91, Issue 3, pp. 289-299.
- Elahi, A. (2009), "*Properties of High Performance Concrete with Supplementary Cementitious Materials*", Ph.D Thesis, University of Engineering & Technology, Pakistan.
- El-Hadj, K. and Duval, R. (2009), "Hydration Heat Kinetics of Concrete With Silica Fume", *Construction and Building Materials*, Volume 23, Issue 11, pp. 3388-3392.
- Esfahani, M. (2007), "*Fracture Mechanics of Concrete*", Tehran, Iran: Tehran Polytechnic Press.
- Ezeokonkwo, J. and Nwoji, C. (2011), "Uniaxial Compressive Strength of Polypropylene Fibre Reinforced Sandcrete Cubes", *Journal of Emerging Trends in Engineering and Applied Sciences (JETEAS)*, Volume 2, Issue 6, pp. 1020-1025.
- Farahi, E. (2009), "*Advanced Calcareous Ceramics via Novel Green Processing and Super-Critical Carbonation*", PhD Thesis, University of Warwick.
- Felekoglu, B., Tosun, K. and Baradan, B. (2009), "Effects of Fibre Type and Matrix Structure on the Mechanical Performance of Self Compacting Micro-Concrete Composites", *Cement and Concrete Research*, Volume 39, Issue 11, pp. 1023-1032.
- Fidelis, M., Pereira, T., Gomes, O., Silva, F. and Filho, R. (2013), "The Effect of Fibre Morphology on The Tensile Strength of Natural Fibres", *Journal of materials Research Technology*, Volume 2, Issue 2, pp. 149-157.
- Filho, T. and Sanjuan, M. (1999), "Effect of Low Modulus Sisal and Polypropylene Fibre on The Free And Restrained Shrinkage of Mortars at Early Age", *Cement and Concrete Research*, Volume 29, Issue 10, pp. 1597-1604.

- Fu, X. and Chung, D. (1995), "Contact Electrical Resistivity between Cement and Carbon Fibre: Its Decrease with Increasing Bond Strength and its Increase During Fibre Pull-out", *Cement and Concrete Research*, Volume 25, Issue 7, pp. 1391-1396.
- Fu, X., Lu, W. and Chung, D. (1996), "Improving the Bond Strength between Carbon Fibre and Cement by Fibre Surface Treatment and Polymer Addition to Cement Mix", *Cement and Concrete Research*, Volume 26, Issue 7, pp. 1007-1012.
- Fu, X. and Chung, D. (1998), "Improving the Bond Strength of Concrete to Reinforcement by Adding Methylcellulose to Concrete", *ACI Materials Journal*, Volume 95, Issue 5, pp. 601-608.
- Gadpalliwar, S., Deotale, R. and Narde, A. (2014), "To Study the Partial Replacement of Cement by GGBS & RHA and Natural Sand by Quarry Sand in Concrete", *IOSR Journal of Mechanical and Civil Engineering (IOSR-JMCE)*, Volume 11, Issue 2, pp. 69-77.
- Gambhir, M. (2006), *Concrete Technology*, Third Edition, Tata McGraw-Hill, 532 Pages.
- Garces, P., Fraile, J., Vilaplana, O., Cazorla, A., Alcocelc, E. and Andion, L. (2005), "Effect of Carbon Fibres on the Mechanical Properties and Corrosion Levels of Reinforced Portland Cement Mortars", *Cement and Concrete Research*, Volume 35, Issue 2, pp. 324-331.
- Gdoutos, E. (2005), *Cementitious Materials*, Chapter 14, Fracture Mechanics: An Introduction (Solid Mechanics and Its Applications), 2nd edition, Springer, pp 353-366.
- Gelman, A. (2013), "P-Values and Statistical Practice", *Epidemiology*, Volume 24, Issue 1, pp. 69-72.
- Gilbert, G. (2004), "GFRC-30 Years of High Fibre Cement Composite Applications Worldwide", *ACI Special Publications*, Volume 224, pp. 2-20.
- Gopalaratnam, V. and Shah, S. (1987), "Failure Mechanisms and Fracture of Fibre Reinforced Concrete, Fibre Reinforced Concrete Properties and Applications", *SP-105, American Concrete Institute, Detroit*, pp. 1-25.

- Griffith, A. (1921), "The Phenomena of Rupture and Flow in Solids", *Philosophical Transactions of Royal Society*, London, A221, pp. 163-198.
- Gulvanessian, H., Galgaro, J., and Holicky, M. (2002), "*Designers' Guide to EN 1990 Eurocode: Basic of Structural Design*", Thomas Telford, London.
- Gurit (2011), "*Guide to Composites*", Report No. GTC-3-0509 <http://www.gurit.com/guide-to-composites.aspx>, [Accessed 08 November 2011].
- Haddad, R. and Smadi, M. (2004), "Role of Fibres in Controlling Unrestrained Expansion and Arresting Cracking in Portland Cement Concrete Undergoing Alkali-Silica Reaction", *Cement and Concrete Research*, Volume 34, Issue 1, pp. 103-108.
- Hanjari, K. (2006), "*Evaluation of WST Method as a Fatigue Test for Plain and Fibre Reinforced Concrete Experimental and Numerical Investigation*", MSc Thesis, Chalmers University of Technology, Goteborg, Sweden.
- Hannant, D. (1978), "*Fibre Cements and Fibre Concretes*", Chichester, John Wiley and Sons, Ltd., New York, 219 Pages.
- Hannant, D. and Hughes, D. (1986), "Durability of Cement Sheets Reinforced with Layers of Continuous Networks of Fibrillated Polypropylene Film", In: Swamy, R., Wagstaffe, R. and Oakley, D. (eds) *Developments in Fibre Reinforced Cement and Concrete, Proceedings of the RILEM Symposium*, University of Sheffield, Sheffield, Paper 7.8.
- Harris, B. (1999), "*Engineering Composite Materials*", The Institute of Materials, London, 193 Pages.
- Haupt, G. (1997), "*Study of Cement Based Composites Manufactured by Extrusion, Compression Moulding and Filament Winding*", Msc Thesis, Arizona State University, USA.
- Hegger, J., Bentur, A., Curbach, M., Mobasher, B., Peled, A. and Wastiels, J. (2006), "Mechanical behaviour of textile reinforced concrete, Chapter 6, Textile Reinforced Concrete" - *State-of-the-Art Report of RILEM TC 201-TRC. RILEM Publications SARL*, pp. 133-186.

- Hibbertand, A. and Hannant, D. (1982), "Toughness of Fibre Cement Composites", *Composites*, Volume 13, Issue 2, pp. 105-111.
- Hillerborg, A., Modeer, M. and Petersson, P. (1976), "Analysis of Crack Formation and Crack Growth in Concrete by Means of Fracture Mechanics and Finite Elements", *Cement and Concrete Research*, Volume 6, Issue 6, pp. 773-781.
- Hillerborg, A. (1980), "Analysis of Fracture by Means of the Fictitious Crack Model, Particularly for Fibre Reinforced Concrete", *The International Journal of Cement Composites*, Volume 2, Issue 4, pp., 177-184.
- Hofstetter, G. and Meschke, G. (2011), "*Numerical Modeling of Concrete Cracking*", Springer, 328 Pages.
- Htut, T. and Foster, S. (2010), "Unified Model for Mixed Mode Fracture of Steel Fibre Reinforced Concrete", *In: Proceedings of the 7th International Conference on Fracture Mechanics of Concrete and Concrete Structures*, Korea, pp. 1469-1477.
- Huang, X. (2009), "Fabrication and Properties of Carbon Fibres", *Materials*, Volume 2, Issue 4, pp. 2369-2403.
- Idiart, A. (2009), "*Coupled Analysis of Degradation Processes in Concrete Specimens at the Meso-Level*", PhD Thesis, Polytechnic University of Catalonia, Barcelona, Spain.
- Inagaki, M. (1991), "Research and Development on Carbon/Ceramic Composites in Japan", *Carbon*, Volume 29, Issue 3, pp. 287-295.
- Irwin, G. (1957), "Analysis of Stresses and Strain Near the End of a Crack Traversing a Plate", *Journal of Applied Mechanics, A.S.M.E.*, Volume 24, pp. 361-364.
- Ismeik, M. (2010), "Environmental Enhancement through Utilization of Silica Fume as a Partial Replacement of Fine Aggregate in Concrete", *Journal of Civil Engineering Research and Practice*, Volume 7, Issue 2, pp. 11-21.
- Jenq, Y. and Shah, S. (1985), "Two Parameter Fracture Model for Concrete", *Journal of Engineering Mechanics, ASCE*, Volume 111, Issue 10, pp. 1227-1241.

- Johnson, C. (2001), "*Fibre Reinforced Cements and Concretes*", Gordon and Research Science Publishers, 372 Pages.
- Kakemi, M., Hannant, D. and Mulheron, M. (1996), "Techniques for Determining Some Microstructural Parameters in Glass Reinforced Cement", *Magazine of Concrete Research* Volume 48, Issue 176, pp. 229-236.
- Kalliopi, K. (2006), "*Pore Structure of Cement Based Materials; Testing, Interpretation and Requirements*", Taylor and Francis, 1st Edition, 432 Pages.
- Kamiura, M. (2010), "Toray's Strategy for Carbon Fibre Composite Materials", *Toray Industries, Inc. 3rd IT-2010 Strategy seminar (Carbon Fibre Composite Materials) Presentation*.
- Kanda, T. and Li, V. (1998), "Interface Property and Apparent Strength of High-Strength Hydrophilic Fibre in Cement Matrix", *Journal of Materials in Civil Engineering*, Volume 10, Issue 1, pp. 5-13.
- Kanellopoulos, A. (2004), "*Autogenous Shrinkage of CARDIFRC*", PhD Thesis, Cardiff University, UK.
- Kannadaguli, M., Rong, H., Hegde R., Dahiya, A. and Kamath, M. (2004), "Carbon Fibres", <http://web.utk.edu/~mse/pages/Textiles/CARBON%20FIBERS.htm> [Accessed 03 August 2010].
- Kaplan, M. (1961), "Crack Propagation and the Fracture of Concrete", *ACI Journal*, Volume 58, Issue 5, pp.591-610.
- Kar, J. and Pal, A. (1972), "Strength of Fibre-Reinforced Concrete", *American Society of Civil Engineers [ASCE], Journal of the Structural Division*, Volume 98, Issue ST5, pp. 1053-1068.
- Karihaloo, B. (1995), "*Fracture Mechanics and Structural Concrete*", Longman Scientific & Technical, London, UK, 330 pages.

Katz, A., Li, V. and Kazmer, A. (1995), "Bond Properties of Carbon Fibres in Cementitious Matrix", *Journal of Materials in Civil Engineering*, Volume 7, Issue 2, pp. 125-128.

Katz, A. and Li, V. (1996), "A Special Technique for Determining the Bond Strength of Micro Fibres in Cement Matrix by Pull-out Test", *Journal of Material Science*, Volume 15, Issue 20, pp. 1821-1823.

Keller, T. (2003), "*Use of Fibre Reinforced Polymers in Bridge Construction*", First Edition, International Association for Bridge and Structural Engineering, Zurich, Switzerland, 131 Pages.

Khan, M., Lyndsedale, C. and Waldron, P. (2000), "Porosity and Strength of PFA/SF/OPC/Ternary Blended Paste", *Cement and Concrete Research*, Volume 30, Issue 8, pp. 1225-1229.

Khorami, M. (2011), "*Application of Natural and Synthetic Fibres as a Replacement for Asbestos Fibres in Cement Boards*", PhD thesis, Coventry University.

Kim, D., Naaman, A. and El-Tawil, S. (2008), "Comparative Flexural Behaviour of Four Fibre Reinforced Cementitious Composites", *Cement and Concrete Composites*, Volume 30, Issue 10, pp. 917-928.

Knott, J. (1973), "*Fundamental of Fracture Mechanics*", Butterworths, London, 286 pages.

Kolle, B. (2006), "*Behaviour of Steel Fibre Reinforced High Performance Concrete Under Biaxial Loading Conditions*", PhD thesis, University of Glasgow.

Konrad, M. (2008), "*Effect of Multifilament Yarn Crack Bridging on Uniaxial Behaviour of Textile Reinforced Concrete*", PhD Thesis, RWTH Aachen University, Germany.

Krenchel, H. (1964), "*Fibre Reinforcement: Theoretical and Practical Investigations of the Elasticity and Strength of Fibre-Reinforced Materials*", Akademisk Forlag, Copenhagen.

Kuder, K. and Shah, S. (2010), "Processing of High-Performance Fibre-Reinforced Cement-Based Composites", *Construction and Building Materials*, Volume 24, Issue 2, pp. 181-186.

- Kruger, M., Reinhardt, H. and Yong, X. (2003), "Sulphoaluminate Cement Matrices Used for Textile and Glass Fibre Reinforced Concrete Elements", *International Workshop High Performance Fibre Reinforced Cement Composites (RILEM Publications SARL)*, pp. 349-360.
- Krus, M., Hansen, K. and Hunzel, H. (1997), "Porosity and Liquid Absorption of Cement Paste", *Materials and structures*, Volume 30, Issue 201, pp. 394-398.
- Kullaa, J. (1994), "Constitutive Modelling of Fibre-Reinforced Concrete Under Uniaxial Tensile Loading", *Composites*, Volume 25, Issue 10, pp. 935-944.
- Kullaa, J. (1998), "*Constitutive Modelling of Fibre-Reinforced Brittle Materials*", PhD Thesis, Helsinki University of Technology, Finland.
- Kumar, S. and Barai, S. (2012), "*Concrete Fracture Models and Applications*", Springer, 406 Pages.
- Kumar, S. and Barai, S. (2012), "Size-Effect of Fracture Parameters for Crack Propagation in Concrete: A Comparative Study", *Computers and Concrete*, Volume 9, Issue 1, pp. 1-19.
- Kumar, S., Pandey, S. and Srivastava, A. (2013), "Analytical Methods for Determination of Double-K Fracture Parameters of Concrete", *Advances in Concrete Construction*, Volume 1, Issue 4, pp. 319-340.
- Larbi, J., Fraay, A. and Bijen, J. (1990), "The Chemistry of the Pore Fluid of Silica Fume Blended Cement Systems", *Cement and Concrete Research*, Volume 20, Issue 4, pp. 506-516.
- Larrinaga, P., Chastre, C., Biscaia, H. and San-Jose, J. (2014), "Experimental and Numerical Modelling of Basalt Textile Reinforced Mortar Behaviour under Uniaxial Tensile Stress", *Materials and Design*, Volume 55, pp. 66-74.
- Larson, B., Drzal, L. and Sorousian, P. (1991), "Carbon Fibre Cement Adhesion in Carbon Fibre Reinforced Cement Composites", *Construction & Building Materials*, Volume 5, Issue 2, pp. 83-92.

Laws, V. (1971), "The Efficiency of Fibrous Reinforcement of Brittle Matrices", *Journal of Physics D: Applied Physics*, Volume 4, Issue 11, pp. 1737-1746.

Laws, V. (1982), "Micromechanical Aspects of the Fibre-Cement Bond", *Composites*, Volume 13, Issue 2, pp. 145-151.

Li, M. and Li, V. (2012), "Rheology, Fibre Dispersion, and Robust Properties of Engineered Cementitious Composites", *Materials and Structures*, Volume 46, Issue 3, pp. 405-420.

Li, V., Wang, Y. and Backer, S. (1990), "Effect of Inclining Angle, Bundling and Surface Treatment on Synthetic Fibre Pull-out from a Cement Matrix", *Composites*, Volume 21, Issue 2, pp. 132-140.

Li, V. and Obla, K. (1994), "Effect of Fibre Length Variation on Tensile Properties of Carbon Fibre Cement Composites", *International Journal of Composite Engineering*, Volume 4, Issue 9, pp. 947-964.

Li, V. (2002), "Large Volume, High-Performance Applications of Fibres in Civil Engineering", *Journal of Applied Polymer Science*, Volume 83, Issue 3, pp. 660-686.

Li, V. and Stang, H. (1997), "Interface Property Characterization and Strengthening Mechanisms in Fibre Reinforced Cement Based Composites", *Advance Cement Based Materials*, Volume 6, Issue 1, pp. 1-20.

Li, V., Liu, A. and Leung, C. (2002), "PVA Polymer Modified Glass Fibre Reinforced Cementitious Composites", *ACI Materials Journal*, Volume 206, SP206-24, pp. 401-410.

Li, V. (2003), "On Engineered Cementitious Composites (ECC) -A Review of the Material and Its Applications", *Journal of Advanced Concrete Technology*, Volume 1, Issue 3, pp. 215-230.

Lin, Z., Kanda, T. and Li, V. (1999), "On Interface Property Characterization and Performance of Fibre Reinforced Cementitious Composites", *Concrete and Science Engineering*, Volume 1, pp. 173-184.

- Liu, B., Xie, Y., Zhou, S. and Yuan, Q. (2000), "Influence of Ultrafine Fly Ash Composite on the Fluidity and Compressive Strength of Concrete", *Cement and Concrete Research*, Volume 30, Issue 9, pp. 1489-1493.
- Lofgren, I. (2005), "*Fibre-Reinforced Concrete for Industrial Construction- A Fracture Mechanics Approach to Material Testing and Structural Analysis*", PhD Thesis, Chalmers University of Technology, Goteborg, Sweden.
- Lothenbach, B., Scrivener, K. and Hooton, R. (2011), "Supplementary cementitious materials", *Cement and Concrete Research*, Volume 41, Issue 12, pp. 1244-1256.
- Lu, W., Fu, X. and Chung, D. (1998), "A Comparative Study of the Wettability of Steel, Carbon, and Polyethylene Fibres by Water", *Cement and Concrete Research*, Volume 28, Issue 6, pp. 783-786.
- Luo, R., Cai, Y., Wang, C. and Huang, X. (2003), "Study of Chloride Binding and Diffusion in GGBS Concrete", *Cement and Concrete Research*, Volume 33, Issue 1, pp. 1-7.
- Ma, Y., Zhu, B. and Tan, M. (2005), "Properties of Ceramic Fibre Reinforced Cement Composites", *Cement and Concrete Research*, Volume 35, Issue 2, pp. 296-300.
- Machida, A. (1993), "State-of-the-Art Report on Continuous Fibre Reinforcing Materials", *Research Committee on Continuous Fibre Reinforcing Material, Concrete Engineering Series*. No.3. Ed., Japanese Society of Civil Engineers (JSCE), Tokyo, pp. 1-68.
- Majumdar, J. (1974), "The Role of the Interface in Glass Fibre Reinforced Cement", *Cement and Concrete Research*, Volume 4, Issue 2, pp. 247-266.
- Majumdar, J. and Laws, V. (1991), "*Glass Fibre Reinforced Cement*", Oxford, UK, BSP Professional Books, 208 Pages.
- Marikunte, S., Aldea, C. and Shah, S. (1997), "Durability of Glass Fibre Reinforced Cement Composites: Effect of Silica Fume and Metakaolin", *Advanced Cement Based Materials*, Volume 5, Issue 3-4, pp. 100-108.

- Metaxa, Z., Konsta-Gdoutos, M. and Shah, S. (2010), "Mechanical Properties and Nanostructure of Cement-Based Materials Reinforced with Carbon Nanofibers and Polyvinyl Alcohol (PVA) Microfibers", *ACI Committee 267 Special Publication: Advances in the Material Science of Concrete SP-270*, Ideker, J. and Radlinska, A. Editors, pp.115-124.
- Middendorf, B., Martirena, J., Gehrke, M. and Day, R. (2005), "Lime Pozzolan Binders: An Alternative to OPC", *In: Proceedings of the International Building Lime Symposium*, Orlando, Florida, USA.
- Mihai, I. (2012), "*Micromechanical Constitutive Models for Cementitious Composite Materials*", PhD Thesis, Cardiff University, UK.
- Miller, E. (1993), "Blended Cements-Applications and Implications", *Cement and Concrete Composites*, Volume 15, Issue 4, pp. 237- 245.
- Mindess, S. (1983), "The Fracture of Fibre Reinforced and Polymer Impregnated Concretes: A Review", *In Wittmann, F. (ed.) Fracture Mechanics of Concrete*, Elsevier Science Publishers, Amsterdam, pp. 481-501.
- Mobasher, B. and Shah, S. (1989), "Test Parameters in Toughness Evaluation of Glass Fibre Reinforced Concrete Panels", *ACI Materials Journal*, Volume 86, Issue 5, pp. 448-458.
- Mobasher, B., Stang, H., and Shah, S. (1990), "Microcracking in Fibre Reinforced Concrete", *Cement and Concrete Research*, Volume 20, Issue 5, pp. 665-676.
- Mobasher, B. and Li, C. (1996), "Mechanical Properties of Hybrid Cement-Based Composites", *ACI Materials Journal*, Volume 93, Issue 3, pp. 284-292.
- Mobasher, B., Pivacek, A. and Haupt, G. (1997), "Cement Based Cross-Ply Laminates", *Journal of Advanced Cement Based Materials*, Volume 6, Issues 3-4, pp. 144-152.
- Mobasher, B., Peled, A. and Jitendra, P. (2004), "Pultrusion of Fabric Reinforced High Fly Ash Blended Cement Composites", *Proceedings of the RILEM Technical Meeting*, BEFIB, pp. 1473-1482.

Mobasher, B., Pahilajani, J. and Peled, A. (2006(a)), "Analytical Simulation of Tensile Response of Fabric Reinforced Cement Based Composites", *Cement and Concrete Composites*, Volume 28, Issue 1, pp. 77-89.

Mobasher, B., Peled, A. and Pahilajani, J. (2006(b)), "Distributed Cracking and Stiffness Degradation in Fabric-Cement Composites", *Materials and Structures*, Volume 39, Issue 3, pp. 317-331.

Mobasher, B. (2011), "Development of Design Procedures for Flexural Applications of Textile Composite Systems Based on Tension Stiffening Models", *Proceedings of the 6th Colloquium on Textile Reinforced Structures (CTRS6)*, Joint Colloquium of the Collaborative Research Centres 528 (Dresden) and 532 (Aachen), Berlin, Germany, pp. 297-314.

Mumenya, S. (2007), "*Evaluation of Mechanical Properties of Textile Concrete Subjected to Different Environmental Exposures*", PhD Thesis, University of Cape Town, South Africa.

Naaman, A. and Najm, H. (1991), "Bond-Slip Mechanisms of Steel Fibres in Concrete", *ACI Materials Journal*, Volume 88, Issue 2, pp. 135-145.

Naaman, A., Namur, G., Alwan, J. and Najm, H. (1991), "Fibre Pull-out and Bond Slip II: Experimental Validation", *Journal of Structural Engineering*, Volume 117, Issue 9, pp. 2791-2800.

Naaman, A. and Reinhardt, H. (2006), "Proposed Classification of HPFRC Composites Based on Their Tensile Response", *Materials and Structures*, Volume 39, Issue 5, pp. 547-555.

Naaman, A. (2007), "Tensile Strain-Hardening FRC Composites: Historical Evolution since the 1960". In: *Advances in Construction Materials 2007*; Grosse, C. (editor), Berlin: Springer, pp. 181-202.

Naaman, A. (2008), "*High Performance Fibre Reinforced Cement Composites*", Chapter 3, in: Shi, C. and Mo Y. (editors), *High-Performance Construction Materials: Science and Applications*, World Scientific Publishing Co. Pte. Ltd., pp. 91-153.

- Nakagawa, H., Akihama, S., Suenaga, T., Taniguchi, Y. and Yoda, K. (1993), "Fibre Reinforced Concrete: Developments and Applications to Buildings", *Advanced Composite Materials*, Volume 3, Issue 2, pp. 123-131.
- Neville, A. (1995), "*Properties of concrete*", 4th Edition, Longman Group Limited, 864 Pages.
- Neville, A. (2001), "Seawater in the mixture", *ACI, Concrete International*, Volume 23, Issue 1, pp. 48-51.
- Neville, A. (2003), "*Neville on concrete*", Farmington Hills, Michigan, ACI International, 510 Pages.
- Nicolaides, D. (2004), "*Fracture and Fatigue of CARDIFRC*", PhD Thesis, Cardiff University, UK.
- Nili, M. and Afroughsabet, V. (2010), "The Effects of Silica Fume and Polypropylene Fibres on the Impact Resistance and Mechanical Properties of Concrete", *Construction and Building Materials*, Volume 24, Issue 6, pp. 927-933.
- Nilufer, O., Woo, L., Mu, B., Shah, S. and Mason, T. (2004), "Detection of Fibre Dispersion in Fresh and Hardened Cement Composites", *In: Workshop on Improving the Performance of Concrete Through Science and Engineering, RILEM Publications, Bagnoux, France*, pp. 1-12.
- Nishioka, K., Yamakawa, S. and Shirakawa, K. (1986), "Properties and Applications of Carbon Fibre Reinforced Cement Composites", *In R.N. Swamy, R.L.Wagstaffe and D.R. Oakley (eds) Developments in Fibre Reinforced Cement and Concrete, Proceedings of the RILEM Symposium*, University of Sheffield, Sheffield, RILEM Technical Committee 49-FTR, Paper 2.2.
- Nuruddin, M., Khan, S., Shafiq, N. and Ayub, T. (2014), "Strength Development of High-Strength Ductile Concrete Incorporating Metakaolin and PVA Fibres", *Hindawi Publishing Corporation, The Scientific World Journal*, Volume 2014, Article ID 387259, 11 pages.

- Oakley, D. and Procter, B. (1975), "Tensile Stress-Strain Behaviour of Glass Fibre Reinforced Cement Composites", *In: Proceedings of the RILEM Symposium, Fibre Reinforced Cement and Concrete*, Construction Press, UK, pp. 347-360.
- Ogawa, A. and Hoshiro, H. (2011), "Durability of Fibres", *RILEM State of the ART Reports*, Volume 4, pp. 81-88.
- Ohama, Y., Amano, M., and Endo, M. (1985), "Properties of Carbon Fibre reinforced Cement with Silica Fume", *Concrete International: Design and Construction*, Volume 7, Issue 3, pp. 58-62.
- Ohama, Y. (1989), "Carbon-Cement Composites", *Carbon*, Volume 27, Issue 5, pp. 729-737.
- Oliver, J., Husepe, A., Pulido, M. and Chaves, E. (2002), "From Continuum Mechanics to Fracture Mechanics: The Strong Discontinuity Approach", *Engineering Fracture Mechanics*, Volume 69, Issue 2, pp.113-136.
- Oliver, J. and Huespe, A. (2004), "Continuum Approach to Material Failure in Strong Discontinuity Settings", *Computer Methods in Applied Mechanics and Engineering*, Volume 193, Issue 30-32, pp. 3195-3220.
- Ombres, L. (2012), "Debonding Analysis of Reinforced Concrete Beams Strengthened With Fibre Reinforced Cementitious Mortar", *Engineering Fracture Mechanics*, Volume 81, pp. 94-109.
- Pachow, U. (2003), "Textile Reinforced Concrete - New Manufacturing Technologies and Applications", *In: Proceedings of the 12th International Tectextile Symposium for Technical Textiles, Nonwovens and Textile Reinforced Materials*, Paper 4.17, 24 Seiten, Frankfurt, Germany.
- Pandey, S. and Sharma, R. (2000), "The Influence of Mineral Additives on the Strength and Porosity of OPC Mortar", *Cement and Concrete Research*, Volume 30, Issue 1, pp. 19-23.

- Parimi, S. and Rao, J. (1971), "Effectiveness of Random Fibres in Fibre-Reinforced Concrete", *In: Proceedings of the International Conference Mechanical Behaviour of Materials*, Volume 5, Kyoto, pp. 176-186.
- Park, S., Lee, B. and Lim, Y. (1991), "Experimental Study on the Engineering Properties of Carbon Fibre Reinforced Cement Composites", *Cement and Concrete Research*, Volume 21, Issue 4, pp. 589-600.
- Park, S. and Lee, B. (1993), "Mechanical Properties of Carbon Fibre Reinforced Polymer Impregnated Cement Composites", *Cement and Concrete Composites*, Volume 15, Issue 3, pp. 153-163.
- Pavia, S. and Condren, E. (2008), "Study of the Durability of OPC versus GGBS Concrete on Exposure to Silage Effluent", *Journal of Materials in Civil Engineering*, Volume 20, Issue 4, pp. 313-320.
- Peled, A., Bentur, A. and Yankelevsky, D. (1998), "Effects of Woven Fabrics Geometry on the Bonding Performance of Cementitious Composites: Mechanical Performance", *Journal Advanced Cement Based Materials*, Volume 7, Issue 1, pp. 20-27.
- Peled, A., Bentur, A. and Yankelevsky, D. (1999), "Flexural Performance of Cementitious Composites Reinforced by Woven Fabrics", *Journal Materials in Civil Engineering (ASCE)*, Volume 11, Issue 4, pp. 325-330.
- Peled, A. and Bentur, A. (2000), "Geometrical Characteristics and Efficiency of Textile Fabrics for Reinforcing Cement Composites", *Cement and Concrete Research*, Volume 30, Issue 5, pp. 781-790.
- Peled, A. and Bentur, A. (2003), "Fabric Structure and its Reinforcing Efficiency in Textile Reinforced Cement Composites", *Composites: Part A*, Volume 34, Issue 2, pp. 107-118.
- Peled, A. and Shah, S. (2003), "Processing Effects in Cementitious Composites: Extrusion and Casting", *Journal of Materials and Civil Engineering, ASCE*, Volume 15, Issue 2, pp. 192-199.
- Peled, A., Mobasher, B. and Sueki, S. (2004), "Technology Methods in Textile Cement-Based Composites Concrete Science and Engineering", *A Tribute to Arnon Bentur, In:*

Kovler K, Marchand J, Mindess S, Weiss J, editors, *RILEM Proceedings PRO*, Volume 36, pp. 187-202.

Peled, A., Jones, J. and Shah, S. (2005), "Effect of Matrix Modification on Durability of Glass Fibre Reinforced Cement Composites", *Materials and Structures*, Volume 38, Issue 2, pp. 163-171.

Peled, A., Sueki, S. and Mobasher, B. (2006), "Bonding in Fabric-Cement Systems: Effects of Fabrication Methods", *Cement and Concrete Research*, Volume 36, Issue 9, pp. 1661-1671.

Peled, A., Zvi, C., Pasder, Y., Roye, A. and Gries, T. (2008), "Influences of Textile Characteristics on the Tensile Properties of Warp Knitted Cement Based Composites", *Cement and Concrete Composites*, Volume 30, Issue 3, pp. 174-183.

Peled, A. (2009), "Cement Penetrability Characteristics in Textile Cement Systems", *In: Proceedings of the 4th Colloquium on Textile Reinforced Structures (CTRS4)*, pp. 99-114.

Purnell, P. (1998), "*The Durability of Glass Fibre Reinforced Cements Made With New Cementitious Matrices*", PhD Thesis, Aston University. UK.

Purnell, P., Short, N., Page, C., Majumbar, A. and Walton, P. (1999), "Accelerated Ageing Characteristics of Glass-Fibre Reinforced Cement Made With New Cementitious Matrices", *Composites: Part A*, Volume 30, Issue 9, pp. 1073-1080.

Purnell, P., Buchanan, A., Short, N., Page, C. and Majumdar, A. (2000), "Determination of Bond Strength in Glass Fibre Reinforced Cement Using Petrography and Image Analysis", *Journal of Material Science*, Volume 35, Issue 18, pp. 4653-4659.

Purnell, P., Short, N. and Page, C. (2001), "Super-critical Carbonation of Glass-Fibre Reinforced Cement. Part 1: Mechanical Testing and Chemical Analysis", *Composites: Part A*, Volume 32, Issue 12, pp. 1777-1787.

Purnell, P. and Beddows, J. (2005), "Durability and Simulated Ageing of New Matrix Glass Fibre Reinforced Concrete", *Cement and Concrete Composites*, Volume 27, Issues 9-10, pp. 875-884.

Purnell, P. (2007), "*Degradation of Fibre-Reinforced Cement Composite*" Chapter 9, In: Page CL; Page MM (ed.) *Durability of Concrete and Cement Composites*, Woodhead, pp. 316-363.

Purnell, P. (2010), "*Mechanical Behaviour of FRC Construction*", Chapter 48, *Materials Their Nature and Behaviour*, Fourth edition, Spon Press.

Rabczuk, T. (2013), "Computational Methods for Fracture in Brittle and Quasi-Brittle Solids: State-of-the-Art Review and Future Perspectives", *Hindawi Publishing Corporation ISRN Applied Mathematics*, Volume 2013, Article ID 849231, 38 pages.

Radtke, F. (2012), "*Computational Modelling of Fibre-Reinforced Cementitious Composites: an Analysis of Discrete and Mesh-Independent Techniques*", PhD Thesis, Delft University of Technology, Netherlands.

Ramakrishnan V., Wu, G. and Hosalli, G. (1989), "Flexural Behaviour and Toughness of Fibre Reinforced Concretes", *Transportation Research Record 1226*, National Research Council, Washington, DC, pp. 36-47.

Rashad, A. (2014), "A Comprehensive Overview about the Influence of Different Admixtures and Additives on the Properties of Alkali-Activated Fly Ash", *Materials and Design*, Volume 53, pp. 1005-1025.

Rashid, Y. (1968), "Analysis of Prestressed Concrete Pressure Vessels", *Nuclear Engineering and Design*, Volume, 7, Issue 4, pp. 334-344.

Redon, C., Li, V., Wu, C., Hoshiro, H., Saito, T. and Ogawa, A. (2001), "Measuring and Modifying Interface Properties of PVA Fibres in ECC Matrix", *Journal of Materials in Civil Engineering*, Volume 13, Issue 6, pp. 399-406.

RILEM TC 162-TDF (2002), "Design of Steel Fibre Reinforced Concrete Using the σ -w Method: Principles and Applications", (Chairlady: Vandewalle, L.), *Materials and Structures*, Volume 35, Issue 249, pp. 262-278.

RILEM (2006), "*Textile Reinforced Concrete*", RILEM Technical Committee TRC-201, ISBN 2-912143-99-3.

Rodriguez, E., Soriano, L., Paya, J., Borrachero, M. and Monzo, J. (2012), "Increase of the Reactivity of Densified Silica Fume by Sonication Treatment", *Ultrasonics Sonochemistry*, Volume 19, Issue 5, pp. 1099-1107.

Robert, M., Cousin, P. and Benmokrane, B. (2009), "Durability of GFRP Reinforcing Bars Embedded in Moist Concrete", *Journal of Composites for Construction*, Volume 13, Issue 2, pp. 66-73.

Robert, M. and Benmokrane, B. (2010), "Physical, Mechanical, and Durability Characterisation of Preloaded GFRP Reinforcing Bars", *Journal of Composites for Construction*, Volume 14, Issue 4, pp. 368-375.

Robert, M. and Benmokrane, B. (2013), "Combined Effects of Saline Solution and Moist Concrete on Long-term Durability of GFRP Reinforcing Bars", *Construction and Building Materials*, Volume 38, pp. 274-284.

Rols, S., Ambroise, J. and Pera, J. (2000), "Durability of Fibre Reinforced Composites", *ACI Materials Journal*, Volume 192, SP192-51, pp. 843-858.

Romualdi, J. and Batson, G. (1963), "Mechanics of Crack Arrest in Concrete", *Journal of the Engineering Mechanics Division, ASCE*, Volume 89, Issue 3, pp. 147-168.

Romualdi, J. and Mandel, J. (1964), "Tensile Strength of Concrete Affected by Uniformly Distributed Closely Spaced Short Lengths of Wire Reinforcement", *Journal of the American Concrete Institute (ACI)*, Volume 61, Issue 6, pp. 657-670.

Sadrmomtazi, A. and Fasihi, A. (2010), "Influence of Polypropylene Fibres on the Performance of Nano-SiO₂-Incorporated Mortar", *Iranian Journal of Science & Technology, Transaction B: Engineering*, Volume 34, Issue B4, pp. 385-395.

Sahmaran, M., Christianto, H. and Yaman, I. (2006), "The Effect of Chemical Admixtures and Mineral Additives on the Properties of Self-Compacting Mortars", *Cement and Concrete Composites*, Volume 28, Issue 5, pp. 432-440.

Sanchez, P., Huespe, A., Oliver, J., Diaz, G. and Sonzogni, V. (2012), "A Macroscopic Damage-Plastic Constitutive Law for Modelling Quasi-Brittle Fracture and Ductile

Behaviour of Concrete", *International Journal for Numerical and Analytical Methods in Geomechanics*, Volume 36, Issue 5, pp. 546-573.

Saraswathy, V., Muralidharan, S., Thangavel, K. and Srinivasan, S. (2003), "Influence of Activated Fly Ash on Corrosion-Resistance and Strength of Concrete", *Cement and Concrete Composites*, Volume 25, Issue 7, pp. 673-680.

Sengul, O, Tas-demir, M. and Sonmez, R. (2003), "Chloride Permeability of Ordinary and High Strength Concrete Containing High Volume Fly Ash", *TMMOB, Chamber of Civil Engineers, In: 5th National Concrete Congress Proceedings*, Istanbul, Turkey, pp. 75-86.

Sengupta, B. and Bhanja, S. (2003), "Optimum Silica Fume Content and Its Mode of Action on Concrete", *ACI Material Journal*, Volume 100, Issue 5, pp. 407-412.

Shah, S. (1985), "Reinforcement Mechanism in GFRC Composites", *In: Proceedings of the 12th International Symposium on Durability of Glass Fibre Reinforced Concrete*, Edited by Diamond, S., PCI, Illinois, USA, pp. 91-109.

Shah, S., Swartz, S. and Ouyang, C. (1995), "*Fracture Mechanics of Concrete: Applications of Fracture Mechanics to Concrete, Rock and Other Quasi-Brittle Material*", John Wiley and Sons, New York, USA, 588 Pages.

Shah, S., Peled, A., Aldea, C. and Akkaya, Y. (1999), "Scope of High Performance Fibre Reinforced Cement Composites", *In: Proceedings of the 3rd International Workshop on High Performance Fibre Reinforced Cement composites (HPFRCC3)*, Reinhardt, H. and Naaman, A. (editors), Mains, Germany, pp. 113-129.

Shahbazpanahi, S., Ali, A., Aznieta, F., Kamgar, A. and Farzadnia, N. (2013), "Modelling of the Fracture Process Zone to Improve the Crack Propagation Criterion in Concrete", *Journal of the South African Institution of Civil Engineering*, Volume 55, Issue. 3, pp. 2-9.

Shannang, M. and Yeginobali A. (1995), "Properties of Pastes, Mortars and Concretes Containing Natural Pozzolans", *Cement and Concrete Research*, Volume 25, Issue 3, pp. 647-657.

Shannag, M. (2000), "High Strength Concrete Containing Natural Pozzolan and Silica Fume", *Cement and Concrete Composites*, Volume 22, Issue 6, pp. 399-406.

Shao, Y. and Shah, S. (1997), "Mechanical Properties of PVA Fibre Reinforced Cement Composites by Extrusion Processing", *ACI Material Journal*, Volume 94, Issue 6, pp. 555-564.

Shao, Y. and Qiu, J. (2002), "The Role of Polymer Additives in Extrusion of Fibre-Cement Composites", *In: Proceedings of the 2nd Material Specialty Conference of the Canadian Society for Civil Engineering*. Montreal, Quebec, Canada, pp. 1-8.

Shen, B., Hubler, M., Paulino, G. and Struble, L. (2008), "Functionally-Graded Fibre Reinforced Cement Composite: Processing, Microstructure, and Properties", *Cement and Concrete Composites*, Volume 30, Issue 8, pp. 663-673.

Shi, Y., Rabin, T., Mark, C., Tony, C., Mohan, J. and Robert, S. (2013), "Mechanical Properties of Recycled Plastic Fibres for Reinforcing Concrete", *In: Proceedings of the 7th International Conference on Fibre Concrete*, Prague, Czech Republic, pp. 1-10.

Shihada, S. and Arafa, M. (2010), "Effects of Silica Fume, Ultrafine and Mixing Sequences on Properties of Ultra High Performance Concrete", *Asian Journal of Materials Science*, Volume 2, Issue 3, pp. 137-146.

Siang, T. (2006), "*Flexural Behaviour of Concrete Beam Reinforced With Glass Fibre Reinforced Polymer (GFRP) Section*", BSc Report, University Technology Malaysia.

Siddique, R. (2011), "Utilization of Silica Fume in Concrete: Review of Hardened Properties", *Resources, Conservation and Recycling*, Volume 55, Issue 11, pp. 923-932.

Silva, F., Mobasher, B., Soranakom, C. and Filho, R. (2011), "Effect of Fibre Shape and Morphology on Interfacial Bond and Cracking Behaviours of Sisal Fibre Cement Based Composites", *Cement and Concrete Composites*, Volume 33, Issue 8, pp. 814-823.

Singh, N. (2000), "Hydration of Bagasse-Ash Blended Portland Cement", *Cement and Concrete Research*, Volume 30, Issue 9, pp. 1485-1488.

Singh, S., Shukla, A. and Brown, R. (2004), "Pull-out Behaviour of Polypropylene Fibres from Cementitious Matrix", *Cement and Concrete Research*, Volume 34, Issue 10, pp. 1919-1925.

Siddique, R. and Khan, M. (2011), "*Supplementary Cementing Materials*", 1st Edition, Springer Heidelberg Dordrecht London New York, 304 Pages.

Sivakumar, A. and Santhanam, M. (2007), "Mechanical Properties of High Strength Concrete Reinforced With Metallic and Non-Metallic Fibres", *Cement and Concrete Composites*, Volume 29, Issue 8, pp. 603-608.

Smith, W. and Hashemi, J. (2004), "*Foundations of Materials Science and Engineering*", Mc Graw Hill Professionals, 1st Edition, 908 Pages.

Snelson, D. and Kinuthia, J. (2010), "Resistance of Mortar Containing Unprocessed Pulverised Fuel Ash (PFA) to Sulphate Attack", *Cement and Concrete Composites*, Volume 32, Issue 7, pp. 523-531.

Soleimani, M. (1991), "*Flexural Response of Hybrid Fibre Reinforced Cementitious Composites*", MSc Thesis, Sharif University of Technology, Iran.

Song, P., Hwang, S. and Sheu, B. (2005), "Strength Properties of Nylon and Polypropylene-Fibre-Reinforced Concretes", *Cement and Concrete Research*, Volume 35, Issue 8, pp. 1546-1550.

Stang, H. (1996), "Significance of Shrinkage-Induced Clamping Pressure in Fibre-Matrix Bonding in Cementitious Composite Materials", *Advanced Cement Based Materials*, Volume 4, Issues 3-4, pp. 106-115.

Stang, H. and Li, V. (2004), "Classification of Fibre Reinforced Cementitious Materials for Structural Applications", In: *Proceedings of the 6th RILEM Symposium on Fibre Reinforced Concrete (FRC)*, Varenna, Italy, PRO 39, RILEM Publications S.A.R.L, Bagneaux, pp. 197-218.

Stutzman, P. (2001), "Scanning Electron Microscopy in Concrete Petrography", *Materials Science of Concrete Special Volume: Calcium Hydroxide in Concrete, Proceedings*, Anna Maria Island, FL, American Ceramic Society, pp. 59-72.

Stynoski, P., Mondal, P. and Marsh, C. (2015), "Effects of Silica Additives on Fracture Properties of Carbon Nanotube and Carbon Fibre Reinforced Portland Cement Mortar", *Cement and Concrete Composites*, Volume 55, pp. 232-240.

Suneel, N. (2004), "The Advances and Barriers in Application of New Concrete Technology", *In: Proceedings of the International Workshop on Sustainable Development and Concrete Technology*, Beijing, China, Iowa State University, pp. 25-33.

Suwannakarn, S. (2009), "*Post Cracking Characteristics of High Performance Fibre Reinforced Cementitious Composites*", PhD Thesis, The University of Michigan, USA.

Tjiptobroto, P. and Hansen, W. (1991), "Mechanism for Tensile Strain Hardening in High Performance Cement-based Fibre Reinforced Composites", *Cement and Concrete Composites*, Volume 13, Issue 4, pp. 265-273.

Tjiptobroto, P. and Hansen, W. (1993), "Tensile Strain Hardening and Multiple Cracking in High Performance Cement-Based Composites Containing Discontinuous Fibres", *ACI Materials Journal (American Concrete Institute)*, Volume 90, Issue 1, pp 16-25.

Tonoli, G., Fuente, E., Negro, C., Lahr, F., Blanco, A. and Savastano, H. (2008), "Hardwood Pulp Fibre as Alternative to Engineered Cement Cased Composites", *In: Proceedings of the 11th International Inorganic Bonded Fibre Composites Conference*, Madrid Spain, pp. 46-51.

Topcu, I. and Canbaz, M. (2007), "Effect of Different Fibres on The Mechanical Properties of Concrete Containing Fly Ash", *Construction and Building Materials*, Volume 21, Issue 7, pp. 1486-1491.

Tosun, K., Yazici, H., Yigiter H., and Aydin, S. (2003), "An Investigation on Sulphate Resistance of Mortars Containing Fly Ash", *TMMOB, Chamber of Civil Engineers, In: 5th National Concrete Congress Proceedings*, Istanbul, Turkey, pp. 17-26.

Toutanji, H., El-Korchi, T., Katz, R. and Leatherman, G. (1993), "Behaviour of Carbon Fibre Reinforced Cement Composites in Direct Tension", *Cement and Concrete Research*, Volume 23, Issue 3, pp. 618-626.

Toutanji, H., Mcneil, S. and Bayasi, Z. (1998), "Chloride Permeability and Impact Resistance of Polypropylene-Fibre-Reinforced Silica Fume Concrete", *Cement and Concrete Research*, Volume 28, Issue 7, pp. 961-968.

- Toutanji, H., Delatte, N., Aggoun, S., Duval, R. and Danson, A. (2004), "Effect of Supplementary Cementitious Materials on the Compressive Strength and Durability of Short-Term Cured Concrete", *Cement and Concrete Research*, Volume 34, Issue 2, pp. 311-319.
- Unal, O. and Uygunoglu, T. (2004), "An Investigation on Freezing-Thawing Durability of Concretes with Fly Ash", *Turkish Ready Mixed Concrete Association, Concrete Congress Proceeding*, Turkey, Istanbul, pp. 376-86.
- Urban, M. (2003), "Properties of Hardened Self-Compacting Concrete with Fly Ash", *In: Proceedings of the 3rd International Scientific Conference Quality and Reliability in Building Industry*, Levoca, Slovakia, pp. 533-538.
- Uzal, B., Turanl, L., Yucel, H., Goncuoglu, M. and Culfaz, A. (2010), "Pozzolanic Activity of Clinoptilolite: A Comparative Study with Silica Fume, Fly Ash and a Non-Zeolitic Natural Pozzolan", *Cement and Concrete Research*, Volume 40, Issue 3, pp. 398-404.
- Van-Mier, J. (1997), *Fracture Processes of Concrete: Assessment of Material Parameters for Fracture Models*, CRC Press, Boca Raton, 464 Pages.
- Van-Mier, J. (2013), *Concrete Fracture A Multiscale Approach*, 1st Edition, Taylor & Francis Group, 331 Pages.
- Vitro M. (2008), *Portland Cement and Pozzolans, Technical Background for the Effective Use of VCAS Pozzolans in Portland Cement Concrete*, Lawrenceville, Georgia, www.vitrominerals.com, [Accessed 20 June 2010].
- Voo, J. and Foster, S. (2003), "Variable Engagement Model for the Design of Fibre Reinforced Concrete Structures", *In: Proceedings of Advanced Materials for Construction of Bridges, Buildings, and Other Structures III*, Switzerland, pp.1-10.
- Wang, S. and Li, V. (2006), "Polyvinyl Alcohol Fibre Reinforced Engineered Cementitious Composites: Material Design and Performances", *International RILEM Workshop on High Performance Fibre Reinforced Cementitious Composites in Structural Applications*, pp. 65-73.

- Wang, Z., Gao, J., Ai, T., Jiang, W. and Zhao, P. (2014), "Quantitative Evaluation of Carbon Fibre Dispersion in Cement Based Composites", *Construction and Building Materials*, Volume 68, pp. 26-30.
- Wates, C. (2009), "*Taking the Flak: Novel Systems for Personal Ballistics Protection*", ES4B8 Individual Project Report, The University of Warwick.
- Wecharatana, M. and Shah, S. (1983), "Prediction of Nonlinear Fracture Process Zone in Concrete", *Journal of Engineering Mechanics*, Volume 109, Issue 5, pp. 1231-1246.
- Wiberg, A. (2003), "*Strengthening of Concrete Beams Using Cementitious Carbon Fibre Composites*", PhD Thesis, Royal Institute of Technology, Stockholm, Sweden.
- Wille, K., El-Tawil, S. and Naaman, A. (2014), "Properties of Strain Hardening Ultra High Performance Fibre Reinforced Concrete (UHP-FRC) Under Direct Tensile Loading", *Cement and Concrete Composites*, Volume 48, pp. 53-66.
- Wittmann, F. and Hu, X. (1991), "Fracture Process Zone in Cementitious Materials", *International Journal of Fracture*, Volume 51, Issue 1, pp. 3-18.
- Wouters, M. (2002), "*Effects of Fibre Bundle Size and Stitch Pattern on the Static Properties of Unidirectional Carbon-Fibre non-Crimp Fabric Composites*", MSc Thesis, Lulea University of Technology, Sweden.
- Xu, S. and Reinhardt, H. (1999), "Determination of Double-K Criterion for Crack Propagation in Quasi brittle Materials, Part II: Analytical Evaluating and Practical Measuring Methods for Three-Point Bending Notched Beams", *International Journal of Fracture*, Volume 98, Issue 2, pp. 151-177.
- Xu, Y. and Chung, D. (1999), "Carbon Fibre Reinforced Cement Improved by Using Silane-Treated Carbon Fibres", *Cement and Concrete Research*, Volume 29, Issue 3, pp. 773-776.
- Yazdanbakhsh, A., Grasley, Z., Tyson, B. and Abu Al-Rub, R. (2009), "Carbon Nano Filaments in Cementitious Materials: Some Issues on Dispersion and Interfacial Bond", *American Concrete Institute (ACI)*, Volume 267, Issue 3, pp. 21-34.

- Yogendran, V., Langan, B., Haque, M. and Ward, M. (1987), "Silica Fume in High Strength Concrete", *ACI Materials Journal*, Volume 84, Issue 2, pp. 124-129.
- Yuan, R., Jin, S. and Qian, J. (1982), "Effects of Fly Ash on Rheology of Fresh Cement paste", *Materials and Research Society Symposium Proceedings*, pp. 182-191.
- Yun, Y. and Kyum, K. (2005), "Corrosion Resistance of Concrete With Ground Granulate Blast-Furnace Slag", *Cement and Concrete Research*, Volume 35, Issue 7, pp. 1391-1399.
- Yurtseven, A. (2004), "*Determination of Mechanical Properties of Hybrid Fibre Reinforced Concrete*", MSc Thesis, Middle East Technical University, Turkey.
- Yusof, A., Nor, N., Zain, M., Peng, N., Ismail, A., Sohaimi, M. and Zaidi, A. (2011), "Mechanical Properties of Hybrid Steel Fibre Reinforced Concrete with Different Aspect Ratio", *Australian Journal of Basic and Applied Sciences*, Volume 5, Issue 7, pp. 159-166.
- Zhang, J. and Li, V. (2004), "Simulation of Crack Propagation in Fibre-Reinforced Concrete by Fracture Mechanics", *Cement and Concrete Research*, Volume 34, Issue 2, pp. 333-339.
- Zheng, Q. and Chung, D. (1989), "Carbon Fibre Reinforced Cement Composites Improved by Using Chemical Agents", *Cement and Concrete Research*, Volume 19, Issue 1, pp. 25-41.
- Zheng, Z. and Feldman, D. (1995), "Synthetic Fibre-Reinforced Concrete", *Progress in Polymer Science*, Volume 20, Issue 2, pp. 185-210.
- Zhou, X., Slater, J., Wavell, S. and Oladiran, O. (2012), "Effects of PFA and GGBS on Early-Ages Engineering Properties of Portland Cement Systems", *Journal of Advanced Concrete Technology*, Volume 10, Issue 2, pp. 74-85.
- Zhu, W. and Bartos, P. (1993), "Effects of Combined Fibre Treatments and Matrix Modifications on Toughness of Aged GRC", In: *Proceedings of the 9th Biennial Congress, Glass Fibre Reinforced Cement Association*, Copenhagen, Denmark, paper 1\4.

Zhu, W. and Bartos, P. (1997), "Assessment of Interfacial Microstructure and Bond Properties in Aged GRC Using a Novel Microindentation Method", *Cement and Concrete Research*, Volume 27, Issue 11, pp. 1701-1711.

Zhu, M., Wetherhold, R., and Chung, D. (1997), "Evaluation of the Interfacial Shear in a Discontinuous Carbon Fibre/Mortar Matrix Composite", *Cement and Concrete Research*, Volume 27, Issue 3, pp. 437-451.

Zulkarnain, F. and Ramli, M. (2011), "Performance of Foamed Concrete Mix Design with Silica Fume for General Housing Construction", *European Journal of Technology and Advanced Engineering Research*, ISSN: 1433-2248, Issue 2, pp. 18-28.

APPENDICES

APPENDIX A

Table A.6.1: Results from four-point bending test, water reduction, coefficient of variation, and standard deviation of six cementitious specimens containing 2% of CF1 were manufactured via compression moulding.

(1)	(2)			(3)		(4)	(5)
Specimen code	Water/binder ratio			Stress (MPa)		Strain at peak stress (%)	Toughness at peak stress (J/m ³)
	Before pressing	After pressing	Difference (%)	LOP	Peak		
CF1-CM-50-01	0.4	0.26	35	8.3	8.3	0.034	0.0014
CF1-CM-50-02	0.4	0.31	23	7.4	7.4	0.035	0.0013
CF1-CM-50-03	0.4	0.29	28	9.5	9.5	0.031	0.0015
CF1-CM-50-04	0.4	0.27	33	8.3	8.3	0.019	0.0008
CF1-CM-50-05	0.4	0.28	30	8.4	8.4	0.024	0.0010
CF1-CM-50-06	0.4	0.3	25	7.3	7.3	0.029	0.0010
Mean	0.4	0.29	29	8.2	8.2	0.029	0.0012
SD				0.8	0.8	0.006	0.0003
Characteristic strength (MPa)				6.8	6.8		
Max		0.31	35	9.5	9.5	0.035	0.0015
Min		0.26	23	7.3	7.3	0.019	0.0008

Table A.6.2: Results from four-point bending test, coefficient of variation, and standard deviation of six cementitious specimens containing 2% of CF1 were manufactured via hand lay-up.

(1)	(2)	(3)		(4)	(5)
Specimen code	Water/binder ratio	Stress (MPa)		Strain at peak stress (%)	Toughness at peak stress (J/m ³)
		LOP	Peak		
CF1-HU-50-01	0.4	7.8	7.8	0.029	0.0012
CF1-HU-50-02	0.4	7.6	7.6	0.028	0.0012
CF1-HU-50-03	0.4	7.7	7.7	0.034	0.0016
CF1-HU-50-04	0.4	7.1	7.1	0.023	0.0008
CF1-HU-50-05	0.4	8.4	8.4	0.035	0.0013
CF1-HU-50-06	0.4	6.8	6.8	0.037	0.0013
Mean		7.6	7.6	0.031	0.0012
SD		0.6	0.6	0.005	0.0003
Characteristic strength (MPa)		6.6	6.6		
Max		8.4	8.4	0.037	0.0016
Min		6.8	6.8	0.023	0.0008

Table A.6.3: Results from four-point bending test, water reduction, coefficient of variation, and standard deviation of six specimens containing 2% of CF2 were manufactured via compression moulding.

(1)	(2)			(3)		(4)	(5)
Specimen code	Water/binder ratio			Stress (MPa)		Strain at peak stress (%)	Toughness at peak stress (J/m ³)
	Before pressing	After pressing	Difference (%)	LOP	Peak		
CF2-CM-50-01	0.4	0.27	33	12.0	12.4	0.045	0.0031
CF2-CM-50-02	0.4	0.33	18	8.1	10.8	0.038	0.0028
CF2-CM-50-03	0.4	0.28	30	10.3	11.4	0.051	0.0034
CF2-CM-50-04	0.4	0.27	33	10.1	11.5	0.043	0.0029
CF2-CM-50-05	0.4	0.24	40	11.4	12.0	0.050	0.0037
CF2-CM-50-06	0.4	0.26	35	9.1	10.2	0.051	0.0031
Mean		0.27	31	10.2	11.4	0.046	0.0032
SD				1.4	0.8	0.005	0.0003
Characteristic strength (MPa)				7.7	10		
Max		0.33	40	12.0	12.4	0.051	0.0037
Min		0.24	18	8.1	10.2	0.038	0.0028

Table A.6.4: Results from four-point bending test, coefficient of variation, and standard deviation of six specimens containing 2% of CF2 were manufactured via hand lay-up.

(1)	(2)	(3)		(4)	(5)
Specimen code	Water/binder ratio	Stress (MPa)		Strain at peak stress (%)	Toughness at peak stress (J/m ³)
		LOP	Peak		
CF2-HU-50-01	0.4	9.3	11.2	0.056	0.0045
CF2-HU-50-02	0.4	6.0	10.0	0.055	0.0044
CF2-HU-50-03	0.4	7.9	10.4	0.030	0.0028
CF2-HU-50-04	0.4	8.1	9.3	0.040	0.0023
CF2-HU-50-05	0.4	9.8	10.5	0.039	0.0030
CF2-HU-50-06	0.4	8.0	9.6	0.044	0.0026
Mean		8.2	10.2	0.044	0.0033
SD		1.3	0.7	0.01	0.0009
Characteristic strength (MPa)		5.9	9		
Max		9.8	11.2	0.056	0.0045
Min		8.0	9.3	0.030	0.0023

Table A.6.5: Results from four-point bending test, water reduction, coefficient of variation, and standard deviation of five specimens containing 2% of CF3 were manufactured via compression moulding.

(1)	(2)			(3)		(4)	(5)
Specimen code	Water/binder ratio			Stress (MPa)		Strain at peak stress (%)	Toughness at peak stress (J/m ³)
	Before pressing	After pressing	Difference (%)	LOP	Peak		
CF3-CM-50-02	0.4	0.28	30	6.5	9.5	0.059	0.0034
CF3-CM-50-03	0.4	0.28	30	10	11.0	0.047	0.0034
CF3-CM-50-04	0.4	0.27	33	8.1	8.8	0.030	0.0024
CF3-CM-50-05	0.4	0.27	33	8.2	9.4	0.071	0.0044
Mean	0.4	0.28	30	8.0	9.4	0.051	0.0032
SD				1.4	1.0	0.015	0.0009
Characteristic strength (MPa)				5.6	7.6		
Max		0.30	33	10	11.0	0.071	0.0044
Min		0.27	25	6.5	8.2	0.030	0.0023

Table A.6.6: Results from four-point bending test, coefficient of variation, and standard deviation of six specimens containing 2% of CF3 were manufactured via hand lay-up.

(1)	(2)	(3)		(4)	(5)
Specimen code	Water/binder ratio	Stress (MPa)		Strain at peak stress (%)	Toughness at peak stress (J/m ³)
		LOP	Peak		
CF3-HU-50-01	0.4	8.4	8.4	0.061	0.0035
CF3-HU-50-02	0.4	7.0	7.2	0.035	0.0016
CF3-HU-50-03	0.4	7.7	7.7	0.048	0.0031
CF3-HU-50-04	0.4	6.7	8.9	0.071	0.0039
CF3-HU-50-05	0.4	7.2	8.8	0.078	0.0042
CF3-HU-50-06	0.4	7.2	8.2	0.053	0.0023
Mean		7.4	8.2	0.058	0.0031
SD		2.4	0.7	0.016	0.001
Characteristic strength (MPa)		1.9	7.1		
Max		7.2	8.9	0.078	0.0042
Min		1.2	7.2	0.035	0.0016

Table A.6.7: Results from four-point bending test, water reduction, coefficient of variation, and standard deviation of five specimens containing 2% of PP were manufactured via compression moulding.

(1)	(2)			(3)		(4)	(5)
Specimen code	Water/binder ratio			Stress (MPa)		Strain at peak stress (%)	Toughness at peak stress (J/m ³)
	Before pressing	After pressing	Difference (%)				
				LOP	Peak		
PP-CM-50-01	0.4	0.29	28	7.8	7.8	0.036	0.0014
PP-CM-50-02	0.4	0.28	30	8.2	8.2	0.053	0.0024
PP-CM-50-03	0.4	0.30	25	10.8	10.8	0.048	0.0025
PP-CM-50-04	0.4	0.28	30	9.4	9.4	0.043	0.0020
PP-CM-50-05	0.4	0.27	32	9.5	9.5	0.040	0.0021
Mean		0.26	29	9.1	9.1	0.044	0.0021
SD				1.2	1.2	0.007	0.0004
Characteristic strength (MPa)				7.1	7.1		
Max		0.29	40	10.8	10.8	0.053	0.0025
Min		0.24	28	7.8	7.8	0.036	0.0014

Table A.6.8: Results from four-point bending test, coefficient of variation, and standard deviation of six specimens containing 2% of PP were manufactured via hand lay-up.

(1)	(2)	(3)		(4)	(5)
Specimen code	Water/binder ratio	Stress (MPa)		Strain at peak stress (%)	Toughness at peak stress (J/m ³)
		LOP	Peak		
PP-HU-50-01	0.4	7.8	9.2	0.029	0.0016
PP-HU-50-02	0.4	9.3	9.3	0.023	0.0011
PP-HU-50-03	0.4	8.9	8.9	0.022	0.0012
PP-HU-50-04	0.4	10.0	10.0	0.034	0.0017
PP-HU-50-05	0.4	11.5	11.5	0.033	0.0018
PP-HU-50-06	0.4	10.5	10.5	0.035	0.0017
Mean		9.7	9.9	0.033	0.0015
SD		1.3	1.0	0.006	0.0003
Characteristic strength (MPa)		7.4	8.2		
Max		11.5	11.5	0.035	0.0018
Min		7.8	8.9	0.022	0.0011

Table A.6.9: Results from four-point bending test, water reduction, coefficient of variation, and standard deviation of six specimens containing 2% of PVA were manufactured via compression moulding.

(1)	(2)			(3)		(4)	(5)
Specimen code	Water/binder ratio			Stress (MPa)		Strain at peak stress (%)	Toughness at peak stress (J/m ³)
	Before pressing	After pressing	Difference (%)				
				LOP	Peak		
PVA-CM-50-01	0.4	0.25	38	10.4	13.4	0.27	0.027
PVA-CM-50-02	0.4	0.30	25	12.6	14.5	0.26	0.031
PVA-CM-50-03	0.4	0.26	35	12.4	12.6	0.11	0.010
PVA-CM-50-04	0.4	0.26	35	6.3	12.4	0.37	0.035
PVA-CM-50-05	0.4	0.29	28	7.4	11.5	0.30	0.027
PVA-CM-50-06	0.4	0.28	30	8.7	12.5	0.67	0.068
Mean	0.4	0.27	31	9.6	12.8	0.33	0.033
SD				2.6	1.0	0.2	0.02
Characteristic strength (MPa)				5.1	11.1		
Max		0.30	38	12.6	14.5	0.67	0.068
Min		0.25	25	6.3	11.5	0.11	0.010

Table A.6.10: Results from four-point bending test, coefficient of variation, and standard deviation of six specimens containing 2% of PVA were manufactured via hand lay-up.

(1)	(2)	(3)		(4)	(5)
Specimen code	Water/binder ratio	Stress (MPa)		Strain at peak stress (%)	Toughness at peak stress (J/m ³)
		LOP	Peak		
PVA-HU-50-01	0.4	7.3	10.6	0.31	0.027
PVA-HU-50-02	0.4	8.0	10.3	0.24	0.019
PVA-HU-50-03	0.4	6.6	8.0	0.35	0.023
PVA-HU-50-04	0.4	7.7	7.7	0.03	0.001
PVA-HU-50-05	0.4	6.8	6.9	0.25	0.013
PVA-HU-50-06	0.4	7.6	10.0	0.58	0.048
Mean		7.3	8.9	0.29	0.022
SD		0.5	1.6	0.2	0.02
Characteristic strength (MPa)		6.4	6.2		
Max		8.0	10.6	0.58	0.048
Min		6.6	6.9	0.03	0.001

APPENDIX B

Table B.7.1: Results from four point bending test, water reduction and standard deviation of six control specimens were manufactured via compression moulding.

(1)	(2)			(3)	(4)	(5)
Specimen code	Water/binder ratio			Stress at peak (MPa)	Strain at peak stress (%)	Toughness at peak stress (J/m ³)
	Before	After	Difference %			
CS1-CM-50-01	0.35	0.20	43	7.4	0.036	0.0013
CS1-CM-50-02	0.35	0.22	37	8.8	0.083	0.0040
CS1-CM-50-03	0.35	0.19	46	8.2	0.036	0.0017
CS1-CM-50-04	0.35	0.24	31	6.0	0.040	0.0013
CS1-CM-50-05	0.35	0.21	40	7.8	0.072	0.0030
CS1-CM-50-06	0.35	0.21	40	7.5	0.068	0.0026
Mean	0.35	0.21	40	7.6	0.056	0.0023
SD				0.9	0.021	0.0011
Characteristic strength (MPa)				6		
Max		0.24	46	8.8	0.083	0.0040
Min		0.19	31	6.0	0.036	0.0013

Table B.7.2: Results from four point bending test and standard deviation of six control specimens were manufactured via hand lay-up.

(1)	(2)	(3)	(4)	(5)
Specimen code	Water/binder ratio	Stress at peak (MPa)	Strain at peak stress (%)	Toughness at peak stress (J/m ³)
CS1-HU-50-01	0.35	5.8	0.012	0.00040
CS1-HU-50-02	0.35	7.4	0.013	0.00043
CS1-HU-50-03	0.35	7.9	0.010	0.00034
CS1-HU-50-04	0.35	8.5	0.011	0.00040
CS1-HU-50-05	0.35	7.7	0.011	0.00036
CS1-HU-50-06	0.35	6.8	0.013	0.00044
Mean		7.4	0.012	0.00040
SD		0.9	0.001	0.00004
Characteristic strength (MPa)		5.7		
Max		8.5	0.013	0.00044
Min		5.8	0.010	0.00034

Table B.7.3: Results from four point bending test, water reduction and standard deviation of six CF4 (sheets) were manufactured via compression moulding.

(1)	(2)			(3)		(4)	
Specimen code	Water/binder ratio			Stress (MPa)		Strain (%)	
	Before pressing	After pressing	Difference (%)	LOP	Peak	At LOP	At peak stress
CF4-CM-50-01	0.35	0.22	37	35	41.6	0.19	0.25
CF4-CM-50-02	0.35	0.25	29	30.1	43.2	0.17	0.30
CF4-CM-50-03	0.35	0.23	34	26.4	39.8	0.15	0.34
CF4-CM-50-04	0.35	0.24	31	30	38.2	0.17	0.26
CF4-CM-50-05	0.35	0.25	29	20.1	38.3	0.10	0.99
CF4-CM-50-06	0.35	0.22	37	35	44	0.19	0.3
Mean	0.4	0.24	33	29.4	40.9	0.16	0.41
SD				5.6	2.5	0.03	0.29
Characteristic strength (MPa)				19.7	36.6		
Max		0.25	37	35	44	0.19	0.99
Min		0.22	29	20.1	38.2	0.10	0.25

Table B.7.4: Toughness at two positions; at LOP and peak stress of six CF4 (sheet) specimens were manufactured via compression moulding.

Specimen code	Toughness (J/m ³)	
	At LOP	At peak stress
CF4-CM-50-01	0.035	0.058
CF4-CM-50-02	0.027	0.078
CF4-CM-50-03	0.022	0.089
CF4-CM-50-04	0.030	0.060
CF4-CM-50-05	0.012	0.27
CF4-CM-50-06	0.038	0.081
Mean	0.027	0.11
SD	0.01	0.08
Max	0.038	0.27
Min	0.012	0.058

Table B.7.5: Results from four point bending test and standard deviation of five CF4 (sheet) specimens were manufactured via hand lay-up.

(1)	(2)	(3)		(4)	
Specimen code	Water/ binder ratio	Stress (MPa)		Strain (%)	
		LOP	Peak	At LOP	At peak stress
CF4-HU-50-01	0.35	10.5	43.4	0.040	0.32
CF4-HU-50-02	0.35	8.0	47.1	0.039	0.39
CF4-HU-50-03	0.35	8.6	45.3	0.031	0.45
CF4-HU-50-04	0.35	12.2	34.6	0.063	0.25
CF4-HU-50-05	0.35	11.4	44.3	0.041	0.32
Mean		10.1	42.9	0.043	0.35
SD		1.8	4.9	0.012	0.076
Characteristic strength (MPa)		7	34.6		
Max		12.2	47.1	0.063	0.45
Min		8.0	34.6	0.031	0.25

Table B.7.6: Toughness at two positions; at LOP and peak stress of five CF4 (sheet) specimens were manufactured via hand lay-up.

Specimen code	Toughness (J/m ³)	
	At LOP	At peak stress
CF4-HU-50-01	0.0025	0.087
CF4-HU-50-02	0.0032	0.11
CF4-HU-50-03	0.0014	0.13
CF4-HU-50-04	0.0042	0.049
CF4-HU-50-05	0.0025	0.085
Mean	0.0028	0.092
SD	0.001	0.03
Max	0.0042	0.13
Min	0.0014	0.049

Table B.7.7: Results from four point bending test and standard deviation of five CF5 (sheets) were manufactured via hand lay-up.

(1)	(2)	(3)		(4)	
Specimen code	Water/ binder ratio	Stress (MPa)		Strain (%)	
		LOP	Peak	At LOP	At peak
CF5-HU-50-01	0.35	28.0	33.0	0.18	0.44
CF5-HU-50-02	0.35	20.0	28.3	0.15	0.35
CF5-HU-50-03	0.35	31.1	39.0	0.22	0.36
CF5-HU-50-04	0.35	31.0	37.3	0.23	0.30
CF5-HU-50-05	0.35	30.0	32.4	0.33	0.38
Mean		28	34.0	0.22	0.37
SD		4.7	4.2	0.07	0.05
Characteristic strength (MPa)		20	26.7		
Max		31.1	39.0	0.33	0.96
Min		20	28.3	0.15	0.36

Table B.7.8: Toughness at two positions; at LOP and peak stress of five CF5 (sheet) specimens were manufactured via hand lay-up.

Specimen code	Toughness (J/m ³)	
	At LOP	At peak stress
CF5-HU-50-01	0.029	0.22
CF5-HU-50-02	0.016	0.23
CF5-HU-50-03	0.040	0.088
CF5-HU-50-04	0.038	0.11
CF5-HU-50-05	0.047	0.065
Mean	0.034	0.14
SD	0.01	0.08
Max	0.047	0.23
Min	0.016	0.065

Table B.7.9: Results from four point bending test, water reduction and standard deviation of six CF5 (sheets) were manufactured via compression moulding.

(1)	(2)			(3)		(4)	
Specimen code	Water/binder ratio			Stress (MPa)		Strain (%)	
	Before pressing	After pressing	Difference (%)	LOP	Peak	At LOP	At peak stress
CF5-CM-50-01	0.35	0.25	29	20.1	31.5	0.10	0.55
CF5-CM-50-02	0.35	0.24	31	21.1	30.1	0.12	0.60
CF5-CM-50-03	0.35	0.23	34	30.1	44.6	0.10	0.40
CF5-CM-50-04	0.35	0.24	31	28.2	35.3	0.13	0.56
CF5-CM-50-05	0.35	0.22	37	29.0	34.6	0.16	0.45
CF5-CM-50-06	0.35	0.25	29	35.1	37.5	0.16	0.35
Mean	0.4	0.24	32	27.3	35.6	0.13	0.49
SD				5.7	5.2	0.03	0.09
Characteristic strength (MPa)				17.5	26.7		
Max		0.25	37	35.1	44.6	0.16	1.3
Min		0.22	29	20.1	30.1	0.10	0.6

Table B.7.10: Toughness at two positions; at LOP and peak stress of six CF5 (sheet) specimens were manufactured via compression moulding.

Specimen code	Toughness (J/m ³)	
	At LOP	At peak stress
CF5-CM-50-01	0.012	0.16
CF5-CM-50-02	0.014	0.13
CF5-CM-50-03	0.020	0.15
CF5-CM-50-04	0.022	0.13
CF5-CM-50-05	0.033	0.16
CF5-CM-50-06	0.035	0.18
Mean	0.023	0.15
SD	0.01	0.02
Max	0.035	0.18
Min	0.012	0.13

Table B.7.11: Results from four point bending test and standard deviation of five CF6 were manufactured via hand lay-up.

(1)	(2)	(3)		(4)	
Specimen code	Water/ binder ratio	Stress (MPa)		Strain (%)	
		LOP	Peak	At LOP	At peak stress
CF6-HU-50-01	0.35	41.8	41.8	0.22	0.22
CF6-HU-50-02	0.35	35.1	35.1	0.23	0.23
CF6-HU-50-03	0.35	33.4	38.7	0.20	0.71
CF6-HU-50-04	0.35	35.5	35.5	0.23	0.23
CF6-HU-50-05	0.35	28.7	28.7	0.15	0.15
Mean		34.9	36.0	0.21	0.31
SD		4.7	4.9	0.03	0.2
Characteristic strength (MPa)		26.8	27.6		
Max		41.8	41.8	0.23	0.71
Min		28.7	28.7	0.15	0.15

Table B.7.12: Toughness at two positions; at LOP and peak stress of five CF6 specimens were manufactured via hand lay-up.

Specimen code	Toughness (J/m ³)	
	At LOP	At peak stress
CF6-HU-50-01	0.052	0.052
CF6-HU-50-02	0.043	0.043
CF6-HU-50-03	0.039	0.20
CF6-HU-50-04	0.048	0.048
CF6-HU-50-05	0.026	0.026
Mean	0.042	0.074
SD	0.01	0.07
Max	0.052	0.20
Min	0.026	0.026

Table B.7.13: Results from four point bending test, water reduction and standard deviation of four CF6 were manufactured via compression moulding.

(1)	(2)			(3)		(4)	
Specimen code	Water/binder ratio			Stress (MPa)		Strain (%)	
	Before pressing	After pressing	Difference (%)	LOP	Peak	At LOP	At peak stress
CF6-CM-50-02	0.35	0.22	37	15.0	23.3	0.11	1.1
CF6-CM-50-03	0.35	0.25	29	24.7	27.2	0.13	0.2
CF6-CM-50-04	0.35	0.26	26	20.7	28.3	0.10	0.2
Mean	0.35	0.24	31	19.3	24.6	0.12	0.70
SD				4.3	3.9	0.02	0.5
Characteristic strength (MPa)				11.9	17.9		
Max		0.26	37	24.7	28.3	0.15	1.2
Min		0.22	26	15.0	19.7	0.10	0.2

Table B.7.14: Toughness at two positions; at LOP and peak stress of four CF6 specimens were manufactured via compression moulding.

Specimen code	Toughness (J/m ³)	
	At LOP	At peak stress
CF6-CM-50-01	0.015	0.19
CF6-CM-50-02	0.014	0.21
CF6-CM-50-03	0.021	0.043
CF6-CM-50-04	0.012	0.045
Mean	0.016	0.12
SD	0.004	0.09
Max	0.021	0.21
Min	0.014	0.043

Table B.7.15: Results from four point bending test, water reduction and standard deviation of six CF7 were manufactured via compression moulding.

(1)	(2)			(3)		(4)	
Specimen code	Water/binder ratio			Stress (MPa)		Strain (%)	
	Before pressing	After pressing	Difference (%)	LOP	Peak	At LOP	At peak stress
CF7-CM-50-01	0.35	0.23	34	6.0	16.9	0.036	0.48
CF7-CM-50-02	0.35	0.25	29	6.2	15.2	0.038	0.47
CF7-CM-50-03	0.35	0.26	26	5.0	18.1	0.027	0.62
CF7-CM-50-04	0.35	0.23	34	7.0	17.4	0.037	0.49
CF7-CM-50-05	0.35	0.24	31	6.1	17.3	0.023	0.43
CF7-CM-50-06	0.35	0.26	26	5.2	14.1	0.032	0.34
Mean		0.25	30	5.9	16.5	0.032	0.47
SD				0.7	1.5	0.006	0.09
Characteristic strength (MPa)				4.7	13.9		
Max		0.26	34	7.0	18.1	0.038	0.62
Min		0.23	26	5.0	14.1	0.023	0.34

Table B.7.16: Toughness at two positions; at LOP and peak stress of six CF7 specimens were manufactured via compression moulding.

Specimen code	Toughness (J/m ³)	
	At LOP	At peak stress
CF7-CM-50-01	0.0012	0.060
CF7-CM-50-02	0.0013	0.053
CF7-CM-50-03	0.0007	0.079
CF7-CM-50-04	0.0014	0.063
CF7-CM-50-05	0.0018	0.053
CF7-CM-50-06	0.0009	0.035
Mean	0.0012	0.057
SD	0.0004	0.01
Max	0.0018	0.079
Min	0.0007	0.035

Table B.7.17: Results from four point bending test and standard deviation of six CF7 were manufactured via hand lay-up.

(1)	(2)	(3)		(4)	
Specimen code	Water/ binder ratio	Stress (MPa)		Strain (%)	
		LOP	Peak	At LOP	At peak stress
CF7-HU-50-01	0.35	5.5	33.2	0.032	0.64
CF7-HU-50-02	0.35	14.1	34.0	0.069	0.50
CF7-HU-50-03	0.35	11.5	37.3	0.015	0.69
CF7-HU-50-04	0.35	15.0	37.2	0.052	0.49
CF7-HU-50-05	0.35	11.8	34.5	0.053	0.59
CF7-HU-50-06	0.35	10.1	34.0	0.10	0.60
Mean		11.3	35.0	0.05	0.59
SD		3.4	1.8	0.03	0.08
Characteristic strength (MPa)		5.5	32		
Max		15	37.3	0.10	0.69
Min		5.5	33.2	0.015	0.49

Table B.7.18: Toughness at two positions; at LOP and peak stress of six CF7 specimens were manufactured via hand lay-up.

Specimen code	Toughness (J/m ³)	
	At LOP	At peak stress
CF7-HU-50-01	0.11	0.13
CF7-HU-50-02	0.0048	0.12
CF7-HU-50-03	0.0015	0.21
CF7-HU-50-04	0.0052	0.13
CF7-HU-50-05	0.0038	0.14
CF7-HU-50-06	0.0052	0.12
Mean	0.022	0.14
SD	0.04	0.03
Max	0.11	0.21
Min	0.0015	0.12

Table B.7.19: Results from four point bending test, water reduction and standard deviation of six CF8 were manufactured via compression moulding.

(1)	(2)			(3)		(4)	
Specimen code	Water/binder ratio			Stress (MPa)		Strain (%)	
	Before pressing	After pressing	Difference (%)	LOP	Peak	At LOP	At peak stress
CF8-CM-50-01	0.35	0.23	34				
CF8-CM-50-02	0.35	0.25	29	3.3	20.5	0.044	0.45
CF8-CM-50-03	0.35	0.23	34	2.6	20.9	0.027	0.43
CF8-CM-50-04	0.35	0.26	26	3.5	22.0	0.043	0.51
CF8-CM-50-05	0.35	0.24	31	2.1	20.7	0.024	0.47
CF8-CM-50-06	0.35	0.25	29	6.5	20.6	0.15	0.55
Mean	0.35	0.24	30	3.6	21.2	0.054	0.47
SD				1.5	0.8	0.05	0.05
Characteristic strength (MPa)				0.9	19.8		
Max		0.26	34	6.5	22.4	0.15	0.86
Min		0.23	26	2.1	20.5	0.024	0.62

Table B.7.20: Toughness at two positions; at LOP and peak stress of six CF8 specimens were manufactured via compression moulding.

Specimen code	Toughness (J/m ³)	
	At LOP	At peak stress
CF8-CM-50-01	0.00076	0.10
CF8-CM-50-02	0.00084	0.09
CF8-CM-50-03	0.00037	0.08
CF8-CM-50-04	0.00078	0.12
CF8-CM-50-05	0.00024	0.10
CF8-CM-50-06	0.0056	0.09
Mean	0.0014	0.10
SD	0.002	0.01
Max	0.0056	0.12
Min	0.00024	0.08

Table B.7.21: Results from four point bending test and standard deviation of five CF8 specimens were manufactured via hand lay-up.

(1)	(2)	(3)		(4)	
Specimen code	Water/ binder ratio	Stress (MPa)		Strain (%)	
		LOP	Peak	At LOP	At peak stress
CF8-HU-50-01	0.35	8.2	27.7	0.072	0.50
CF8-HU-50-02	0.35	9.6	35.8	0.065	0.55
CF8-HU-50-03	0.35	6.1	36.7	0.057	0.55
CF8-HU-50-04	0.35	8.5	43.5	0.071	0.30
CF8-HU-50-05	0.35	9.3	35.3	0.14	0.78
Mean		8.3	35.8	0.081	0.54
SD		1.4	5.6	0.03	0.2
Characteristic strength (MPa)		6.0	26.1		
Max		9.6	43.5	0.14	0.78
Min		6.1	27.7	0.057	0.30

Table B.7.22: Toughness at two positions; at LOP and peak stress of five CF8 specimens were manufactured via hand lay-up.

Specimen code	Toughness (J/m ³)	
	At LOP	At peak stress
CF8-HU-50-01	0.0031	0.22
CF8-HU-50-02	0.0045	0.18
CF8-HU-50-03	0.0014	0.17
CF8-HU-50-04	0.0035	0.18
CF8-HU-50-05	0.0073	0.20
Mean	0.0040	0.19
SD	0.002	0.02
Max	0.0073	0.22
Min	0.0014	0.17

Table B.7.23: Results from four point bending test, water reduction and standard deviation of four GF were manufactured via compression moulding.

(1)	(2)			(3)		(4)	
Specimen code	Water/binder ratio			Stress (MPa)		Strain (%)	
	Before pressing	After pressing	Difference (%)				
				LOP	Peak	At LOP	At peak stress
GF-CM-50-01	0.35	0.25	29	3.0	23.4	0.029	0.90
GF-CM-50-02	0.35	0.26	26	4.0	26.7	0.039	0.97
GF-CM-50-03	0.35	0.23	34	3.2	24.5	0.043	1.03
GF-CM-50-04	0.35	0.27	23	3.2	23.6	0.024	0.93
Mean	0.35	0.25	28	3.4	24.6	0.034	0.96
SD				0.4	1.5	0.009	0.02
Characteristic strength (MPa)				2.6	22		
Max		0.27	34	4.0	26.7	0.043	1.03
Min		0.23	23	3.0	23.4	0.024	0.90

Table B.7.24: Toughness at two positions; at LOP and peak stress of four GF specimens were manufactured via compression moulding.

Specimen code	Toughness (J/m ³)	
	At LOP	At peak stress
GF-CM-50-01	0.00046	0.12
GF-CM-50-02	0.00095	0.15
GF-CM-50-03	0.00084	0.14
GF-CM-50-04	0.00041	0.13
Mean	0.00067	0.14
SD	0.0003	0.01
Max	0.00095	0.15
Min	0.00041	0.12

Table B.7.25: Results from four point bending test and standard deviation of five GF specimens were manufactured via hand lay-up.

(1)	(2)	(3)		(4)	
Specimen code	Water/ binder ratio	Stress (MPa)		Strain (%)	
		LOP	Peak	At LOP	At peak stress
GF-HU-50-01	0.35	7.9	12.9	0.038	0.37
GF-HU-50-02	0.35	8.2	12.8	0.041	0.26
GF-HU-50-03	0.35	7.8	14.9	0.053	0.50
GF-HU-50-04	0.35	7.1	13.5	0.040	0.44
GF-HU-50-05	0.35	8.0	14.4	0.039	0.38
Mean		7.8	13.7	0.042	0.39
SD		0.4	0.9	0.006	0.09
Characteristic strength (MPa)		7.1	12.1		
Max		8.2	14.9	0.053	0.50
Min		7.1	12.8	0.038	0.26

Table B.7.26: Toughness at two positions; at LOP and peak stress of five GF specimens were manufactured via hand lay-up.

Specimen code	Toughness (J/m ³)	
	At LOP	At peak stress
GF-HU-50-01	0.0018	0.037
GF-HU-50-02	0.0017	0.025
GF-HU-50-03	0.0025	0.054
GF-HU-50-04	0.0019	0.046
GF-HU-50-05	0.0018	0.042
Mean	0.0019	0.041
SD	0.0003	0.01
Max	0.0025	0.054
Min	0.0017	0.025

Table B.7.27: Results from four point bending test, water reduction and standard deviation of six CF9 were manufactured via compression moulding.

(1)	(2)			(3)		(4)	
Specimen code	Water/binder ratio			Stress (MPa)		Strain (%)	
	Before pressing	After pressing	Difference (%)	LOP	Peak	At LOP	At peak stress
CF9-CM-50-01	0.35	0.28	20	10.2	50.5	0.028	0.45
CF9-CM-50-02	0.35	0.26	26	13.0	45.0	0.045	0.37
CF9-CM-50-03	0.35	0.28	20	10.1	41.8	0.026	0.33
CF9-CM-50-04	0.35	0.27	23	20.0	43.7	0.074	0.37
CF9-CM-50-05	0.35	0.25	29	28.1	44.2	0.12	0.29
CF9-CM-50-06	0.35	0.27	23	14.0	44.1	0.084	0.57
Mean	0.4	0.27	24	15.9	44.9	0.063	0.40
SD				7.0	3.0	0.04	0.1
Characteristic strength (MPa)				3.9	39.8		
Max		0.28	29	28.1	50.5	0.12	0.57
Min		0.25	20	10.1	41.8	0.026	0.29

Table B.7.28: Toughness at two positions; at LOP and peak stress of six CF9 specimens were manufactured via compression moulding.

Specimen code	Toughness (J/m ³)	
	At LOP	At peak stress
CF9-CM-50-01	0.0018	0.16
CF9-CM-50-02	0.0034	0.11
CF9-CM-50-03	0.0020	0.09
CF9-CM-50-04	0.0083	0.13
CF9-CM-50-05	0.02	0.09
CF9-CM-50-06	0.0057	0.18
Mean	0.0069	0.13
SD	0.007	0.04
Max	0.02	0.18
Min	0.0018	0.09

Table B.7.29: Results from four point bending test and standard deviation of five CF9 were manufactured via hand lay-up.

(1)	(2)	(3)		(4)	
Specimen code	Water/ binder ratio	Stress (MPa)		Strain (%)	
		LOP	Peak	At LOP	At peak stress
CF9-HU-50-01	0.35	10.5	45.9	0.037	0.85
CF9-HU-50-02	0.35	10.0	49.2	0.040	0.67
CF9-HU-50-03	0.35	10.0	44.0	0.048	0.76
CF9-HU-50-04	0.35	12.0	48.8	0.072	0.69
CF9-HU-50-05	0.35	10.1	51.3	0.041	0.78
Mean		10.5	47.8	0.048	0.75
SD		0.9	2.9	0.01	0.1
Characteristic strength (MPa)		9.1	42.9		
Max		12.0	51.3	0.072	0.85
Min		10.0	44.0	0.037	0.67

Table B.7.30: Toughness at two positions; at LOP and peak stress of five CF9 specimens were manufactured via hand lay-up.

Specimen code	Toughness (J/m ³)	
	At LOP	At peak stress
CF9-HU-50-01	0.0024	0.26
CF9-HU-50-02	0.0019	0.22
CF9-HU-50-03	0.0036	0.21
CF9-HU-50-04	0.0048	0.22
CF9-HU-50-05	0.0032	0.26
Mean	0.0032	0.23
SD	0.001	0.02
Max	0.0048	0.26
Min	0.0019	0.21

Table B.7.31: Results from four point bending test, water reduction and standard deviation of six CF4 (strips) cementitious specimens ($V_f=5\%$) produced with compression moulding.

(1)	(2)			(3)		(4)	
Specimen code	Water/binder ratio			Stress (MPa)		Strain (%)	
	Before pressing	After pressing	Difference (%)	LOP	Peak	At LOP	At peak stress
CF4S-CM-50-01	0.35	0.25	29	23.8	75.2	0.072	0.45
CF4S-CM-50-02	0.35	0.25	29	20.2	66.2	0.062	0.49
CF4S-CM-50-03	0.35	0.27	23	14.0	72.6	0.036	0.48
CF4S-CM-50-04	0.35	0.23	34	14.0	61.0	0.037	0.39
CF4S-CM-50-05	0.35	0.26	26	20.1	62.8	0.072	0.38
CF4S-CM-50-06	0.35	0.22	37	22.2	60.2	0.081	0.39
Mean	0.35	0.25	30	19.1	66.3	0.06	0.43
SD				4.1	6.3	0.019	0.049
Characteristic strength (MPa)				11.9	55.6		
Max		0.27	37	23.8	75.2	0.081	0.49
Min		0.22	23	14.0	60.2	0.036	0.38

Table B.7.32: Toughness at two positions; at LOP and peak stress of six CF4 (strips) specimens were manufactured via compression moulding.

Specimen code	Toughness (J/m^3)	
	At LOP	At peak stress
CF4S-CM-50-01	0.0096	0.22
CF4S-CM-50-02	0.01	0.22
CF4S-CM-50-03	0.0033	0.21
CF4S-CM-50-04	0.0029	0.14
CF4S-CM-50-05	0.0081	0.14
CF4S-CM-50-06	0.010	0.15
Average	0.0073	0.18
SD	0.003	0.04
Max	0.01	0.22
Min	0.0029	0.14

Table B.7.33: Results from four point bending test and standard deviation of five CF4 (strips) cementitious specimens ($V_f=5\%$) produced with hand lay-up.

(1)	(2)	(3)		(4)	
Specimen code	Water/ binder ratio	Stress (MPa)		Strain (%)	
		LOP	Peak	At LOP	At peak stress
CF4S-HU-50-01	0.35	55	55.6	0.39	0.52
CF4S-HU-50-02	0.35	44	62.5	0.21	0.52
CF4S-HU-50-03	0.35	44	61.4	0.22	0.44
CF4S-HU-50-04	0.35	38	51.9	0.22	0.43
CF4S-HU-50-05	0.35	50.2	61.3	0.22	0.36
Mean	0.35	46.2	58.5	0.25	0.45
SD		6.5	4.6	0.08	0.07
Characteristic strength (MPa)		35	50.6		
Max		55	62.5	0.39	0.52
Min		38	51.9	0.21	0.36

Table B.7.34: Toughness at two positions; at LOP and peak stress of five CF4 (strips) specimens ($V_f=5\%$) were manufactured via hand lay-up.

Specimen code	Toughness (J/m^3)	
	At LOP	At peak stress
CF4S-HU-50-01	0.190	0.20
CF4S-HU-50-02	0.052	0.22
CF4S-HU-50-03	0.054	0.17
CF4S -HU-50-04	0.047	0.15
CF4S-HU-50-05	0.062	0.14
Mean	0.08	0.18
SD	0.06	0.34
Max	0.19	0.22
Min	0.047	0.14

Table B.7.35: Results from four point bending test, water reduction and standard deviation of six CF5 (strips) were manufactured via compression moulding.

(1)	(2)			(3)		(4)	
Specimen code	Water/binder ratio			Stress (MPa)		Strain (%)	
	Before pressing	After pressing	Difference (%)	LOP	Peak	At LOP	At peak stress
CF5S-CM-50-01	0.35	0.26	26	50.9	70.2	0.20	0.41
CF5S-CM-50-02	0.35	0.28	20	48.6	62.4	0.21	0.34
CF5S-CM-50-03	0.35	0.26	26	64.1	65.0	0.38	0.44
CF5S-CM-50-04	0.35	0.24	31	56.0	63.8	0.25	0.39
CF5S-CM-50-05	0.35	0.25	29	54.1	65.5	0.21	0.36
CF5S-CM-50-06	0.35	0.23	34	50.1	63.2	0.17	0.41
Mean	0.4	0.25	28	54.0	65.0	0.24	0.39
SD				5.7	2.8	0.08	0.04
Characteristic strength (MPa)				44.2	60.2		
Max		0.28	34	64.1	70.2	0.38	0.44
Min		0.23	20	48.6	62.4	0.17	0.34

Table B.7.36: Toughness at two positions; at LOP and peak stress of six CF5 (strips) specimens were manufactured via compression moulding.

Specimen code	Toughness (J/m ³)	
	At LOP	At peak stress
CF5S-CM-50-01	0.057	0.19
CF5S-CM-50-02	0.068	0.14
CF5S-CM-50-03	0.15	0.18
CF5S-CM-50-04	0.081	0.17
CF5S-CM-50-05	0.064	0.16
CF5S-CM-50-06	0.05	0.19
Mean	0.078	0.17
SD	0.04	0.02
Max	0.15	0.19
Min	0.05	0.14

Table B.7.37: Results from four point bending test and standard deviation of six CF5 (strips) cementitious specimens ($V_f=5\%$) produced with hand lay-up.

(1)	(2)	(3)		(4)	
Specimen code	Water/ binder ratio	Stress (MPa)		Strain (%)	
		LOP	Peak	At LOP	At peak stress
CF5S-HU-50-01	0.35	13	52.3	0.03	0.52
CF5S-HU-50-02	0.35	20.7	52.8	0.12	0.45
CF5S-HU-50-03	0.35	20.2	49.9	0.10	0.45
CF5S-HU-50-04	0.35	12.1	52.7	0.06	0.57
CF5S-HU-50-05	0.35	20	55.5	0.14	0.72
CF5S-HU-50-06	0.35	10	56.2	0.02	0.66
Mean		16	53.2	0.08	0.56
SD		4.8	2.3	0.05	0.11
Characteristic strength (MPa)		7.7	49.3		
Max		20.7	56.2	0.14	0.72
Min		10	49.9	0.02	0.45

Table B.7.38: Toughness at two positions; at LOP and peak stress of six CF5 (strips) specimens ($V_f=5\%$) were manufactured via hand lay-up.

Specimen code	Toughness (J/m^3)	
	At LOP	At peak stress
CF5S-HU-50-01	0.022	0.19
CF5S-HU-50-02	0.13	0.15
CF5S-HU-50-03	0.012	0.14
CF5S -HU-50-04	0.004	0.20
CF5S-HU-50-05	0.015	0.27
CF5S-HU-50-06	0.002	0.25
Mean	0.031	0.20
SD	0.05	0.05
Max	0.13	0.27
Min	0.002	0.14

Table B.7.39: Results from four point bending test and standard deviation of six CF4 (surface treatment) cementitious specimens ($V_f=3\%$) produced with compression moulding.

(1)	(2)			(3)		(4)	
Specimen code	Water/binder ratio			Stress (MPa)		Strain (%)	
	Before pressing	After pressing	Difference (%)	LOP	Peak	At LOP	At peak stress
CF4T-CM-50-01	0.35	0.22	37	54.4	56.7	0.27	0.31
CF4T-CM-50-02	0.35	0.24	31	49.1	58.7	0.28	0.38
CF4T-CM-50-03	0.35	0.23	34	51.5	55.3	0.28	0.37
CF4T-CM-50-04	0.35	0.23	34	56.0	60.5	0.39	0.48
CF4T-CM-50-05	0.35	0.25	29	55.2	55.2	0.36	0.36
CF4T-CM-50-06	0.35	0.26	26	49.6	56.4	0.26	0.36
Mean	0.35	0.24	32	52.6	57.1	0.31	0.38
SD				3.0	2.1	0.05	0.06
Characteristic strength (MPa)				47.5	53.6		
Max		0.26	37	56.0	60.5	0.39	0.48
Min		0.22	26	49.1	55.2	0.26	0.31

Table B.7.40: Toughness at two positions; at LOP and peak stress of six treated CF4 specimens were manufactured via compression moulding.

Specimen code	Toughness (J/m^3)	
	At LOP	At peak stress
CF4T-CM-50-01	0.081	0.10
CF4T-CM-50-02	0.074	0.13
CF4T-CM-50-03	0.080	0.13
CF4T-CM-50-04	0.13	0.19
CF4T-CM-50-05	0.11	0.11
CF4T-CM-50-06	0.07	0.12
Mean	0.091	0.13
SD	0.02	0.03
Max	0.13	0.19
Min	0.07	0.1

Table B.7.41: Results from four point bending test and standard deviation of five treated CF4 ($V_f=5\%$) were manufactured via hand lay-up.

(1)	(2)	(3)		(4)	
Specimen code	Water/ binder ratio	Stress (MPa)		Strain (%)	
		LOP	Peak	At LOP	At peak stress
CF4T-HU-50-01	0.35	22.1	49	0.09	0.53
CF4T-HU-50-02	0.35	21	45	0.10	0.60
CF4T-HU-50-03	0.35	10.4	50.7	0.01	0.52
CF4T-HU-50-04	0.35	24.1	48.3	0.09	0.44
CF4T-HU-50-05	0.35	18	46.8	0.09	0.65
Mean		19.1	48	0.08	0.55
SD		5.4	2.2	0.04	0.08
Characteristic strength (MPa)		9.9	44.2		
Max		24.1	50.7	0.10	0.65
Min		10.4	46.8	0.01	0.44

Table B.7.42: Toughness at two positions; at LOP and peak stress of five treated CF4 specimens ($V_f=5\%$) were manufactured via hand lay-up.

Specimen code	Toughness (J/m^3)	
	At LOP	At peak stress
CF4T-HU-50-01	0.012	0.18
CF4T-HU-50-02	0.013	0.20
CF4T-HU-50-03	0.010	0.19
CF4T-HU-50-04	0.014	0.15
CF4T-HU-50-05	0.010	0.22
Mean	0.01	0.19
SD	0.002	0.03
Max	0.014	0.22
Min	0.01	0.15

Table B.7.43: Results from four point bending test, water reduction and standard deviation of five treated CF5 were manufactured via compression moulding.

(1)	(2)			(3)		(4)	
Specimen code	Water/binder ratio			Stress (MPa)		Strain (%)	
	Before pressing	After pressing	Difference (%)	LOP	Peak	At LOP	At peak stress
CF5T-CM-50-01	0.35	0.24	31	20.5	51.4	0.072	0.74
CF5T-CM-50-02	0.35	0.25	29	30.1	56.8	0.11	0.44
CF5T-CM-50-03	0.35	0.25	29	42.1	52.4	0.19	0.37
CF5T-CM-50-04	0.35	0.26	26	30.1	51.0	0.10	0.27
CF5T-CM-50-05	0.35	0.23	34	40.0	54.4	0.16	0.34
Mean	0.35	0.25	30	32.6	53.2	0.13	0.43
SD				8.7	2.4	0.05	0.2
Characteristic strength (MPa)				17.6	49.1		
Max		0.26	34	42.1	56.8	0.19	0.74
Min		0.23	26	20.5	51.0	0.072	0.27

Table B.7.44: Toughness at two positions; at LOP and peak stress of five treated CF5 specimens were manufactured via compression moulding.

Specimen code	Toughness (J/m ³)	
	At LOP	At peak stress
CF5T-CM-50-01	0.0088	0.29
CF5T-CM-50-02	0.020	0.18
CF5T-CM-50-03	0.043	0.13
CF5T-CM-50-04	0.017	0.09
CF5T-CM-50-05	0.037	0.13
Mean	0.025	0.16
SD	0.01	0.08
Max	0.043	0.29
Min	0.0088	0.09

Table B.7.45: Results from four point bending test and standard deviation of five treated CF5 ($V_f=5\%$) were manufactured via hand lay-up.

(1)	(2)	(3)		(4)	
Specimen code	Water/ binder ratio	Stress (MPa)		Strain (%)	
		LOP	Peak	At LOP	At peak stress
CF5T-HU-50-01	0.35	18	43.3	0.08	0.40
CF5T-HU-50-02	0.35	12.1	43.6	0.05	0.51
CF5T-HU-50-03	0.35	12	41.3	0.06	0.70
CF5T-HU-50-04	0.35	21	43.9	0.15	0.64
CF5T-HU-50-05	0.35	19	43.2	0.12	0.55
Mean		16.4	43.1	0.092	0.56
SD		4.1	1.0	0.04	0.12
Characteristic strength (MPa)		9.3	41.03		
Max		12	43.9	0.15	0.70
Min		19	41.3	0.05	0.40

Table B.7.46: Toughness at two positions; at LOP and peak stress of five treated CF5 specimens ($V_f=5\%$) were manufactured via hand lay-up.

Specimen code	Toughness (J/m^3)	
	At LOP	At peak stress
CF5T-HU-50-01	0.009	0.12
CF5T-HU-50-02	0.004	0.15
CF5T-HU-50-03	0.004	0.21
CF5T-HU-50-04	0.02	0.19
CF5T-HU-50-05	0.013	0.16
Mean	0.01	0.17
SD	0.007	0.04
Max	0.02	0.21
Min	0.004	0.12

Table B.7.47: Results from four point bending test, water reduction and standard deviation of four hybrid (CF3+PVA+CF8) specimens were manufactured via compression moulding.

(1)	(2)			(3)		(4)	
Specimen code	Water/binder ratio			Stress (MPa)		Strain (%)	
	Before pressing	After pressing	Difference (%)	LOP	Peak	At LOP	At peak stress
H-CM-50-01	0.35	0.23	34	41.8	74.3	0.42	0.61
H-CM-50-02	0.35	0.22	37	40.4	55.7	0.51	0.63
H-CM-50-03	0.35	0.25	29	33.4	44.3	0.33	0.59
H-CM-50-04	0.35	0.23	34	25.3	51.9	0.37	0.66
Mean		0.23	34	35.2	56.6	0.41	0.62
SD				7.6	12.8	0.08	0.03
Characteristic strength (MPa)				22	35		
Max		0.25	37	41.8	74.3	0.08	0.66
Min		0.22	29	25.3	44.3	0.04	0.59

Table B.7.48: Toughness at two positions; at LOP and peak stress of four hybrid (1%CF3+1%PVA+3%CF8) specimens were manufactured via compression moulding.

Specimen code	Toughness (J/m ³)	
	At LOP	At peak stress
H-CM-50-01	0.02	0.22
H-CM-50-02	0.02	0.19
H-CM-50-03	0.01	0.21
H-CM-50-04	0.005	0.23
Mean	0.014	0.21
SD	0.01	0.02
Max	0.02	0.23
Min	0.005	0.19

Table B.7.49: Results from four point bending test, water reduction and standard deviation of four hybrid (1%CF3+1%PVA+3%CF8) specimens were manufactured via hand lay-up.

(1)	(2)	(3)		(4)	
Specimen code	Water/ binder ratio	Stress (MPa)		Strain (%)	
		LOP	Peak	At LOP	At peak stress
H-HU-50-01	0.35	43	54.1	0.4	0.9
H-HU-50-02	0.35	68.3	68.3	0.5	0.5
H-HU-50-03	0.35	54.1	57.2	0.5	0.6
H-HU-50-04	0.35	48.5	55.0	0.6	0.7
H-HU-50-05	0.35	50.1	64.1	0.4	0.77
Mean		52.8	59.7	0.48	0.69
SD		9.5	6.2	0.08	0.15
Characteristic strength (MPa)		36	49		
Max		68.3	68.3	0.6	0.9
Min		43	54.1	0.4	0.5

Table B.7.50: Toughness at two positions; at LOP and peak stress of five hybrid (1%CF3+1%PVA+3%CF8) specimens were manufactured via hand lay-up.

Specimen code	Toughness (J/m ³)	
	At LOP	At peak stress
H-HU-50-01	0.1	0.30
H-HU-50-02	0.2	0.2
H-HU-50-03	0.16	0.22
H-HU-50-04	0.18	0.32
H-HU-50-05	0.11	0.33
Mean	0.15	0.27
SD	0.04	0.07
Max	0.18	0.32
Min	0.1	0.2

APPENDIX C

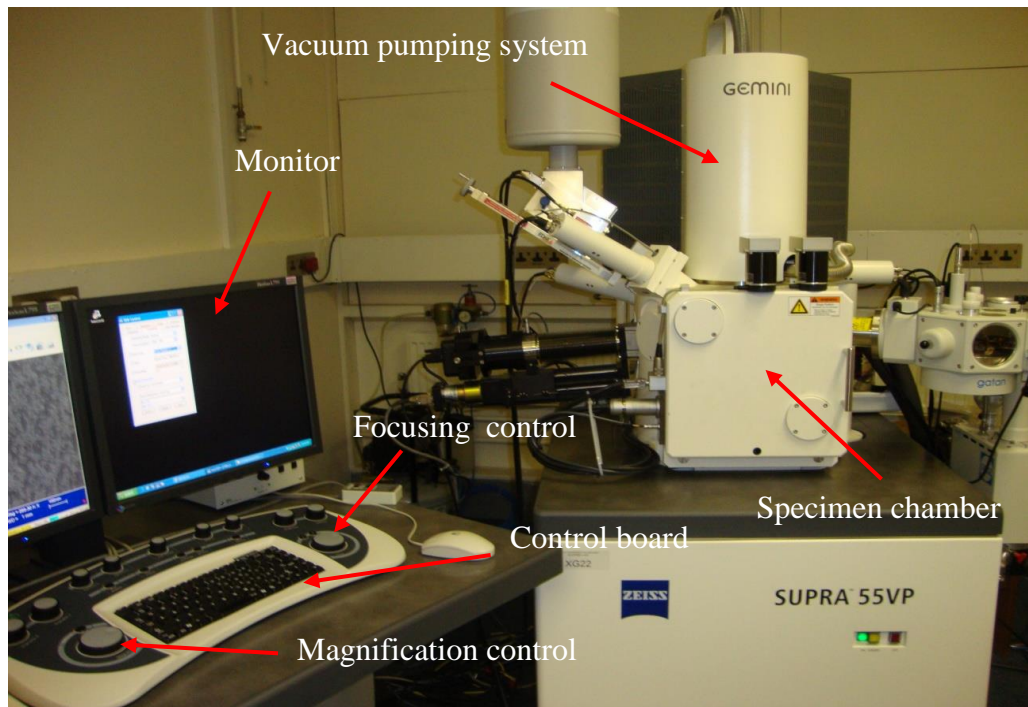


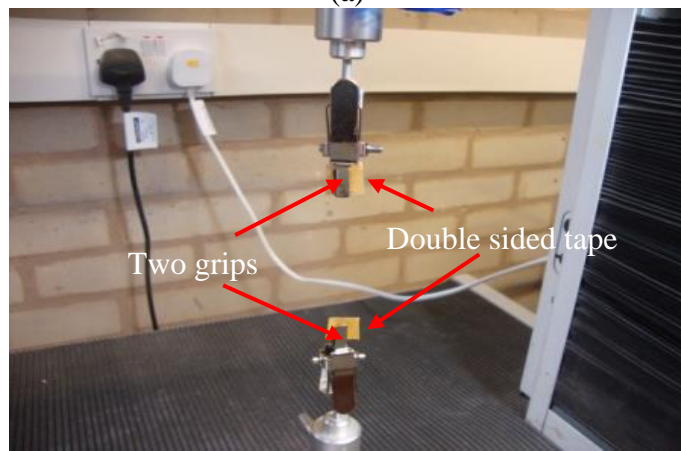
Figure C1: Photo of the ZEISS SUPRA 55VP SEM.



Figure C2: In-house ceramic mould used for slump test.



(a)



(b)



(c)

Figure C3: Arrangement of single fibre tensile strength test, a) Lloyd's universal testing machine with a load cell of 10 N, b) two grips with double-sided tape for better grip, and c) lighting magnifying lens for making the small diameter/length of the single fibre look bigger.



Figure C4: Hobart mixer.

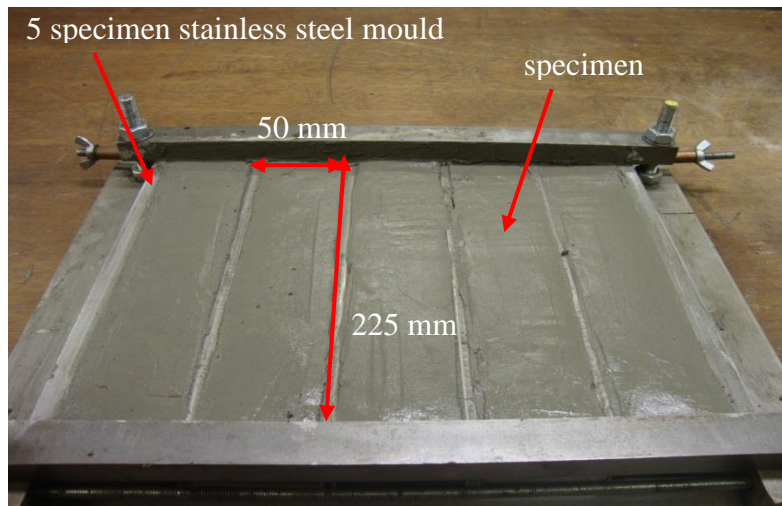


Figure C5: The five specimen stainless steel mould.

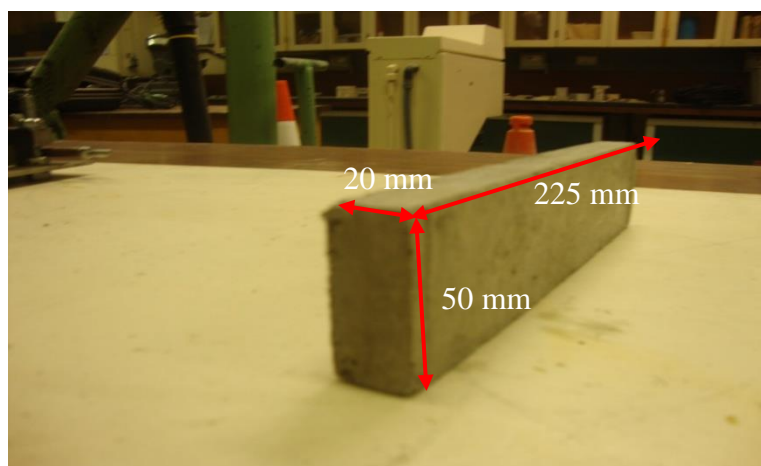


Figure C6: A typical specimen from the stainless steel mould.

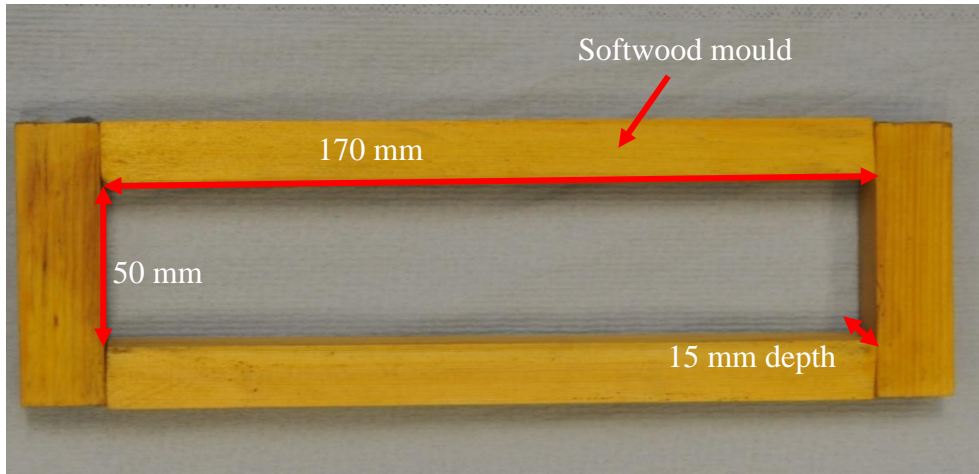


Figure C7: The single softwood mould.



Figure C8: The Denison 7231 compression machine.



Figure C9: The WMG DASSETT compression machine.

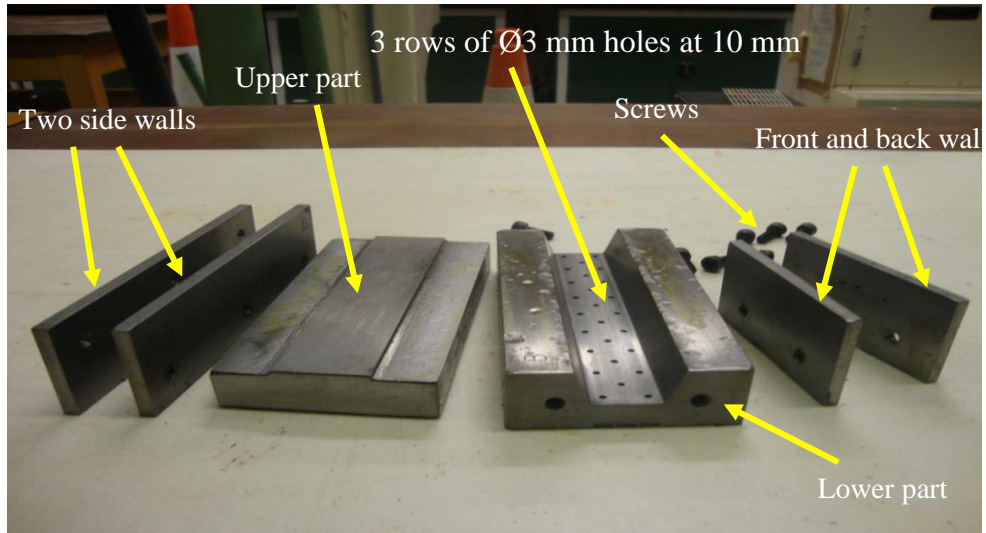


Figure C10: Six pieces of mild steel single trapezoid mould.

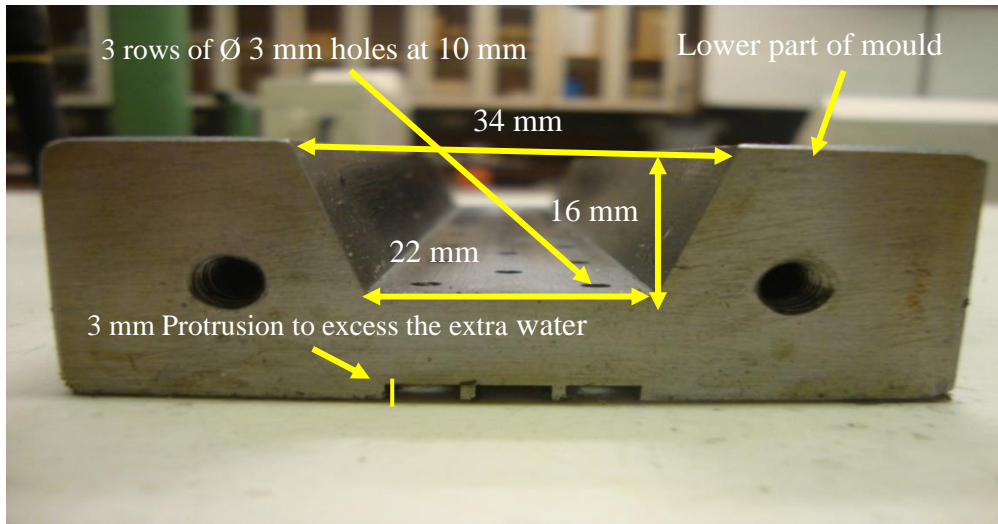


Figure C11: Protrusion of 3 mm holes in the lower part to access the extra water.

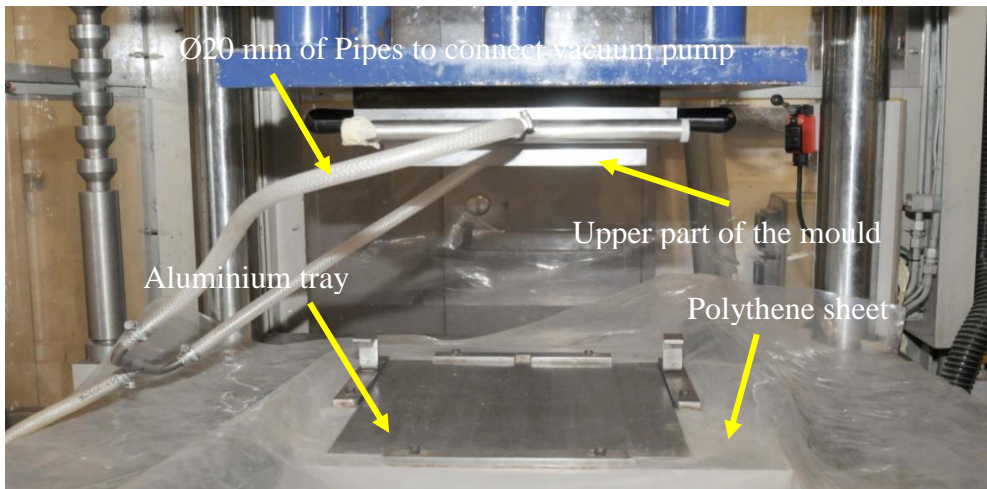


Figure C12: Six samples trapezoid mould and the arrangement when the upper part is fixed in the DASSET machine.

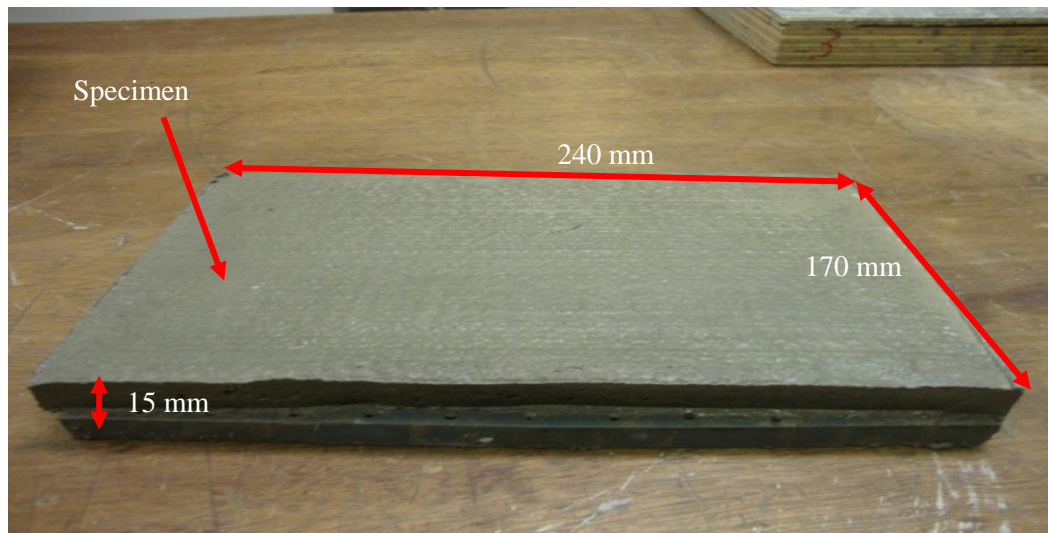


Figure C13: A green specimen from the single rectangular slab plate mould formed by compression moulding.

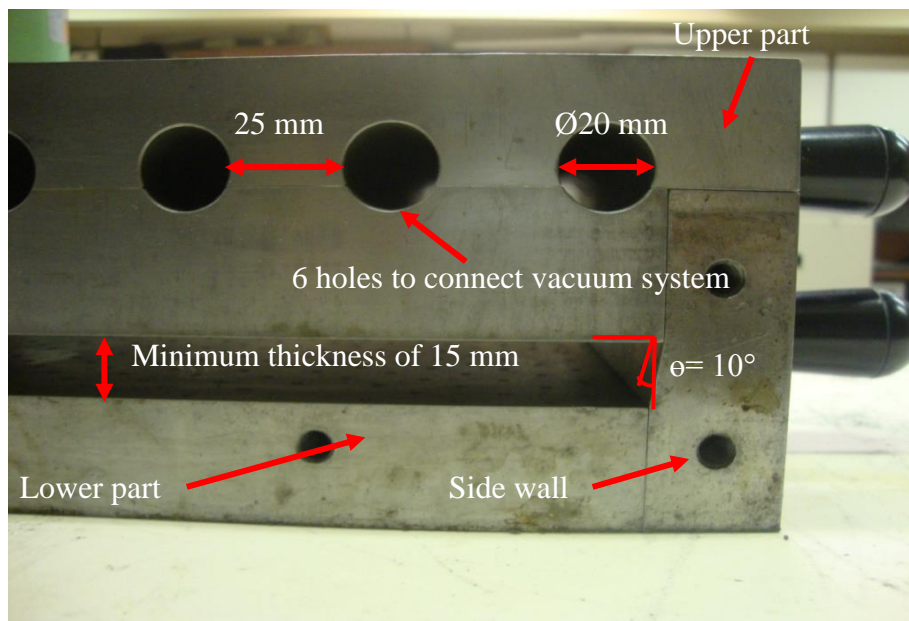


Figure C14: Assembled mould without end wall plate to show the 10° incline in the lower section of the side walls.

APPENDIX D

Table D.6.1: ANOVA test results for control specimens.

Groups	Count	Sum	Mean	Variance	
HLU	6	36.9	6.15	0.563	
CM	6	40.3	6.72	0.294	
ANOVA					
Source of Variation	SS	DF	MS	F	P-value
Between Groups	0.963	1	0.963	2.249	0.1646
Within Groups	4.283	10	0.428		
Total	5.246	11			

Table D.6.2: ANOVA test results for CF1 specimens.

Groups	Count	Sum	Mean	Variance	
HLU	6	45.4	7.57	0.315	
CM	6	49.2	8.20	0.64	
ANOVA					
Source of Variation	SS	DF	MS	F	P-value
Between Groups	1.203	1	1.203	2.522	0.1434
Within Groups	4.773	10	0.477		
Total	5.976	11			

Table D.6.3: ANOVA test results for CF2 specimens.

Groups	Count	Sum	Mean	Variance	
HLU	5	51.7	10.34	0.358	
CM	5	55.9	11.18	0.482	
ANOVA					
Source of Variation	SS	DF	MS	F	P-value
Between Groups	1.764	1	1.764	4.20	0.0746
Within Groups	3.360	8	0.420		
Total	5.124	9			

Table D.6.4: ANOVA test results for CF3 specimens.

Groups	Count	Sum	Mean	Variance	
HLU	5	42	8.40	0.235	
CM	5	46.9	9.38	1.092	
ANOVA					
Source of Variation	SS	DF	MS	F	P-value
Between Groups	2.401	1	2.401	3.619	0.0936
Within Groups	5.308	8	0.6635		
Total	7.709	9			

Table D.6.5: ANOVA test results for PVA specimens.

Groups	Count	Sum	Mean	Variance	
HLU	6	53.5	8.92	2.462	
CM	6	76.9	12.82	1.046	
ANOVA					
Source of Variation	SS	DF	MS	F	P-value
Between Groups	45.630	1	45.630	26.0198	0.0004
Within Groups	17.537	10	1.754		
Total	63.167	11			

Table D.6.6: ANOVA test results for PP specimens.

Groups	Count	Sum	Mean	Variance	
HLU	6	59.4	9.90	0.956	
CM	5	45.7	9.14	1.408	
ANOVA					
Source of Variation	SS	DF	MS	F	P-value
Between Groups	1.575	1	1.575	1.362	0.2732
Within Groups	10.412	9	1.157		
Total	11.987	10			

APPENDIX E

Table E.7.1: ANOVA test results for control specimens.

Groups	Count	Sum	Mean	Variance	
HLU	6	44.1	7.35	0.89	
CM	6	45.7	7.62	0.89	
ANOVA					
Source of Variation	SS	DF	MS	F	P-value
Between Groups	0.21	1	0.213	0.24	0.64
Within Groups	8.90	10	0.890		
Total	9.11	11			

Table E.7.2: ANOVA test results for CF4 specimens.

Groups	Count	Sum	Mean	Variance	
HLU	5	214.7	42.94	23.62	
CM	6	245.1	40.85	6.13	
ANOVA					
Source of Variation	SS	DF	MS	F	P-value
Between Groups	11.91	1	11.913	0.86	0.38
Within Groups	125.13	9	13.903		
Total	137.04	11			

Table E.7.3: ANOVA test results for CF5 specimens.

Groups	Count	Sum	Mean	Variance	
HLU	5	170	34	17.99	
CM	6	213.6	35.6	26.55	
ANOVA					
Source of Variation	SS	DF	MS	F	P-value
Between Groups	6.98	1	6.982	0.31	0.60
Within Groups	204.7	9	22.744		
Total	211.68	10			

Table E.7.4: ANOVA test results for CF6 specimens.

Groups	Count	Sum	Mean	Variance	
HLU	5	179.8	35.96	23.82	
CM	4	98.5	24.63	15.38	
ANOVA					
Source of Variation	SS	DF	MS	F	P-value
Between Groups	285.51	1	285.516	14.13	0.0071
Within Groups	141.42	7	20.203		
Total	426.93	8			

Table E.7.5: ANOVA test results for CF7 specimens.

Groups	Count	Sum	Mean	Variance	
HLU	6	210.2	35.03	3.13	
CM	6	99	16.5	2.32	
ANOVA					
Source of Variation	SS	DF	MS	F	P-value
Between Groups	1030.45	1	1030.453	378.38	2.82×10^{-9}
Within Groups	27.23	10	2.723		
Total	1057.68	11			

Table E.7.6: ANOVA test results for CF8 specimens.

Groups	Count	Sum	Mean	Variance	
HLU	5	179	35.8	31.49	
CM	6	127.1	21.18	0.65	
ANOVA					
Source of Variation	SS	DF	MS	F	P-value
Between Groups	582.67	1	582.673	40.58	0.00013
Within Groups	129.23	9	14.359		
Total	711.90	10			

Table E.7.7: ANOVA test results for CF9 specimens.

Groups	Count	Sum	Mean	Variance	
HLU	5	239.2	47.84	8.31	
CM	6	269.3	44.88	8.71	
ANOVA					
Source of Variation	SS	DF	MS	F	P-value
Between Groups	23.84	1	23.841	2.79	0.13
Within Groups	76.80	9	8.533		
Total	100.64	10			

Table E.7.8: ANOVA test results for GF specimens.

Groups	Count	Sum	Mean	Variance	
HLU	5	68.5	13.70	0.86	
CM	4	98.2	24.55	2.28	
ANOVA					
Source of Variation	SS	DF	MS	F	P-value
Between Groups	261.61	1	261.606	178.31	3.10×10^{-6}
Within Groups	10.27	7	1.467		
Total	271.88	8			